Advanced modelling of wave penetration in ports

Konstantina Aikaterini Maroudi

Advanced modelling of wave penetration in ports

By

Konstantina Aikaterini Maroudi

in partial fulfilment of the requirements for the degree of

Master of Science
in Civil Engineering

at the Delft University of Technology,
to be defended publicly on Thursday May 23, 2019 at 10:30 AM.

Supervisor:	Prof. dr. ir. M. Van Koningsveld	TU Delft
Thesis committee:	Dr. ir. M. Zijlema,	TU Delft
	Ir. A.J. Van der Hout,	TU Delft / Deltares
	Ir. S.P. Reijmerink,	Deltares

An electronic version of this thesis is available at http://repository.tudelft.nl/.

iii

Front cover: Aerial view of moored container ships.
Downloaded from:

Back cover: Artistic impression of the front cover picture showing a wave entering the port.

Acknowledgments

This thesis reflects the knowledge and skills I have developed in pursuit of my Master of Science in Hydraulic Engineering at Delft University of Technology and it would not be complete without acknowledging all the people who supported me in this achievement.

Firstly, I would like to thank the members of my graduation committee for their guidance and constructive suggestions during this research work. I would like to express my deep gratitude to my daily supervisor, Mr. Bas Reijmerink, for his thoughtful feedback, continuous support and enthusiastic encouragement. He has always been generous with his time and helped me to learn and work with SWASH and MATLAB. I would like to offer my special thanks to Mr. Arne van der Hout for his constructive criticism and inspiring discussions which helped me to acquire an in depth knowledge of my thesis topic. My grateful thanks also extend to Mr. Marcel Zijlema for his insightful comments and his advice on setting up the SWASH simulations. Last but not least, I would like to thank the chairman, Mr. Mark Van Koningsveld, whose experience and critical approach on my results and ideas were always valuable for the progress of my work.

I am honoured to be one of the recipients of the Scholarship for Hellenes by the Onassis Foundation to which I would like to express my gratitude for supporting me in my studies abroad. I would like to express my great appreciation to Professor Dimas who helped me to quest a master of outstanding academic quality and always guided me through the process. Additionally, I would like to thank the Deltares staff for enabling me to work in such a motivating, friendly and challenging working environment.

The experience of carrying out my thesis at Deltares would not have been the same without my fellow interns. I am particularly grateful to Vassia for her friendship and constant support whenever I needed advice, which allows me to call her 'extra supervisor'. I feel incredibly lucky to have been a part of the amazing tower group of friends: Alexia, Antonio, Anna, Andrea & Andrea, Bauke, Eugenio, Irene, Joe, Kostas & Kostas, Odilia and Sara made the last months unforgettable.

I am really glad for all the people I met during my staying in Netherlands and all the amazing times we had together. To my fellow students in the hydraulic engineering track, Vasso, Fontas, Alejandra, Maria and Lina I want to express my appreciation for their friendship and kindness. Special thanks to my friends Juan, Ioanna, Luis and Maria for their contagious enthusiasm and for the countless board game nights. I wish to thank also my roommates for introducing me to the Dutch culture. I could not forget to thank two cheerful people from the beautiful island of Corfu, who were always by my side: my beloved friend Juliette and darling Lala. Last but not least, I would like to thank my cousins, Chris and Kostas, as well as my aunt, Efi for their tenderness and their support in my first experience living abroad.

The completion of my master would not have been possible without the love and unconditional support of my family, who encouraged me to pursue my goals. My parents Ioannis and Aristea, my sister Stefanie and my grandmother Kaiti have always inspired me to follow my dreams and wanted the best for me. This thesis is dedicated with all my love to them.

Konstantina Aikaterini (Teni) Maroudi
Delft, April 2019

Acknowledgments in Greek/Ευχαριστίες

Executive summary

Wave penetration inside a harbour is one of the main challenges that port planners and engineers had to tackle in recent years. Wave conditions near the harbour entrance and inside the harbour basins determine vessels' safe sailing and mooring, possibly causes unwanted vessel movements, and unequivocally regulate the execution of port operations. Wave penetration can be described in a complete way by means of physical scale modelling. However, the construction of a physical scale model is expensive and time consuming. For this reason, in recent past maritime and port engineers have used several numerical models to describe wave penetration in ports, affected by multiple processes such as diffraction, partial reflection, etc.

In this study, the simulation of wave penetration with the non-hydrostatic model SWASH is examined. To validate the numerical model, output of an open benchmark dataset of Deltares (Deltares, 2016) is used, consisting of physical scale model tests of schematic port layouts. As wave penetration is a summation of physical processes, each process should be described accurately by SWASH. This thesis focuses on assessing how SWASH models wave penetration per wave process first separately by means of simplified models and then combined in a model describing the full harbour layout resulting to the final wave field inside a port. As the amount of processes influencing wave penetration increases for higher layout complexity, the research was targeted at the simplest port layout considered in the benchmark dataset (Deltares, 2016). Moreover, only regular waves were taken into account, as in this case wave penetration becomes less complex. Thus, when comparing computational results to measurement results differences are most easily identified.

The main topics of interest of the formulated research questions are the ability of SWASH to simulate wave propagation, wave celerity and the effect of two dominant wave processes: reflection and diffraction. Hence, the first part of the research aimed to obtain knowledge about these topics from the measurements. Consequently, this information was used as comparison material to evaluate the SWASH results.

To better understand the influence of reflection the waves, two simplified one-dimensional SWASH models were designed. The first model simulated reflection in front of a gravel slope, located outside the harbour basin, and the second model reflection in front of the harbour basin end, consisting of a gravel slope and a concrete quay wall behind it. The results suggest that outside the basin the reflection off the gravel slope has a minor effect in comparison to the reflection off a vertical quay wall. Inside the harbour basin, wave reflection played a dominant role on the resulting wave field there. It should be emphasised that the standing wave heights were altering fast within a short horizontal distance. As a consequence, the precise wave height values were strongly influenced by the exact location of the output points examined.

The importance of diffraction inside the harbour was demonstrated by a simplified two-dimensional model in which the harbour end, at which waves get reflected, was not included. The information that could be obtained from the measurements about the wave height changes due to diffraction was limited. However, the initial trends due to diffraction were also identified in SWASH. From the comparison of the wave height in the SWASH model, influenced only by diffraction, to the respective measured value, it was confirmed that the total measured wave penetration inside the harbour was significantly influenced by diffraction. Nevertheless, reflection off the harbour end played also an important role inside the basin and both wave processes should be modelled accurately to reproduce the wave field in the measurements.

The comparison of the measurements to the results of the final SWASH model, which included the full version of the simplest physical model, showed that the overall wave field pattern is in agreement. The numerical model was able to reproduce the diffraction and reflection patterns observed in the

measurements. At many output locations in SWASH the measured wave height values were simulated with high accuracy. On the downside, at other locations the measured and the modelled wave height deviated significantly. The large deviations can be explained by the fact that the standing wave patterns change within a short distance and thus the wave height can vary significantly at the area close to a specific output point. It may be possible that the measured wave height at a specific point can be identified in SWASH in the region close to the exact point coordinates. All in all, it was concluded that for non-breaking, relatively low waves, with wave-height-to-water-depth ratio lower than 0.2, the accuracy of SWASH in modelling the wave processes of reflection and diffraction is sufficiently well for engineering purposes. For relatively high waves and/or breaking waves, numerical instabilities were detected. It is assumed that the numerical instabilities can be attributed to the relatively low number of grid cells per wave length. However, this assumption has not been verified within this study.

This study advances our understanding of the wave penetration simulation in SWASH. The approach followed allows investigating the ability of the model to simulate, separately and combined, two wave processes which predominantly contribute to wave penetration in harbour: reflection and diffraction. With further validation to guarantee the model stability, the strategy of this thesis can be a useful tool to understand the performance of SWASH in modeling wave penetration per wave process and in combination. The knowledge obtained enlightens the possible reasons leading to deviations between the measurements and the model outputs. This can be valuable assistance in the course of further improving the model accuracy. The next step would be to apply the technique of examining wave penetration in SWASH as a summation of different wave processes in more complex layouts and wave conditions.

Executive summary in Greek/ Περίληψη

Η κυματική διείσδυση αποτελεί μια από τις κυριότερες προκλήσεις που οι σχεδιαστές και μηχανικοί λιμένων καλούνται να αντιμετωπίσουν τα τελευταία χρόνια. Οι κυματικές συνθήκες κοντά στην είσοδο του λιμένα και μέσα στη λιμενολεκάνη καθορίζουν την ασφαλή πλεύση και πρόσδεση των πλοίων, ενδεχομένως προκαλούν ανεπιθύμητες κινήσεις τους και αδιαμφισβήτητα ρυθμίζουν την εκτέλεση των δραστηριοτήτων του λιμένα. Η κυματική διείσδυση δύναται να περιγραφεί πλήρως με χρήση ενός φυσικού ομοιώματος. Παρόλα αυτά η κατασκευή ενός υδραυλικού ομοιώματος είναι δαπανηρή και χρονοβόρα. Για αυτό το λόγο, τα τελευταία χρόνια οι ναυπηγοί μηχανικοί και οι υδραυλικοί μηχανικοί λιμένων χρησιμοποιούν διάφορα αριθμητικά μοντέλα για να περιγράψουν την κυματική διείσδυση στα λιμάνια, η οποία επηρεάζεται απο πληθώρα διαδικασιών όπως περίθλαση, μερική ανάκλαση κλπ.

Στην παρούσα μελέτη εξετάζεται η προσομοίωση της κυματικής διείσδυσης με χρήση του μη-υδροστατικού αριθμητικού μοντέλου SWASH. Για την επιβεβαίωση της ορθότητας του μοντέλου χρησιμοποιήθηκαν τα αποτελέσματα ενός σημείου αναφοράς συνόλου δεδομένων (Deltares, 2016), ελεύθερα διαθέσιμα, τα οποία περιλαμβάνουν τα πειράματα σε ένα φυσικό ομοίωμα σχηματικών διατάξεων λιμένα. Καθώς η κυματική διείσδυση είναι ένας συνδυασμός φυσικών διεργασιών, κάθε επιμέρους διεργασία πρέπει να μπορεί να περιγραφεί με ακρίβεια από το SWASH. Η παρούσα διπλωματική εστιάζει στην αξιολόγηση του τρόπου με τον οποίο το SWASH περιγράφει την κυματική διείσδυση ανά κυματική διεργασία, πρώτα ξεχωριστά με χρήση απλουστευμένων μοντέλων και ύστερα συνδυαστικά σε ένα μοντέλο που περιλαμβάνει την πλήρη διάταξη λιμένα, οδηγώντας στο τελικό κυματικό πεδίο εντός και πλησίον του λιμένα. Καθώς ο αριθμός των φυσικών διεργασιών που επηρεάζουν την κυματική διείσδυση αυξάνει όταν η διάταξη του λιμένα γινεται πιο πολύπλοκη, η έρευνα εστίασε στην απλούστερη διάταξη λιμένα που περιλαμβανόταν στο σύνολο δεδομένων (Deltares, 2016). Επιπροσθέτως, μόνο μονοχρωματικοί κυματισμοί ελήφθησαν υπόψη καθώς σε αυτή την περίπτωση οι διαφορές μεταξύ αριθμητικών αποτελεσμάτων και τις μετρήσεων εντοπίζονται πιο εύκολα.

Τα κύρια θέματα ενδιαφέροντος των ερευνητικών ερωτήσεων που διαμορφώθηκαν είναι η δυνατότητα του SWASH να προσομοιώσει την κυματική διείσδυση, την ταχύτητα των μονοχρωματικών κυματισμών και την επίδραση δύο κυρίαρχων κυματικών διεργασιών: της ανάκλασης και της περίθλασης. Επομένως, το πρώτο μέρος της έρευνας στόχευε στη συλλογή πληροφοριών για αυτά τα θέματα από τις μετρήσεις. Στη συνέχεια, οι πληροφορίες αυτές συγκρίθηκαν με τα αποτελέσματα του αριθμητικού μοντέλου προκειμένου να αξιολογηθεί η απόδοση του SWASH.

Για την καλύτερη κατανόηση της επίδρασης της ανάκλασης των κυμάτων, δύο απλουστευμένα μονοδιάστατα μοντέλα δημιουργήθηκαν στο SWASH. Το πρώτο μοντέλο προσομοίωνε την ανάκλαση από ένα κεκλιμένο πρανές με πέτρες, ευβρισκόμενο εκτός της λιμενολεκάνης, ενώ το δεύτερο μοντέλο προσομοίωνε την ανάκλαση στο κλειστό τέλος της λιμενολεκάνης, που αποτελούνταν από ένα πρανές με πέτρες και ένα κρηπιδότοιχο από σκυρόδεμα ακριβώς από πίσω. Τα αποτελέσματα έδειξαν ότι στην περιοχή εκτός της λιμενολεκάνης η επίδραση της ανάκλασης από το κεκλιμένο πρανές με πέτρες είναι μικρή σε σχέση με την επίδραση ενος κατακόρυφου κρηπιδότοιχου. Εντός της λιμενολεκάνης, η κυματική ανάκλαση διαδραματίζει κυρίαρχο ρόλο στο τελικό κυματικό πεδίο. Αξίζει να τονιστεί ότι το ύψος κύματος των στάσιμων κυμάτων μεταβαλλόταν σημαντικά εντός μικρού οριζόντιου διαστήματος. Συνεπώς, οι ακριβείς τιμές του ύψους κύματος επηρεάζονται έντονα από την ακριβή θέση των σημείων που εξετάζονται.

Η επίδραση της περίθλασης εντός του λιμένα αναδείχθηκε μέσω ενός απλουστευμένου μοντέλου το οποίο δεν περιελάμβανε το κλειστό άκρο του λιμένα στο οποίο τα κύματα ανακλώνται.Οι πληροφορίες που προέκυψαν από τις μετρήσεις σχετικά με τις αλλαγές του ύψους κύματος λόγω

περίθλασης ήταν περιορισμένες. Παρόλα αυτά οι αρχικές τάσεις λόγω περίθλασης εντοπίστηκαν και στο SWASH. Από τη σύγκριση του ύψους κύματος στο SWASH, επηρεασμένο μόνο από το φαινόμενο της περίθλασης, με την αντίστοιχη μετρηθείσα τιμή, επιβεβαιώθηκε ότι η συνολική μετρηθείσα κυματική διείσδυση επηρεάζεται αισθητά από την περίθλαση. Ωστόσο, και η ανάκλαση στο κλειστό άκρο του λιμένα διαδραματίζει σημαντικό ρόλο εντός της λιμενολεκάνης. Επομένως, είναι απαραίτητο να προσομοιώνονται με ακρίβεια και οι δύο διεργασίες, περίθλαση και ανάκλαση, ώστε να αναπαραχθεί στο μοντέλο το κυματικό πεδίο των μετρήσεων.

Η σύγκριση των μετρήσεων με τα αποτελέσματα του τελικού μοντέλου στο SWASH, το οποίο περιελάμβανε την πλήρη έκδοση της απλούστερης διάταξης λιμένα, έδειξε ότι εν γένει τα κυματικά πεδία είναι σε συμφωνία. Το αριθμητικό μοντέλο είναι εν γένει σε θέση να προσομοιώσει τις μετρηθείσες τιμές, που αποτελούν συνδυασμό δύο κυρίαρχων φαινομένων: της περίθλασης και την ανάκλασης. Σε πολλές θέσεις καταγραφής αποτελεσμάτων στο SWASH οι μετρηθείσες τιμές του ύψους κύματος περιγράφονται με μεγάλη ακρίβεια. Από την άλλη πλευρά, σε αρκετές θέσεις οι μετρηθείσες τιμές του ύψους κύματος και οι αντίστοιχες τιμές του αριθμητικού μοντέλου παρουσιάζουν σημαντική απόκλιση. Αξίζει να σημειωθεί ότι στην παρούσα προσέγγιση οι μετρήσεις και τα αποτελέσματα του SWASH συγκρίνονται στις ακριβείς θέσεις των μετρητικών οργάνων. Όμως, όπως προαναφέρθηκε, στο αριθμητικό μοντέλο παρατηρήθηκε ότι το ύψος στα στάσιμα κύματα αλλάζει εντός μικρής οριζόντιας απόστασης. Επομένως, το ύψος κύματος ενδέχεται να διαφέρει σημαντικά στην περιοχή κοντά στο συγκεκριμένο σημείο που εξετάζεται. Αυτή η παρατήρηση αποτελεί μια καλή εξήγηση για τις αποκλίσεις που παρατηρήθηκαν σε αρκετά σημεία. Είναι πιθανό το μετρηθέν ύψος κύματος σε μια συγκεκριμένη τοποθεσία να εντοπίζεται στο SWASH στην περιοχή κοντά στην ακριβή τοποθεσία που εξετάζεται. Εν γένει, συμπεραίνεται ότι για μη-θραυόμενους, σχετικά ασθενείς κυματισμούς, με λόγο ύψους-κύματος-προς-βάθος μικρότερο του 0.2, η ακρίβεια του SWASH στην προσομοίωση των κυματικών διεργασιών της ανάκλασης και της περίθλασης είναι επαρκώς ακριβής για μελέτες μηχανικού. Για σχετικά ισχυρούς κυματισμούς και/ή θραυόμενους κυματισμούς, παρατηρήθηκαν αριθμητικές αστάθειες. Θεωρείται ότι οι αριθμητικές αστάθειες μπορούν να αποδοθούν στον σχετικά χαμηλό αριθμό κελιών ανά μήκος κύματος.

Η παρούσα έρευνα διευρύνει την κατανόηση της προσομοίωσης της κυματικής διείσδυσης μέσω του αριθμητικού μοντέλου SWASH. Η προσέγγιση που ακολουθήθηκε επιτρέπει τη διερεύνηση της ικανότητας προσομοίωσης του μοντέλου, ξεχωριστά και σε συνδυασμό, δύο κυματικών διεργασιών που συμβάλλουν πρωταρχικά στην κυματική διείσδυση σε λιμένες: την ανάκλαση και την περίθλαση. Με επιπλέον επαλήθευση, που θα εξασφαλίσει την αριθμητική σταθερότητα του μοντέλου, η στρατηγική της παρούσας διπλωματικής μπορεί να αποτέλεσει ενα χρήσιμο εργαλείο κατανόησης της απόδοσης του SWASH στην περιγραφή της κυματικής διείσδυσης ανά κυματική διεργασία και συνολικά. Η αποκτηθείσα γνώση διαφωτίζει σχετικά με τους πιθανούς λόγους που οδηγούν σε αποκλίσεις ανάμεσα στις μετρήσεις και τα αριθμητικά αποτελέσματα. Μπορεί να αποτελέσει πολύτιμη βοήθεια στην πορεία βελτιστοποίησης της ακρίβειας του μοντέλου. Το επόμενο βήμα μπορεί να είναι η εφαρμογή της παρούσας μεθόδου εξέτασης της κυματικής διείσδυδης στο SWASH ως άθροισμα διαφορετικών κυματικών διεργασιών σε πιο σύνθετες διατάξεις λιμένα και πιο πολύπλοκες κυματικές συνθήκες.

Contents

List of figures

List of tables

List of abbreviations

Abbreviation	Description
1D	one-dimensional
2D	two-dimensional
ARC	Active Reflection Compensation
m	meter
PHAROS	Program for Harbour Oscillations
s	second
SWASH	Simulating WAves till Shore
SWL	Shallow water level

Chapter 1   Introduction

Financially, downtime in ports is of major importance as it refers to the period of time when normal port operations cannot be executed. Depending on the type of vessels in a port there are limits to a number of wave parameters below which safe sailing and mooring is guaranteed. Moreover, during severe wave conditions it may not be safe for vessels to stay at a berth. The wave field inside a harbour is one of the most important parameters required to estimate the downtime of a port. Other factors influencing a port's downtime may be wind conditions, collapse of a structure or damage repair operations (Allsop, 1998).

Different phenomena affect the wave penetration into ports including diffraction, refraction, shoaling, reflection and transmission (Holthuijsen, 2007). The importance of each wave process depends on the design and the special characteristics of a specific port. Complex geometry and specific bathymetry influences, such as the effect of dredged entrance channels, may also play a role. Other processes that influence wave propagation into ports are harbour oscillations, low frequency waves, wave breaking, dispersion and non-linear wave-wave interactions. It is obvious that calculating the wave field inside a port area is not straightforward.

Wave penetration can be described in a complete way by means of physical scale modelling. The high costs and the long construction process of a scale model, as well as the need to check alternative port layouts in early design stages may lead an engineer to use numerical tools. Several types of numerical wave models can potentially be used to predict wave penetration. Even though the wave models have generally been validated in detail for wave propagation and wave growth in open water, validation of their performance for representing wave penetration into harbours has been rather limited.

1.1   Problem description

A numerical wave model is considered suitable depending on the application for which it is applied. To assess the model performance on a specific application, it is common practice to compare the model results to measurements. In this thesis the application examined is wave penetration in harbours. A set of experiments in a physical scale model conducted by Deltares in 2014 aimed to form a complete dataset for numerical model validation for wave penetration in ports (Deltares, 2016). The available datasets include test series of three schematic port layouts. A certain part of the datasets has been used previously by a few master students in Delft University of Technology for their graduation thesis (e.g. Van Mierlo, 2014, Monteban, 2016 etc.).

A limited number of tests for the most complex port layout (layout 3) and spectrum wave conditions are simulated with the mild slope model PHAROS (Deltares, 2013), the Boussinesq type model TRITON (Deltares, 2008) and the non-hydrostatic wave model SWASH (Zijlema, Stelling and Smit, 2011) by Van Mierlo (2014). One test from the same sub-dataset and a different test also for layout 2 with spectral wave conditions have been used by Monteban (2016) to compare the performance of the Boussinesq-type model MIKE 21BW (DHI, 2007) to the non-hydrostatic wave model SWASH. The computed values by the models are considered accurate if the relative bias percentages and/or the mean absolute percentage error are less than ±15% deviating from the measured values. In both master theses, the performance of the models regarding the wave height of primary waves was examined.

The performance of the non-hydrostatic model, SWASH, for modelling wave penetration in ports is chosen to be studied in this thesis. As both master students, Van Mierlo and Monteban, modelled a part of the dataset of the schematic port layouts using SWASH their work is carefully examined and is considered a stepping stone for this thesis. According to both students' conclusions, SWASH has been proven able to describe accurately the propagation of primary waves. The wave height of primary waves was predicted with an error lower than 15%. Finally, if two vertical layers are used, the model is considered robust and no numerical instabilities are expected.

In the aforementioned theses, tests for the most complex layouts were examined. This means that a lot of physical processes influence simultaneously the wave field that enters the harbour. Therefore, the final errors in wave prediction inside the port are attributed to a group of processes modelled in SWASH. Using the previous work results it is not possible to evaluate if SWASH is able to describe accurately each wave process that contributes to the total wave penetration. To improve the model performance and obtain more accurate results it is necessary to find the reasons causing the errors. Moreover, the errors can be related to the ability of the model to describe the governing wave processes influencing wave penetration.

1.2   Strategy

This thesis focuses on explaining how SWASH models wave penetration per wave process and finding the possible factors causing errors in the predictions. To better understand the performance of SWASH in calculating waves in ports, it is necessary to identify which physical processes contribute to wave penetration. As wave penetration is a summation of physical processes, each process should be described accurately by SWASH. As the complexity of the layout increases, the amount of processes influencing wave penetration is also increased. To be able to identify the separate wave processes, the research is therefore focused on the simplest port layout. In the chosen layout the most important wave processes involved in wave penetration are examined separately and combined.
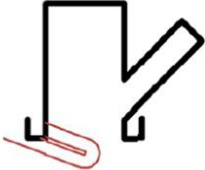
The previous theses focus on complex wave conditions. The water level time series used as input in SWASH are derived form a JONSWAP spectrum (Hasselmann et al., 1973). This means that the water level entering the domain consists of a series of superpositioned regular waves with different characteristics and duration. As every few seconds the wave characteristics are changing, it is not possible to check if the model can perform well for all wave heights and wave periods. An alternative approach is to study only monochromatic wave conditions. If only regular waves are taken into account, wave penetration becomes less complex and when comparing computational results to measurement results differences are most easily identified.

The strategy of this thesis is to decompose the test cases in very simplified models for which behaviour of waves can be predicted in advance. This means that the simplified tests will be performed for regular wave conditions in simplistic layouts to obtain results, which can be more easily understood and related to specific wave processes.

1.3 The dataset of schematic port layouts (Deltares, 2014) and the selection of specific group of tests

The open benchmark dataset of schematic port layouts (Deltares, 2016) is designed for examining wave penetration in ports. Three different layouts are studied. The layouts and the relevant physical processes are increasing stepwise in complexity. The simplest layout, layout 1, consists of a main harbour basin. In addition to the main basin, in layout 2 a side basin is included. In the most complex layout, layout 3, a breakwater is added at the harbour entrance. The three harbour layouts and the relevant wave process contributing to wave penetration in each case are presented in Table 1.1.

Table 1.1 The three schematic port layouts of the physical model and the wave processes that influence wave penetration (Adapted from Van Mierlo, 2014).

Wave processes influencing wave penetration		Layout 1	Layout 2	Layout 3
Reflection	at the main basin end	✓	✓	✓
	at the harbour head walls	✓	✓	✓
	at the side basin end	-	✓	✓
	at the breakwater slope	-	-	✓
Diffraction	as waves enter the main basin	✓	✓	✓
	as waves enter the side basin	-	✓	✓
Refraction	over the breakwater	-	-	✓
Transmission	through the breakwater	-	-	✓
Harbour oscillations		✓	✓	✓
Transversal reflections	in the main basin	✓	✓	✓
	in the side basin	-	✓	✓

With respect to the geometry, a real port may be complex, consisting of multiple basins. For simplicity the layout examined in detail is Layout 1. A sketch of Layout 1 as constructed in the physical scale model is presented in Figure 1.1. By choosing a simple layout the amount of wave processes involved in wave penetration is minimized.

The governing wave processes taking place in the harbour basin of Layout 1 are stated in Table 1.1. The processes that consider influencing mainly the wave field are reflection in the main basin and the harbour head walls and diffraction as waves enter the harbour. The harbour oscillations and the transversal reflections are considered to have a minor effect. In the area outside the harbour basin reflection at the outer slopes 2a and 2b are considered of major importance. The transversal reflections at slopes 3a and 3b influence mainly the adjacent area. These transversal reflections are not important for in the mooring area and the harbour entrance and thus they can be ignored. As the water depth in the physical model is constant wave processes, such as shoaling and refraction are not relevant for the specific layout.
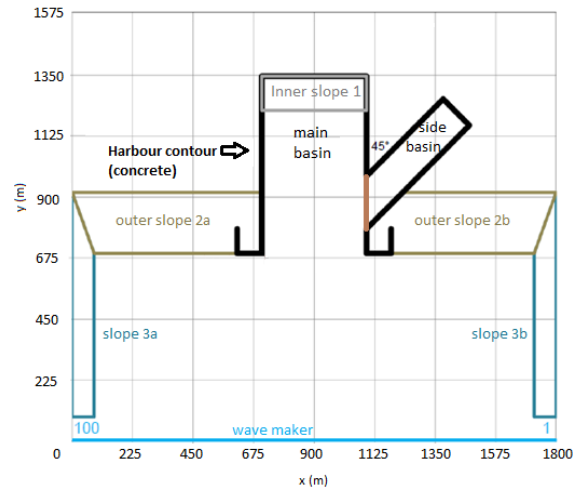
Figure 1.1-Sketch of physical scale model for Layout 1 in prototype scale. The scale used is scale 1:45. (Figure adapted from Deltares, 2016).

The wave conditions examined for the three layouts are by increasing complexity: monochromatic, bi-chromatic and spectral (JONSWAP spectrum). Only for layout 3 various sea and swell wave conditions are examined. In reality, a port is attacked by a wave spectrum, which is the summation of regular waves with different wave heights, periods and wave directions. Regular waves, also called monochromatic waves, are the simplest waves forms used as initial step of defining the majority of wave theories. To keep the cases as simple as possible this thesis is focused on studying the monochromatic wave conditions approaching the harbour with a 90° angle of incidence.

From the tests performed in the physical scale model, seven tests are selected to be studied and modelled in SWASH. In the following table basic information about the seven tests that have been conducted in the physical scale model (Deltares, 2016) is presented. To provide general conclusions the selected tests cover a wide range of wave heights and periods.

Table 1.2-The characteristics of the selected set of tests in prototype scale.

Test	Wave conditions	Layout	H [m]	T [s]	Depth [m]	Angle [°]
T001	Monochromatic	1	0.99	7.51	19.8	90
T002	Monochromatic	1	1.44	10.00	19.8	90
T003	Monochromatic	1	2.39	16.97	19.8	90
T010	Monochromatic	1	2.97	5.03	19.8	90
T011	Monochromatic	1	3.02	8.99	19.8	90
T012	Monochromatic	1	2.75	15.03	19.8	90
T013	Monochromatic	1	1.94	4.49	19.8	90

During the experiments the water level time series are measured at 21 measurement locations. The measurement devices are placed in the centre of the harbour and in the mooring areas close to the quay walls as well as in the area in front of the harbour. A complete overview of the full dataset and the measurement locations is provided in Section 2.2 . Moreover, the details about the seven selected tests are discussed in Section 2.3 .

1.4   Research questions

The open benchmark dataset for wave penetration in ports conducted in Deltares in 2014 includes a wide range of layouts and wave conditions (Deltares, 2016). This thesis is focused on a specific set of tests for the simplest layout and the simple monochromatic wave conditions. As described in Section 1.3 , the selected set of tests consists of 7 cases. The following research questions are referring to this specific set of tests.

Question 1: How accurate can SWASH reproduce wave propagation, the incoming wave height and the wave celerity of individual waves measured in the physical scale model tests?

Question 2: Can wave reflection and diffraction, measured in the physical scale model tests, be modelled accurately by SWASH?

Question 3: Can a two-dimensional SWASH model representing the simplest layout of the physical scale model tests, describe the wave height changes (temporally and spatially) in the measured water level time series?

1.5   Research approach

The approach formed to answer the research questions stated in the previous section consists of data analysis and numerical modelling. The strategy followed is discussed separately for each question. An essential remark is that the analysis of the measured data and the SWASH simulations are conducted in prototype scale. This choice is clarified in Section 2.5 . It should be mentioned that all the graphs in this report are in prototype scale.

Question 1:   How accurate can SWASH reproduce wave propagation, the incoming wave height and the wave celerity of individual waves measured in the physical scale model tests?

SWASH outputs can be considered as accurate, if they are in agreement with the measurements. Hence, the first step is to examine the wave propagation, the wave celerity and the incoming wave height in the measurements. Ideally the propagation of waves in one direction is inspected in a wave flume. Alternatively, a line of measurement devices perpendicular to the wave maker is studied as it is considered to resemble a wave flume. It is assumed that the simple monochromatic waves follow the linear wave theory. It is anticipated that the waves travel from the wave maker towards the closest measurement locations without any disturbance. After the waves at measurement locations start to be influenced by diffraction and reflections at the different structures, the measurement devices signal does not any longer match with the incoming wave maker signal. The undisturbed part of the time series is used in the calculations of the incoming wave height.

The aforementioned approach is also applied in SWASH. A 1D SWASH model representing the same line of measurement devices used in the measurements analysis is created. As in the 1D model waves propagate in one direction it is considered to represent a wave flume. In the 1D model the geometry of the physical scale model is reproduced. Moreover, the wave conditions are the same as in the experiments. Finally, the SWASH results are compared to the measured water level time series. This enables the assessment of SWASH performance.

Question 2: Can wave reflection and diffraction, measured in the physical scale model tests, be modelled accurately by SWASH?

As discussed in Section 1.2, a group of wave processes governs wave penetration in layout1. Modelling in SWASH the full layout 1 results in a wave field influenced by many wave processes simultaneously. To investigate the impact of each wave process it is necessary to consider simplified

SWASH models focusing on one wave process at a time. As simplified SWASH models are defined the models containing only a part of the full layout. The design of a simplified model aims to focus on a specific wave process, which is consider as dominant and to minimize the influence of other wave phenomena.

This approach of dividing the complex phenomenon of wave penetration into simplified cases leads to the formulation of 2 sub-questions.

Sub question 2a. : Is it possible to accurately reproduce the correct amount of reflection in SWASH, using the porosity and stone values from the scale model?

Sub question 2b. : Is it possible to accurately reproduce the diffraction of wave energy into a harbor basin in SWASH?

Based on, the travelling time of the waves from a specific location to another it is possible to estimate the time interval during which the water level time series at the different wave gauges are influenced by a specific wave process (e.g reflection, diffraction). By doing so, it is possible to divide the measured and simulated time series in separate parts, in which one part consists of only incoming waves and another part consists of a combination of incoming, diffracted and reflected waves. By analysing these different parts of the time series separately, the impact of each individual physical process on the wave height changes can be identified.

Sub question 2a. : Is it possible to accurately reproduce the correct amount of reflection in SWASH, using the porosity and stone values from the scale model?

There are two different cases of reflection at a gravel slope. The first case is at the outer slopes outside the harbour. The second case is reflection at the end of the harbour basin. In the latter case the waves get reflected at the inner gravel slope and the concrete wall located behind it. The two cases are treated separately. It is worth mentioning that the inner and the outer slope consist from the same material and are constructed with the same technique in the physical scale model. Hence, the two slopes are considered to have the same properties for porosity and stone size diameter.

1.   Reflection off the outer gravel slope

As a first step a simplified 1D model representing only the reflection phenomenon off the outer slope is designed. Initially the porosity and stone size values used in the physical scale model are defined in the SWASH simulation. Consequently, the changes in reflection for runs with different porosity and stone size values are investigated. In all cases, the measured time series are used to evaluate the simplified SWASH model performance. For every SWASH case it is examined if the main trends due to reflection in the water level time series are reproduced. Finally, a conclusion about the optimal values for SWASH simulations for both parameters is drawn.

2. Reflection off the harbour end

A 1D SWASH model is created representing a cross section including the inner slope and the concrete wall behind it. The output locations are chosen to be the same as in the cross section line in the physical scale model. As a result, SWASH outputs can be compared to the measurements. A critical view is required as the measurements are also influenced by other processes, such as diffraction. The goal is to identify the basic trends due to reflection in front of the harbour end.

The changes of the water level time series due to reflection in the two aforementioned cases can be compared. Moreover, it is also possible to investigate if the impact of reflection is larger in the outer gravel slope case or in the case of the inner slope and the concrete wall at the harbour end.

Sub question 2b. : Is it possible to accurately reproduce the diffraction of wave energy into a harbor basin in SWASH?

The objective of this sub question is to study the diffraction phenomenon irrespective of reflections. For this purpose the following assumption applies: from the moment waves enter the harbour basin in until the arrival of the reflected wave from the harbour end, the waves measured by the wave gauges at the measurement locations are only influenced by the phenomenon of diffraction. This time interval is determined in the measurements and it is used to obtained information about the wave height changes due to diffraction. However, this time interval may not be long enough to come to conclusions regarding the impact of diffraction on the wave height.

In SWASH a 2D model that helps demonstrate the influence of diffraction on the wave field inside the basin is created. This means that the inner gravel slope and the concrete wall at the end of the harbour basin, on which waves get reflected, are removed. The model includes only the side concrete walls and the head walls at the harbour basin entrance. The simulated time in SWASH should be longer than the calculated interval in the measurements for which diffraction is the dominant process. If the duration of the time series part used to calculate the wave height influenced by diffraction is larger, the results are considered more reliable. Apart from the wave height calculation, the effects of diffraction in the water level can be determined qualitatively, by visual inspections of the time series inside the basin. Finally, the SWASH results can be compared to the measurements to evaluate SWASH performance in describing diffraction.

Question 3: Can a two-dimensional SWASH model representing the simplest layout of the physical scale model tests, describe the wave height changes (temporally and spatially) in the measured water level time series?

To answer the final research question, a 2D SWASH model representing the full simplest layout (layout 1), as constructed in the physical scale model is required. The goal is to model simultaneously in SWASH all wave processes taking place in the measured tests. The wave height changes in SWASH should be compared to the measured values quantitatively as well as qualitatively by observing the main water level trends. The performance of the simplified models focusing on a certain wave process at a time can be compared to the performance of the full model simulating all the prevailing wave processes. Conclusions about which processes play a dominant role in the final wave field can be drawn.

Figure 1.2 summarises the general approach followed in this thesis to address the research questions.
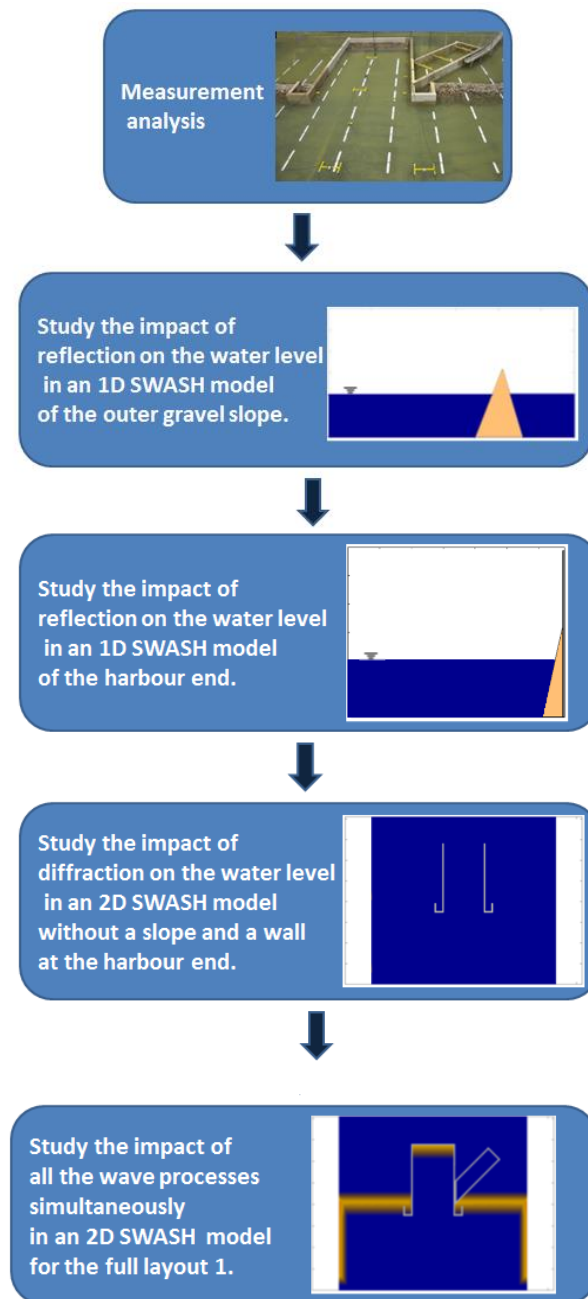
Figure 1.2 – Work flow diagram (source of the photo of Layout 1: Deltares).

Chapter 2 Literature Review

An overview of the background information necessary to address the complex phenomenon of wave penetration in ports is provided in this chapter. Firstly, the physical processes contributing to the formation of the wave field in ports are summarised in Section 2.1 Secondly, key information about the open benchmark dataset of port layouts provided by Deltares, part of which is studied in depth in this thesis, is presented in Section 2.2 . The characteristics of the aforementioned dataset subset studied in this thesis are deliberated in Section 2.3 . The previous work done using a part of the open benchmark data set is briefly discussed in Section 2.4 . Moreover, Section 2.5 deals with the comparison of the numerical wave models regarding the application of wave penetration. Finally, the role of scaling in a physical scale model experiment and the decision of working in prototype scale are explained in Section 2.6 .

2.1   Wave processes related to wave propagation in ports

The most important wave processes related to wave propagation in harbours are in presented in Table 2.1.These phenomena occur in the shallow area connected to the port, in the entrance channel and inside the port area are described. A brief description of the most important wave processes related to wave propagation in harbours is attempted in Appendix A. For a more complete and detailed explanation of the relevant phenomena the reader is referred to Holthuijsen (2007).

Table 2.1 - Governing processes in wave propagation in ports

1. Shoaling
2. Refraction
3. Reflection
4. Transmission
5. Diffraction
6. Wave breaking
7. Low frequency waves
8. Harbour oscillations
9. Dispersion
10. Non-linear wave-wave interactions

2.2   Overview of the full open benchmark dataset of schematic port layouts (Deltares, 2016)

To validate the ability of wave models to reproduce wave penetration, field measurement datasets are usually used. These datasets are often limited in duration and space, refer to present situations instead of future designs and they are unlikely to include extreme conditions. On the contrary, scale model tests provide higher measurement accuracy than field measurements and allow testing of specific and well defined conditions. However, the majority of scale model measurements are performed for commercial projects, they are usually confidential or they do not include all the necessary details for validation purposes.

Deltares proposed an alternative method to validate numerical wave penetration models by using a collection of open benchmark datasets (Van der Ven et al., 2018). There is a set of experiments performed in physical scale model basins that include a wide range of controlled wave conditions and several measurement points at strategic locations of the layout. The available datasets include test series of schematic port layouts. The dataset of this project (Deltares, 2016) is studied in detail in this

master thesis. The most important information about the experiments, which are relevant for this thesis, is summarised in this section.

The modelled port is fictitious and consists of a main basin, a closable side basin and an optional breakwater. The dataset obtained can be used to validate cases for different wave penetration software. The physical model is constructed in the extended directional wave basin of Deltares (Delta Basin), which has outer dimensions of 50x50m and a 40m wide wave maker. The tests are performed at scale 1:45 for three schematic layouts presented in Figure 2.1.
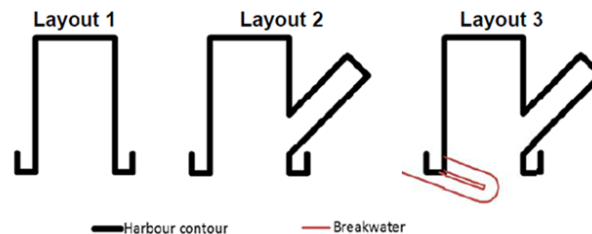
Figure 2.1 - The three layouts of the physical model considered for the dataset (Adapted from Van Mierlo, 2014).

In total, 56 tests are included in the dataset. To represent mild as well as severe wave conditions, a wide range of incoming wave heights (0.5m to 9.5m) and wave periods (4.5s to 17s) is incorporated. The wave conditions applied on each test are provided in Appendix B. The four different types of wave conditions applied in the tests are described below.

1. Monochromatic

   Monochromatic wave conditions are the simplest wave conditions for validation purposes.

2. Bi-chromatic

   In case of Bi-chromatic wave conditions low frequency waves are generated. Moreover, the primary waves can be chosen such that low frequency component induces a particular harbour basin oscillation (seiche).

3. Spectral

   The most realistic wave field is the application of a JONSWAP spectrum, using a distribution in frequency and in some cases a directional spreading.

4. Sea and Swell (applied only for Layout 3)

   Finally, a combination of a sea state from one direction with a swell from a different direction is also included in the dataset.

The incoming waves are imposed at the offshore boundary by a wave maker consisting of 100 individual paddles (Figure 2.2). The paddles can force spread waves into the basin. To avoid excess reflection against the side gravel slopes 3, paddles (1-5) and (96-100), located at the external sides of the wave maker, are not used in full power. Additionally, the wave maker is equipped with an ARC (Active Reflection Compensation) to prevent re-reflection by absorbing nearly all the wave energy hitting the wave maker.

For each test, the incoming wave field is saved in a txt file. This file contains the water surface elevation time series generated by the wave maker displacements in the physical model. For the analytical steps about deriving the files the reader in referred to Appendix B, Van Mierlo (2014). It is worth mentioning that the wave maker displacements signal is created before the start of the experiments. Hence, the signal is not influenced by the active reflection compensation imposed on the maker.

A top view of Layout 1, on which this thesis is focused, is provided in Figure 2.2. Moreover, the properties of the structures in Layout 1 shown in Figure 2.2 are presented in Table 2.2.
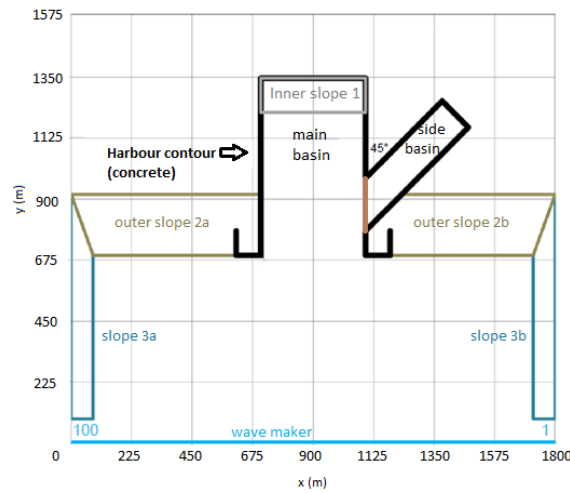
Figure 2.2- Top view of the physical scale mode in prototype scale (scale 1:45). This figure is a repetition of Figure 1.1.

Table 2.2 - The properties of the structures in Layout 1 in prototype scale.

	Quay wall	**Inner slope 1**	**Outer slopes 2a and 2b**	**Slopes 3a and 3b**
Material	Concrete block (Block length: 45m)	Gravel	Gravel	Gravel
Width [m]	0.3	2.8	5	1.8
Height [m]	1.3	0.7	0.7	0.9
Stone size [m]	-	0.675	0.675	0.675
Slope	Vertical	1:2	Front 1:4, Back 1:3	1:2

Measurement devices are placed in front and inside the port. A total of 16 wave height probes (accuracy 0.5%) were used to measure the wave heights and five directional wave height probes (1% accuracy) provided information about the wave heights and the x and y velocities. The measurement set up is presented in Figure 2.3 and the exact locations of the measurement devices are included in Appendix B.
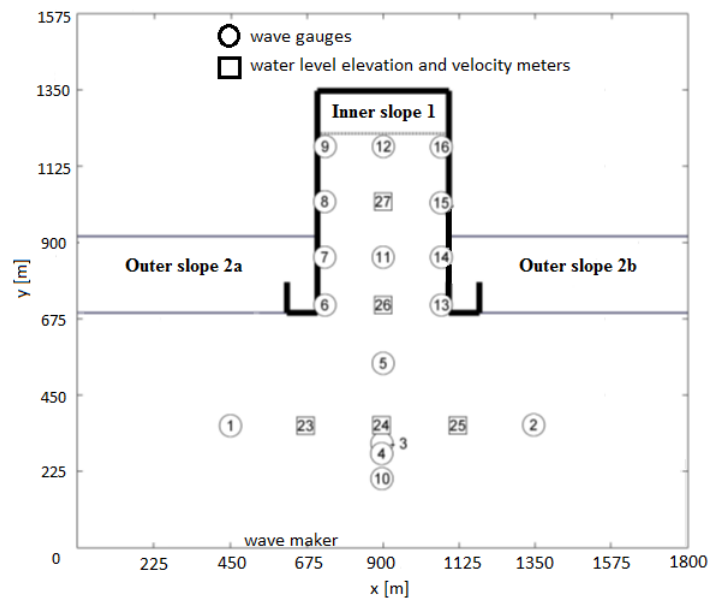
Figure 2.3-Measurement setup in the scale model (wave gauge 3 is located between wave gauges 4 and 24). Outer slopes 3a and 3b are not shown. (Adapted from Van Mierlo, 2014)

The devices are mainly placed close to the quay wall, where the ships are typically moored. The wave height in these locations and in the middle of the basin is required to identify the harbour oscillations. The incoming wave height is measured by 9 devices in front of the harbour area placed forming a cross: a line parallel to the wave direction (gauges 10, 4, 3, 24 and 5) and a line perpendicular to it, which is parallel to the wave maker (gauges 1, 23, 24, 25 and 2). Devices 17 to 20 (in total 6 wave gauges) are placed inside the side basin measuring waves for layout 2 and 3. For layout 1there is a wooden plate preventing waves from entering the side basin.

2.3   The characteristics of the selected dataset

The set of test selected to be studied in detail is presented in Table 2.3. All seven tests are performed for monochromatic wave conditions, in layout 1 (Figure 2.4) and the angle of incidence is 90°. Since layout 1 only has one main basin, it is considered the simplest layout to predict and understand the behaviour of waves in the basin.

Table 2.3 - The characteristics of the seven selected tests. This table is a repetition of Table 1.1, including three additional columns : the wave length L, the kd value and the wave steepness H/L.

Test	Wave conditions	Layout	H [m]	T [s]	Depth [m]	Angle [°]	L [m]	kd	H/L
T001	Monochromatic	1	0.99	7.51	19.8	90	80.48	1.55	0.001
T002	Monochromatic	1	1.44	10.00	19.8	90	120.74	1.03	0.012
T003	Monochromatic	1	2.39	16.97	19.8	90	225.59	0.55	0.011
T010	Monochromatic	1	2.97	5.03	19.8	90	39.38	3.16	0.075
T011	Monochromatic	1	3.02	8.99	19.8	90	104.71	1.19	0.029
T012	Monochromatic	1	2.75	15.03	19.8	90	197.05	0.63	0.014
T013	Monochromatic	1	1.94	4.49	19.8	90	31.52	3.95	0.061
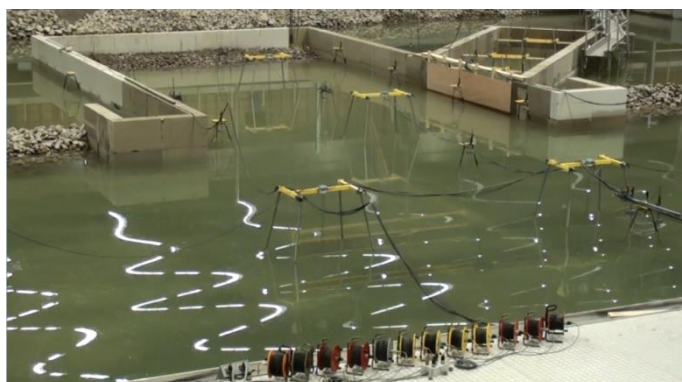
Figure 2.4 -Photograph of the physical scale model for layout 1. In the photograph is captured the start of test T001. (source: Deltares)

It would have been reasonable to study full spectrum cases as they represent better the wave field that enters in a port in reality. However, the purpose of this study is to find out if the numerical model is capable of simulating a simple monochromatic wave and if the outputs are in agreement with the theoretical expectations. Complex wave condition can be interpreted as a summation of individual monochromatic waves. Although it is easier to understand the physical behaviour of only one monochromatic wave it can be more difficult for the numerical model to describe it accurately. For the monochromatic case the numerical diffusion effect is stronger. Moreover, the wave height and the wave direction are constant in time and it is relatively easier to spot errors in the water level time

series. On the other hand, in a spectrum the wave height and the wave direction vary in time. It is possible that different errors in the simulation of individual waves might add up and the total final error of the water level time series is smaller.

To better understand the physics of each test some physical parameters are also included in Table 2.3: the wave length L, the kd value, the wave steepness H/L. The kd value is used as an estimate of the computational effort required for each test. A rule of thumb is that tests with higher kd value are more computationally demanding. Moreover, for higher kd values the non-linear effects become more important. For each test the kd value is determined by the maximum water depth, which in all the cases is 19.8m and by the wave period as it results from the wave maker motion. The wave steepness is an indicator of the wave breaking. If the wave steepness exceeds the value 0.07, then waves start to break.

There are several criteria to specify if the waves are in deep or shallow water. The basin criteria according to Bosboom and Stive (2011) are presented in Table 2.4. The kd values criterion is used to classify the waves of the seven tests in deep, intermediated or shallow water.

Table 2.4-Criteria for deep and shallow water waves with an error of the order of 1% (Bosboom and Stive, 2011).

Shallow water			Deep water		
d/L_0	d/L	kd	d/L_0	d/L	kd
< 0.015	<1/20(=0.05)	$<\pi/10$	>0.5	>0.5	$>\pi$

The seven selected tests can be divided in three groups with similar values of specific parameters. These parameters are the kd value, the wave length L and the wave steepness H/L. The first group consists from test T003 and T012 (Table 2.5). Both tests have a low kd value and represent intermediate water conditions. However, their kd values are close to the shallow water limit (kd< 0.314). Moreover, the two tests have the longest waves, as their wave length values are close or higher than 200m. The second group of tests consists of tests with average kd values from 1.03 to 1.55 (Table 2.6). These are tests T001, T002 and T011. Their wave conditions are classified in intermediate water. Furthermore, their wave length values vary from 80 to 120m. The last group of test are T010 and T013 with kd values higher than π (Table 2.7). Both tests represent deep water conditions. As the kd values are relatively high these test cases are considered computationally demanding. Finally it is worth mentioning that for test T010 the waves have already started breaking while in T013 the wave steepness value is close to the breaking limit.

Table 2.5 – The first group of tests for low kd values.

Test	L [m]	kd	Wave conditions	H/L	Wave breaking
T003	225.59	0.55	Intermediate/shallow water	0.011	-
T012	197.05	0.63	Intermediate/shallow water	0.014	-

Table 2.6 – The second group of tests for average kd values.

Test	L [m]	kd	Wave conditions	H/L	Wave breaking
T001	80.48	1.55	Intermediate water	0.001	-
T002	120.74	1.03	Intermediate water	0.012	-
T011	104.71	1.19	Intermediate water	0.029	-

Table 2.7 – The third group of tests for high kd values.

Test	L [m]	kd	Wave conditions	H/L	Wave breaking
T010	39.38	3.16	Deep/Intermediate water	0.075	yes
T013	31.52	3.95	Deep water	0.061	close to the breaking limit

2.4 Previous work using the benchmark test of schematic port layouts

A part of the dataset described in Section 2.2 has been processed by a number of master students at Delft University of Technology. The students selected certain tests to assess the value and accuracy of numerical wave penetration models. Van Mierlo (2014) used the mild slope model PHAROS (Deltares, 2013), the Boussinesq type model TRITON (Deltares, 2008) and the non-hydrostatic wave model SWASH (Zijlema, Stelling and Smit, 2011). Monteban (2016) worked with SWASH and also the Boussinesq type model Mike21 BW (DHI, 2007). The non-hydrostatic phase resolving setting of the wave model, XBEACH (Roelvink, 2010) was selected by Wong (2016) for wave penetration simulations. SWASH and XBEACH are both non-hydrostatic wave models. In this thesis for the category of non-hydrostatic models SWASH (version 3.14) is chosen to be studied in more depth. Therefore, the literature review is focused only on two of the aforementioned thesis: in the thesis of Van Mierlo and Monteban. The tests studied by Van Mierlo are T076, T079, T080, T081, T084 and T085. The tests studied by Monteban are T035 and T079. For details about the wave conditions of the aforementioned tests the reader is referred to Appendix B.

The main conclusions of the research of Van Mierlo and Monteban are in agreement: wave penetration can be modelled quite accurately for practical engineering purposes, whereas long waves and resonant modes are generally computed with less accuracy. Important remarks mentioned in these MSc reports include data analysis methods (e.g. spectral resolutions), reflection settings in the numerical models, numerical stability, the influence of layout inaccuracies in the physical scale model and averaging of computed wave heights within a circle around a measurement location. Consequently, further research is recommended on validating and improving numerical wave penetration models.

2.5 The wave models performance in simulating wave penetration in harbours

This section summarizes the work of two MSc students, F. Van Mierlo (2014) and D. Monteban (2016) about the performance or wave models regarding the application of wave penetration. The section starts with the criteria used to evaluate the models performance. The three wave models used by Van Mierlo are presented in Section 2.5.2 , while the two wave models examined by Monteban in Section 2.5.3 . The models are compared in terms of theoretical abilities and limitations as well as about the simulation outputs. Lastly, the abilities and the restrictions for the wave model studied in this thesis, SWASH, are discussed. A theoretical comparison of the available wave models and the selection of the most suitable models to simulate wave penetration is provided in Appendix C.

2.5.1 Evaluation criteria of wave penetration simulation by a wave model

To evaluate the ability of a wave model in simulating wave penetration the following factors should be taken into account:
- Ability to describe the most relevant processes related to wave penetration
- Model limitations, for example kd value, minimum water level
- Accurate predictions regarding:
  - primary waves (spectral waves)   - low frequency waves   - harbour oscillations
- Computational cost

Since this thesis focuses on monochromatic sea waves, the performance of the models regarding low frequency waves and harbour oscillations is not relevant and thus is not discussed in the following section. Information about the models abilities in simulating modelling of low frequency waves and harbour oscillations can be found in the thesis of F. Van Mierlo(2014) and D. Monteban(2016).

2.5.2   Comparison of PHAROS, TRITON and SWASH

In this thesis a subset of the dataset for schematic ports layouts (Deltares, 2014) is studied thoroughly. A selection of physical model tests from the same dataset is simulated with PHAROS (Deltares, 2013), TRITON (Deltares, 2008) and SWASH (Zijlema, Stelling and Smit, 2011) by F. Van Mierlo. Taking into account his findings a comparison of the three numerical models is attempted. The type of the three wave models ass wells as the organisation that developed them is presented in Table 2.8. In Table 2.9 selection of the most relevant processes modelled in the three models is shown.

Table 2.8 - Information about the three wave models used by Van Mierlo.

Wave model and Acronym	Model type	Developed by	Capable to model (among other)
PHAROS (Program for HARbour Oscillations)	Mild slope	Deltares	harbour oscillations and wind waves penetration, in harbours with complex geometries
TRITON (-)	Boussinesq	Deltares	wave propagation in nearshore regions and harbours
SWASH (Simulating WAves till Shore)	Non-hydrostatic	TU Delft	waves transformation from offshore towards the shore or into a harbour

Table 2.9-Overview of the wave processes related to wave penetration that can be modelled in PHAROS, TRITON and SWASH.(sources Deltares (2013) , Deltares (2008), The SWASH Team (2016).

Wave process	PHAROS	TRITON	SWASH
Shoaling	✓	✓	✓
Refraction	✓	✓	✓
Diffraction	✓	✓	✓
Dispersion	✓	✓	✓
Non-linear wave interactions	-	✓	✓
Wave breaking	✓	✓	✓
Wave run-up and run-down	-	✓	✓
Partial reflection	✓	✓	✓
Transmission	✓	-	✓
Wave-current interaction	✓	-	✓
Wave induces currents	-	✓	✓

According to Van Mierlo conclusions PHAROS is at least one order of magnitude faster than TRITON and SWASH. SWASH is more efficient than TRITON as the parallelisation option requced significantly the required computational effort. The following sketch provides some insight about the accuracy and the computational efficiency of the three wave models examined.
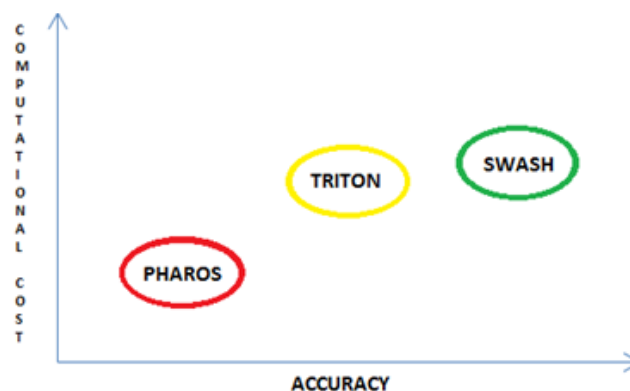
Figure 2.5-A comparison of the three wave models PHAROS, TRITON and SWASH regarding computational cost and accuracy.

Based on the simulations outcomes for the selected six tests, Van Mierlo concludes that TRITON and SWASH can model primary waves more accurate than PHAROS. The errors in wave height for the two models are on average less than 15%, for all examined wave conditions. It is mentioned that PHAROS overestimated the wave height in areas which sheltered from direct wave attack by breakwaters and are enclosed by highly reflective boundaries. The overestimation is highly related to the reflection coefficients that are set by the user. Moreover, numerical instabilities were observed in TRITON simulations for significant wave heights (up to a quarter of the water depth). Therefore, the wave height prediction by SWASH is more accurate for all the simulations, including tests with high significant wave height.

Taking into account the errors in wave penetration predictions some conclusions the performance of the three models can be drawn. PHAROS can be very useful for obtaining a quick estimate of wave heights in ports. Its main advantages are computational efficiency and robustness. Attention should be paid in determining the reflection coefficients. TRITON and SWASH should be preferred when accurate values are necessary. Due to the numerical instabilities in TRITON performance, SWASH can be considered more robust. Van Mierlo also mentions that for breakwaters in ports, the resulting computation time for SWASH is significantly lower.

2.5.3 Comparison of MIKE 21 BW and SWASH

The same dataset of schematic port layouts was used, among others, from D. Monteban to compare the performance of MIKE 21 BW (DHI, 2007) to SWASH (Zijlema, Stelling and Smit, 2011). The model type of the two wave models are presented in Table 2.10 In the following paragraphs some of his results and conclusions will be discussed.

Monteban compared the limitations of the two models. One of the main differences between SWASH and MIKE 21 BW is the application range of kd value, show in in Table 2.10. Using 2 vertical layers in SWASH can lead to more accurate results, but also to high computation cost. As in SWASH there is no limit about maximum frequency the model is able to resolve the total wave spectrum. Moreover, it can model sloping boundaries in full detail, as there is no minimum water depth restriction. On the contrary, MIKE 21 BW is a commercial model which provides customer support and can be used when the computational power is limited (i.e. the available computer has less than 10 processors).

Table 2.10 - Information about the two wave models used by Monteban. The application limits based on the kd value.

Wave model	Model type	Developed by	Suitable model based on the kd value		
			kd<0.5	0.5<kd<3.1	kd>3.1
MIKE 21 BW	Boussinesq	DHI	✓	✓	-
SWASH	Non-hydrostatic	TU Delft	✓ (using 1 vertical layer)	✓ (using 2 vertical layers)	✓ (using 2 or more vertical layers)

To avoid scaling effects Monteban started running his simulations at physical model scale, but the results for both models show numerical instabilities, especially in MIKE 21 BW. The main problems were a strange symmetrical pattern in front of the breakwater in SWASH and in MIKE 21 BW an unwanted resonant standing wave in the side basin. A possible explanation can be that the models work with double precision and for small scales rounding errors may be important. However, double precision results in output files with significantly larger size.

The rest of the analysis was performed in prototype scale. The accuracy of predicting primary waves (f >0.067 Hz) using prototype scale was considerably higher than for the simulations using physical model scale. For both numerical wave models the deviation from the measured primary waves is below ± 15%. The significant wave height was computed with mean average percentage errors 8% and 7.8% in SWASH and MIKE 21 BW respectively.

2.5.4   Selection of using SWASH

Taking into account the relatively good performance of SWASH in describing wave penetration as well as the recommendations of further investigating the wave height errors, it was decided to focus in this thesis on the wave model SWASH. This thesis can be considered as a continuation of the theses of F.Van Mierlo (2014) and D.Monteban (2016). While the previous theses aimed in examining the performance of SWASH in describing wave penetration in a harbour under various complex wave conditions, this thesis focuses more in understanding which of the wave processes influencing the total wave penetration can be modelled accurately by SWASH. Whereas, in the previous theses more complex port layouts and wave conditions were examined, in this thesis the simplest layout 1 and the simplest monochromatic wave conditions are elaborated. By doing so, the amount of the relevant wave processes is reduced and the wave penetration becomes less complex, making the identification of the differences between the SWASH outputs and the measurement more straightforward.

SWASH has an open source code which can freely be downloaded from http://SWASH.sourceforge.net. In previous theses version 3.14 is used. In this thesis the new version of the software package SWASH 4.01 is used. In the two SWASH versions the method of solving the shallow water equations remains the same. As the differences between the two versions are not fundamental, it can be claimed that the main performance of SWASH regarding wave propagation towards and inside the port is the same. Hence, it can be assumed that the main findings of the previous research also hold for the current version.

According to the previous theses, SWASH has been proven to can describe the propagation of primary waves with a good level of accuracy, as the errors are on average less than 15%.Based also on the theoretical comparison (Table 2.9), the most important processes related to wave penetration are included in SWASH. Moreover, it was mentioned that by using two vertical layers the model is considered robust and no numerical instabilities are expected. Furthermore, it should be kept in mind that SWASH is a computational demanding model. Nevertheless, the higher computational time is considered acceptable, as this thesis is carried out for academic purposes and the time restrictions are not so strict as in a commercial project.

2.6   Scaling

The physical scale model of port layouts is designed on model scale to be small enough to fit inside a laboratory. However, the dimensions of a port in reality are much larger, for example two orders of magnitude larger, than the physical scale model dimensions. A real port is described by prototype scale. To switch from model scale to prototype scale and vice versa, scaling laws are applied.

2.6.1   Scaling laws

In hydraulic experiments, the most commonly used similitude laws are Froude and Reynolds similarity. Reynolds similarity guarantees the correct scaling of inertia and viscous forces. The Froude scaling assumes that gravity is the governing force balancing the inertia forces. The schematic port layouts physical scale model was conducted based on Froude scaling. The most important scaling factors for Froude scaling are presented in Table 2.11.

Table 2.11-Froude scaling. Note that α is the scaling factor when a scale 1 : α is used, ρ_m is the density on model scale and ρ_f the density on full scale or prototype scale. (Monteban, 2016)

Physical parameters	Unit	Multiplication factor
Length	[m]	α
Volume	[m^3]	α^3
Structural mass	[kg]	$\alpha^3 * \rho_f / \rho_m$
Time	[s]	$\sqrt{\alpha}$
Frequency	[Hz]	$1/\sqrt{\alpha}$

2.6.2 Scale effects

Scale effects are observed when the employed scaling law does not correctly reproduce the physical conditions from prototype at model scale. For the schematic port layouts physical scale model Froude scaling is assumed as the correct scaling of gravity and inertia forces is important to model precisely wave propagation. Other processes, such as viscosity, elasticity and surface tension are considered to play a minor role and the fact that they are not scaled correctly is considered acceptable. However, this can lead to scale effects related to the physical processes of wave penetration, wave transmission, wave energy frictional dissipation and wave breaking dissipation.

To prevent significant scale effects on wave reflection, the physical model scale should be sufficiently large. It is logical that for a small scale, for example 1:100, the scale effects are becoming important and influence the examined application of wave penetration. On the contrary, constructing a physical model based on a large scale, i.e. 1:10, is relatively costly and time consuming. The selected scale for the schematic port layouts physical model is 1:45. This scale is considered large enough to consider the scale effects as insignificant. Moreover, it the resulting construction cost is acceptable. This scale is a good compromise and it is often used in this type of studies. For an analytical description of scaling laws and scale effects the reader is referred to Frostick et al., 2011.

2.6.3 Selection of prototype scale for the measurement analysis and SWASH simulations

In this thesis it is chosen to perform the measurement analysis and SWASH simulations in prototype scale. It is obvious that measured data and the numerical model data must be compared using the same scale. To be consisted in the whole report, the information about the open benchmark dataset is provided in prototype scale. Appendix B includes data about the harbour contour, the location of the wave gauges and the wave conditions for all 56 tests conducted in prototype scale.

The use of prototype scale is supported by three arguments. Firstly, it is desirable to demonstrate SWASH ability to model the wave phenomena related to wave penetration in real scale. After all, in common engineering practice numerical models, such as SWASH, are used to describe or predict wave penetrations for a real port design project. Secondly, as discussed in Section 2.6.2 scale effects are considered significantly small or not relevant for the purpose of this thesis. Finally, the full scale is chosen to avoid numerical instabilities, observed by Monteban (2016), when running the simulation in model scale for SWASH.

Chapter 3 Methodology of measurement processing

The formulated research questions aim to evaluate SWASH performance regarding wave penetration. For this purpose, the SWASH outputs should be compared to the physical scale model measurements, as they considered representing reality.

The main topics of interest of the formulated research questions are the ability of SWASH to simulate wave propagation, wave celerity and the effect of two dominant wave processes: reflection and diffraction. Hence, it is desirable to obtain knowledge about these topics from the measurements. The approach to analyse the measured data is amply illustrated in this chapter.

To begin with, the initial measurement processing required is briefly described in Section 3.1 . In Section 3.2 the equation for calculating the wave celerity according to the linear wave theory is provided. Furthermore, the approach used for calculating the wave celerity in the measurements is extensively clarified. In addition, the method of calculating the fully developed incoming wave height measured at the wave gauges is discussed. The wave gauges inside the harbour basin that are influenced by diffraction are treated separately from the wave gauges outside the basin. In Section 3.3 is presented a methodology about determining the time moments when wave get reflected and when they arrive at the measurement locations along the model centreline. Finally, in Section 3.4 the method of determining the steady state at all measurement locations is presented.

3.1   Preliminary measurement processing

For each of the seven selected experiments, the water level in time is measured at 27 locations. To obtain useful information from the data some initial preparations is done. The preliminary analysis of the measurements includes the following three steps.

Step 1: Removing the average
According to theory, the mean water level at each wave gauge represents the still water level and should be equal to zero. To achieve that the wave height meters are calibrated by setting the water surface at two different levels. Nevertheless, in a laboratory experiment the average water level is expected to deviate slightly from zero. This is also the case for the selected experiments. For water level measurements it is common practice to set the water level oscillating around zero. The average water level value is calculated separately at each wave gauge for each test. Then, the average water level values are subtracted from the time series of each wave gauge for the seven selected tests.

Step 2: Detrending
After removing the average, a linear trend is observed in the measurements. This trend can be attributed to the behaviour of the wave probes. The probe of each wave height meter device is constructed of two parallel stainless steel rods. The rods act like electrodes of an electric conduction meter (Deltares, 2016). As more and more waves are being measured the rods temperature is increased linearly. This explains the linear increase of the still water level in time. However, this linear trend does not represent the physical behaviour of the still water level which remains constants during the experiments as no water is added or removed by the basin. Therefore, the linear trend is also removed from the measured water level time series.

Step 3: Switching from model to prototype scale
After processing the measurements to oscillate around zero, the next step is to convert them into prototype scale. As discussed in Section 2.6 , it is chosen the measurement analysis and the SWASH simulations to be performed in prototype scale. The scale used in the open benchmark dataset of port

layouts is 1:45. Thus, the wave gauges measurements for the selected 7 tests are expressed in prototype scale by multiplying the water level values with 45 and the time values by $\sqrt{45}$ (for the multiplication factors see Table 2.11).

An example of the water level time series after the initial processing is shown in Figure 3.1.
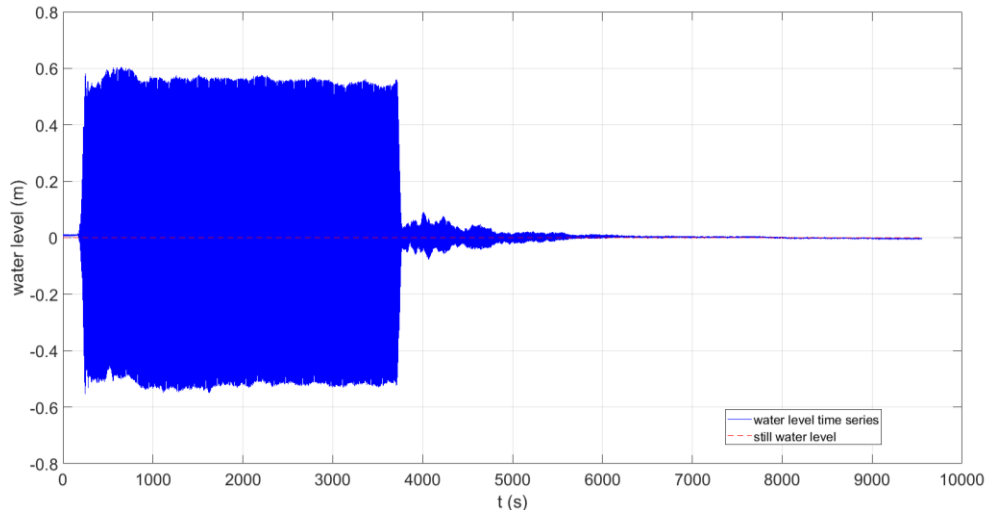
Figure 3.1 The final time series oscillating around the still water level (dashed red line) at Point 11 for T001.

In Figure 3.1 it is observed that the water level does not show a constant behaviour. Waves reach at Point 11 after the first 160 seconds. This time interval is describing the initial time when the wave gauges are recording, but the wave maker has not started operating and the time required from the waves to travel from the wave maker to the point. In this initial part from t=0s until t=160s, an offset of approximately +0.01m is observed, while the water level is expected to be equal to zero. This offset is considered small compared to the incoming wave height and thus can be ignored. As shown in Figure 3.2, the wave height is gradually increasing until approximately t=240 s. This is because a taper function is applied to the wave maker motion. By doing so, the waves enter the basing gradually and the occurrence of shock waves is prevented.
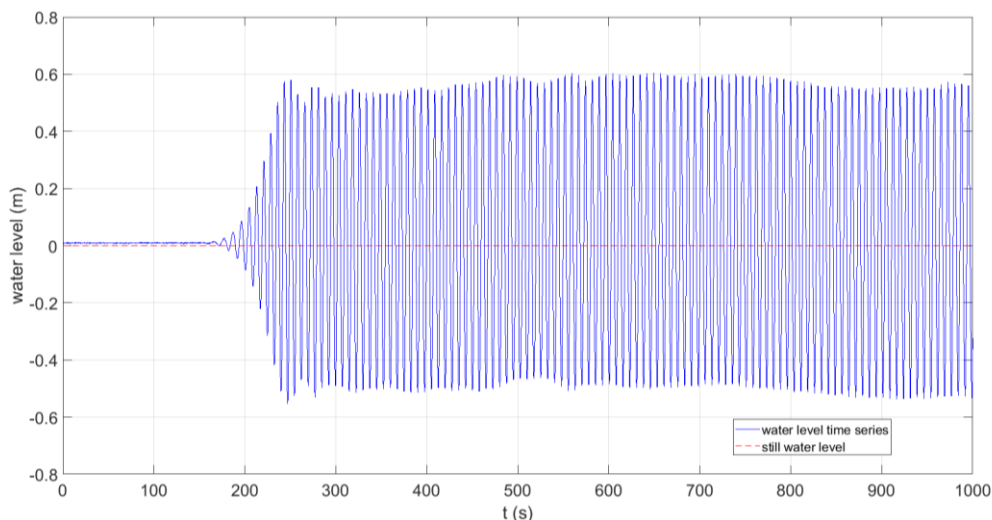
Figure 3.2-The initial part of the water level time series at wave gauge 11 for T001.

The wave height at Point 11 starts becoming lower at t=3750 s as shown in Figure 3.3. The wave height is reduced gradually as a taper function is applied again to the wave maker's motion. After stopping the wave maker's motion the water level is not reduced to zero and oscillating patterns still can be observed. Although new waves are not generated from the wave maker, the already existing

20

waves in the basin continue propagating and get reflected at the port walls and the gravel slopes. From Figure 3.1 it can be estimated that the water level drops to zero at t =6500 s approximately.

The reflections part at the end of the record shows that the waves get reflected at the harbour walls, the damping slopes and the wave maker. This behaviour verifies that only a part of the wave energy is absorbed by ARC (Active Reflection Compensation) applied at the wave maker. Moreover, at the damping material at inner slope slope1 and outer slopes 2 only a part of the wave energy is damped or transmitted. The rest of the energy is re-reflected towards the experiment area. The same holds for the concrete walls of the harbour. The only difference is that there is no wave energy transmission trough the walls.
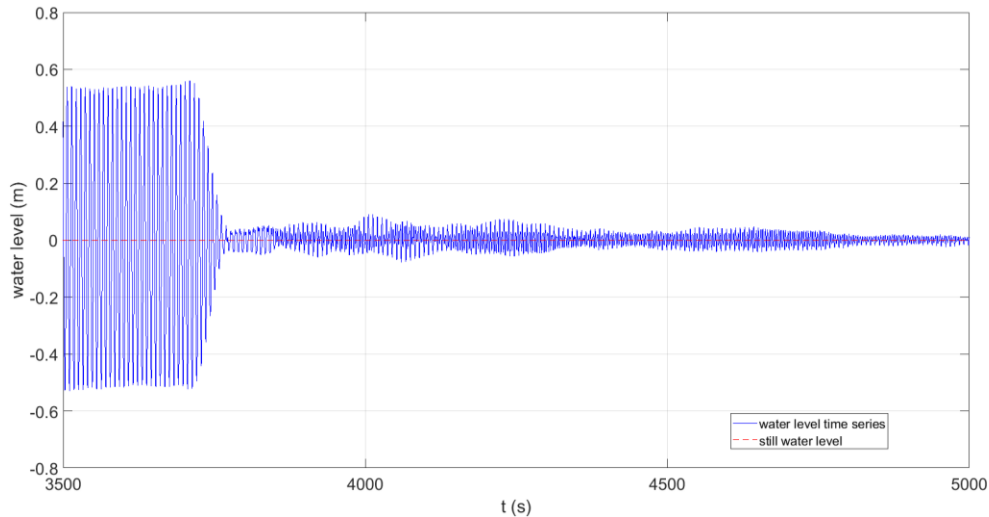
Figure 3.3-The water level time series at wave gauge 11 for T001 when the wave maker stops operating.

In all the remaining five tests, apart from T010, the water level time series are similar to the time series already presented in Figure 3.1.for wave gauge 11 and test T001: a time delay until the waves reach the location, a gradual increase, a constant part (Figure 3.4), a gradual decrease and a long period until the reflections in the basin become negligible and finally the water level drops to zero. However, in the time series for test T010 there is not a clear constant part as in the rest of the cases. This is shown in Figure 3.5. This behaviour can be explained by the high H/L ratio, equal to 0.075, for which wave breaking starts occurring.
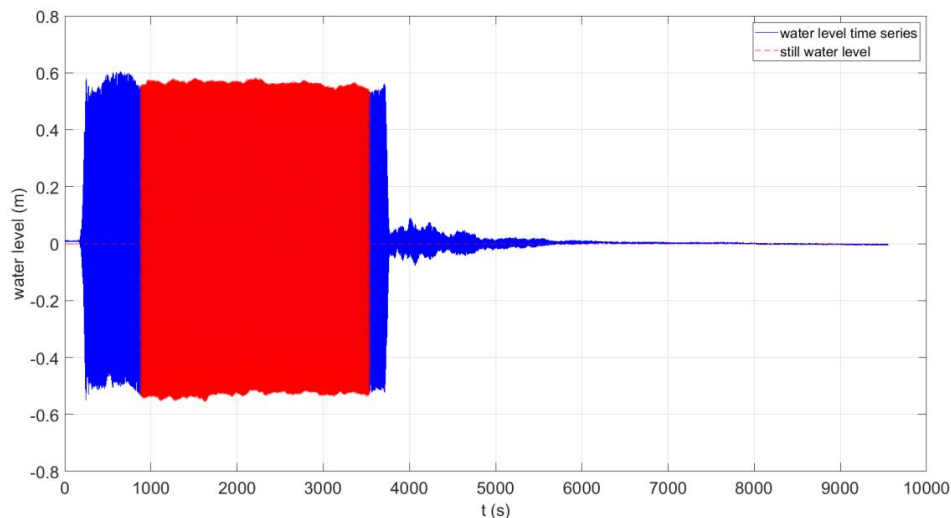
Figure 3.4- The measured water level time series at Point 11 for T001. This figure is a repetition of Figure 3.1 including a read area that represents the constant part when a temporal steady state is reached.

21
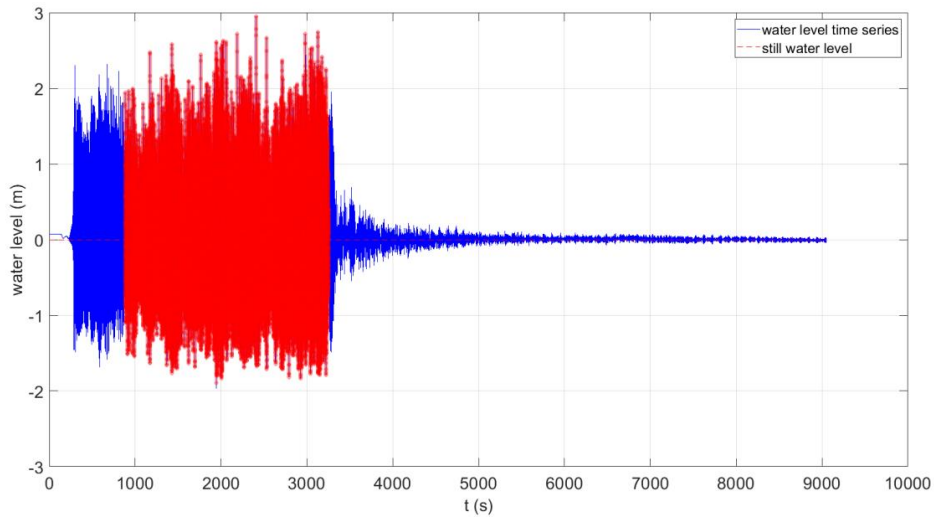
Figure 3.5-Water level time series at Point 11 for T010.

When the wave height in the measurements remains constant a temporal steady state is reached. During the constant part the changes in the wave height are not significant. It is selected to study the first 15 minutes (900 s) of the measurements. The first reason of this choice is that useful knowledge can be obtained by studying either the first few minutes of the constant part or the whole constant part. Secondly, the end part of multiple reflections is out of interest for engineering purposes. Finally, as SWASH is a computationally demanding model, this choice aims to reduce the time required for SWASH simulations.

3.2 Computation of the wave celerity in the measurements

3.2.1 Computation of the theoretical celerity according to the linear wave theory

The comparison of the wave celerity in the measurements and in SWASH is the objective of the first research question. This section focuses on determining the wave celerity in the measurements. It is assumed that the monochromatic waves in the examined experiments follow the linear theory. Instead of calculating explicitly the wave celerity, first the theoretical celerity determined by linear wave theory is calculated. Then it is examined if the theoretical wave celerity, calculated by using the wave parameters of each test, is in agreement with the measurement outputs. By doing so the measurements follow the linear wave theory and hence the measured and the theoretical celerity coincide.

The first step of the method is the calculation of the theoretical wave celerity according to Equation 3.1. It is worth mentioning that the radian frequency in the formula results from the linear dispersion relationship.

$$\mathbf{c} = \frac{\mathbf{L}}{\mathbf{T}} = \frac{\boldsymbol{\omega}}{\mathbf{k}} = \sqrt{\frac{\mathbf{g}}{\mathbf{k}} \ \mathbf{tanh\,kd}} = \frac{\mathbf{g\,T}}{2\boldsymbol{\pi}} \ \mathbf{tanh\,kd} \qquad\qquad (3.1)$$

where: c = the wave celerity (m/s)   L= the wave length (m)   T= the wave period (s)

       ω = radian frequency (rad/s)   k= the wave number (rad/m)   d= the water depth (m)

       g = gravitational acceleration (m/s^2)

3.2.2 An example of the calculation method of the wave celerity in the measurement: a wave flume case

In every test the wave period and the water depth remain constant during the test. Assuming linear waves, it holds that the wave celerity is considered constant during each test. The principles of motion with constant speed are used to confirm that the computed celerity matches with the measurements. The method is illustrated for a simple example in a wave flume.

In the wave flume depicted in Figure 3.6 there is a wave maker to the left, two wave gauges in the middle and an outflow in the centre. The distance between the two wave gauges is equal to x. The bottom of the flume is horizontal and the water depth is constant. A linear sinusoidal wave of constant wave height is generated by the wave m. The wave gauges are measuring the water level in time.
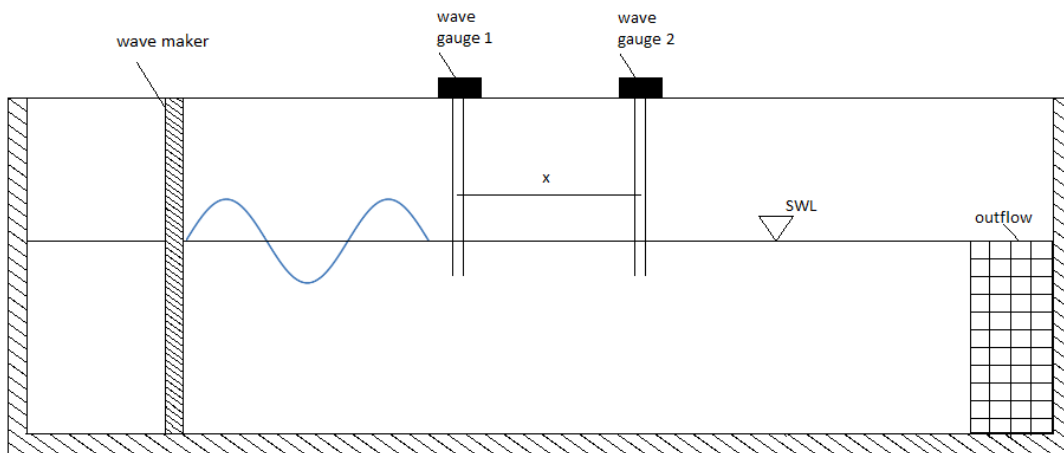
Figure 3.6-A simple example of monochromatic waves in a wave flume.
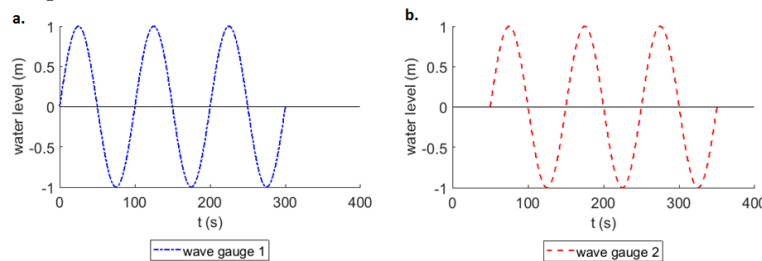
Figure 3.7-a. Water level in time at wave gauge 1, b. Water level in time at wave gauge 2.

As shown in Figure 3.7 a. and Figure 3.7 b., the time series in wave gauge 2 is exactly the same as in wave gauge 1 simply shifted in time. The wave pattern arrives at Point 2 with a delay of Δt. For a constant celerity, it holds: $\Delta t = \Delta x / c$. The wave celerity can be calculated by Equation 3.1. If the time series at wave gauge 2 is shifted Δt seconds earlier in time, it coincides with the time series at wave gauge 2. This can be illustrated by plotting the original time series at wave gauge 1 and the shifted time series at wave gauge 2 in the same graph. The following graph can only be created if measurements follow the linear theory and hence the measurements celerity is equal to the theoretical celerity. In a different case, the two time series will not match.
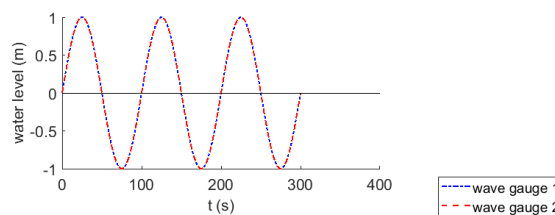
Figure 3.8-Original time series at wave gauge 1 and time series at wave gauge 2 shifted in time.

To sum up, the method requires:
- assuming that linear wave theory applies
- computing the theoretical wave celerity by Equation 3.1
- plotting the times series of different points in the same graph by shifting them in time
- checking if there is a good agreement between the time series
- confirming that the initially assumed celerity is correct or not

3.2.3 The calculation method of the wave celerity in the measurements

The same process described in the example of Section 3.2.2 can be applied for the wave gauges in the schematic port layout tests. For every point in model centre line (line AA') the wave pattern is the same as in the previous point shifted in time. Line AA' is parallel to the basin length and is located in the middle of the basin width dividing the basin in two symmetrical parts (Figure 3.9). Points 10, 4, 3, 5, 26, 11, 27 and 12 are considered to lie on this line.
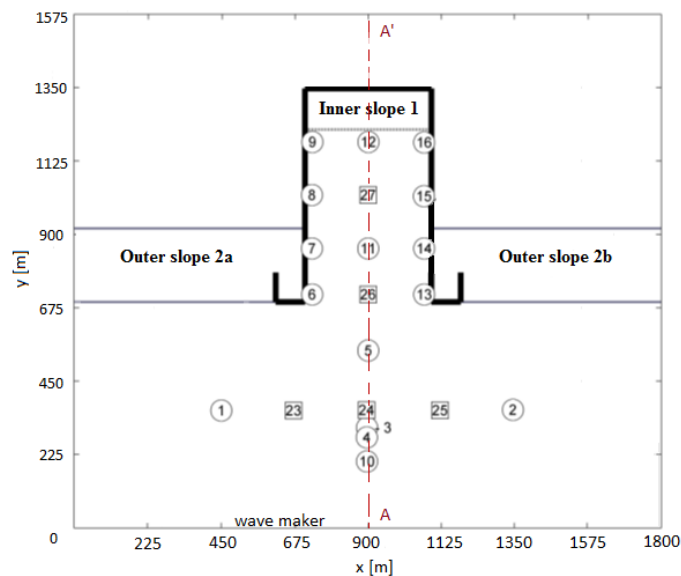
Figure 3.9-Model centre line (AA') is located in the middle of the basin in terms of width. Outer slopes 3a and 3b are not shown.

The times series of points on line AA' will be plotted in the same graph for Point 10 by shifting them in time. Instead of Point 10, another location to shift the time series would be the wave maker. However, there is no information when the wave maker started operating relative to the wave gauges records. A possible estimation about the starting moment of the wave maker would introduce additional errors in the process. Thus, the time series are not shifted at the wave maker location, but at wave gauge 10, which is located closest to the wave make. By doing so, all the records are shifted earlier in time.

The time for the wave to travel from Point 10 to every other point in line AA', $\Delta t_{10-Point}$, is calculated as follows:

$$\Delta t_{10-Point} = \frac{y_{Point} - y_{10}}{c} \tag{3.2}$$

where: $\Delta t_{10-Point}$: travelling time from Point 10 to another point.
c : the wave celerity for the selected test.
y_{Point} : y coordinate of the point in question.
y_{10} : y coordinate of Point 10.

The time series of wave gauges on line AA' can be plotted at the same graph for Point 10 by shifting each point time series earlier in time by $\Delta t_{10-Point}$. The water level time series are expected to be the same for the part of the measurements that is not influenced by reflections, as this phenomenon causes changes in the wave height. To apply the proposed methodology it is required to define when the wave records are starting to be influenced by reflections. The method used to determine the arrival of the reflected waves is explained in Section 3.2.5 .

The methodology of computing the wave celerity in the measurements is elaborated here for T001. The same approach is applied for the rest of the selected tests of which the results are presented in Chapter 4 . Initially, the theoretical wave celerity is calculated. According to Equation 3.1 the wave celerity is equal to $c_{T001} = 10.71$ m/s. The output after shifting the time series of each point at line AA' earlier in time by $\Delta t_{10-Point}$ is presented Figure 3.10.
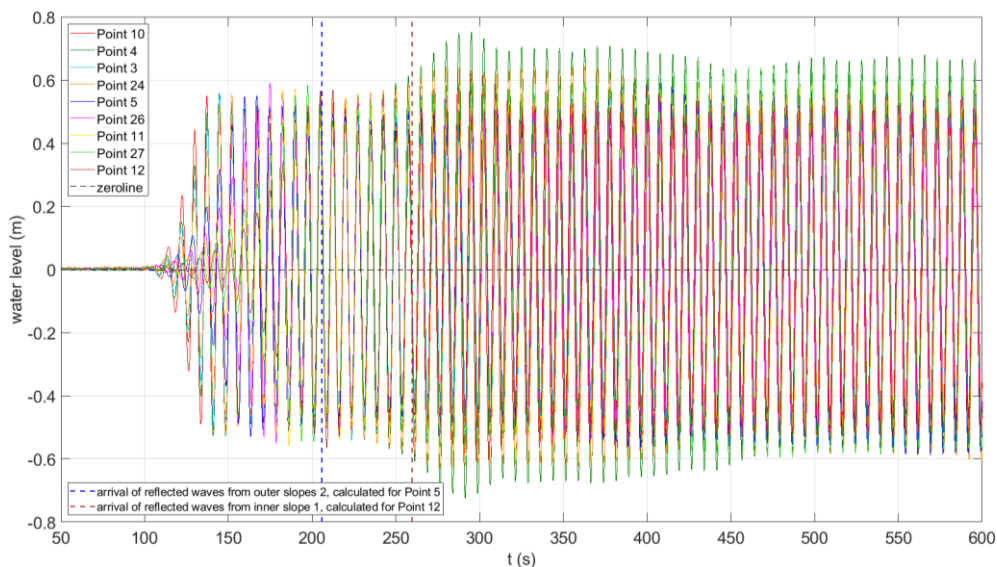
Figure 3.10-T001, measured water level time series of points on Line AA' shifted earlier in time to match with Point 10. The vertical blued dashed line represents the arrival of reflected waves from outer slopes 2 at Point 5. The vertical light brown dashed line represents the arrival of reflected waves from inner slope 1 at Point 12.

In Figure 3.10 the first vertical dashed line (colour: blue) represents the arrival of the reflected wave from outer slopes 2 at Point 5, which is located closer to this slope. The rest of the points outside the basin are expected to be influenced a few seconds later by the reflected waves from outer slopes 2. The second vertical dashed line (colour: light brown) represents the arrival of the reflected wave from inner slope 1 at Point 12, which is located closer to this slope. The rest of the wave records are expected to be influenced a few seconds later by the reflected waves from slope 1. Detailed information about how the reflection areas are defined is provided in Section 3.2.5 . A zoomed in part of Figure 3.10 is shown in Figure 3.11, in which it is easier to observe the changes after the reflections.

Focusing on the general trends of Figure 3.10 and Figure 3.11, it can be said that there is a good match with regard to the wave period. This does not hold for the first 170 s, but this behaviour is explained in Section 0. If the first 170 seconds are not taken into account, it is observed that the phase shift between the time series of the different points is negligible (170-250 s) or there is a small time shift (from 250 s until the end). The varying phase shift between the different points is detected after the arrival of reflected waves from inner slope 1. Moreover, the wave height values vary significantly mainly after the arrival of reflected waves. This holds especially in the case of reflections coming back from inner slope 1. This phenomenon is reasonable as in the wave record not only the incoming wave is measured, but also the reflected waves. However, after the first 500 seconds the wave height at the different points and the phase shift between the time series of the points are remaining constant. A temporal steady state has then been developed in the test.
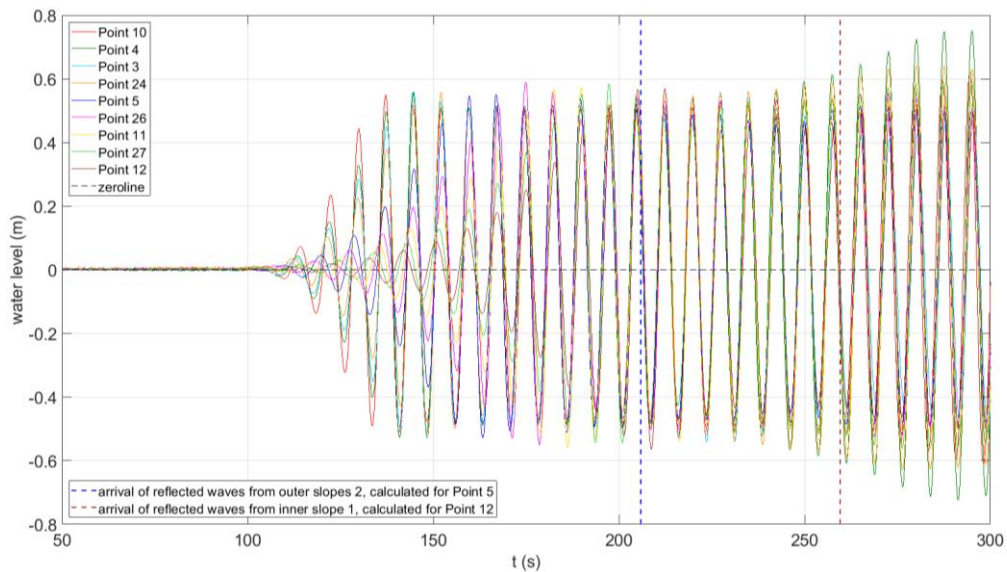
Figure 3.11- T001, measured water level time series of points on Line AA' shifted earlier in time at Point 10. This figure is a zoomed part of Figure 3.10.

The initial part of the wave records before the arrival of reflected waves, indicated by the vertical dashed blue line at t=210s (Figure 3.11) is not disturbed by reflections. Therefore, it is expected this initial part to be very similar to the wave signal generated by the wave machine. The result is expected to be similar to Figure 3.8 for the wave flume case. Despite the expectations the part of the measurements before any reflection is not exactly the same. There is a first part (t<170s) in which the time series do not match and a second part (170s<t<210s) where there is a good agreement between the records. In the first part the wave height is varying, while in the second part it remains constant in time.

It is important to realize that points outside the basin are influenced first by reflection at slope 2 and later by reflection at slope 1. However, the points inside the basin are not influenced by reflection at slope 2. This holds if perfect absorption of the ARC (Active Reflection Compensation) mode of the wave maker is assumed. The first reflected waves recorded at the gauges inside the harbour basin are coming from slope 1. The vertical dashed line representing reflected waves from slope 2 is not relevant for points inside the harbour. Hence, it is useful to examine separately the two groups of points: points inside the harbour basin and points outside the basin.

Figure 3.12 shows the time series of the points outside the harbour basin are plotted, while Figure 3.13 shows the time series of points inside the basin. In both group of points the same pattern is observed: There is a not a good match of the initial part of the time series, but in the second part the time series almost coincide. The good agreement in the second part indicates that for T001 the assumption of linear wave theory is correct and the wave celerity in the measurements is equal to the theoretical wave celerity.
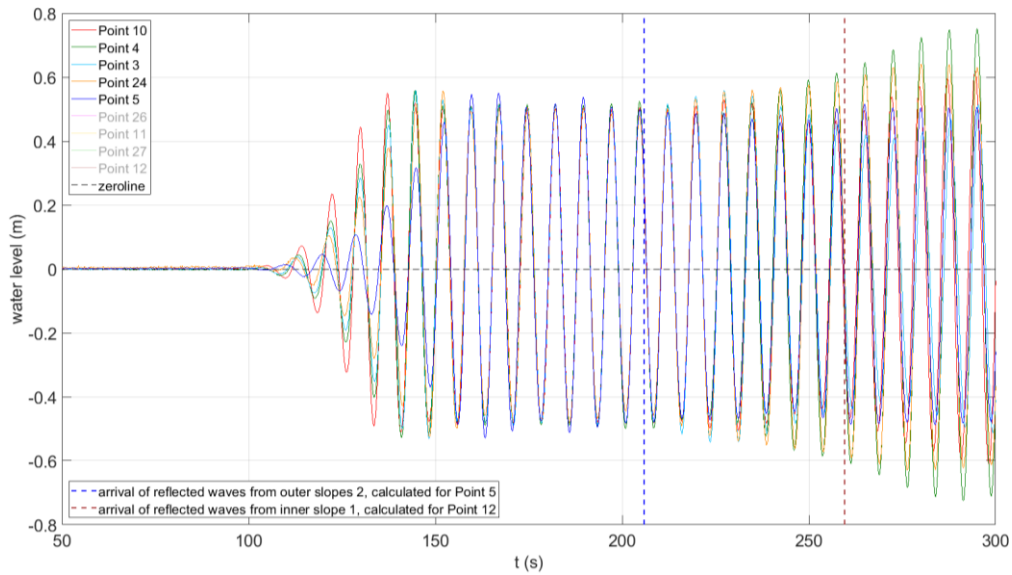
Figure 3.12- T001, measured water level time series of points outside the harbour basin on Line AA' shifted earlier in time at Point 10, before the arrival of the first reflected wave from outer slopes 2 (time axis: 50-210 s)
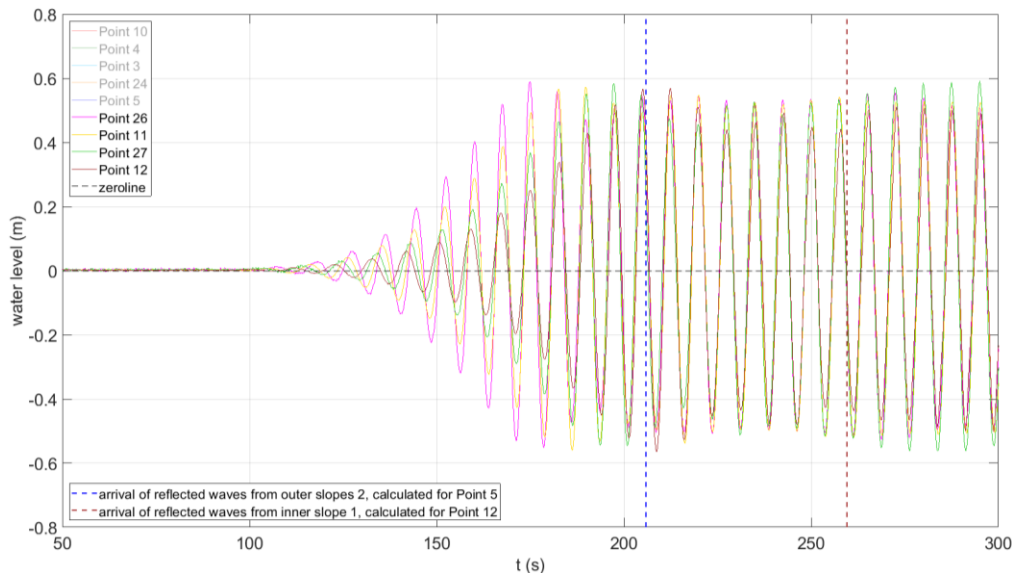
Figure 3.13- T001, measured water level time series of points inside the harbour basin on Line AA' shifted earlier in time at Point 10, before the arrival of the first reflected wave from outer slopes 2 (time axis: 50-270 s)

According to Figure 3.12, the wave height reaches a constant value at t=135s for Point 4, while this occurs at t=160s for Point 5. For all the points outside the basin the wave height remains constant until the arrival of reflected waves from outer slope 3 at t=210s (blue dashed line). Thus, the duration of the fully developed wave height part differs from a point to another. The comparison between the different points becomes easier, if the time interval of the constant fully developed incoming wave is longer. The constant wave height at the points outside the basin is determined in Section 3.2.5 .

As can be seen in Figure 3.13 for Point 26 the wave height remains constant from t=180s to t=210s and for point 12 from t=195s to t=210s. Although the reflected waves starting influencing the records after the dashed, light brown vertical line the waves are already influenced by diffraction as they enter the harbour basin. The waves enter the basin a few seconds before the vertical dashed blue line, so approximately at t=200s. The constant wave height at the points outside the basin is computed in Section 3.2.6 .

27

3.2.4   The behaviour of the taper function part

To interpret the behaviour of waves before the arrival of reflected waves, the wave signal generated by the wave machine must be studied. To avoid a shock wave in the basin a taper function has been applied at the start-up of the wave generator, so that the wave height increases gradually to finally reach a constant value (Figure 3.14). Based on this observation the undisturbed incoming wave time interval can be divided in the taper function part and the fully developed incoming part. It is worth mentioning that the zero of the wave maker motion is not related to the zero of the wave gauges records. It is not known when exactly the wave maker motion started relative to the wave records at the wave gauges. However, the travelling time of a wave with celerity c_{T001} from the wave machine to wave gauge 10 is 19s. Therefore, it is estimated that the wave machine started generating waves at approximately 80 s using the time reference of the wave records of the gauges.
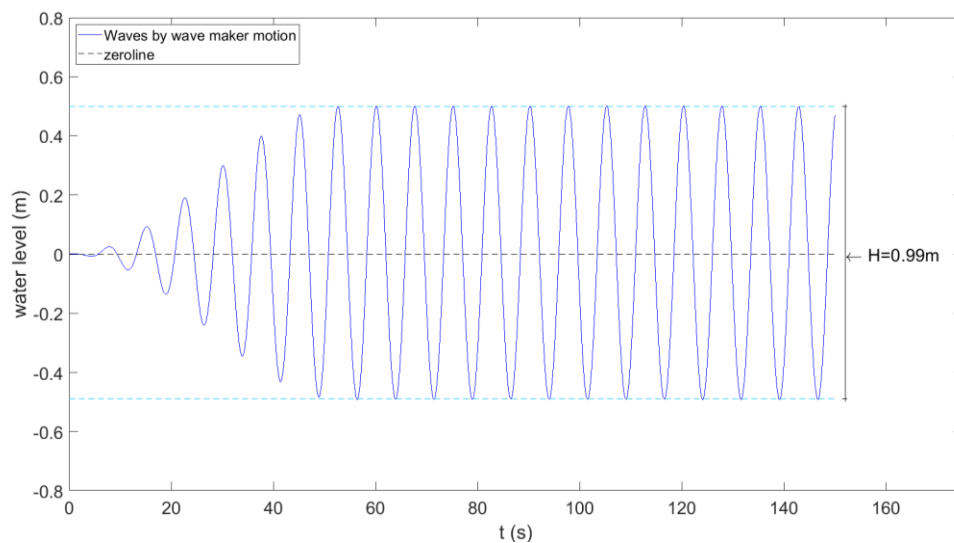
Figure 3.14 - Wave signal generated by wave maker motion for T001. The time axis differs from the wave records.

In Figure 3.11, Figure 3.12 and Figure 3.13 the same trends are observed. In every case it is clear that there is a good agreement in the constant fully developed incoming wave height. However, this is not the case for the taper function part. It is observed that the wave celerity in the taper function part is higher than celerity calculated based on the linear wave theory. Moreover, the wave amplitudes are becoming smaller as the distance from the wave generator increases. For an increasing distance between the examined point and the wave maker, the taper function part is becoming longer and the increase of the wave height until it reaches the full developed incoming wave height is slower. All in all, a non-linear behaviour is observed for the taper function part. It is important to realize that this non- linear behaviour of the taper function part results in the distorted wave signal that is different from the original signal of the wave maker and also changes from one point to another. This non-linear effect explains the non-good agreement in the first part of the plot with the time series shifted at Point 10 (Figure 3.11).

As it does not remain constant, the duration of the taper function has to be calculated at each point. The beginning of the taper function is defined as the start point (first zero down crossing) of the first wave with a wave height larger than 0.02m. This limit is set to exclude the part of the wave record before the arrival of the waves generated from the wave machine. Before the wave arrival, the wave gauges are measuring the still water level. As observed in Figure 3.11 the initial, still water level part is not a straight horizontal line, but there are small fluctuations occurring. These fluctuations can be described as white noise and are related to the accuracy of the measurement device and can be clearly seen in Figure 3.15, in which is the first 100s of Figure 3.11are shown. When the water level is fluctuating it may change sign from negative to positive or the opposite and this is defined as zero crossing. So waves defined in the still water level part are not realistic waves, but measurement errors. The accuracy of the wave gauges used in the experiments is 0.5% of the measuring range (Deltares,

2016). To avoid taking into account these non-realistic waves, the wave height threshold of 0.02m is set.
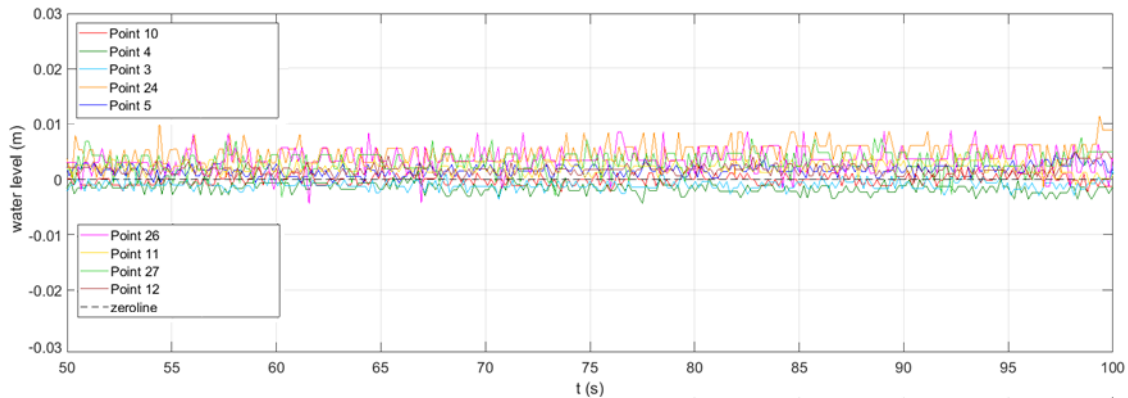
Figure 3.15-White noise observed during the first 100s of the time series of all points of line AA' shifted earlier in time to match with point 10. This figure is a zoomed part of Figure 3.10 and Figure 3.11.

The end of the taper function for Point 10 is the beginning of the first wave after which the wave height remains constant. The wave height is considered constant if the following condition holds:

$$\left|\frac{H_i - H_{i+1}}{H_i}\right| < 2\% \tag{3.3}$$

where: i is the sequence number of the wave in the record (i.e., i = 1 is the first wave in the record, i = 2 is the second wave, etc.).

In Figure 3.16 the start of the taper function for Point 10 is plotted by the vertical line 1a and the end of the taper function by the vertical line 1b. For this figure the limitation of Equation 3.3 can be explained. The wave height of the 6th wave the wave height of the 7th wave differ less than 2%. The same holds for the wave height of the 7th and the 8th wave, and so forth. The beginning of the 6th wave is the end of the taper function. For the rest of the wave gauges the end of the taper function is computed by adding the additional travelling time from 10 to the specific point $\Delta t_{10-Point}$ (Equation 3.2) to the ending time of taper function at Point 10. In the graphs of the time series of each point the start of the taper function is defined as "Moment 1a" and the end of the taper function as "Moment 1b".
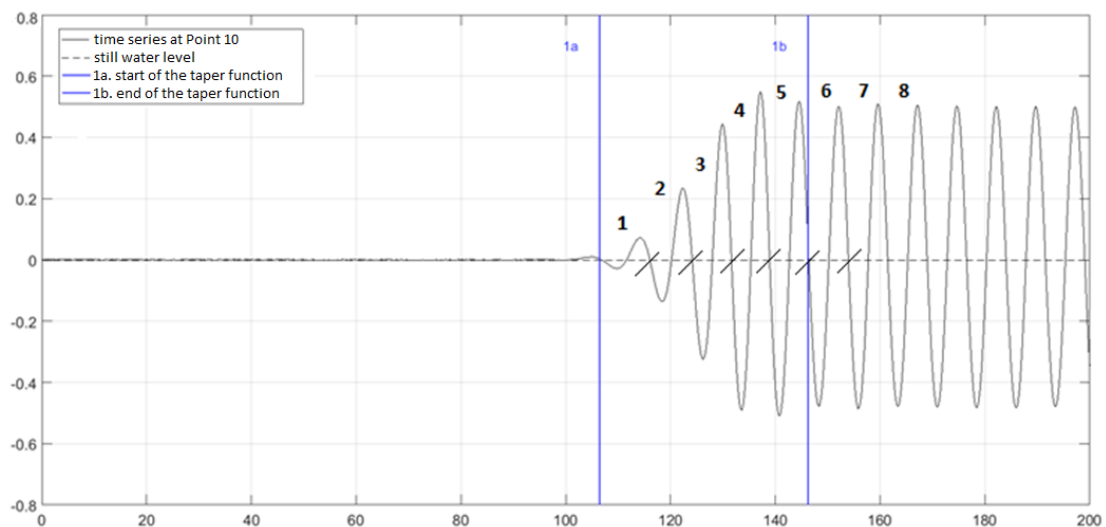
Figure 3.16 - Measured water level time series at Point 10 for T001. The taper function is defined between the two blue vertical lines. The individual waves are indicated by numbers (1, 2, 3, 4 and so froth).

It is essential to realize that the taper function part behaves in a different way than the fully incoming wave part. Therefore, the two parts should be examined separately. However, it should be kept in mind that the taper function is applied only at the first seconds of the wave machine signal and after the occurrence of the first few reflections all the energy of this part is damped. So after this moment the waves of the taper function part are not found in the basin while at the same time the wave machine produces only waves with the fully developed wave height.

The interaction between the taper function part of the incoming wave and the corresponding reflected wave, as well as the interaction between the fully developed incoming wave and the taper function reflected wave result in maximum wave height values which are not critical for the wave field in the harbour. On the contrary, the interaction between the fully developed incoming waves and the corresponding reflected waves are of major importance as their summation can lead to high wave height values. This case is critical for the safety of the vessels in the port. Consequently, this thesis is mainly focused on the fully developed waves.

3.2.5 Calculation of the measured fully developed incoming wave height at the wave gauges outside the basin

After the end of the taper function and before the arrival of reflected waves, the wave gauges outside the basin measure only the constant full developed incoming wave height. The wave height for the constant part should be equal to the incoming wave height coming from the wave machine. This constant part measured at all the gauges can be used to verify the good agreement in terms of wave height of the different time series plotted at the same graph.

It is expected that the time series of the different points, plotted in the same graph, do not coincide perfectly in terms of height, as in the simplified example of the two wave gauges in the flume. As the time series in the basin are measured data, errors are included in the records. The deviations in the incoming wave height, calculated based on the time series of the different points are expected to be within a limit of 2%.

By comparing the part of the different time series before the occurrence of reflections, information about the incoming wave height can be obtained. It is necessary to verify that the incoming wave height at the wave gauges locations is indeed equal to the wave height generated by the wave machine. For this purpose, the average wave height of the part of the time series measuring only the fully developed incoming wave is calculated at all the wave gauges. For a point outside the harbour basin this part starts at the end of the taper function (Moment 1b in Figure 3.16) until the moment of the arrival of the reflected wave from outer slopes 2. This latter moment is different for every wave gauge. The method for calculating this arrival moment (later refer as Moment 2a) is explained in Section 3.3.

In Table 3.1 the results for the five measurement locations outside the basin on model centre line AA' are presented. At each wave gauge, the mean wave height is calculated after determining the wave height of the individual waves is the wave record. The individual waves are identified by zero crossing analysis. This process is explained in detail in Appendix B. It is worth mentioning that for Point 5 there is no part of the wave record describing only the full developed incoming wave. This can be attributed to the fact that the distance from outer slopes 2 to Point 5 is small compared to the rest of the points. Therefore, the reflected waves come back within a short time and influence the wave record and no solely incoming part can be distinguished.

Table 3.1 includes also the standard deviation determined from the wave height values at the four wave gauges. Moreover, the last column of the table is the ratio $\overline{H}_{mean,measured}/H_{inc,wave\ maker}$, which can be used to compare the average incoming wave height measured at the wave gauges outside the harbour basin to the incoming wave height generated by the wave maker. The two values are considered to coincide if the ratio lies within the limits from 0.98 to 1.02.

Table 3.1-Mean, measured wave height values for the incoming wave part at wave gauges outside the basin for T001. For these gauges computation of average measured wave height and standard deviation. Comparison to the incoming wave height generated by the wave maker.

T001	
Point	$H_{mean,measured}$ (m)
10	0.99
4	1.00
3	1.01
24	1.01
5	-
$\overline{H}_{mean,measured} =$ 1.00 m	
Std. deviation = 0.01 m	
$H_{inc,wave\ maker} =$ 0.99 m	
$\overline{H}_{mean,measured}/H_{inc,wave\ maker}$ =1.012	

For T001, the ratio $\overline{H}_{mean,measured}/H_{inc,wave\ maker}$ is smaller 1.02 and thus it is considered acceptable. Moreover, the standard deviation of the wave height in the measurement locations is in the order of centimetre. It can be confirmed that the wave signal generated from the wave machine for T001 travels towards the harbour basin and it is represented in the signal before the occurrence of reflections at the wave gauges 10, 4, 3 and 24 located outside the basin. The results for the rest of the tests are discussed in Section 4.2 .

3.2.6   The influence of diffraction on the incoming wave height measured at the wave gauges inside the basin

After the end of the taper function (Moment 1b in Figure 3.16) and before the arrival of reflected waves, the wave gauges inside the basin measure only the constant full developed incoming wave height. However, this part is not expected to be equal to the incoming wave height generated by the wave maker, as it is influenced by diffraction. By comparing the part of the different time series before the occurrence of reflections, information about the influence of diffraction on the wave height can be obtained. For this purpose, the average wave height of the part of the time series undisturbed from reflections is calculated at all the wave gauges. This part starts at the end of the taper function until the moment of the arrival of the reflected wave from inner slope 1. This latter moment is different for every wave gauge. The method for calculating this arrival moment (later refer as moment 4a) is explained in Section 3.2.5

In Table 3.2 the results for the four measurement locations inside the basin on line AA' are presented. At each wave gauge, the mean wave height is calculated after determining the wave height of the individual waves is the wave record. The method of zero crossing analysis used for determining the wave height is illustrated in Appendix C. In Table 3.2 there is a wave height value only for two of the wave gauges. For Points 27 and 12, the reflected waves from inner slope 1 return within a short time and influence the wave record and no solely incoming part can be distinguished. These points are located close to the harbour end and the reflected waves arrive first at these locations.

Table 3.2 includes also the standard deviation determined from the wave height values at the two wave gauges. Moreover, the last column of the table is the ratio $H_{inc,wave\ maker}/\overline{H}_{mean,measured}$, which can be used to compare the incoming wave height generated by the wave maker to the average incoming wave height measured at the wave gauges outside the harbour basin.

Table 3.2- Mean, measured wave height values for the incoming wave part at wave gauges inside the basin for T001. For these gauges computation of average measured wave height and standard deviation. Comparison to the incoming wave height generated by the wave maker.

T001	
Point	$H_{mean,measured}$ (m)
26	0.93
11	0.81
27	-
12	-
$\overline{H}_{mean,measured} = 0.87$ m	
Std. deviation $= 0.21$ m	
$H_{inc,wave\ maker} = 0.99$ m	
$H_{inc,wave\ maker}/\overline{H}_{mean,measured} = 0.88$	

For T001, the ratio $\overline{H}_{mean,measured}/H_{inc,wave\ maker}$ is equal to 0.88. This value is much smaller than the limit 0.98 set for the points outside the basin. For this experiment, diffraction causes a reduction in the wave height. Moreover, the standard deviation of the wave height in the measurement locations is in the order of decimetre. So the spread is higher than for the points outside the basin. The results for the rest of the tests are discussed in Section 4.3 .

3.3 Estimation of the reflection locations and the return time of the resulting reflected waves at the measurement locations

In this chapter is described how to calculate the arrival of reflected waves at the wave gauges. The units in all the equations provided are meters for length, m/s for the celerity and s for time.

3.3.1 Estimation of the arrival time of the incoming waves at the wave gauges

As explained by the example of the wave flume in Section 3.2 the travelling time from one location or a point to another is calculated by assuming that the wave celerity is constant. It is important to define which measured point will be the starting point for the calculations to which the additional traveling time will be added to.

It can be claimed to use t=0s as a reference point for the calculations. However, t=0s is just the moment when all the wave gauges started recording simultaneously and it does not coincide with the start of the wave maker motion. Thus, t=0s is not related to the wave behaviour. An alternative option would be to use the first zero-down-crossing at Point 10 as reference point. Point 10 is the first point at which the incoming waves arrive, as it is the closest to the wave maker. The next step would be to check how this zero-crossing pattern travels in space and arrives at different gauges. Though, this is not possible due to the distortion of the wave pattern over taper function part of the incoming signal. The part of the wave signal which does not alter during travelling is the fully developed incoming wave part. Consequently, the chosen reference point for the calculations is the beginning of the fully developed incoming wave at wave gauge 10 (t_{10}). To sum up, using as a reference point t_{10} and assuming that the wave celerity c is constant , the arrival time of the fully developed incoming wave arrives at a specific point ($t_{f.d.H_{inc},Point}$) can be calculated. This is done by adding to the reference point the time for the wave to travel from Point 10 to the point examined (Equation 3.4).

$$t_{f.d.HH_{inc},Point} = t_{10} + \frac{y_{Point}-y_{10}}{c} \qquad (3.4)$$

3.3.2 The main reflection locations

By observing the water level time series as measured at all the wave gauges, it is obvious that the wave height is not constant in time. It is observed that there are parts during which the wave height is increasing, decreasing or remaining constant. An approach to explain these variations in the water level time series is presented in this chapter. As reflection is one of the main wave processes influencing the wave field, the approach is focussed on determining where the reflection occurs and when the reflected waves are coming back at the measurement locations. The time intervals during which the waves are only influenced by diffraction are also defined.

It is important to determine first the locations where reflection occurs. These locations, presented in Figure 3.17, are the following:

1. Outer slopes 2a and 2b and harbour head walls (at line y=693m)
2. Inner slope 1(y=1300m)
3. Wave maker
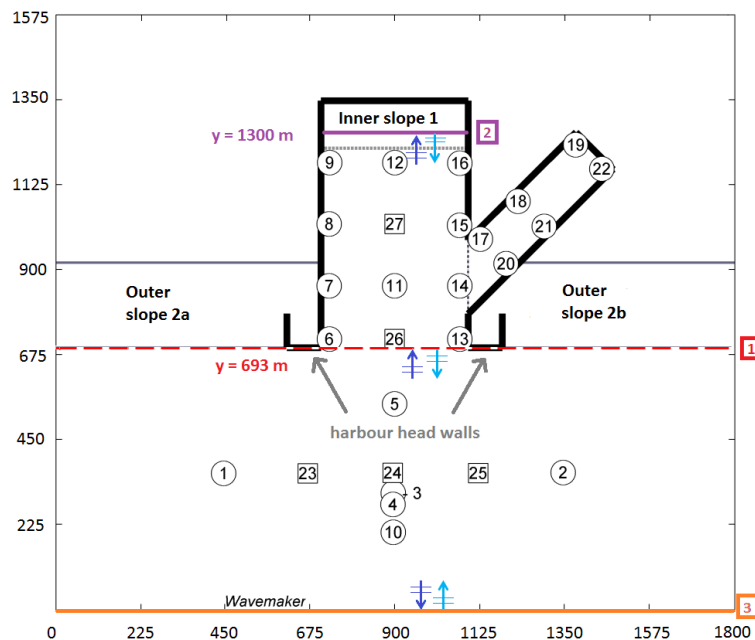
Figure 3.17-The three most important locations where reflection occurs : 1. Outer slopes 2a and 2b and harbour head walls, 2.Inner slope 1, 3.Wave maker. Axes units: m. In the picture outer slopes 3a and 3b are not shown.

As explained in Section 2.2 the paddles of the wave maker located in front of outer slopes 3a and 3b (Figure 2.2) are not functioning in full power. As discussed also in Section 1.3, the influence of reflection off slopes 3a and 3b is considered to be minor and therefore the two slopes are not included in the reflection study in the following paragraphs.

3.3.3 The first reflection at the outer slopes 2 and the harbour head walls

The first location where the reflection occurs is the outer slopes 2a and 2b and tips of the concrete quay walls of the harbour. For simplification it is considered that the reflection occurs at the horizontal line at the y= 693 m which coincides with the line of the quay wall and the bottom line of slope 2. It is assumed that the waves hit the structures on this line and return. In Figure 3.18 the incoming wave lines and the reflected wave lines sketched are representing the crests of the waves. The theoretical reflection line is interrupted by the harbour entrance in which no reflection occurs. So, as the waves return, there is a lack of energy in front of the harbour basin. As sketched in Figure 3.18 the reflected waves will undergo diffraction. However, in the selected approach the curved lines

caused by diffraction are simplified by straight lines. As the goal is to calculate when the reflected waves will come back the use of straight lines is in favour of safety, as the waves arrive relatively earlier if the curvature of the line is ignored. Moreover, the time difference between the arrival of the curved line and the straight line will be small and not significant based on the accuracy achieved while examining the phenomenon. It should be kept in mind that this is a simplified approach as in reality the reflection over the cross section of the porous slope. Furthermore, it has to be clarified that for simplicity the reflection occurring at line y= 693 m is most of the times referred as reflection at outer slopes 2.
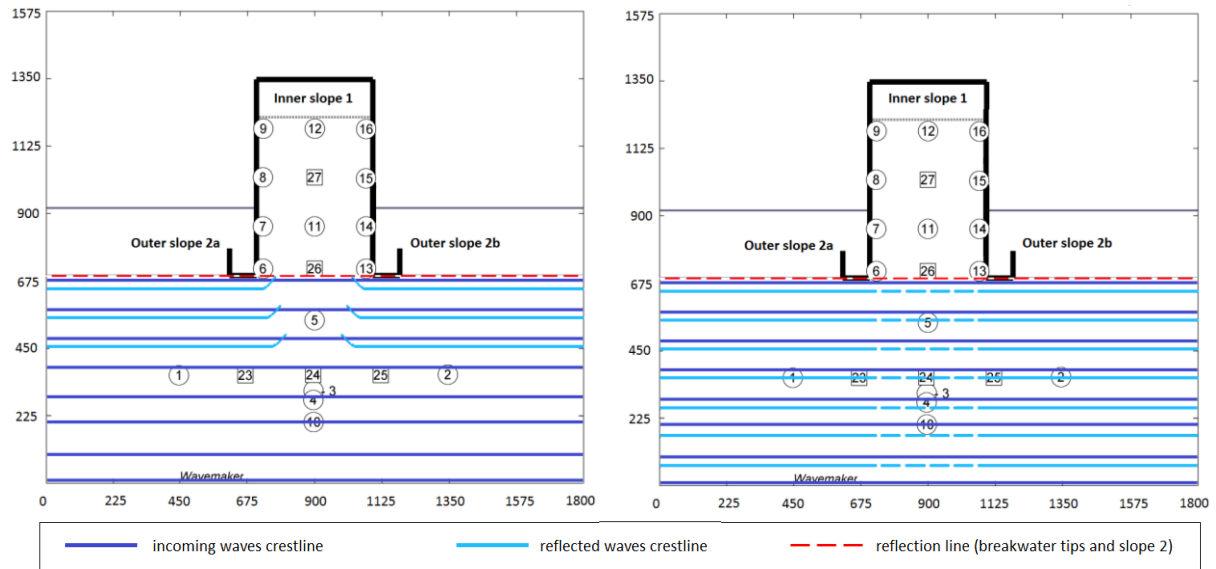
Figure 3.18 The reflected waves undergoe diffraction (left panel). The reflected wave crestlines are simplified to straight lines (right panel). Axes units: m.

For this reflection case the time for a wave to travel from the wave gauge hit outer slopes 2 and return at the gauge is calculated. The arrival of the reflected wave at a specific wave gauge occurs at time $t_{r,outer,1st}$ is calculated by Equation 3.5. In the graphs of the time series of each point this moment is defined as "Moment 2". The reflected waves from outer slopes 2 influence directly only the points outside of the basin. Thus, Equation 3.5 is applied for points with y coordinate smaller than 693m, so for wave gauges located outside the harbour basin. It should be noticed that in the following equation the term $y_{slope\ 2}$ represents the reflection line at 693m, so it holds $y_{slope\ 2} = 693$m.

$$t_{r,outer,1st,Point} = t_{f.d.H_{inc},Point} + 2 * \frac{y_{slope\ 2} - y_{Point}}{c} \tag{3.5}$$

3.3.4 The first reflection at the inner slope 1

The second location where reflection occurs is inner slope 1 at the closed end of the main harbour basin. It is considered that the reflection occurs at a fictitious wall located at the cross section line between the still water level (SWL) and the inner slope 1. A cross section parallel to the basin length (Figure 3.19) provides more insight about the imaginary wall simplification. The grey wall located close to x=0m is the real concrete wall at the closed end of the basin. The light brown slope depicts the rubble mound slope. The light blue wall is the fictitious wall on which it is assumed that the reflection takes place. The fictitious wall is located at 1300m.

34
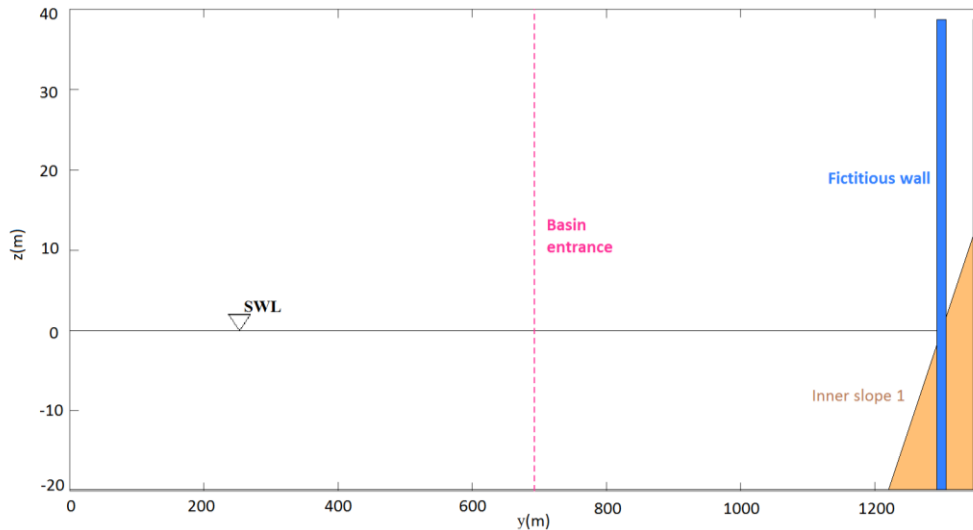
Figure 3.19 Cross section of the main basin including the fictitious wall at which reflection is assumed to take place.

It is important to point out that the incoming wave entering the basin and also the reflected wave coming out of the basin are influenced by diffraction. However, for estimating the moments when the wave reflects at inner slope 1 and returns at the wave gauges the diffraction phenomena are being ignored here. Again, the curved lines are simplified and replaced by straight lines. This simplification is shown in the right sketches of Figure 3.20 and Figure 3.21.
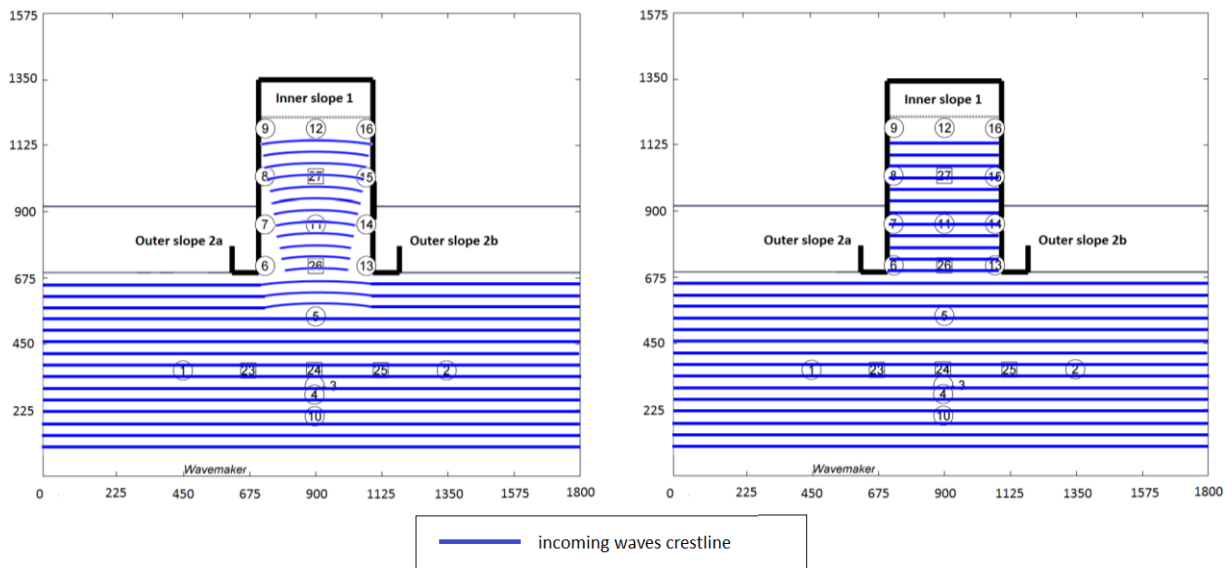
Figure 3.20 – Sketches of the incoming waves entering the harbour. In the harbour, waves are influenced by diffraction (left panel). In the simplified approach the crest lines are straight lines (right panel). Axes units: m.
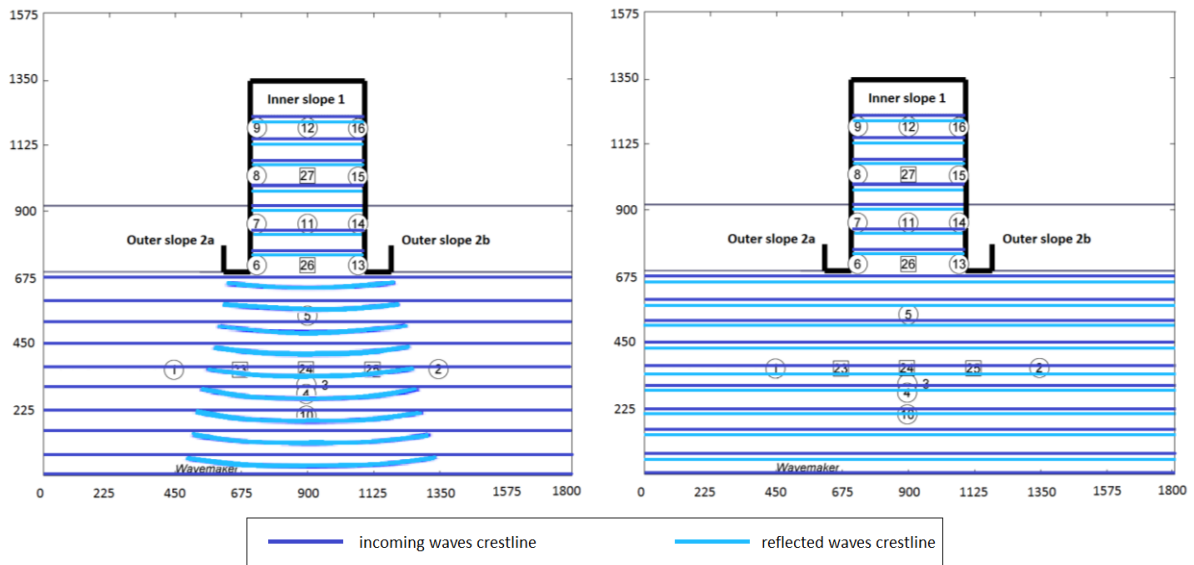
Figure 3.21 Sketches of the simplified incoming wave height entering the basin and the reflected wave travelling out of the basin. Outside the harbour basin the reflected waves will be influenced by diffraction (left panel). In the simplified approach the crest lines are straight lines (right panel).Axes units: m.

For this reflection case the time for the wave to travel from a specific point to the slope, reflect and then return at the point is calculated. The arrival of the reflected wave at a specific point occurs at time $t_{r,inner,1st,point}$ is calculated by Equation 3.6. In the graphs of the time series of each point this moment is defined as "Moment 4". The term $y_{Slope\ 1}$ represents the fictitious wall, so it holds $y_{slope\ 2} = 1300m$.

$$t_{r,inner,1st,point} = t_{f.d.H_{inc},Point} + 2 * \frac{y_{Slope\ 1} - y_{Point}}{c} \tag{3.6}$$

As shown in Figure 3.20, the incoming waves experience diffraction after entering the harbour basin. For the reflection calculation simplifications are made and the influence of diffraction is not taken into account. However, the wave gauges inside the basin are measuring the waves undertaking diffraction. The waves inside the basin are only influenced by diffraction before the occurrence of reflection at inner slope 1. To obtain information about the diffraction phenomenon only the wave record from the arrival of the fully developed incoming wave until the arrival of the reflected wave at inner slope 1 should be studied.

3.3.5   The second reflections at the wave maker and the third reflections at the slopes

The last location examined where reflection occurs is the wave machine. When the incoming waves hit either inner slope 1 or outer slope 2, a part of the energy is damped and the rest of the energy returns back through the reflected waves. The reflected waves travel towards the wave machine. The wave machine is set in an ARC mode (Active Reflection Compensation mode), absorbing partially the reflected wave energy. When the waves hit the wave board nearly all their energy is absorbed. However, the remaining energy travels again in forms of waves towards the basin. It is the second time that the wave gets reflected. In every reflection wave energy is lost. In other words, when the waves hit either inner slope 1 or outer slope 2, the wave amplitude of the reflected wave is lower than the incoming one. When the reflected wave hits the wave board, the reflected wave amplitude is further decreased.

Both reflected waves at inner slope 1 and outer slope 2will travel towards the wave maker reflect and come back. Both secondary reflected waves can influence all the wave gauges. This case differs from the reflected wave caused by the first reflection at outer slope 2, because then the points inside the main harbour basin are not influenced by the reflected wave.
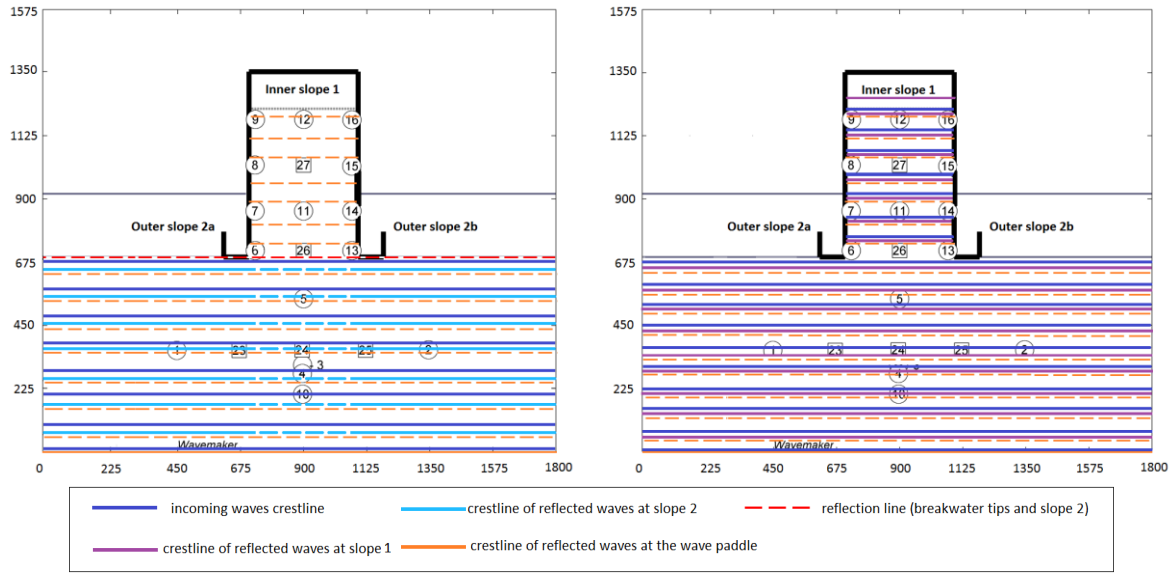
Figure 3.22 Left panel: A simplified approach as the reflected waves at outer slopes 2 hit the wave maker resulting into new reflected waves. Right panel: A simplified approach as the reflected waves at inner slope 1 hit the wave maker resulting into new reflected waves. Axes units: m.

The arrival of the new reflected wave at the wave maker resulting from the reflected wave at outer slopes 2 occurs at time $t_{maker,outer,2nd}$. This moment is calculated by Equation 3.7 for points outside the harbour basin and by Equation 3.8 for points inside the basin. In the graphs of the time series of each point this moment is defined as "Moment 3".

$$t_{maker,outer,2nd} = t_{f.d.H_{inc},Point} + 2 * \frac{y_{Slope\,2} - y_{Point}}{c} + 2 * \frac{y_{Point} - y_{maker}}{c} \tag{3.7}$$

$$t_{maker,outer,2nd} = t_{f.d.H_{inc},Point} + 2 * \frac{y_{Slope\,2} - y_{10}}{c} + 2 * \frac{y_{10} - y_{maker}}{c} + \frac{y_{Point} - y_{10}}{c} \tag{3.8}$$

The new reflected wave is travelling towards outer slopes 2 and gets again reflected. This is the 3rd reflection this wave experiences. It is calculated by Equation 3.9. In the graphs of the time series of each point this moment is defined as "Moment 5". The reflected waves from outer slopes 2 influence directly only the points outside of the basin. Thus, Equation 3.9 is applied for points with y coordinate smaller than 693m.

$$t_{r,outer,3rd} = t_{f.d.H_{inc},Point} + 4 * \frac{y_{Slope\,2} - y_{Point}}{c} + 2 * \frac{y_{Point} - y_{maker}}{c} \tag{3.9}$$

After getting reflected at outer slopes 2 and later at the wave maker the wave travels towards inner slope 1 and gets reflected for third time. The arrival of the reflected wave at inner slope 1 moment is defined as "Moment 6" and influences only the points inside the basin. The exact time is calculated by the following equation.

$$t_{r,inner,2nd} = t_{f.d.H_{inc},Point} + 2 \frac{y_{Slope\,2} - y_{10}}{c} + 2 \frac{y_{10} - y_{maker}}{c} + 2 \frac{y_{Slope\,1} - y_{Point}}{c} \tag{3.10}$$

The arrival of the new reflected wave at the wave maker resulting from the reflected wave at inner slope 1 occurs at time $t_{maker,inner,3rd}$ is calculated by Equation 3.11. In the graphs of the time series of each point this moment is defined as "Moment 7".

$$t_{maker,inner,3rd} = t_{f.d.H_{inc},Point} + 2 * \frac{y_{Slope\ 1} - y_{Point}}{c} + 2 * \frac{y_{Point} - y_{maker}}{c} \qquad (3.11)$$

3.3.6 The graph with the arrival moments of reflected waves

The graph created for all the wave gauges measuring for experiment T001 includes seven vertical lines representing the seven characteristic moments in time (picture A in Figure 3.23)

All the aforementioned calculations for the reflected waves are executed for the fully developed incoming wave. At every point the taper function part arrives before the fully developed wave. This holds for any examined location at which reflection occurs. To calculate the moment when the reflected taper function part comes back in every case the taper function duration at the specific point is extracted from the moment when the reflected fully developed incoming wave arrives. The moments 3 to 7 discussed previously take the suffix b which represents the arrival of the beginning of the fully developed incoming wave part. The arrival of the beginning of the taper function part of the incoming wave is represented by the suffix a. The calculation method is illustrated clearly by the following equation.

$$t_{a,r,outer,Point} = t_{b,r,outer,Point} - taper\ function_{Point} \qquad (3.12)$$

Picture B in in Figure 3.23 is the final plot with all the characteristic moments in time.
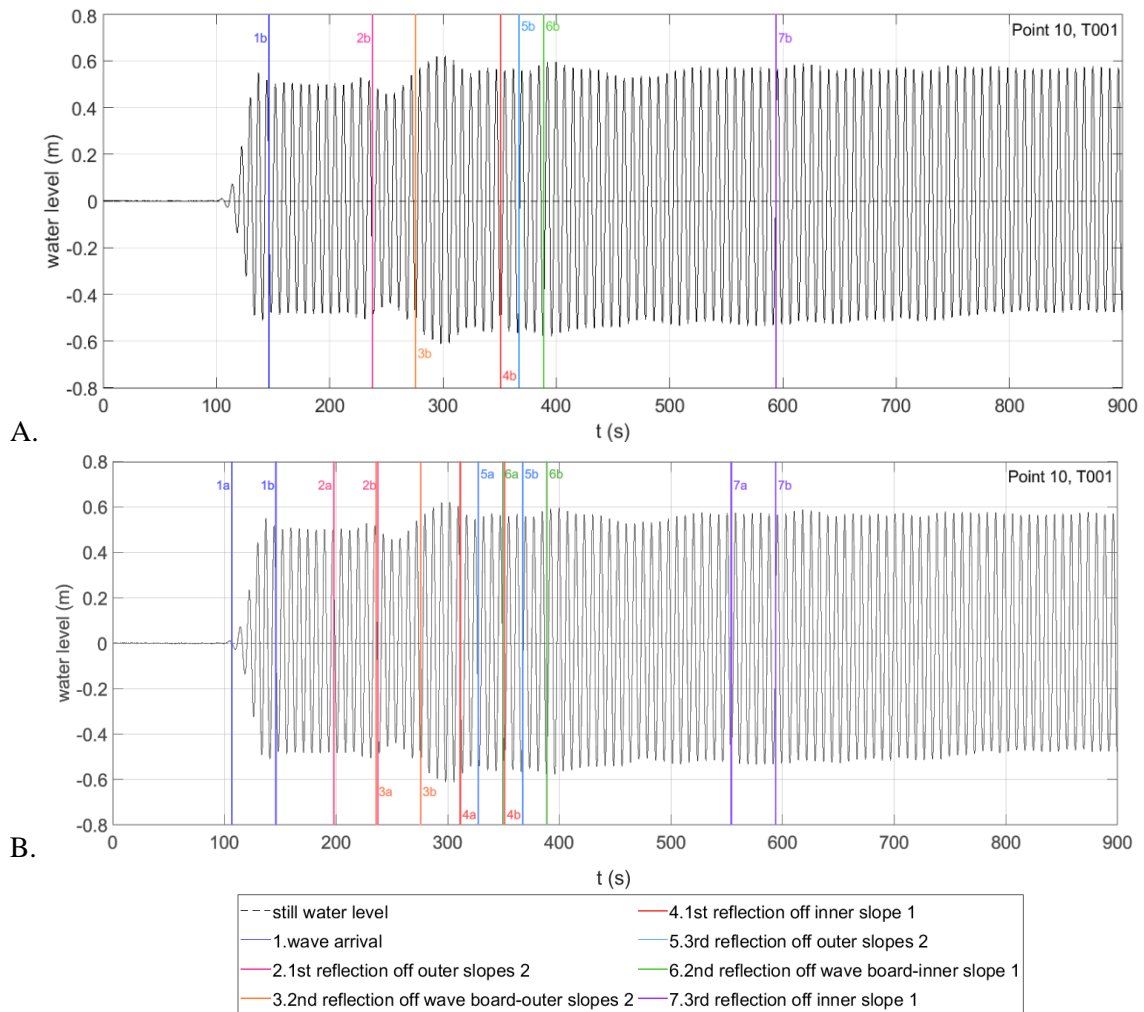
Figure 3.23 The seven characteristic moments in time for the water level time series of point 10 for test T001

As observed in both pictures of Figure 3.23, after moment 7b the wave height remains constant. A steady state has been developed in the basin for this specific experiment. This steady state condition is detected in all the wave gauges records.

3.4   Computation of the steady state wave height at all measurement locations

The characteristic moments indicating the arrival of reflected waves (Section 3.3) were determined for the wave gauges located along the model centreline AA' (Figure 3.9). These lines help identifying the part of the time series influenced by reflected waves off a specific structure and also the intervals that are no influenced by reflected waves but are mainly influenced by diffraction. The analysis of the water level time series at the rest of the measurement locations is less detailed. More precisely, at the wave gauges that are not located along the model centreline, only the time moment when the steady state part begins is determined.

The start of the steady state part is defined as the moment in time after which the wave height remains constant until the end of the time series at t=900s. The wave height is considered constant if the following condition holds:

$$\left| \frac{H_i - H_{i+1}}{H_i} \right| < 2\%$$

(3.13)

where: i is the sequence number of the wave in the record (i.e., i = 1 is the first wave in the record, i = 2 is the second wave, etc.).

The same condition was used for defining Moment 1b (Equation 3.3). However, in this case an extra restriction is applied. The wave height of the first individual wave after the beginning of the steady state moment and the wave height of the final individual wave before the end of the time series at t=900s should also differ less than 2%. This is done to guarantee than not only each wave does not differ in terms of height form the previous one but also the wave height remains constant and does not change gradually. To ensure that in between the two moments in time the wave height does not change the graphs for all the points and all the tests are also visually inspected. Figure 3.24 shows two examples of the steady state beginning moment for test T001: at Point 9, located inside the harbour basin and at Point 25, located outside the basin.

In Section 4.1.3 it will be explained that for T010, in which wave breaking occurs a temporal steady state condition is not reached. For this tests it was decided to consider as 'steady state' the last 300s of the water level time series from t=600s to t=900s.

The time interval from the steady state beginning until the end of the time series at t=900s is used to determine the constant steady state wave height at all points that are not located along the model centreline. For the points along the model centreline the time interval from Moment 7b until t-=900s is used. Subsequently, the steady state wave height at each location is divided by the incoming wave height for the specific test examined. The incoming wave height generated by the wave maker is used, because as it will be discussed in Section 4.2 it differs less than 2% from the average fully developed wave height measured at the wave gauges outside the harbor basin. The ratio $\overline{H}_{steady\ state,diffracrion\ model}/H_{incoming}$ is calculated for all the seven tests. By dividing with the incoming wave height the results for all the seven tests examined can be compared. To demonstrate how the wave height differs at various locations it was decided to create a top view showing the steady state at each output location. Figure 3.24 is a top view in which the value of the ratio at every point is indicated by colours. The exact values of the ratio are presented in Table 3.3. The results for the remaining 6 test are presented in Appendix E.

A.

B.
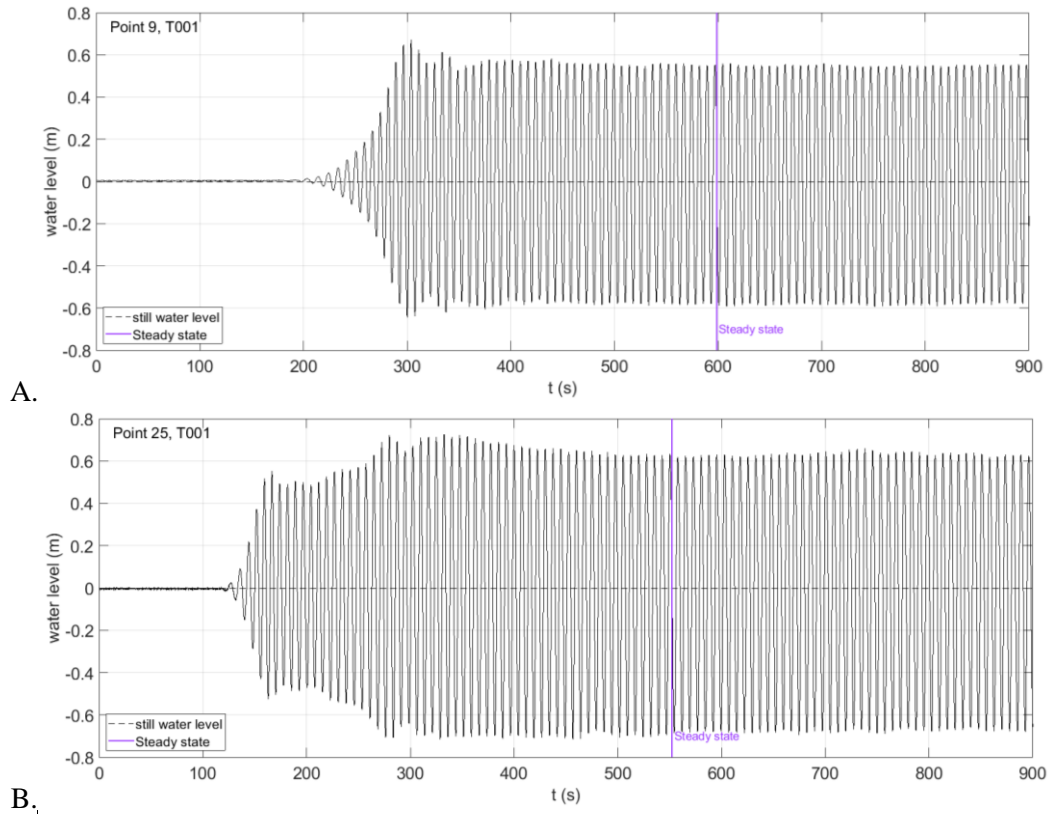
Figure 3.24- The steady state beginning at water level time series generated by the 2D simplified SWASH model at Point 9 and Point 25 for test T001.
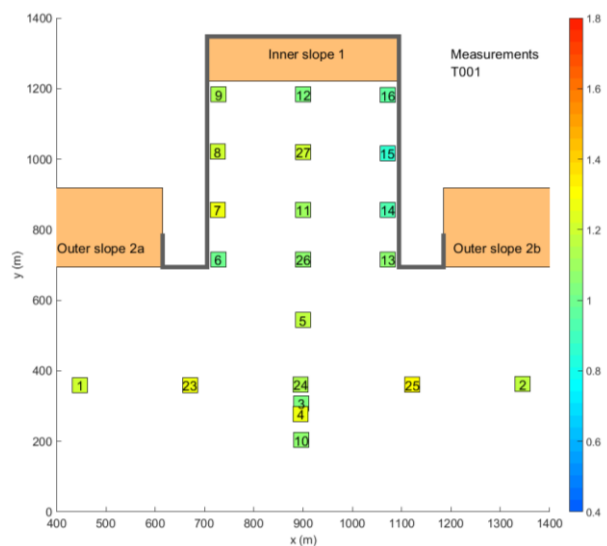
Figure 3.25 – Top view of the ratio $\bar{H}_{steady\ state}/H_{incoming}$ in the measurements for T001.

Table 3.3 - The exact values of the ratio $\bar{H}_{steady\ state}/H_{incoming}$ in the measurements for T001.

Outside the harbour basin			
Wave Gauge	Measured $H_{steady\ state}/H_{inc.}$	Wave Gauge	Measured $H_{steady\ state}/H_{inc.}$
1	1.20	10	1.08
2	1.18	23	1.28
3	1.03	24	1.14
4	1.26	25	1.32
5	1.17		

Inside the harbour basin			
Wave Gauge	Measured $H_{steady\ state}$	Wave Gauge	Measured $H_{steady\ state}$
6	1.00	13	1.07
7	1.27	14	0.94
8	1.21	15	0.87
9	1.15	16	0.98
11	1.10	26	1.07
12	1.03	27	1.20

Chapter 4 Results of measurement analysis

In Chapter 3 the process followed to analyse the measurement outputs for T001 is described in detail. The same approach is applied to all the selected tests. In Section 4.1 the results for the remaining six tests are presented. Possible similarities between the different tests are commented at the end of the section. In Section 4.2 , the measured incoming wave height at the wave gauges outside the basin is determined. Moreover, in Section 4.3 the influence of diffraction on the wave height as measured at the wave gauges inside the harbour basin is discussed. Finally, in Section 4.4 the trends observed in the measurements outside and inside the basin are explained based on the vertical lines representing the arrival of reflected waves (determined in Section 3.3).

4.1   Computation of the wave celerity in the measurements

To confirm if linear theory holds and indeed the theoretical celerity matches with the measurements a plot including the time series of points of model centre line AA'(Figure 3.9.) shifted earlier in time to match with Point 10 is created. Two versions of this plot are presented for every test: one from 50 s to 600s and a zoomed version from 50s to 300s. The wave behaviour is discussed for all the cases. For an overview of the incoming water level generated by the wave maker the reader is refer to Appendix F. This is the signal that in theory is expected to arrive at the wave gauges. By comparing the theoretical signal with the measurements, the plots with all the wave signals at Point 10 can be more easily understood.

The values of the incoming wave height, the wave period and the theoretical wave celerity for the six tests are presented in Table 4.1.

Table 4.1 The wave celerity according to linear wave theory and the characteristics of the seven selected tests.

Test	$H_{incoming}$	$T_{incoming}$	c_{linear}	kd	Wave condition	H/L
T001	0.99m	7.51s	10.71 m/s	1.55	Intermediate water	0.001
T002	1.44 m	10.00 s	12.08 m/s	1.03	Intermediate water	0.012
T003	2.39 m	16.97 s	13.29 m/s	0.55	Intermediate/Shallow water	0.011
T010	2.97 m	5.03 s	7.83 m/s	3.16	Deep/Intermediate water	0.075
T011	3.02 m	8.99 s	11.65 m/s	1.19	Intermediate water	0.029
T012	2.75 m	15.03 s	13.11 m/s	0.63	Intermediate/Shallow water	0.014
T013	1.94 m	4.49 s	7.01 m/s	3.95	Deep water	0.061

4.1.1   Wave celerity in the measurements for T002

Figure 4.1 and Figure 4.2 are created assuming that the wave celerity equal to c_{T002}=12.08 $^m/_s$. A general remark for both figures is that the zero crossings as well as the wave crests and wave troughs occur either at the same time or with a small time shift. However, this is not the case for the taper function part. For all the points it holds that the taper function part travels faster than the wave celerity c_{T002} and the wave becomes smaller in amplitude. Until all the points reach the constant incoming wave height at approximately 140s it is clear that the signals do not match. It is worth mentioning that for the points outside the basin the constant incoming wave height has been reached relatively earlier at 125s.

In Figure 4.2, the wave height for Point 5 starts decreasing (at t=150s) before the arrival of the reflected wave from outer slopes 2 calculated using the celerity c_{T002}. This can be attributed to the fact that the reflected wave resulting from the taper function part has already arrived at Point 5. This wave travels with a faster speed than the theoretical celerity used to determine the vertical dashed, light brown line defining the reflected waves from slope 2. It is logical that this change is observed at Point 5 which is closer to outer slopes 2. As the light brown dashed line of reflection off

outer slopes 2 is calculated for this specific point the rest of the points are not influenced yet by the reflected waves.

Figure 4.1 Time series of all points of Line AA' shifted earlier in time to match with Point 10, for T002.

Figure 4.2 Time series of all points of Line AA' shifted earlier in time to match with Point 10, for T002. This figure is a zoomed part of Figure 4.1.

After the first reflections (blue and light brown dashed vertical lines) changes in the wave height are detected for all the points. Significant changes in the wave height are observed for Points 24 and 5. After the first dashed line the wave gauges are recording the summation of the incoming wave and the reflected wave. The wave height of the resulting standing waves may be higher than the incoming wave height, if the incoming and the reflected wave enhance each other or lower, if the waves cancel each other. After the reflected waves arrival higher of lower wave heights are observed in the wave record. The increase or decrease of the wave height is related to the location of the point. If at a specific location the incoming and the reflected wave are in phase, the wave height is increased. On the contrary, if they are out of phase the total wave height is decreased. It is worth mentioning that after the blue dashed line the points outside the basin are influenced by reflection, while the points inside the basin are influenced by diffraction. For the points inside the basin reflection plays a role after the second vertical line representing the arrival of reflected waves from inner slope 1.

After the first 510 seconds (coinciding with Moment 7b for Point 10) it can be noticed that the wave height at the different points and the phase shift between the time series of the points is remaining constant (Figure 4.1). For this specific experiment a steady state has been reached. It is worth mentioning that the highest wave crest value is observed at Point 24 and the lowest at Point 5. The difference between the two crest values is larger than 0.5m.

4.1.2 Wave celerity in the measurements for T003

From the selected monochromatic experiments, test T003 is the test with the longest wave conditions and the maximum wave period value. Moreover, the wave celerity for this test has the highest value, $c_{T003} = 13.29 \, {}^m/_s$. As the waves travel faster the number of wave crests before any reflection is only 5. In contrast, for a test with smaller wave speed, such as T002, the number of crests before any reflections is 7. Due to the high speed the taper function disappears faster from the measurements. Focusing on the taper function part (approximately from 85 s to 115s) the wave behaviour is clear: the waves travel faster than the celerity based on the linear theory and the wave height is decreases over the distance from the wave machine. This means that the wave height in the taper function part for Point 12 is smaller than Point 27, which is located closer to the wave machine and so on.

An essential observation about the wave's shape is that the crests are sharp and higher, while the troughs are smooth and elongated. This is the typical form of the waves in shallow water. According to Table 4.1, the waves in T003 are indeed classified in intermediate to shallow water.

An important remark about the graphs for test T003 is the shape of the wave troughs after the arrival of reflected waves. For Points 10, 4 and 3, in the intervals of negative water level there are two local minimum values. This effect is a result of the summation of two shallow water waves travelling in opposite direction. At the locations of the three points, the peaks and the troughs of the incoming and the reflected wave do not occur at simultaneously. This means that for some intervals the water level for the incoming wave is negative and for the reflected wave positive and vice versa. This deformed shape only for troughs observed for T003, can be attributed to the shallow water wave shape with elongated troughs. As the crests are sharper and have shorter duration there is not enough time to observe the distortion due to time delay of the reflected wave.
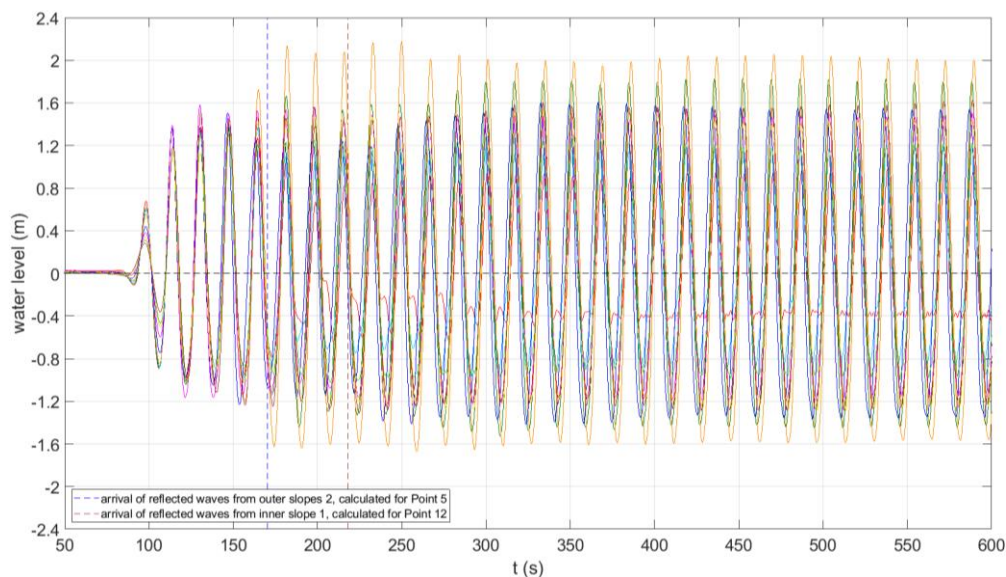
Figure 4.3 Time series of all points of Line AA' shifted earlier in time to match with Point 10, for T003.
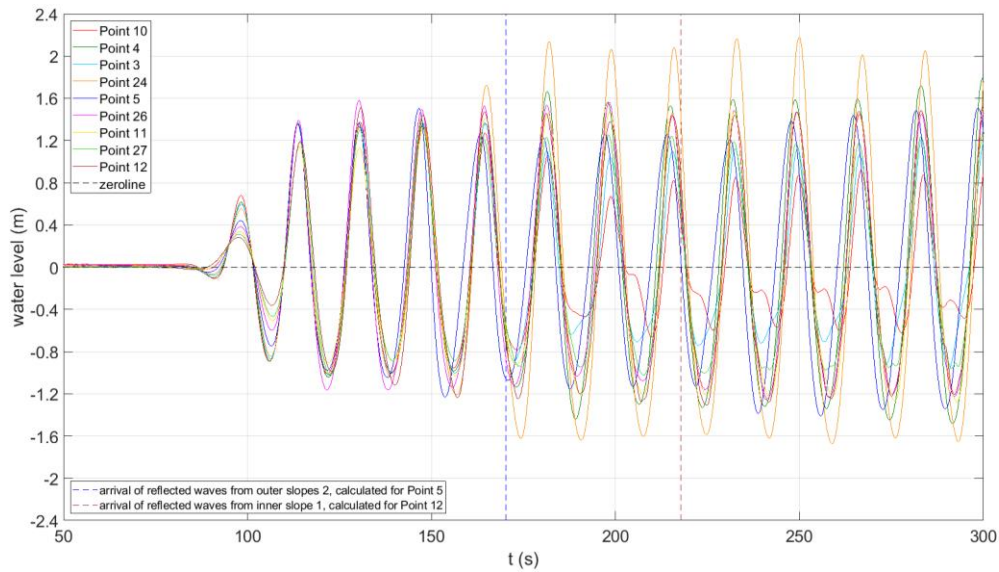
Figure 4.4 Time series of all points of Line AA' shifted earlier in time to match with Point 10, for T003. This figure is a zoomed part of Figure 4.3.

4.1.3 Wave celerity in the measurements for T010

Observing Figure 4.5 and Figure 4.6 it is difficult to detect sinusoidal individual waves. Both pictures create the impression of chaotic wave field. The water level time series for T010 is clearly different than the previous tests examined. Overall, in both pictures the wave signals of the wave gauges appear as random lines. This behaviour can be attributed to wave breaking. In T010 the wave height to wave length ratio H/L exceeds 0.007 and the waves start breaking.

In Figure 4.6 it is observed that the waves are water level is varying from 1.8 to -1.2m. At the arrival of the waves at Points 10, 4, 3, 24 a peak value is detected (140-150s) that is not shown in the signal from the wave machine.

As shown in Figure 4.5, after t=350 s the wave crests become higher than 1.8 with peaks higher than 3m. Moreover, the wave troughs become lower than -1.2m with minimum values smaller than -2m. It is clear after t=350 s, that the wave gauges with the higher wave height values are Point 10, 4 and 3, which are all located outside the harbour basin. Contrary to the previous test examined for T010 a steady state is not noticed.

Due to the difficulty to detect the individual waves it is not feasible to examine a match among the water level signals at the different wave gauges. Therefore it is not possible to come to conclusions whether the theoretical wave celerity is in agreement with the achieved wave celerity in the experiment.
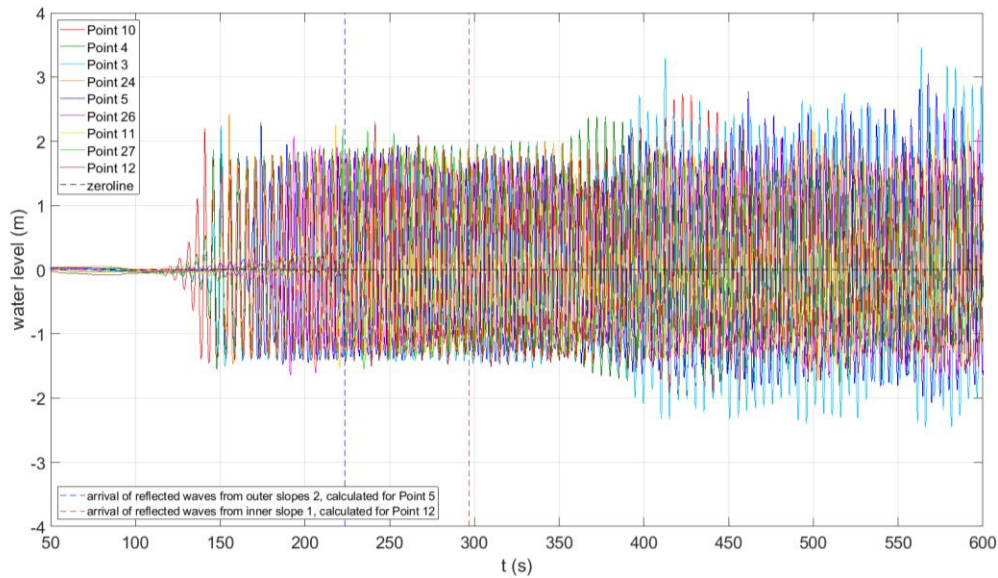
Figure 4.5 Time series of all points of Line AA' shifted earlier in time to match with Point 10, for T010.
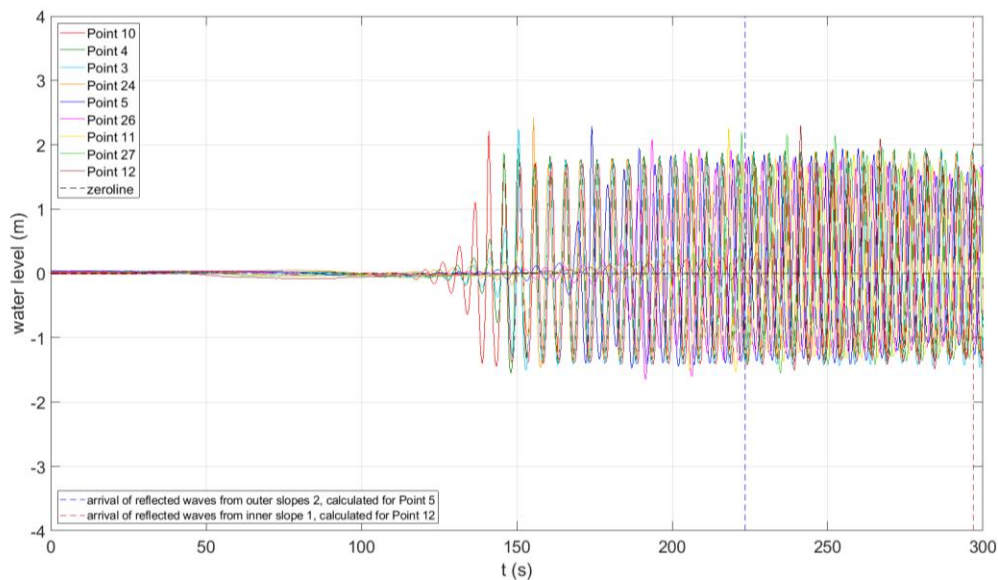
Figure 4.6 Time series of all points of Line AA' shifted earlier in time to match with Point 10, for T010. This figure is a zoomed part of Figure 4.5.

4.1.4 Wave celerity in the measurements for T011

In Figure 4.8 the most important observations made for the previous tests, apart from T010, can be detected. Firstly, the taper function part (90-150s) travels faster than the theoretical celerity. As the distance of the point from the wave machine increases, the decrease of the wave height of the taper function part is also increased. Secondly, from 150 s until 184s, when the first reflected signal arrives, there is a good agreement between the wave signals in terms of height and there is no phase shift between the different time series. This verifies that the waves in the experiment travel with a celerity equal to the theoretical celerity $c_{T011} = 11.65$ m/s. After the arrival of the reflected waves from slope 2 and before the arrival of the reflected waves from slope 1, there is still a good agreement in terms of phase shift as the zero crossings occur almost simultaneously. However, this is not the case for the wave height which varies for the different points.

In Figure 4.7 the same wave pattern is repeated for every wave gauge after t = 400s, so after this moment a steady state is reached. Moreover, there is a wide spread of wave height values at the different wave gauges. The highest peaks occur with decreasing order at Point 24, 3, 26, 11, 10, 27, 12 and finally at Point 4. It is worth mentioning that for T011 there is a good agreement between the measured wave signals and is relatively easy to detect the different trends. This is also the case for T001. The difference between the wave celerity values for the tests is 8%, as $c_{T011} = 11.65$ m/s and $c_{T001} = 10.71$ m/s.

For Points 4, 11, 27 and 12 there are two local minimums in the intervals of negative water level instead of one minimum value, which would be the trough. The same behaviour was also observed for a number of wave gauges for T003. For T011 this behaviour occurs for the wave signal after the arrival of the reflected wave from inner slope 1. This behaviour can be explained by the summation of an incoming and a reflected wave.
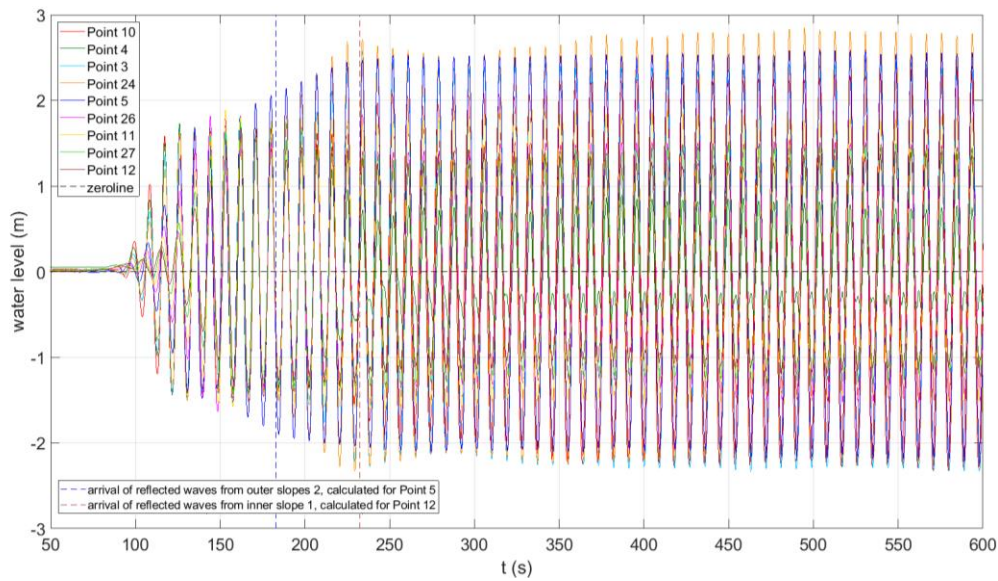
Figure 4.7 Time series of all points of Line AA' shifted earlier in time to match with Point 10, for T011.
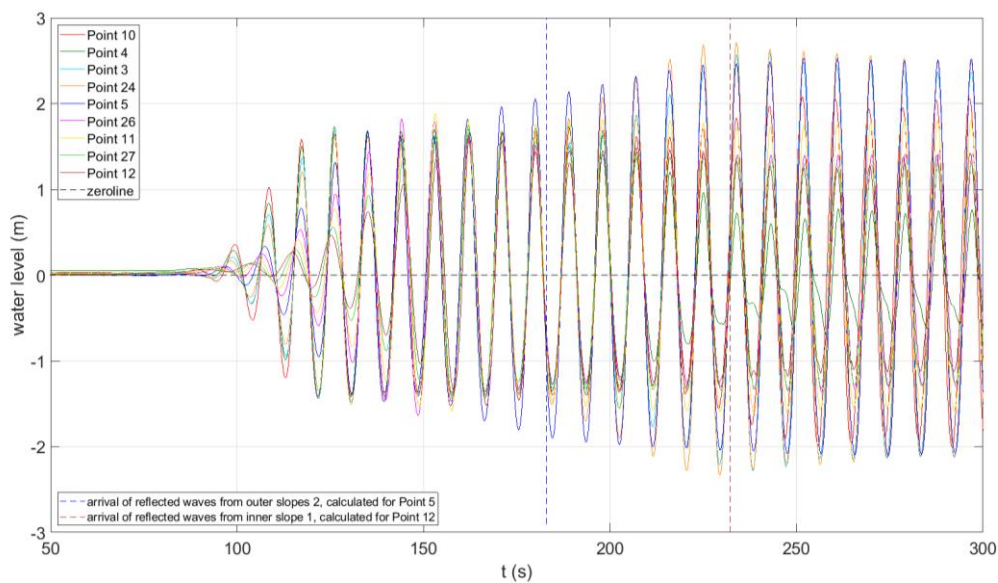
Figure 4.8 Time series of all points of Line AA' shifted earlier in time to match with Point 10, for T011. This figure is a zoomed part of Figure 4.7.

4.1.5   Wave celerity in the measurements for T012

The wave celerity for test T012 is the second highest celerity for all the examined tests. Moreover, as waves are in intermediate to shallow water (Table 4.1) for test T012 the wave signal shows the characteristic of shallow water waves with sharp, high crests and relatively flat, elongated troughs. The taper function part behaviour is similar to the one described for the previous tests. The taper function celerity is higher than the linear celerity, while the taper function wave amplitude decreases over the distance from the wave maker. From t=110s to t=170s the time shift between the time series is small. However, the agreement in terms of wave height is not so well, especially for Point 5.

Already before the arrival of reflected waves the wave trough are distorted. This can be explained by the fact that the wave signal is a summation of the incoming and the reflected wave. The later arrives with a time delay as reflection does not occur instantaneously. The fact that the distortion is observed for a few points before the first dashed line can be attributed to the fact that the line is calculated using the theoretical celerity. It is known that the reflected taper function parts travel faster. The distortion of the wave trough is clear for Points 4, 24, 5, 11 and 27.
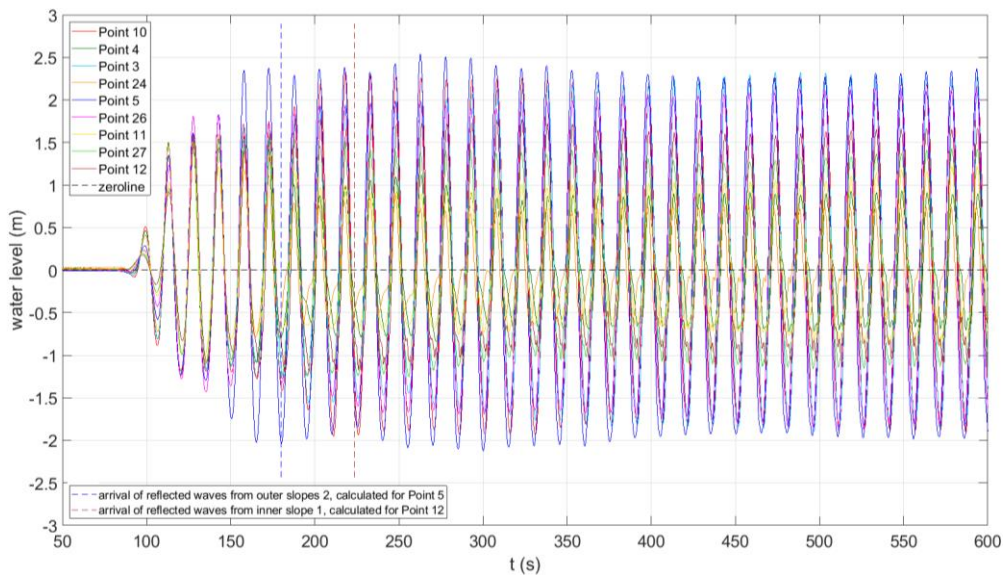
Figure 4.9 Time series of all points of Line AA' shifted earlier in time to match with Point 10, for T012.
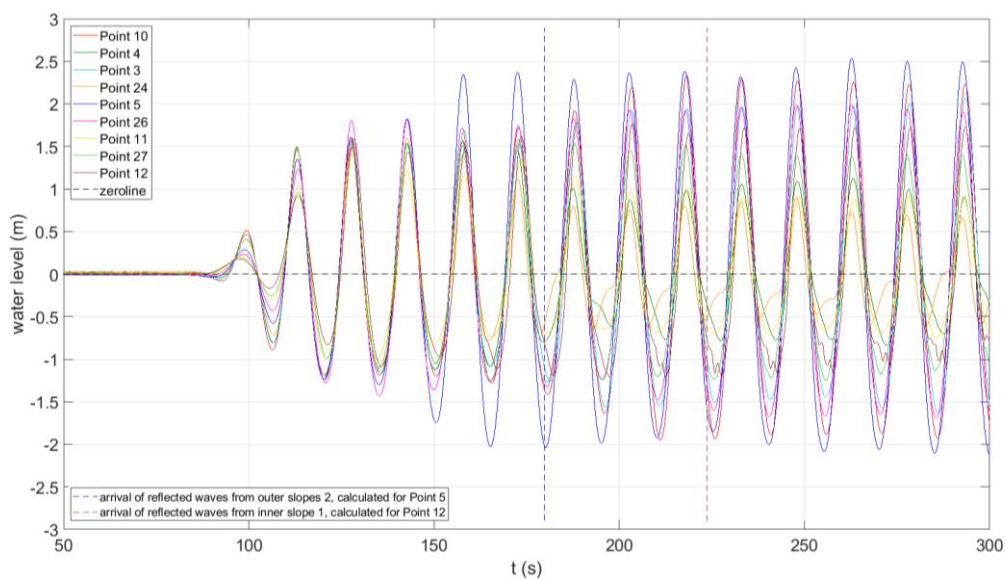
Figure 4.10 Time series of all points of Line AA' shifted earlier in time to match with Point 10, for T012. This figure is a zoomed part of Figure 4.10.

4.1.6　Wave celerity in the measurements for T013

In T013 the kd value is 3.95, indicating a non-linear behaviour of the waves. This kd value is the highest form all the seven tests. Moreover, for T013 the incoming wave height and the incoming wave period are the minimum compared to the values for the other tests. In the Figure 4.11 and Figure 4.12 it is clear that there is not a good match in the wave records. Due to the chaotic wave field in T013 it is not possible to come to conclusions if the theoretical wave celerity is in agreement with the wave celerity in the experiment.

Figure 4.11 and Figure 4.12 for T013 resemble Figure 4.5 and Figure 4.6 for T010. In the pictures of both tests an impression of chaotic wave field is created. Although it is easier for T013 to spot the sinusoidal waves the measurements, still the time shift between the wave signals is so different that the measurements undoubtedly do not match. A possible explanation of this wave signals is the waves are becoming non-linear and the wave celerity deviates from the value calculated according to the linear theory.

Figure 4.12 shows that before the occurrence of reflections the wave crests and the wave through occur approximately for the same water level values. The wave height values start deviating close to the first dash line for reflection from outer slopes 2. For example, the wave height at wave gauges 4 and 24 are increasing. Although in Figure 4.11 there is no good agreement in the wave signals as observed in other tests, it can be claimed that after t=450s the wave patterns remain constant. The peaks and troughs have constant amplitude and also the phase shift between the wave gauges signals remains constant. A steady state seems to be reached.
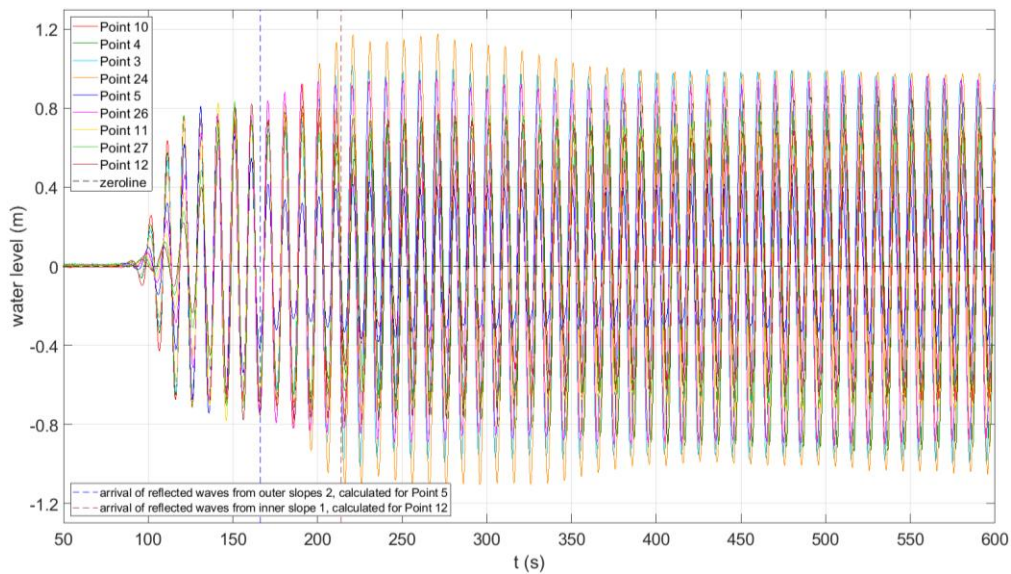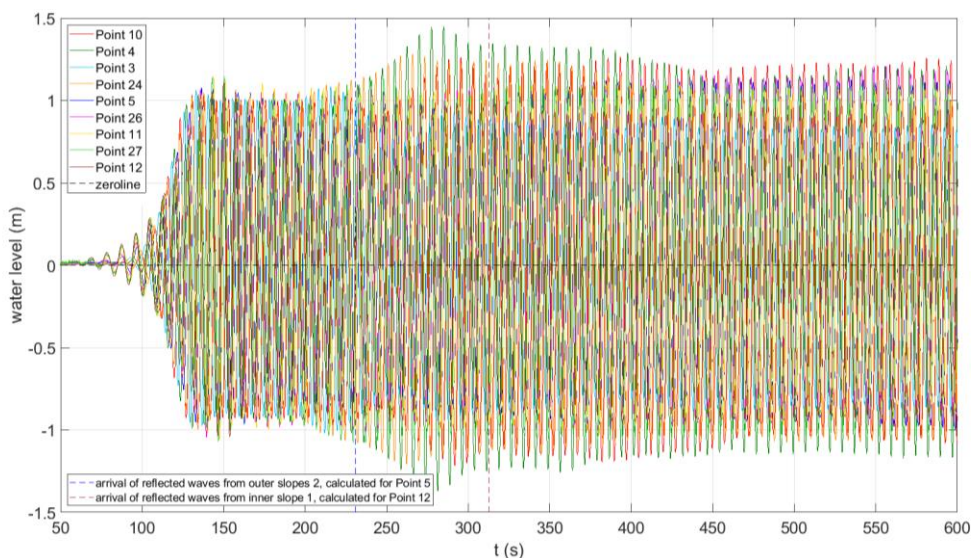

Figure 4.11 - Time series of all points of Line AA' shifted earlier in time to match with Point 10, for T013.
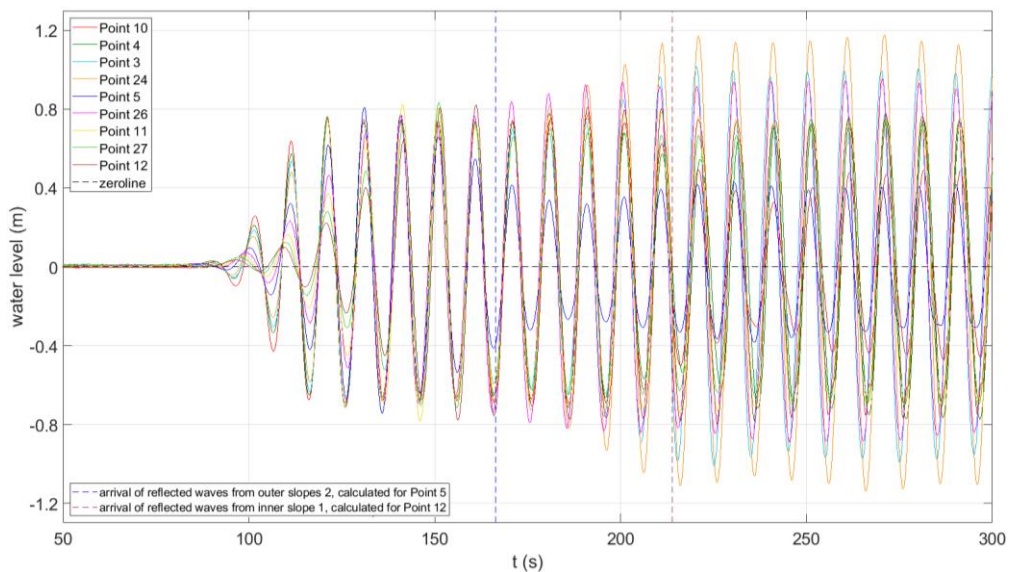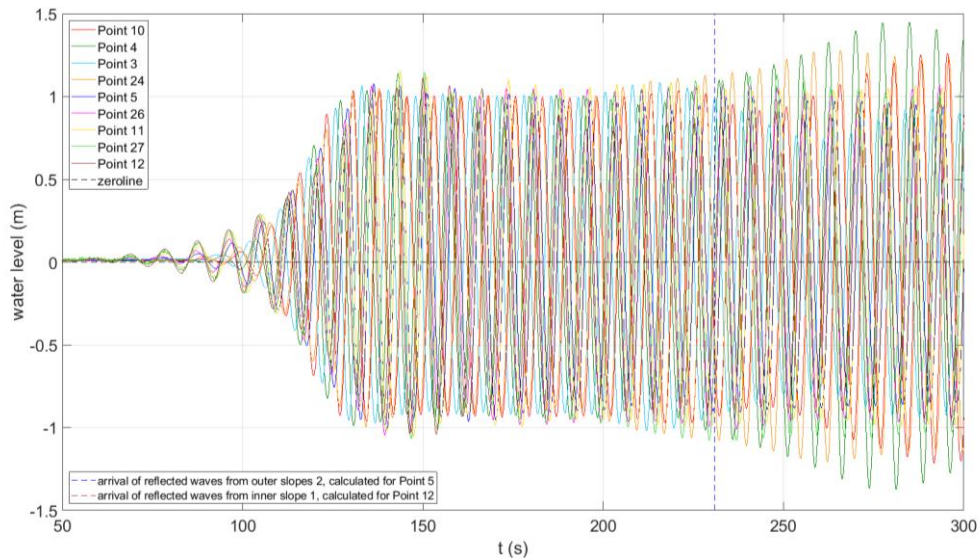
Figure 4.12 - Time series of all points of Line AA' shifted earlier in time to match with Point 10, for T013. This figure is a zoomed part of Figure 4.11.

4.1.7 Remarks about the wave celerity in the measurements for the selected tests

In the previous sections the graphs of the water level measured at the different wave gauges shifted at Point 10 for all the seven selected test are studied in detail. Test T001 is described in Section 3.2 , while the rests of the tests are analysed in Sections 4.1.1 - 4.1.6 . The most important information obtained from the analysis is summarised here.

- The method of verifying the wave celerity by examining the agreement of the wave signals shifted at the same locations cannot be applied for tests with wave height to wave length ratio higher than the breaking limit 0.007 and for kd values higher than 3. For H/L values higher than 0.007 the waves are breaking. For kd values higher than 3 the waves become non-linear. In both cases the picture of the different wave signals is chaotic and does not resemble the simple example of the wave flume presented in Section 3.2 . This phenomenon is observed for tests T010 and T013. Both tests are classified to the third group of tests with high kd values in Table 2.7.

- For the rest of the tests the method provides good results. The agreement of the wave signal is examined for the time interval after the end of the taper function and before the arrival of the reflected waves. For tests with low or average kd values (Table 2.5 and Table 2.6 respectively) there is a good match in terms of wave height and the phase shift between the different wave gauges time series is small or negligible. It can be confirmed that the wave celerity in the measurements is equal to the theoretical wave celerity calculated according to the linear wave theory.

- For tests with low or average kd values it is observed that water level time series capturing the taper function signal generated by the wave machine behaves different than the fully developed incoming wave part. The taper function part travels faster than the theoretical wave celerity and the wave crests and troughs are smaller in amplitude. As the distance of the point from the wave machine increases, the decrease of the wave height of the taper function part is also increased. These observations can be attributed to the non-linear behaviour of the taper function part.

- The wave conditions for T003 and T012 represent intermediate /shallow water. Both tests are classified in the first group of tests for low kd values presented in Table 2.5. For these tests the wave crests are sharper and higher, while the troughs are smooth and elongated .This is the typical wave shape for shallow water.

- For tests T003, T011 and T012 it is observed for many wave gauges signals that the wave troughs are distorted showing two local minimums. This occurs after the arrival of reflected waves. Thus, the wave gauges measure the summation of the incoming and the reflected wave. A possible explanation of this deformed shape is the shallow water shape of the waves. The aforementioned tests are classified into intermediate water, but their kd values are close to the shallow water limit. As the crests are sharper and have shorter duration there is not enough time to observe the distortion due to time delay of the reflected wave. Therefore, the distorted shape is observed only for the wave troughs which are elongated and shorter in amplitude.

- For the six tests a steady state is reached. However, in one test, T010, a steady state is not reached at the first 900s of the experiment. At a specific moment in time, which varies among the tests, the wave patterns are repeated. The wave crests and trough amplitude as wells as the phase shift between the different wave gauges signals remain constant.

4.2 Calculation of the fully developed incoming wave height at the measurement locations

As discussed in Section 3.2.5 , the wave gauges measure the constant full developed incoming wave height, for the time interval after the end of the taper function (Moment 1b) and before the arrival of reflected waves (Moment 2a). The mean wave height measured within this interval ($H_{mean,measured}$) at the wave gauges outside the basin (gauges 10, 4, 3 and 5) is presented in Table 4.2. For Point 5 Moment 2a occurs before Moment 1b and no wave height can be determined. As Point 5 is the closest to outer slopes 2, it is the first point to be influenced by the reflected waves.

In Table 4.2 the averaged measured incoming wave height $\overline{H}_{mean,measured}$ is calculated by averaging the measured wave height $H_{mean,measured}$ values for each test. In the next row the standard deviation of is presented. $H_{inc,wave maker}$ is the fully developed wave height generated by the wave maker. The ratio $\overline{H}_{mean,measured}$ / $H_{inc,wave maker}$ is used to evaluate the agreement between the wave height produced by wave maker and the measured value. If this ratio is within the limits from 0.98 to 1.02 the two terms are considered equal. This means that the two values differ less than 2%. A ratio value from 0.98 to 1 means the measured wave height is lower than the wave height generated from the wave maker, while for a ratio from 1 to 1.2 the measured wave height is higher. The results for the six tests are included in the Table 4.2, while the results for T001 can be found in Table 3.1.

Table 4.2 – The measured incoming wave height at the wave gauges outside the basin.

		T001	T002	T003	T010	T011	T012	T013
$H_{mean,measured}$ (m)	Point 10	0.99	1.42	2.37	3.10	3.00	2.74	1.94
	Point 4	1.00	1.42	2.38	3.14	3.09	2.71	1.93
	Point 3	1.01	1.42	2.36	2.95	3.06	-	1.92
	Point 24	1.01	1.40	2.34	2.63	3.04	-	1.90
	Point 5	-	-	-	-	-	-	
$\overline{H}_{mean,measured}$ (m)		1.00	1.42	2.36	2.96	3.05	2.72	1.92
Std. deviation (m)		**0.01**	**0.01**	**0.02**	**0.02**	**0.04**	**0.02**	**0.02**
$H_{inc,wave maker}$ (m)		0.99	1.44	2.39	2.97	3.02	2.75	1.94
$\overline{H}_{mean,measured}/H_{inc,wave maker}$ (−)		**1.01**	**0.99**	**0.99**	**1.00**	**1.01**	**0.99**	**0.99**

For the seven examined tests, the ratio $\overline{H}_{mean,measured}$ / $H_{inc,wave maker}$ is within the limits from 0.98 to 1.02. For all the tests, excepted from T011, the measured wave height is lower than the wave height from the wave maker. Therefore, the average fully developed wave height measured at the wave

gauges outside the harbor basin differs less than 2% from the corresponding wave height generated by the wave machine. For all the cases the standard deviation of the measurement is in the order of centimeter, with a maximum value of 0.04 for T011. It can be supported that there is a good match in terms of wave height between the measurements and the incoming wave signal. This verifies the good agreement in terms of wave height before the arrival of reflected waves at the plots in which the time series are shifted at Point 10.

4.3   The influence of diffraction on the incoming wave height measured at the wave gauges inside the basin

Table 4.3 includes the same terms shown in Table 4.2 with the only difference that in Table 4.3 shows the results for the wave gauges inside the basin. For the point inside the harbour basin the time interval for which the wave height is not influenced by reflections, starts at the end of the taper function (Moment 1b) and ends with the arrival of reflected waves from outer slopes 2 (Moment 4a).

Again the ratio $\overline{H}_{mean,measured}$ / $H_{inc,wave\ maker}$ is used to compare the measured wave height to the wave height generated by wave maker. However, in this case the two values are not expected to be equal as diffraction plays a role inside the harbour basin. This ratio indicates the influence of diffraction on the wave height. It should be kept in mind that for none of the tests it was possible to determine a time interval that is not disturbed by reflections for Point 26, and in many cases for Point 27.

Table 4.3 - The measured incoming wave height at the wave gauges inside the basin.

		T001	T002	T003	T010	T011	T012	T013
$H_{mean,measured}$ (m)	Point 26	0.93	1.36	2.69	1.89	2.97	3.17	2.01
	Point 11	0.81	1.40	2.04	0.13	2.99	1.98	2.04
	Point 27	-	1.02	-	-	2.18	-	2.21
	Point 12	-	-	-	-	-	-	-
$\overline{H}_{mean,measured}$ (m)		0.87	1.26	2.36	1.01	2.71	2.57	2.09
Std. deviation (m)		**0.21**	**0.28**	**0.46**	**3.02**	**0.61**	**0.86**	**0.23**
$H_{inc,wave\ maker}$ (m)		0.99	1.44	2.39	2.97	3.02	2.75	1.94
$\overline{H}_{mean,measured}/H_{inc,wave\ maker}$ (−)		**0.88**	**0.88**	**0.99**	**0.34**	**0.90**	**0.94**	**1.08**

For the seven examined tests, the ratio $\overline{H}_{mean,measured}/H_{inc,wave\ maker}$ varies from 0.341 to 1.078. It should be noticed that the standard deviation of the measurement wave height varies from the order of meter to decimeter. As shown in Table 4.3, the mean wave height values for a specific test may differ significantly between the different points. For example, for T011 vary from 2.99 to 2.18. For test T003, the ratio $\overline{H}_{mean,measured}/H_{inc,wave\ maker}$ is low (0.991), but the wave heights vary by 0.46 m. All in all, the high values of standard deviation indicate that critical view of the results is required.

It is known that the wave height inside the basin is influenced by diffraction. However, it is not safe to determine the role of diffraction on the wave height from the measurements. There are several problems in the approach followed. First, no information can be obtained from Point 12 and in some cases from Point 27. The points are located close to the harbour end and there is no time interval measuring the incoming wave height without the influence of reflection. Secondly, the measured mean wave height varies significantly among the different gauges, as expressed by the high standard deviation values. Moreover, the wave heights for the duration after the end of the taper function and before the arrival of reflected waves from inner slope 1 are not constant (see also Section 4.4.2). The phenomenon of diffraction is examined separately in Chapter 7 by a two-dimensional SWASH model.

4.4 Characteristic moments at every wave gauge for all the tests

4.4.1 Wave gauges outside the harbour basin

The incoming wave height can be determined by the wave record at the following wave gauges outside the basin: 10, 4, 3 and 24. For these points the duration between the end of the taper function and the arrival of reflected waves is enough to determine the wave height of individual waves and finally calculate the average value. However, as shown in Table 4.2, for T012 the incoming wave height cannot be determined at Point 3 and 24, because the time interval is not sufficiently long. For all the examined tests, for wave gauge 5 there is not a time interval in the wave record measuring only the fully developed incoming wave height.

The behaviour of the wave records are discussed in detail for two characteristic cases for T002. In Figure 4.13 the water level time series for Point 24 are presented. The first measured zero crossing occurs at moment 1a. The water level increases until the end of the taper function at moment 1b. For the definition of moments 1a and 1b the reader is referred to Section 3.2.4 and Figure 3.16. From Moment 1b to 2a the wave height remains constant. This is the time interval used to derive the measured fully developed incoming wave height. This time interval is longer for points located further for outer slopes 2.

After moment 3a the wave gauge measures the summation of the incoming wave and the reflected wave from outer slopes 2. The wave height of the standing waves measured may be higher or lower than the incoming wave height. The increase or decrease of the wave height is related to the location of the point. If at a specific location the incoming and the reflected wave are in phase the wave height is increased. On the contrary, if they are out of phase the total wave height is decreased.

After moment 5b the wave height starts decreasing. After moment 7b the wave signal remains constant. As it is expected a steady state is developed.
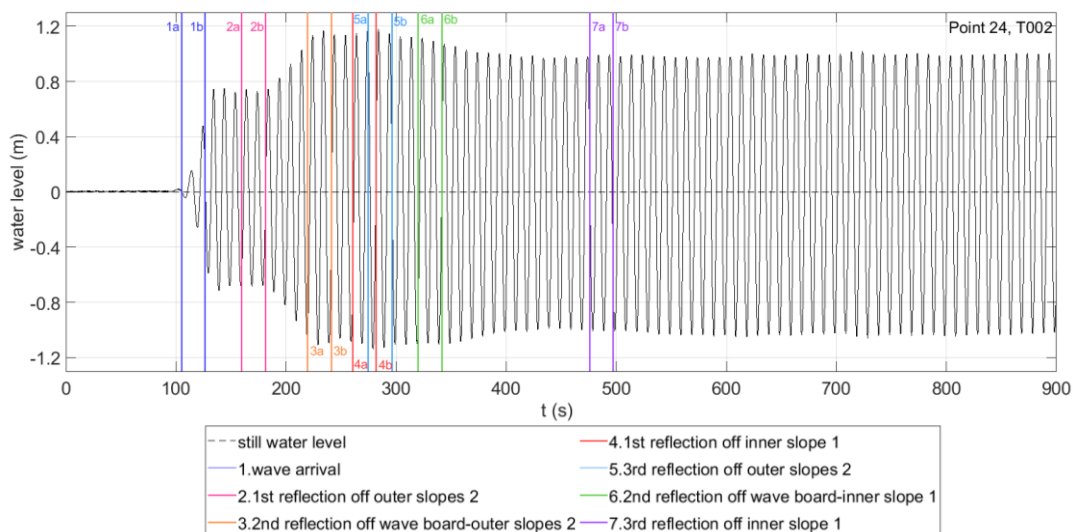
Figure 4.13 The measured water level time series at wave gauge 24 for test T002

In Figure 4.14 the water level time series for Point 5 is plotted. The taper function part is measured from Moment 1a to Moment 1b. As Moments 1b and 2a are almost coinciding the time interval between these moments cannot be used to determine the fully developed wave height. This is because the wave gauge is the closest to outer slopes 2 and the harbour head walls and the reflected waves arrive at the gauge within short time. After Moment 2b the wave height starts decreasing until 10 seconds before Moment 3a. From Moment 3a until Moment 4b there is a slight increase of the wave height. It is reasonable to observe change in the wave height when the reflected waves arrive at the

gauge. After Moment 7b the wave signal remains constant. Thus, it is considered that a steady state is reached.
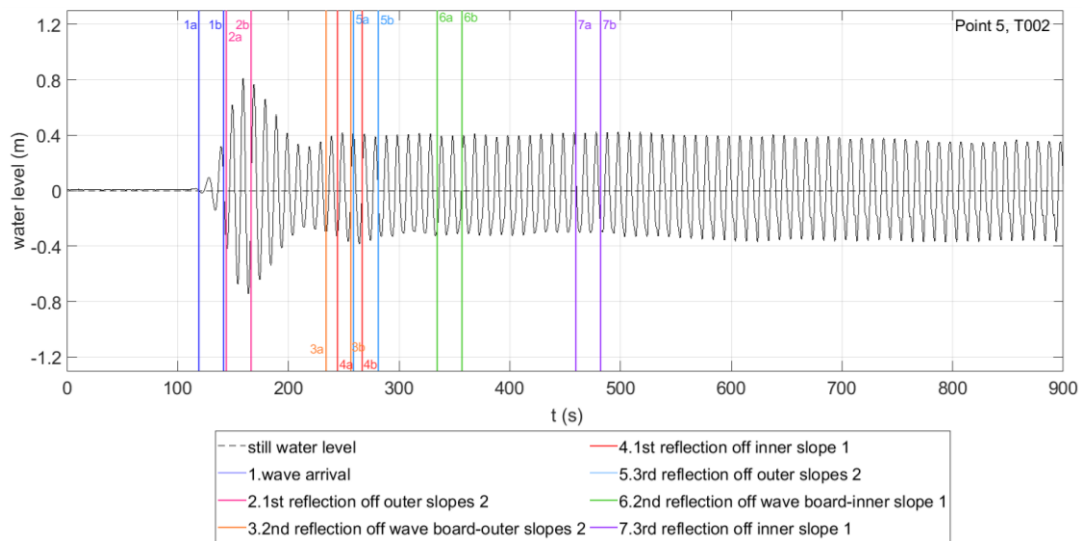
Figure 4.14 The measured water level time series at wave gauge 5 for test T002.

For a full overview of the wave records for all the seven examined tests the reader is referred to Appendix C.

4.4.2 Wave gauges inside the harbour basin

To study the effect of diffraction on the wave height, information about the incoming wave height at the wave gauges inside the basin is required. However, for the points inside the basin the duration of the wave record describing only the incoming wave height is not always long enough. At the point with the furthest distance from the wave maker, Point 12, in every test the reflected taper function wave arrives before the incoming wave can be fully developed. This is illustrated by the water level time series for Point 12 for tests T012 presented in picture D of Figure 4.15. For the majority of the test cases at Point 27 there is no individual wave between the Moments 1b and 4a (picture C of Figure 4.15). For Points 26 and 11 the part of the wave record describing only the fully developed wave height starts at Moment 1b and ends at Moment 4a. In pictures A and B of Figure 4.15, it is clear that during this interval the wave height does not remain constant. The same behaviour is observed for the rest of the selected tests cases. This behaviour is in conflict with the expectations as the wave signal generated from the wave machine is constant after the end of the taper function part. Taking into account the results about the measured incoming wave height inside the basin, it is clear that information about the influence of diffraction inside the basin obtained from the measurements is limited. However, this information can be useful in evaluating the SWASH ability to describe diffraction examined in Chapter 7. Finally, it is worth mentioning that for all the four points inside the basin a steady state is indeed reached after Moment 7b.
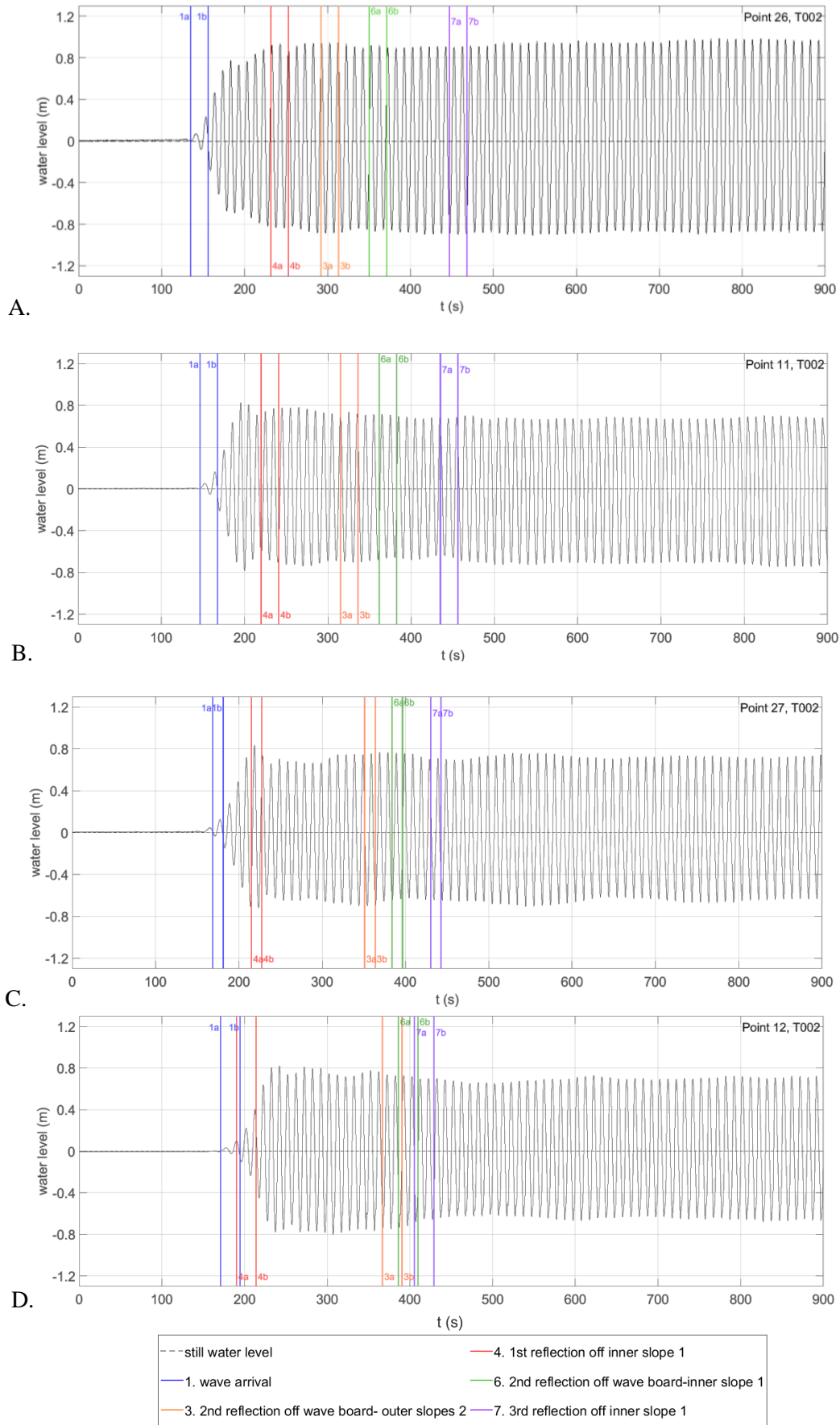
Figure 4.15 - The measured water level time series for test T002 at wave gauge 26 (picture A), at wave gauge 11 (picture B), at wave gauge 27 (picture C) and at wave gauge 12 (picture D).

Chapter 5 The influence of porosity and stone size of a gravel slope on reflection simulated with SWASH

Chapter 5 is the first of a series of chapters (Chapters 5 to 8) in which the setup and the output of SWASH simulations are discussed. Chapter 5 focuses on answering to sub-question 2a. Sub-question 2a aims on testing whether the values of porosity and stone size of the gravel slopes in the physical scale model can be used in SWASH simulations. The gravel slope properties for which the correct amount of reflection is reproduced in SWASH are selected here. In this chapter the reflection off the outer slopes located outside the harbour is assessed. Section 5.1 presents the cross section in the physical scale model selected to be modelled in SWASH. In Section 5.2 the 1D model set up and the examined nine runs for various settings are specified. The results of the model runs are discussed in Section 5.3 . The resulting conclusions that help answering sub-question 2a are summarized in Section 5.4 . Finally, some additional remarks based on the SWASH results are mentioned in Section 5.5 .

5.1   The one-dimensional model in SWASH

With respect to sub-question 2a, gravel slopes reflection is considered to be modelled accurately, if SWASH results are in agreement with the measurements. This means that the wave height trends (increase, decrease or constant part) in time and in space should be reproduced. The steady state wave height observed in the measurement should be reproduced by SWASH within an error of 20%.

To provide an answer to sub-question 2a, it selected to focus on a sub area of the full layout1 that contains a gravel slope and for which the reflection phenomenon is dominant, while the rest of the processes are expected to be negligible. The outer and the inner slopes in layout 1 consist from the same material and are constructed with the same technique in the physical scale model. Hence, the two slopes are considered to have the same properties for porosity and stone size. It is important to mention that the gravel material used in the experiments for the schematic port layouts was previously used in other experiments. The stone size is not measured before the specific experiment examined but earlier. The stones may have been composed out of different rock grading over time. Thus, the gravel sieve curve may have changed and the stone size (D_{n50}) may be slightly different then the value described in the measurements report (Deltares, 2016).

The inner slope 1 is not selected to be modelled for two reasons. Firstly, the reflected wave at the end of the basin results from the incoming wave that hits not only the inner slope 1, but also the concrete wall behind it. Moreover, the measurement devices in front of the inner slope 1 are located inside the harbour basin and thus are influenced also by diffraction. Therefore, it was decided to focus on the outer slopes 2a and 2b.

As mentioned above, the aim within this chapter is to compare the SWASH water level time series to the measured time series at a location that is only influenced by reflection. As discussed in Section 3.3, the reflected waves from inner slope 1 travel out of the basin and their energy gets diffracted (Figure 3.26). It is assumed that the influence of diffraction is important in within in an angle of 15° from the harbour entrance. In Figure 5.1 the cone of influence of diffraction in front of the harbour exit is drawn. Wave gauges 1 and 2 lie out of the cone area. Therefore, it is assumed that wave gauges 1 and 2 are not influenced by the diffracted reflected waves from the inner slope 1.The reflected waves from the harbour head walls are also spread by an angle of 15° due to diffraction. The area influenced by this phenomenon is indicated by red lines. Again Points 1 and 2 are not expected to be influenced by the reflection at the harbour head walls, as the lie out of the red lines.

As shown in Figure 5.1, Point 1 is located in front of outer slope 2a and Point 2 in front of slope 2b. Both wave gauges measure the summation of the incoming wave and the reflected wave from the respective outer slopes. However, behind outer slope 2b the harbour side basin is located. The waves that travel through outer slope 2b may get reflected on the concrete walls of the side basin, travel again trough slope 2b and arrive at wave gauge 2. It is expected that this reflected wave is small in amplitude, since the wave energy is damped two times when passing through the gravel slope. This phenomenon might cause disturbance in the record of wave gauge 2. Therefore, it was chosen to model the outer slope 2a and use the wave record of wave gauge 1 to evaluate SWASH outputs. In Figure 5.1 the blue line represents the cross section chosen to be reproduced in the 1D SWASH model. In this chapter outer slope 2a is described as outer slope 2, gravel slope or slope 2 for simplicity.
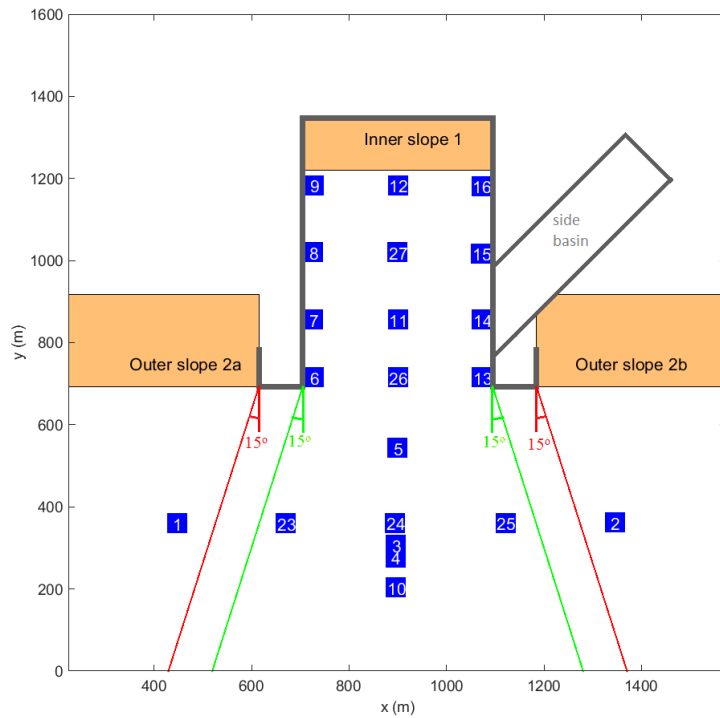
Figure 5.1 - The reflected waves from the harbour end are spread due to diffraction in the area between the two green inclined lines forming an angle of 15° with the harbour exit. The reflected waves from the harbour head walls are spread due to diffraction in the area between the two red inclined lines.
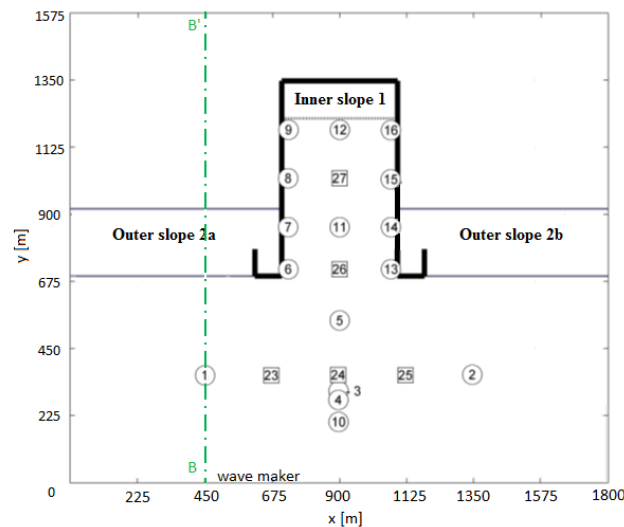
Figure 5.2 – Top view of layout 1. The blue line represents the cross section chosen to be reproduced in the 1D SWASH model.

5.2   The 1D SWASH model setup

The 1D SWASH model domain has a total length of 1152m. A sketch of the model bathymetry is shown in Figure 5.3.The waves enter the domain at y=0m. The only structure included in the model is the outer slope 2a. The porosity and the stone size of the gravel slope are equal to the respective values of the gravel slopes in the physical scale model. Thus, the porosity is 0.4 and the stone size is 6.75m. At the end of the domain a sponge layer is defined. The model boundary behind the sponge layer is set by default as a closed fully-reflective boundary.

An output location is specified at Point 1, as the water level time series at this location will be compared to the measured time series. An extra output location, Point 30, is added behind the gravel slope. This point does not exist as a measurement point in the scale model tests. Point 30 is added for two reasons. The first reason is to confirm that the waves are damped after passing through the outer gravel slope. The second reason is to check if the sponge layer placed at the left end of the cross section (Figure 5.3) is sufficiently large to absorb the transmitted wave energy.
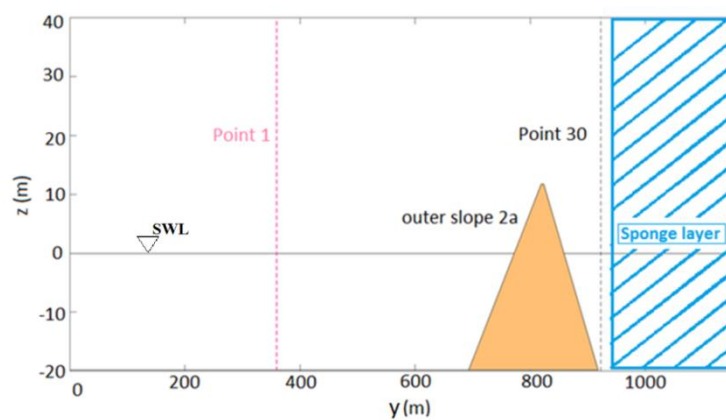
Figure 5.3 – A sketch of the bathymetry of the 1D SWASH model.

Information about the grid resolution, the time step, the bathymetry, the number of layers (2 vertical layers) and other modelling parameters as well as the SWASH command file are provided in Appendix H. The only modelling parameter discussed in this section is the sponge layer length, as the ability of the layer to absorb the wave energy will be examined.

According to SWASH user manual (The SWASH Team, 2016), the sponge layer should have a width of 3 to 5 typical wave lengths to prevent reflections at the open boundaries. To reduce the domain size and thus the computational effort, the sponge layer length was selected to be equal to the largest wave length from all the selected experiments, i.e. T003. The sponge layer width, thus, is equal to 225m to achieve an integer number of cells in the x direction of the cross section. In Table 5.1 is shown that for the rest of the tests this sponge layer might be equal up to 7.1 times the wave length. With the grid boundary behind the sponge layer acting as a closed boundary, the sponge layer becomes double effective as the waves reflect at that boundary and travel back through the sponge layer and their energy gets again absorbed.

Table 5.1 -The number of waves that fit in the sponge layer for all the selected tests.

Test	Wave length L (m)	Ratio $L_{sponge\ layer}/L$
T001	80.48	2.8
T002	120.74	1.9
T003	225.59	1.0
T010	39.38	5.7
T011	104.71	2.1
T012	197.05	1.1
T013	31.52	7.1

From the seven selected tests, described in Section 1.3 it is chosen to study only one representative test. T010 and T013 are excluded as the ratio H/L is high and waves start breaking. The criteria taken into account for the test selection are the wave height and the kd value. The goal is to choose representative, average values and not very high or low values. The final test selected is T002, for which the wave height value is an average value among the tests (H=1.44m). For T002, the kd value is equal to 1.03, which indicates an average computational effort. Finally, according to Table 2.6, for this kd value the waves are classified in intermediate water.

In total, nine runs with different combinations of parameter settings are examined: run 1 for the original values of porosity and stone size, runs 2, 3 and 4, in which the porosity values are varied, runs 5 to 8, in which the stone size values are varied and run 9, in which the outer slope is replaced by a closed wall. The 9 runs are presented in the Table 5.2.

Table 5.2 The nine runs for various porosity and stone size values simulated with SWASH.

Run	Porosity (-)	Porosity change (%)	Stone size (m)	Stone size change (%)
1 (original)	0.40	-	6.75	-
2	0.44	+10%	6.75	-
3	0.36	-10%	6.75	-
4	0.20	-50%	6.75	-
5	0.40	-	7.425	+10%
6	0.40	-	6.075	-10%
7	0.40	-	10.125	+100%
8	0.40	-	3.375	-50%
9 (wall)	0.001	-99.75%	0.045	-99.33%

As explained previously, the SWASH water level time series at wave gauge 1 should be compared to the measured time series. The measured water level time series at wave gauge 1 for test T002 are shown in Figure 5.4. For the derivation of the vertical lines the reader is referred to Section 3.3 . Vertical lines with suffix a represent the arrival of the beginning of the taper function part, while the lines with suffix b represent the arrival of the fully developed wave. The measured incoming wave height equals 1.48m (period between Moment 1b and 2a), which differs by 2.7% from the wave height of 1.44m produced by the wave maker. After Moment 2a, the wave height starts to increase until Moment 5b and then remains constant and equal to 2.34m.
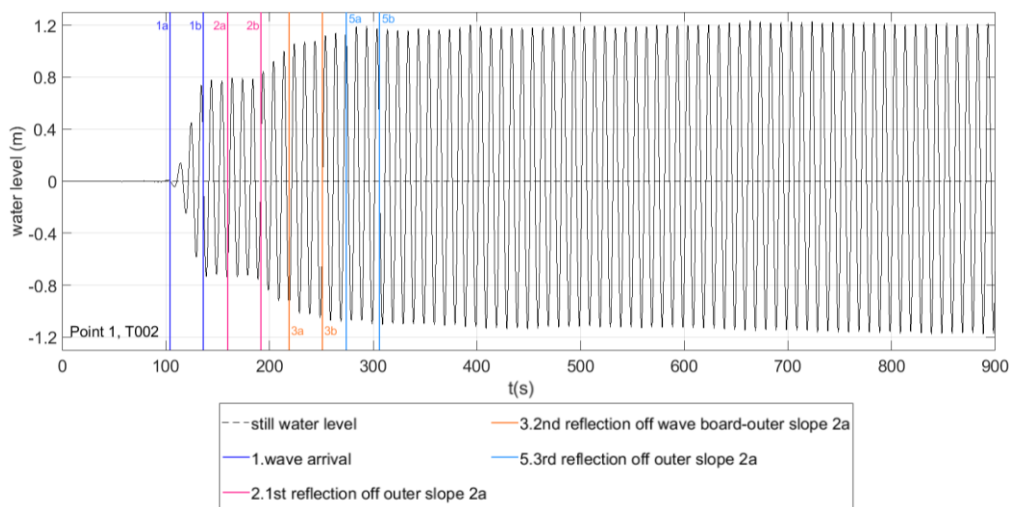
Figure 5.4 – Measured water level time series at Point 1 for T002.

58

5.3 Results

The SWASH results for the nine runs described in Table 5.2 are the following:
- Water level time series at Point 1
- Water level time series at Point 30
- Envelope of the water level during the steady state part of the test (t > Moment 5b).

5.3.1 Water level time series at Points 1 and 30

The water level time series calculated by SWASH for Run 1, in which original values of porosity and stone size are used, is presented in Figure 5.5. The wave height between moment 1b and moment 2a is too short to determine the incoming wave height value. To have a quick estimate whether the incoming wave height at the output location is in agreement with the wave maker wave height defined in the SWASH boundary, the wave height of the first wave after Moment 1b is calculated. This wave is indicated by a brown rectangle in Figure 5.5 and it is assumed that the influence of the reflection is sufficiently small to be ignored. As shown in Figure 5.5, the increase of the wave height after moment 2a is barely visible. The calculated wave height of the first wave after Moment 1b is 1.47m, which deviates by 2% from the wave maker incoming wave height imposed at the boundary (1.44m). However, After moment 5b, a steady state has been developed during which the wave height, $\bar{H}_{\text{steady state,Point 1}}$ is constant and equal to 1.518m. However, the respective value in the measurements is 2.34m. The final constant values of the steady state wave height ($\bar{H}_{\text{steady state,Point 1}}$) for all the runs are summarised in Table 5.3. Moreover, the difference of the measured $\bar{H}_{\text{steady state,Point 1}}$ and the respective value resulting from SWASH is included in the table.
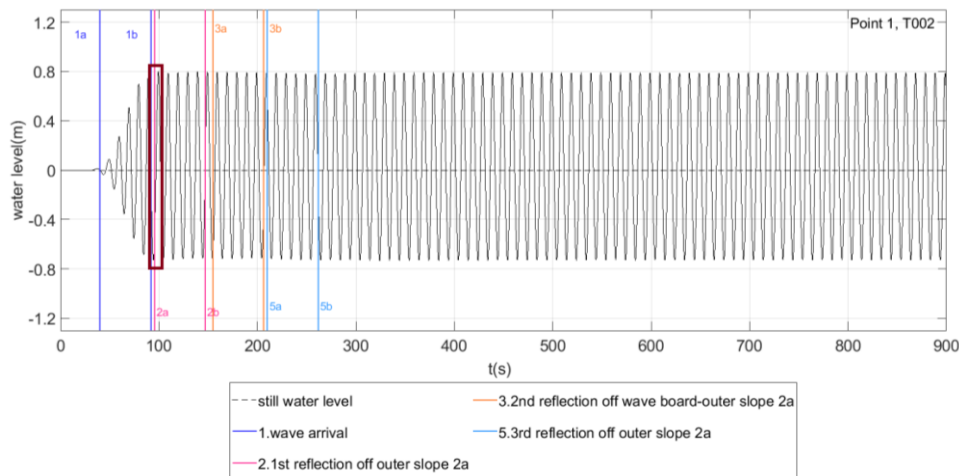
Figure 5.5 – Run 1, water level in time at Point 1 generated by SWASH for T002. The brown rectangle indicates the first wave after Moment 1b.

Table 5.3 – The steady state wave heigt at Points 1 and 30 for the nine runs. In the fifth collumn the difference between the wave height value at Point 1.

Run	Porosity (-)	Stone size (m)	$\bar{H}_{\text{steady state, Point 1}}$ (m)	Difference from the measured $\bar{H}_{\text{steady state, Point 1}}$ (%)	$\bar{H}_{\text{steady state, Point 30}}$ (m)
1 (original)	0.40	6.750	1.52	35.0	0.58
2	0.44	6.750	1.51	35.0	0.67
3	0.36	6.750	1.53	34.0	0.49
4	0.20	6.750	1.64	30.0	0.15
5	0.40	7.425	1.52	35.0	0.62
6	0.40	6.075	1.52	35.0	0.55
7	0.40	10.125	1.50	36.0	0.83
8	0.40	3.375	1.15	51.9	< 0.05 m
9 (wall)	0.001	0.045	0.20	92.0	< 0.05 m

As indicated in Table 5.3 the constant wave height at Point 30, behind the gravel slope is sufficiently small. This means that the larger part of the incoming wave energy either gets reflected at outer slope 2a or is damped while passing through the slope. In Figure 5.6 the times series for Run 1 is plotted. After the end of the taper function part the wave height remains constant and nothing indicates the arrival of reflected waves from the ends of the domain. This means that the wave energy transmitted though the gravel slope gets absorbed by the sponge layer. This is the case for all the 9 runs. Therefore, the sponge layer length is considered efficient.
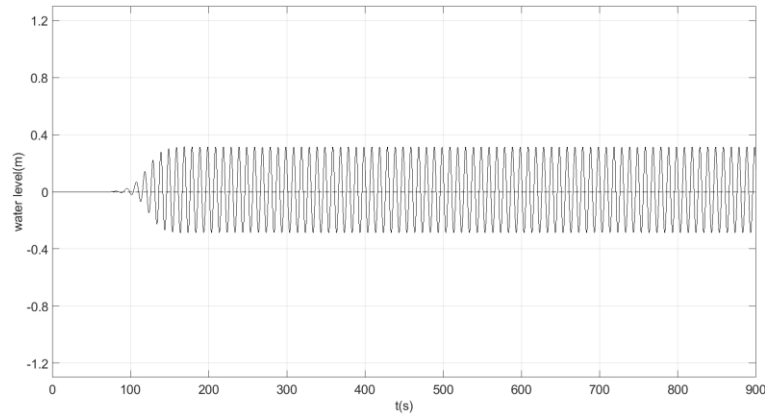
Figure 5.6 – Run 1, Water level in time at Point 30 generated by SWASH for T002.

For runs 2 to 7, the water level time series at Point 1 show behaviour similar to run 1 with the original values as the wave height increases slightly after Moment 2b and reaches a constant value after Moment 5b. The first wave after Moment 1b is again compared to the incoming wave height imposed at the boundary. The deviation is smaller than 3% verifying that no unexpected phenomena take place during the wave propagation from the boundary to Point 1 and the incoming wave height is modelled accurately by SWASH.

The highest $\overline{H}$ steady state,Point 1 of all the different settings examined is observed for run 4 and is equal to 1.64m. As for run 4 the porosity value is lower, the gaps between the stones are smaller and it is more difficult for the waves to pass through them. Hence, a slightly larger amount of wave energy is reflected. However, it the total wave height at Point 1 for run 4 is still much lower than the constant wave height value of 2.34m calculated from the measured time series (Figure 5.4).

For Run 8 after the arrival of the reflected wave from the gravel slope 2 (Moments 2a and 2b) the wave height starts decreasing until it becomes equal to 1.151m at the steady state. This means that a higher amount of wave energy gets reflected when the gravel size becomes half that the initial value. For this case the incoming and the reflected wave are cancelling each other at the location of wave gauge 1. As for runs 1 to 7 the wave height is increasing, it means that for this test the node and antinode pattern is shifted. The water level time series at Point 1 for runs 2 to 8 are presented in Appendix H.

The last run is the wall case. The porosity and the stone size are so small that waves cannot pass through the wall. At Point 30, located behind the gravel slope the water level remains equal to zero. This means that there is no transmission and all the incoming wave energy gets reflected or dissipated. As shown in Figure 5.7, after the arrival of the tapper function part of the reflected wave (Moment 2a) the wave height starts decreasing. The incoming and the reflected wave are cancelling each other. The constant wave height is equal to 0.195m. This value differs by 92% from the measured wave height (Table 5.3).
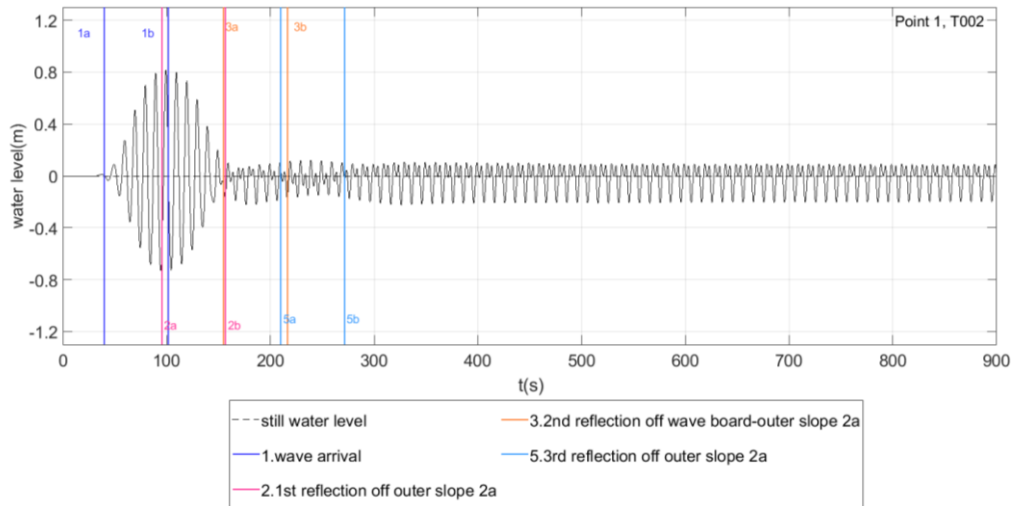
Figure 5.7- Run 9 (wall), Water level in time at Point 1 generated by SWASH for T002.

5.3.2 Envelope of the water level during the steady state of T002

If in the physical scale model the position of the slope or the location of wave gauge 1 is slightly different, the water level time series can be different than the one generated by SWASH. Moreover, for a node-antinode pattern of the standing waves that changes within a short length it is possible that the measured wave height at Point 1 can be observed in the model at a different location, but close to Point 1. To check the influence of standing wave patterns on the modelled wave signals, the wave envelopes during the stationary part of the runs were examined. The envelopes for runs 1, 4, 8 and 9 are shown in Figure 5.8.

Additional information about the node antinode pattern and the theoretical envelope of the surface level motion can be found in Appendix H. The results have been summarized in Table 5.4, which includes maximum and the minimum water level at the whole area in front of the gravel slope. Only for Runs 8 and 9 the wave height values are up to 2 and 3m respectively. It should be mention that run 9 is the extreme case of a wall. Only in this case the wave height can be up to the measured value of 2.34m. The settings of this run are not realistic for a gravel slope. For the rest of the runs the wave heights are much lower than the measured value of 2.34m. This means that even if a region around Point 1 is examined still the measurements and SWASH out puts differ significantly.

Table 5.4 – The maximum and the minimum values for the water level envelope determined for the stationary part of the nine runs.

Run	Porosity (-)	Stone size (m)	Max envelope water level (m)	Min envelope water level (m)
1 (original)	0.40	6.750	0.87	-0.78
2	0.44	6.750	0.86	- 0.79
3	0.36	6.750	0.88	- 0.80
4	0.20	6.750	0.93	- 0.85
5	0.40	7.425	0.87	- 0.79
6	0.40	6.075	0.88	-0.79
7	0.40	10.125	0.88	- 0.79
8	0.40	3.375	1.11	- 0.98
9 (wall)	0.001	0.045	1.65	- 1.42
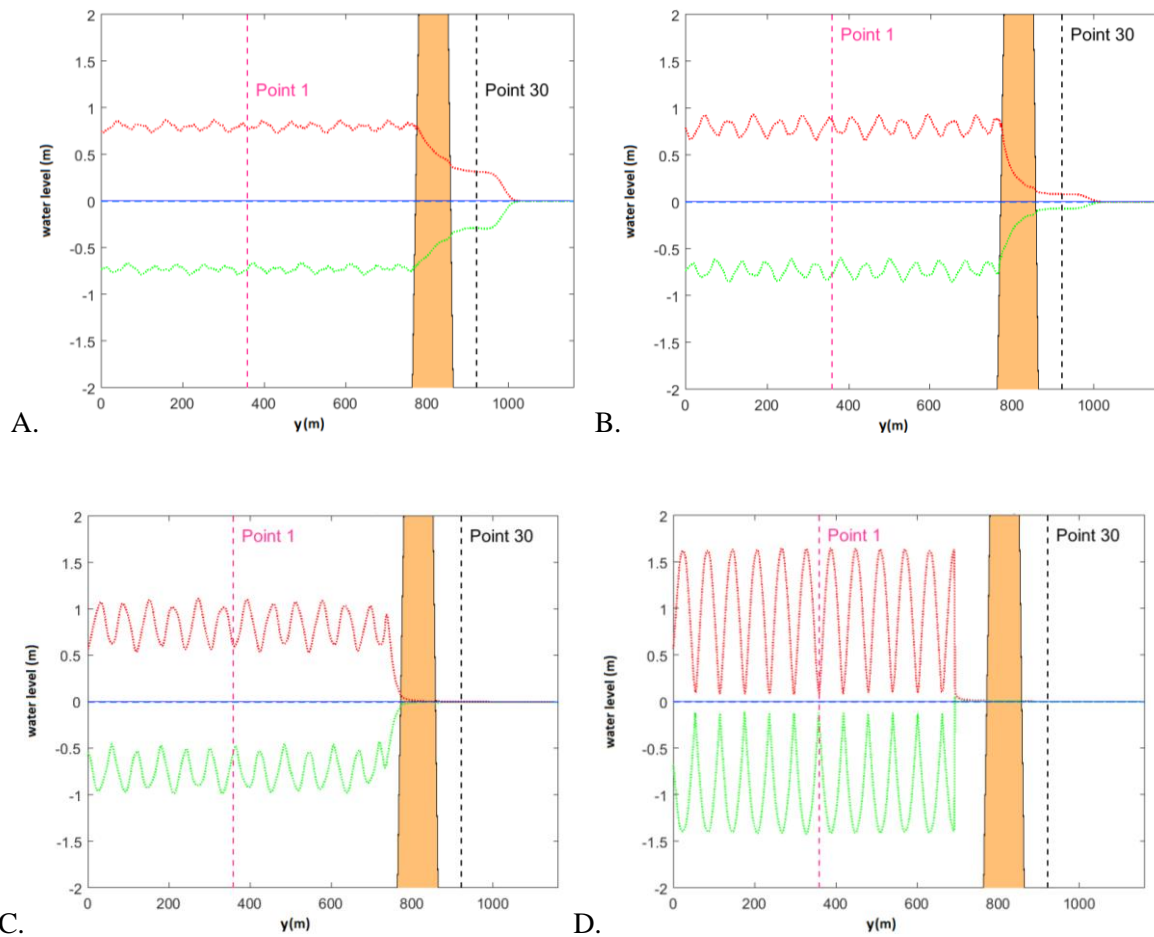
Figure 5.8 – The envelope of the water level during the steady state part for run 1 (original porosity and stone size, picture A), run 4 (picture B), run 8 (picture C) and run 9 (wall case, picture D).

5.4 Conclusions

In Chapter 5 sub-question 2a was assessed. It was examined whether the correct amount of reflection can be reproduced in SWASH, using the porosity and stone values from the scale model. The reflection off the outer slopes located outside the harbour was reproduced in a 1D SWASH model. In total 9 runs with different porosity and stone size settings were studied.

To evaluate the amount of reflection produced by SWASH the measured steady state wave height at Point 1 was compared to the respective value from the different SWASH runs. For all the runs the steady state wave height at Point 1 was lower than the measured value. Using the original porosity and stone size values the wave height was lower by 35%. For an increase or a decrease of the porosity or the stone size by 10%, the steady state wave height remained lower by 34 to 36%. Even for the extreme run of modelling the gravel slope as a concrete wall, the constant wave height at Point 1 is 92% lower than the measurements.

The next step was to examine if the measured wave height at Point 1 is observed in the SWASH model at a different location, but close to Point 1. For this purpose, the wave envelopes during the stationary part of the runs were examined. Only for the wall settings the wave height reaches up to the measured value at wave gauge 1. This observation indicates that another phenomenon apart from reflection at the outer gravel slope is influencing the wave record. It is assumed that the wave record at wave gauge 1 is influenced by the reflection off the head walls at the harbour entrance. This assumption is studied in detail in Chapter 7 .

To sum up, it was not possible to reproduce in SWASH the measured amount of reflection off an outer gravel slope, as according to SWASH results the measured records are likely to be influenced by other wave processes. The process that it is expected to also influence the water level time series in front of the outer gravel slope (e.g at wave gauge 1) is reflection off the head walls at the harbour entrance. Therefore, it is chosen to use in the SWASH simulations the porosity and stone size values of the physical scale model, converted to prototype scale. This choice is also supported by the results of the SWASH runs for different settings. By changing the porosity or the stone size by ±10% it was observed that the resulting steady state wave heights at wave gauge 1 differ in the order of centimetre. This shows that the created SWASH model is robust, as small changes in the gravel slope properties do not lead to noteworthy changes in the results.

5.5   Remarks

Taking into account the 1D SWASH results discussed in the chapter, the most important remarks regarding SWASH performance are summarised in this section. These remarks do not provide an answer to the research question, but they are useful knowledge about setting up a SWASH model.

- The energy of waves travelling through the outer gravel slope in the 1D SWASH model is damped. The wave amplitude for Point 30 behind the slope is approximately 2-3 times smaller than the incoming wave height in front of the slope. SWASH is able to dampen the energy of waves travelling through a gravel slope.

- For all the runs there in no standing wave pattern behind the gravel slope. This means that the wave energy transmitted though the gravel slope gets absorbed by the sponge layer. The sponge layer length is considered efficient.

Chapter 6 Reflection off the harbour end

The aim of this chapter is to answer a part of research Question 1 about the wave celerity in SWASH and a part of sub-question 2a about simulating the reflection at the harbour end with SWASH. For this purpose, a 1D SWASH model is created representing the cross section at the model centre line (Section 6.1).

Regarding Question 1, in Section 6.2 the wave celerity of individual waves in SWASH is determined and compared to the measurements. In Section 6.3 the fully developed wave height at the output location in SWASH is first compared to the measured value and afterwards to the wave height generated by the wave maker, which is prescribed at the offshore SWASH boundary. The ability of SWASH to reproduce the correct amount of reflection off the harbour end, examined in sub-question 2a, is treated in Sections 6.4 and 6.5. Section 6.4 presents the graphs with the vertical lines representing the arrival of reflected waves (determined in Section 3.3). Moreover, the qualitatively changes in the water level due to reflection are discussed. To evaluate quantitatively the SWASH results, the steady state wave height in SWASH due to reflection off the harbour end is compared to the measurements in Section 6.5. Finally, Section 6.6 summarises the conclusions based on the results presented in the chapter.

6.1   The 1D SWASH model for reflection off the harbour end

A one-dimensional SWASH model is set up representing a cross section at the model centre line AA' shown in Figure 6.1. This cross section includes the inner gravel slope and the concrete wall behind it. The aim of this 1D model is to provide insight about modelling of reflection off the harbour end. A sketch of the one-dimensional SWASH model is provided in Figure 6.2. The output locations along line AA' are the same as in the physical scale model (blue points in Figure 6.2). As a result, SWASH outputs can be compared to the measurements.
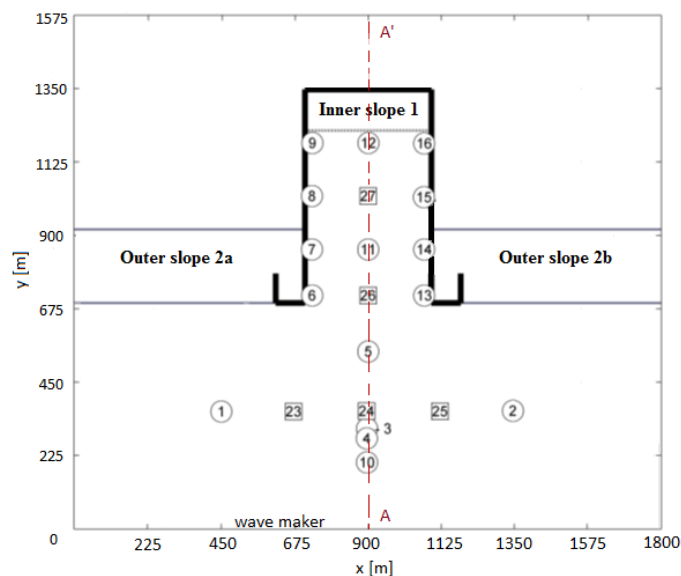
Figure 6.1 - Model centre line (AA') is located in the middle of the basin in terms of width. This figure is a repetition of Figure 3.9.

According to Section 5.4, the porosity and stone size values of the gravel slope in the physical scale model should be used in the SWASH simulations. The model set-up settings and the SWASH command file for this 1D model is presented in the Appendix H. It is worth mentioning that 2 vertical layers are used, as the tests kd values range from 0.55 to 3.95. According to the SWASH user manual

(The SWASH Team, 2016) and also Table 2.10, the use of two vertical layers leads to accurate results.
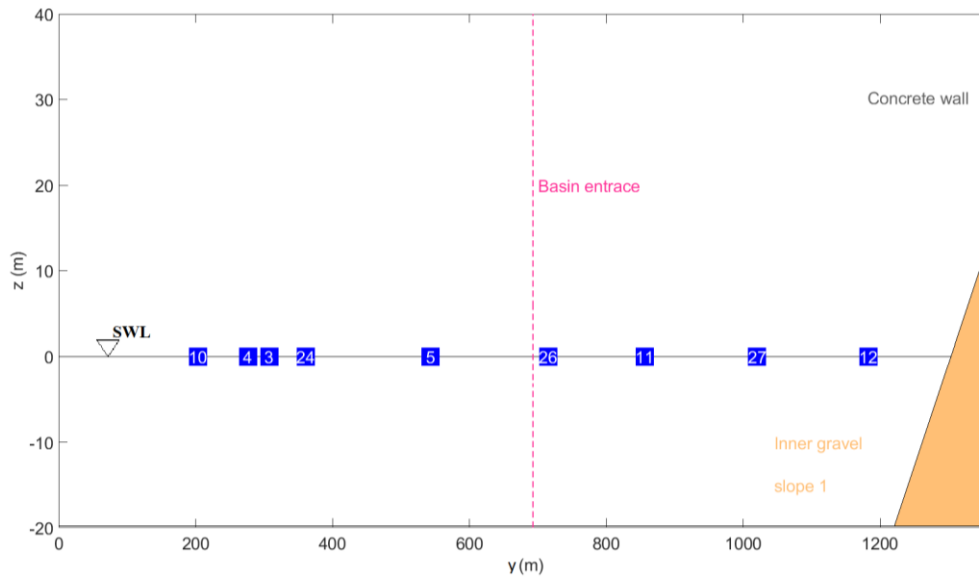
Figure 6.2 -Sketch of the 1D SWASH model representing a cross section in the middle of inner slope 1 and the concrete wall at the basin end. The output locations are specified with blue colour.

6.2   Computation of the wave celerity in the one-dimensional SWASH model

The one-dimensional SWASH model resembles a flume where waves propagate only in one direction. This is the most suitable SWASH model to verify if the wave celerity in SWASH is equal to the wave celerity in the measurements. To determine the wave celerity in SWASH, the approach discussed in Section 3.2.3 is applied. The same method was applied to determine the wave celerity in the measurements (Section 3.2.3 and Section 4.1). The method initially assumes that the waves follow the linear theory and the theoretical wave celerity in determined. The next step is to create graphs including all the water level time series at the output locations along line AA' shifted at Point 10. The agreement between the wave records is examined to verify if the initially assumption about linear waves hold and the theoretical celerity is equal to the celerity in SWASH.

6.2.1   Results for the first and the second group of tests

For the first and the second group of tests (Table 2.5 and Table 2.6), the graphs of the water level at the output locations along line AA' shifted at Point 10 can be used to confirm if the waves in SWASH are linear and their celerity is equal to the theoretical celerity. T003 and T012 belong to the first group of tests for low kd values, while test T001, T002 and T012 are included in the second group for average kd values. The time series shifted at Point 10 for T002 (Figure 6.3) is a typical example of the graphs created for the five tests. The rest of the graphs are presented in Appendix I.

In this section the most important observations for the five tests are discussed, taking into account the remarks for the calculation of the wave celerity in the measurements.

- The method provides good results for the five tests. The agreement of the wave height and the phase shift is examined for the time interval after the end of the taper function and before the arrival of the reflected waves (light brown vertical dashed line in Figure 6.3). As can be observed, for example, in Figure 6.3 for T002 the wave heights are in good agreement in the aforementioned time interval. Moreover, the phase shift between the time series of the different wave gauges is small or negligible. The same holds for the remaining four tests. Therefore, it is

65

verified that the wave celerity in SWASH is equal to the theoretical wave celerity calculated according to the linear wave theory. In Chapter 4 it was confirmed that the wave celerity in the measurements follows the linear theory for these five tests. Overall, for the tests with low or average kd value, the wave celerity in the measurements is equal to the wave celerity in SWASH.

- The behaviour of the taper function part is similar to the non-linear behaviour observed in the measurements. Again the taper function part travels faster than the theoretical wave celerity. Moreover, the wave amplitude decreases over the distance from the wave maker.

- The tests of the first group are classified to intermediate to shallow water waves. In the measurement analysis is it observed that the wave have the typical shallow water shape. This is the case also in SWASH: the wave crests are sharper and higher, while the troughs are smooth and elongated.

- For all the tests a steady state is reached. At a specific moment in time, which varies among the tests, the wave patterns are repeated. The wave crests and trough amplitude as wells as the phase shift between the different wave gauges signals remain constant. This was also the case in the measurements.
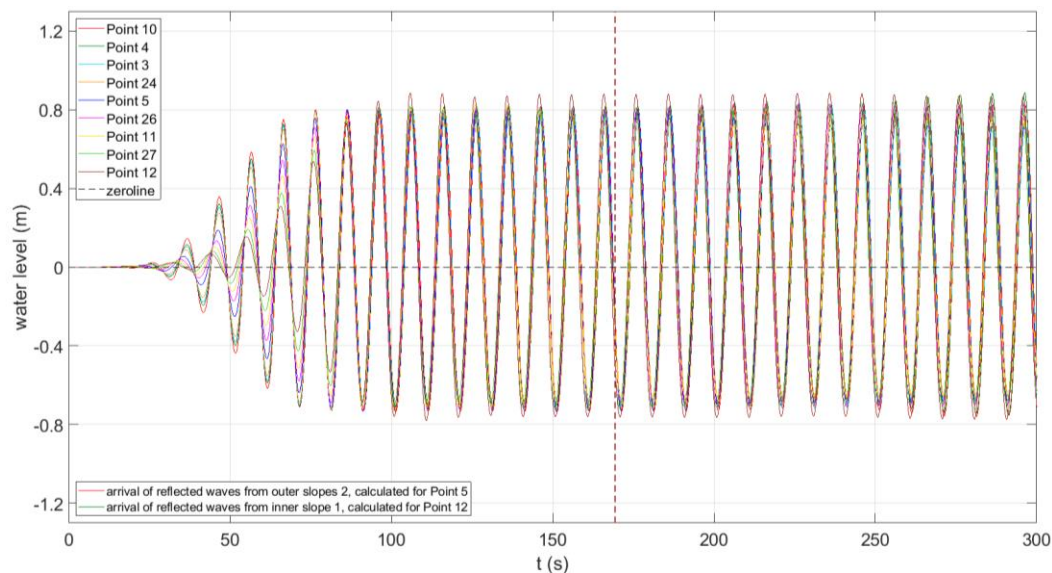
Figure 6.3 - T002, measured water level time series of points on Line AA' shifted earlier in time to match with Point 10.

6.2.2   The application limits of the method

In the measurements, the method of verifying the wave celerity by confirming the agreement of the wave signals shifted at the wave gauge 10 (Section 3.2.3) cannot be applied for all the tests T010 and T013. Both tests are classified to the third group of tests with high kd values in Table 2.7. Moreover, in T010 the wave height to wave length ratio exceeds the breaking limit and thus the waves are breaking.

In SWASH the method presented in Section 3.2.3 cannot be applied for T013, but can be used for T010.As shown in Figure 6.4, for T013 is difficult to detect sinusoidal individual waves. The picture creates the impression of chaotic wave field. In this case the non-linear effects are becoming important. The high kd value for this test (3.95) indicates the non-linear behaviour of the waves. On the contrary, in the graph for T010 the wave signals are in good agreement in terms of phase shift (Figure 6.5). However, for T010 the agreement in terms of wave height is not good as the wave height is decreased for an increasing distance from the wave maker due to wave breaking. As the distance of the point from the wave machine increases, the wave height is reduced. The incoming wave height for

T010 is 2.97m. Nevertheless, due to wave breaking the constant wave height at Point 12, which is the closest to the harbour end, is equal to 1.66m. Consequently, a wave with a height 56% lower than the incoming wave gets reflected at the harbour end. This wave height reduction can be related to the wave breaking which leads to loss of energy.

All in all, the aim of research Question 1 is to compare the wave celerity in the measurements to the celerity in SWASH. This cannot be done as the approach used to determine the celerity (Section 3.2.3) cannot be applied for the third group of tests (Table 2.7). In the measurements the method is not applicable for both tests T010 and T013 and in SWASH for T013.
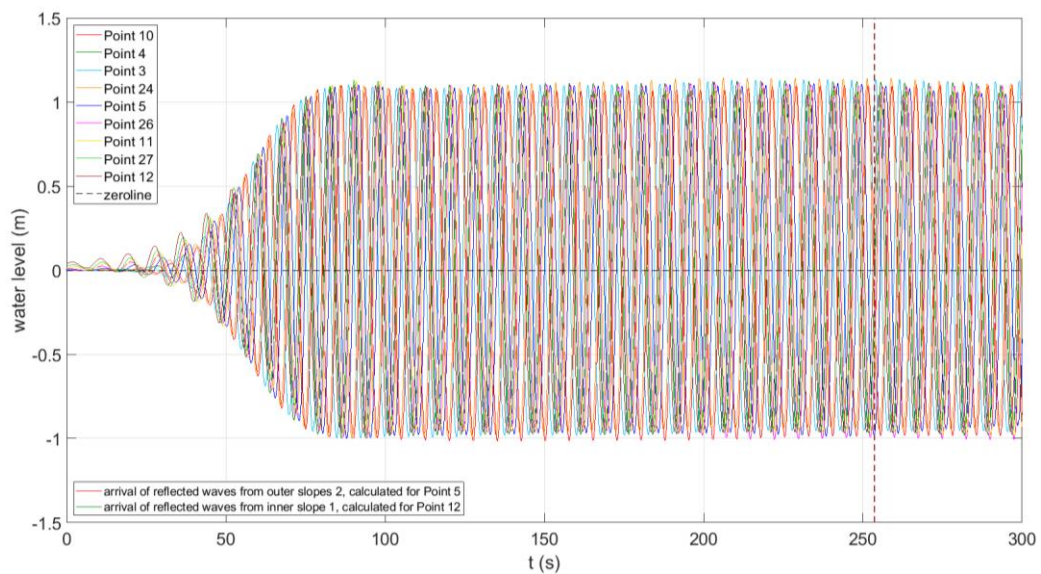
Figure 6.4- T013, measured water level time series of points on Line AA' shifted earlier in time to match with Point 10.
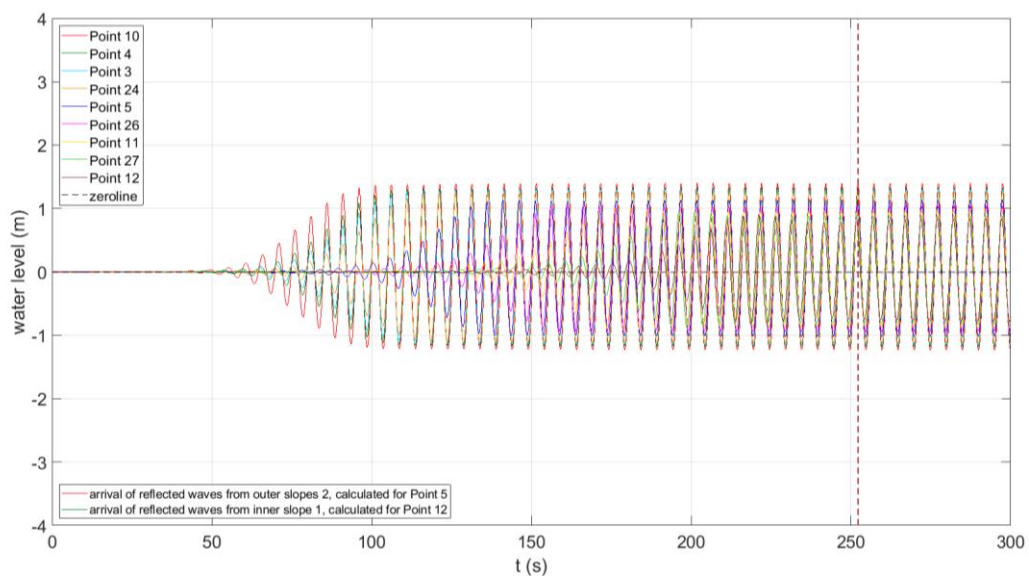
Figure 6.5 - T010, measured water level time series of points on Line AA' shifted earlier in time to match with Point 10.

An alternative method to compare the celerity in the measurements to the celerity in SWASH is presented here. This method is used only for T010 and T013. It was chosen to examine the water level time series only at Point 10 and 5. Point 10 is the closest to the wave maker, while Point 5 is the point outside the basin, which has the largest distance from the wave maker. The measured time series of those points and the time series in SWASH were synchronised based on the 1st zero-down crossing at

Point 10 (Moment 1a). The plots for T010 and T013 are shown in Figure 6.6 and Figure 6.7 respectively.
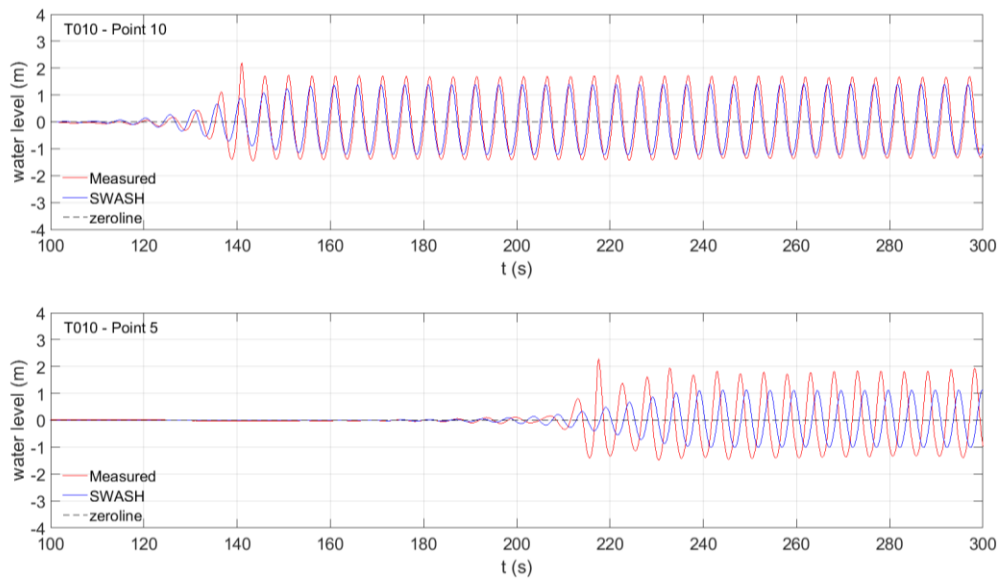
Figure 6.6 – The measured and the SWASH water level time series synchronised at the first zero-down crossing at Point 10, for T010.

For T010, at Point 10 there is a time shift between the measured and the modelled signal. So this means that the first part of the signal does not follow linear wave theory, as expected. However, also in the linear part the SWASH time series arrives after the measured signal. At Point 5 this delay becomes bigger and the two signals are almost out of phase. The required time shift increases from point to point going from the wave maker to the basin end. It can be supported that the celerity in SWASH is lower than the measurements celerity.
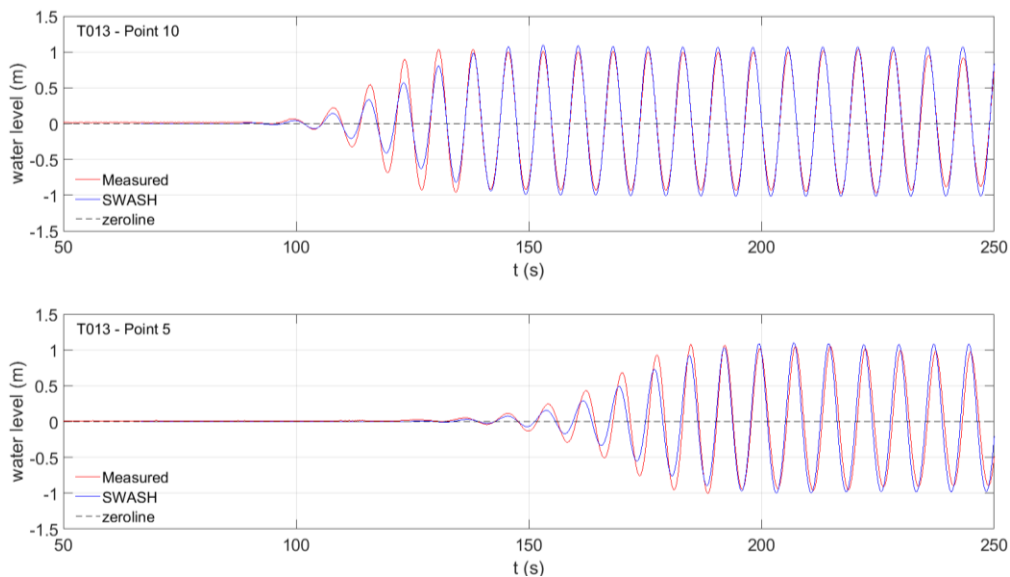
Figure 6.7 - The measured and the SWASH water level time series synchronised at the first zero-down crossing at Point 10, for T013.

For T013, the agreement between the measured and the SWASH water level time series is obviously better than for T010. At Point 10 after the end of the taper function part the two signals almost coincide. However, the taper function part in SWASH is smaller in amplitude than in the measurements. At Point 5 the SWASH signals is shifted relatively earlier in time. This time shift is

68

relatively small. It can be claimed that the agreement between the wave celerity in the measurements and the wave celerity in SWASH is sufficient.

6.3 Comparison of the fully developed incoming wave height in the measurements and in the 1D SWASH model

This section aims to compare the incoming wave height at the output locations outside the basin in SWASH to the measured incoming wave height and to the incoming wave height generated by the wave maker imposed at the offshore SWASH boundary. The incoming wave height at the output points is calculated using the time interval from Moment 1b (end of the taper function) to Moment 4a (arrival of reflected waves from inner slope 1). The results are shown in Table 6.1. It is worth mentioning that this in the only case that information about the fully developed wave height at Point 5 can be derived. This happens because in the 1D SWASH model the outer gravel slopes 2 are not included and the reflected waves off that slopes do not influence the record. Therefore, at Point 5 there is a sufficiently long time interval to determine the fully developed incoming wave height. The table also contains the standard deviation value for the incoming wave height at the five output points outside the harbour basin. The ratio in the last row of Table 6.1 expresses the difference of the mean measured incoming wave height and the mean incoming wave height computed with SWASH. The largest difference is observed for Test T010 in which the waves are breaking. For the rests of the tests the difference may vary from 5% to 8%. The values are considered acceptable taking into account the difficulty to describe numerically a monochromatic wave.

The fully developed incoming wave height generated from the wave maker is prescribed at the SWASH offshore boundary for each experiment. It should arrive at the output locations. As presented in Table 6.2, the difference between the fully developed incoming wave height entering the SWASH domain and the wave height calculated at the output locations is smaller than 8%, excluding tests T010. Thus the SWASH performance in describing the propagation of the simple monochromatic waves in the computational domain is considered sufficient.

Table 6.1 – Comparison of the incoming wave height at the output locations outside the harbour basin in the 1D SWASH model (representing reflection at the harbour end) to the measurements.

		T001	T002	T003	T010	T011	T012	T013
$H_{inc,SWASH}$ (m)	Point 10	1.08	1.52	2.55	2.62	3.25	2.83	2.08
	Point 4	1.08	1.52	2.48	2.49	3.24	2.86	2.08
	Point 3	1.07	1.52	2.47	2.43	3.23	2.85	2.08
	Point 24	1.07	1.51	2.55	2.33	3.23	2.89	2.08
	Point 5	1.07	1.52	2.52	1.90	3.20	2.87	2.07
$\overline{H}_{inc,SWASH}$ (m)		1.07	1.52	2.51	2.35	3.23	2.86	2.08
Std. deviation (m)		< 0.01	< 0.01	0.04	0.27	0.02	0.02	0.01
$H_{inc,measured}$ (m)		1.00	1.42	2.36	2.96	3.05	2.72	1.92
$\left\| \dfrac{\overline{H}_{inc,SWASH} - \overline{H}_{inc,measured}}{\overline{H}_{inc,measured}} \right\|$		7%	7%	6%	20%	6%	5%	8%

Table 6.2 - Comparison of the incoming wave height at the output locations outside the harbour basin in the 1D SWASH model (representing reflection at the harbour end) to the incoming wave height generated by the wave maker prescribed at the offshore SWASH boundary.

	T001	T002	T003	T010	T011	T012	T013
$\overline{H}_{mean,SWASH}$ (m)	1.05	1.50	2.48	1.92	3.16	2.85	2.05
$H_{inc,wave\ maker}$ (m)	0.99	1.44	2.39	2.97	3.02	2.75	1.94
$\dfrac{\left\|\overline{H}_{inc,SWASH} - H_{inc,wave\ maker}\right\|}{H_{inc,wave\ maker}}$	8%	5%	5%	21%	7%	4%	7%

6.4 Comparison of the measured water levels to the SWASH outputs

To begin with, in this section the wave height changes in the SWASH time series are related to the characteristic moments in time described in Section 3.2.5 These moments indicate the arrival of the incoming and the reflected waves in the measured signal at the wave gauges and can also be applied on the time series produced from the 1D SWASH model (Section 6.1). The method is applied only for the first and the second group of tests (Table 2.5 and Table 2.6) for which the wave celerity has been determined in Chapter 6. For the third group (Table 2.7) of tests only the beginning and the end of the taper function is determined. Subsequently, the time series produced from the 1D SWASH model are compared to the measured time series in the physical model. The results for the wave gauges out of the basin and the gauges inside the harbour basin are discussed separately. For a full overview of the water level time series for all the five examined tests the reader is referred to Appendix E.

6.4.1 Output points outside of the harbour basin

The modelled water level time series show similar trends. Figure 6.8 shows a typical example of a produced time series. In all cases, from the first measured zero crossing (Moment 1a) the water level increases until the end of the taper function at Moment 1b. From Moment 1b to 4a the wave height remains constant. The water level start changing after Moment 4a and the changes are more distinguishable after Moment 4b. If at the wave gauge location the incoming and the reflected wave are in phase the wave height is increased. In contrast, if they are out of phase the total wave height is decreased. This is the case at Point 24 presented in Figure 6.9. The wave height changes also after Moments 6a and 6b. These are the moments defining the arrival of the re-reflected wave that has got reflected for the second time at the wave machine. This is change in the wave height is clearly visible at a certain location for T001 (Figure 6.9). For all the cases, after moment 7b a steady state has been developed, as the wave patterns remain constant.
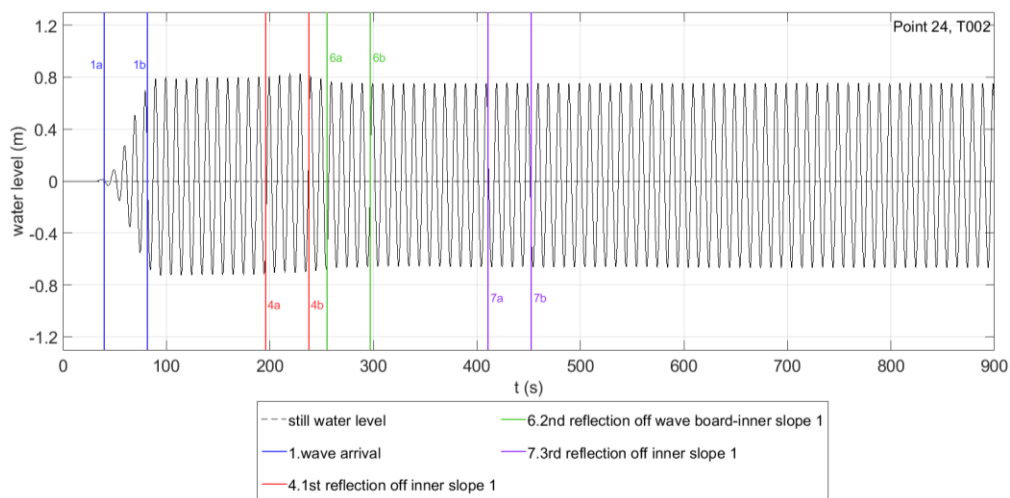
Figure 6.8 - The water level time series generated by SWASH at Point 24 for test T002.

70

To compare the measurements to the SWASH outputs the two time series are plotted in the same graph for all output locations. Two characteristic plots are shown in Figure 6.9 and Figure 6.10. The measured and the SWASH time series are synchronised on Moment 1a, which shows the first zero-down crossing. Moments 4b, 6b and 7b are calculated based on the wave celerity and the locations of the inner slope and the wave board. As the wave celerity and the model geometry are the same in the physical model and in the SWASH model, the characteristic vertical lines for the measured signal and for the SWASH outputs coincide. Focusing on Figure 6.9 it is observed that the measured wave height is fully developed (140<t<200s) and then it increases until Moment 4a. This increase occurs before the arrival of reflected waves form the inner slope (Moment 4a) and thus can be attributed to the reflection off the harbour head walls and the outer slopes 2. As both structures are not included in the SWASH model this change is not shown in the model signal. From Moment 6a and 6b both in the measurements and in SWASH the wave height is decreasing. In both time series a steady state is reached after Moment 7b. However, the wave height in SWASH is significantly lower. In Figure 6.10 some common features can be observed. Firstly, the decrease in the wave height from t=150s to 200s is not shown in the measurement as it is expected to result from reflection at structures which are not included in the SWASH model. Secondly, the measured and the modelled steady state wave height are not in agreement. In this case the wave height in SWASH is higher.
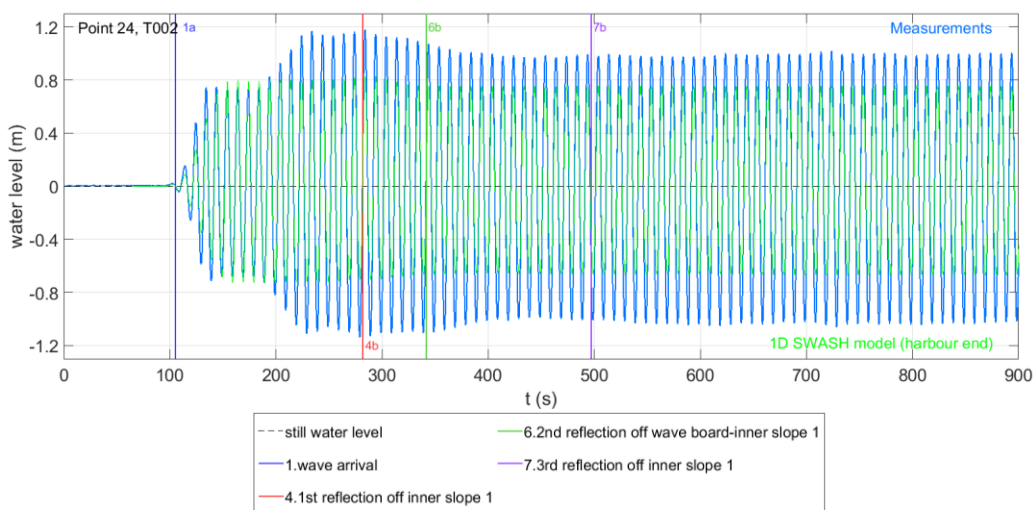
Figure 6.9- The measured water level time series and the time series generated by SWASH at Point 24 for test T002.
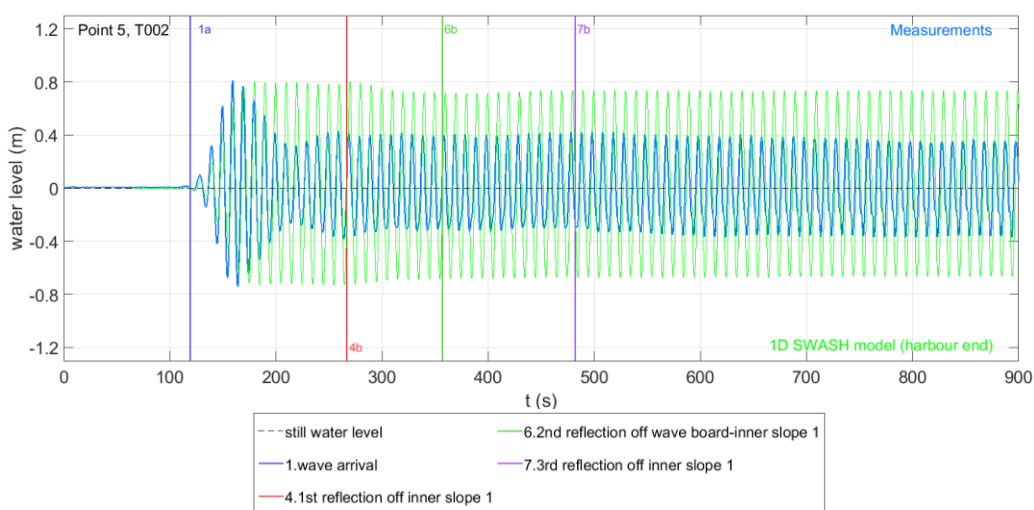
Figure 6.10- The measured water level time series and the time series generated by SWASH at Point 5 for test T002.

6.4.2 Output points inside the harbour basin

A typical example of the water level time series inside the harbour basin is shown in Figure 6.11. The first measured zero crossing occurs at Moment 1a and the water level increases until the end of the taper function at Moment 1b. From Moment1b to 4a the wave height does not remain constant. This can be related to the non-linear taper function behaviour. The further away from the wave maker, the lower the wave amplitude is. After Moment 4b, the water level start increase/reduction is clearly distinguishable. If at the wave gauge location the incoming and the reflected wave are in phase the wave height is increased. In contrast, if they are out of phase the total wave height is decreased (Figure 6.11). For all the cases, after Moment 7b a steady state has been developed, as the wave patterns remains constant.
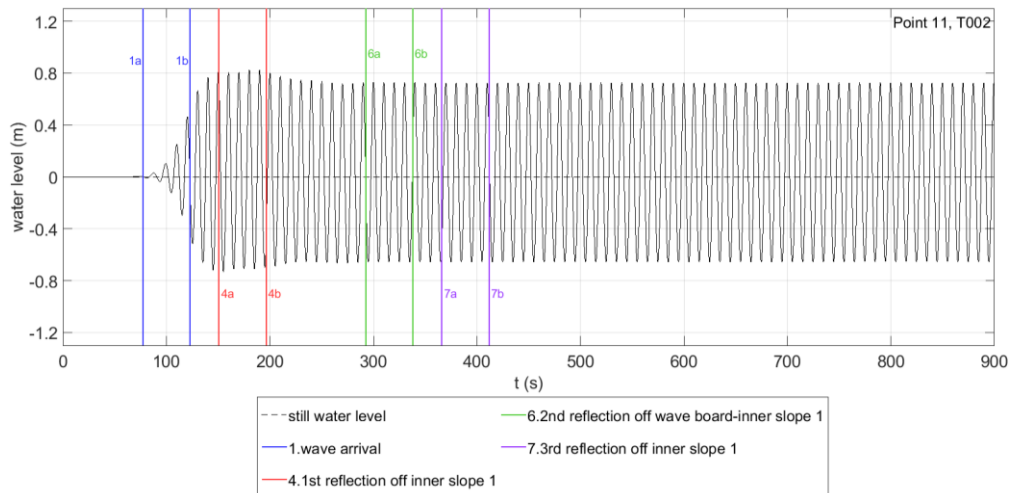
Figure 6.11 - The water level time series generated by SWASH at wave gauge 11 for test T002.

For some of the points inside the basin the duration of the wave record describing only the incoming wave height is not always long enough (for most of the tests Point 27) or there is no such time interval (observed at Point 27, see Figure 6.12 and also for Point 12). In Figure 6.12, Moment 4a occurs simultaneously with Moment 1b .This means that the reflected taper function wave arrives before the incoming wave can be fully developed.
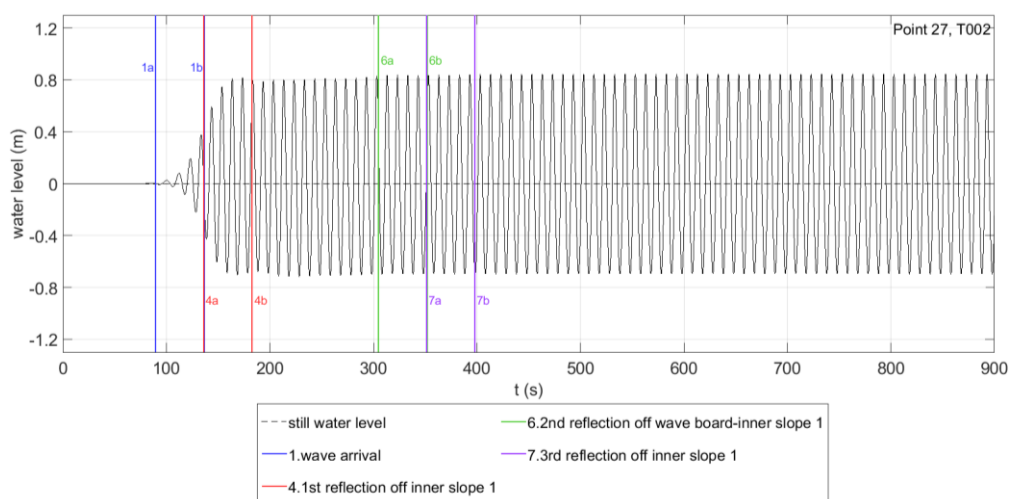
Figure 6.12 - The water level time series generated by SWASH at wave gauge 27 for test T002.

To investigate the agreement between the measurements and the SWASH outputs the respective time series are plotted in the same graph for all output locations. Figure 6.13 and Figure 6.14 present the measured and the modelled water level time series for Points 11 and 27. In Figure 6.13 the agreement

between the measured and the SWASH time series is good in terms of wave height. This means that reflection off the harbour end plays an important role in the final wave height inside the harbour. Taking a closer look at the time series before Moment 4a the measured wave height is lower. This small deviation can be explained by the influence of diffraction in the measurements which is not modelled in this 1D SWASH model. For Point 27 (Figure 6.14) the agreement in terms of wave height is relatively lower than for Point 11(Figure 6.13). However, it still considered sufficient taking into account that the standing wave patterns are influenced by the exact location of the point (see also Section 5.3.1).
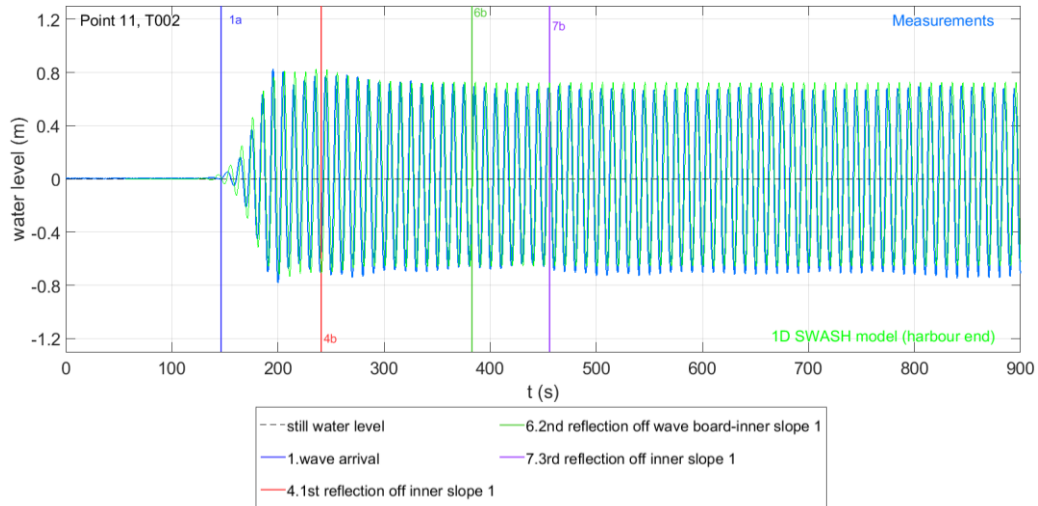
Figure 6.13 - The measured water level time series and the time series generated by SWASH at Point 11 for test T002.
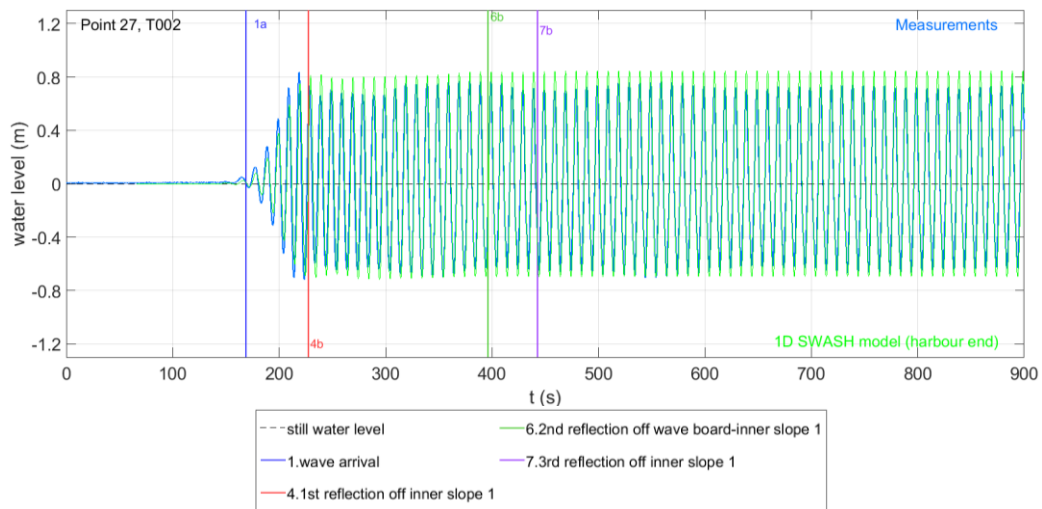
Figure 6.14 - The measured water level time series and the time series generated by SWASH at Point 24 for test T002.

6.5 Comparison of the steady state wave height in the measurement and in SWASH

In this section the final steady state wave height in the measurements will be compared to the respective value in the SWASH model. The values at the points along the model centreline (Figure 3.9), which were included in the 1D model are compared. It should be kept in mind that the only wave process included in the SWASH model is reflection off the harbour end. This comparison is done to quantify the influence of reflection off the harbour end in the total wave penetration.

As discussed in Section 1.3 , there are more wave processes involved. Outside the harbour basin reflection off the harbour head walls and off the outer gravel slopes 2 are influencing the record. Moreover, in Section 5.4 it was concluded that the reflected waves from harbour head walls are probably playing the most important role in the wave field outside the harbour .This assumption will be tested in Chapter 7. Inside the harbour diffraction is expected to influence the records. Therefore, it is expected that only a part of the total wave penetration can be attributed to reflection off the harbour end.

Table 6.3 and Table 6.4 contain the average wave height at the steady state situation (after Moment 7b) both for the measurement and SWASH simulations. For the seven selected tests, the wave height is calculated at the wave gauges along line AA'. Moreover, the differences between the values in the measurement and in SWASH are included. The difference percentage is calculated according to the following equation:

$$\text{Difference}(\%) = \frac{\bar{H}_{\text{steady state,measured}} - \bar{H}_{\text{steady state,SWASH}}}{\bar{H}_{\text{steady state,measured}}} * 100 \tag{6.1}$$

It is shown that the highest differences occur for the points outside the basin. This indicates that the water level outside the basin is mainly influenced by other processes, such as the reflection off the harbour head walls and the outer gravel slope. According to Section 5.4, the influence of reflection at the harbour walls is expected to be higher than the reflection at the gravel slope.

On the contrary, the difference percentages for the gauges inside the basin are lower. The maximum percentages range from 12.1% for T001 to 40.4% for T010. The high value for T010 can be related to the wave breaking occurring during the test, which is a complex phenomenon and difficult to be modelled accurately. The results show that the wave field inside the basin is significantly influenced by the reflection at the harbour end. However, the differences are not small enough to assume that the role of diffraction is not important.

Table 6.3 – Comparison of the steady state wave height in the measurements and in the 1D SWASH model simulating reflection at the harbour end for T001, T002, T003 and T010.

	Wave gauge	T001 Measured $H_{steady\ state}$	T001 SWASH $H_{steady\ state}$	T001 Difference (%)	T002 Measured $H_{steady\ state}$	T002 SWASH $Hs_{teady\ state}$	T002 Difference (%)	T003 Measured $H_{steady\ state}$	T003 SWASH $Hs_{teady\ state}$	T003 Difference (%)	T010 Measured $H_{steady\ state}$	T010 SWASH $Hs_{teady\ state}$	T010 Difference (%)
O U T S I D E	10	1.07	1.09	2.5	1.22	1.60	31.3	1.35	2.31	70.8	2.38	2.71	13.9
	4	1.24	1.17	6.0	1.76	1.67	4.9	3.21	2.42	24.6	2.35	2.51	6.5
	3	1.02	1.11	9.3	1.95	1.39	28.8	2.04	2.09	2.9	4.26	2.44	42.8
	24	1.13	1.16	2.7	2.03	1.42	30.0	3.60	2.91	19.2	2.61	2.47	5.2
	5	1.16	1.00	13.2	0.74	1.40	90.1	2.88	2.24	22.3	4.38	2.09	52.3
		Max percentage Outside		**13.2**	Max percentage Outside		**90.1**	Max percentage Outside		**70.8**	Max percentage Outside		**52.3**
I N S I D E	26	1.09	1.07	1.5	1.40	1.38	1.2	2.65	2.72	2.5	3.337	1.990	40.4
	11	1.19	1.05	12.1	1.38	1.54	11.4	2.72	2.22	18.1	2.752	1.790	35.0
	27	1.02	1.05	2.4	1.34	1.65	22.9	2.17	2.59	18.9	2.827	1.768	37.5
	12	1.06	1.11	4.4	1.84	1.53	16.7	2.83	2.58	8.8	2.742	1.662	39.3
		Max percentage Inside		**12.1**	Max percentage Inside		**22.9**	Max percentage Inside		**18.9**	Max percentage Inside		**39.3**

Table 6.4 - Comparison of the steady state wave height in the measurements and in the 1D SWASH model simulating reflection at the harbour end for T011, T012 and T013.

	Wave gauge	T011 Measured $H_{steady\ state}$	T011 SWASH $H_{steady\ state}$	T011 Difference (%)	T012 Measured $H_{steady\ state}$	T012 SWASH $Hs_{teady\ state}$	T012 Difference (%)	T013 Measured $H_{steady\ state}$	T013 SWASH $Hs_{teady\ state}$	T013 Difference (%)
O U T S I D E	10	4.58	3.23	29.4	4.13	3.02	26.9	2.37	2.14	9.7
	4	1.30	3.22	148.7	1.61	3.11	93.4	2.36	2.22	5.8
	3	4.65	3.21	31.0	4.17	2.97	28.7	1.71	2.11	23.0
	24	4.90	3.26	33.5	1.28	2.88	125.0	2.11	2.21	4.7
	5	4.72	3.19	32.5	4.30	2.66	38.1	2.01	1.96	2.4
		Max percentage Outside		**148.7**	Max percentage Outside		**125.0**	Max percentage Outside		**23.0**
I N S I D E	26	2.98	3.35	12.7	3.92	2.83	27.9	2.12	2.10	1.0
	11	3.23	3.13	3.2	2.05	2.82	37.6	2.07	2.06	0.5
	27	2.70	3.20	18.7	2.60	2.65	1.5	2.14	2.03	4.9
	12	2.44	3.28	34.1	2.76	3.23	17.4	1.77	2.02	14.1
		Max percentage Inside		**34.1**	Max percentage Inside		**37.6**	Max percentage Inside		**14.1**

6.6   Conclusions

In this Chapter a part of research question 1 and a part of the sub-question 2a are assessed. To answer the questions a group of simulations for the seven selected tests were performed in a 1D SWASH model reproducing the reflection off the harbour end (i.e. off the inner gravel slope and the concrete wall behind it). The conclusions regarding each question are discussed separately.

The objective of research question 1 is to examine whether the wave celerity in the measurements is equal to the wave celerity in SWASH. The method of examining whether the wave celerity is equal to the celerity according to linear theory (Section 3.2.3) was applied on the SWASH results. It was found that the method can be used only for the tests with low or average kd values (kd<3) and for non-breaking waves. Thus, for the five examined tests (first and second group in Section 2.3) the agreement of the wave signals shifted at the wave gauge 10 was confirmed. For these tests there is a good agreement between the wave signals in terms of wave height and phase shift. Therefore, it can be concluded that for the tests with low or average kd values (kd<3) and for non-breaking waves the wave celerity in SWASH is equal to the wave celerity calculated according to the linear wave theory. According to Chapter 4, the wave celerity in the measurements is equal to the theoretical wave celerity. Finally, it can be concluded the wave celerity in SWASH is equal to the wave celerity in the measurements.

However, for tests with high kd value (kd>3) two tests were examined: T010 for breaking waves and T013 for non-breaking waves. For these tests an alternative approach was applied: the measured and the SWASH water level time series were directly compared without assuming that linear theory holds. It was concluded that for breaking waves the wave celerity in SWASH was significantly lower than the measured value. For non-breaking waves the agreement between the measured celerity and the celerity computed in SWASH was sufficiently good.

All in all, for kd values lower than 3 and non- breaking waves, the wave celerity in the measurements is equal to the celerity in SWASH and also follows the linear theory. For kd values higher than 3 and non-breaking waves the agreement between wave celerity in the measurements and the wave celerity calculated by SWASH is sufficiently good, even though the linear theory does not hold. Finally, for kd values higher than 3 and breaking wave the wave celerity in SWASH is significantly lower than the measured celerity.

It is important to mention that the proposed methodology initially assumes a value for the wave celerity and then this value is confirmed by visual inspection. The same technique was applied on the measurement and on SWASH results. As the method requires visual inspection it is not possible to give an error percentage for the wave celerity in the measurements and in SWASH. Thus, the answer to the research question 1 about how accurate can SWASH model the wave celerity of individual waves cannot be a percentage.

Apart from the wave celerity, research question 1 also refers to the ability of SWASH to describe wave propagation and the incoming wave height. In this Chapter it was shown that in a simplified 1D SWASH model the incoming wave height measured by the wave gauges matches the respective value in SWASH. Moreover, from the comparison of the 1D SWASH results to the measurements a few similarities are observed. The figures which include all the wave signal plotted at Point 10 for the measurement and for SWASH show some common features: the taper function behaviour, the shallow water wave shape and the final steady state developed at every wave gauge. Therefore, SWASH is able to describe important aspects of wave propagation observed also in the measurements.

Sub-question 2a focuses on the ability of SWASH to reproduce the correct amount of reflection off the harbour end. The porosity and stone size used in the 1D SWASH model are the values from the physical scale model, as chosen in Chapter 5. The changes in the wave records after the arrival of

reflected waves were judged qualitatively. The arrival of reflected waves (Moments 4a, 4b, 6a and 6b) is visible at the wave records as the wave height changes slightly or significantly depending on the location of the wave gauge. After plotting the measured water level time series and the respective SWASH outputs in the same graph it was observed that the agreement in terms of wave height is better for the points inside the harbour basin.

As discussed in Chapter 5, it is not possible to quantify the amount of reflection in the measurements as they are also influenced by other processes. However, the constant, steady state wave height for the measurements and in SWASH are compared to examine the relative importance of each process. The differences for the points outside the basin were larger indicating that reflection off the harbour head walls and reflection off the outer gravel slopes influence more the water level outside the basin. This conclusion is in agreement with the assumption made in Section 5.4 that reflection off the harbour head walls is probably the dominant process outside the harbour basin. This is assumption will be examined in Chapter 7.

On the contrary, the differences inside the basin are smaller. The reflection off the harbour end plays an important role in the wave field inside the harbour basin. The process of diffraction is also expected to influence the wave penetration inside the harbour. The role of diffraction inside the harbour will be studied in Chapter 7.

Chapter 7 The role of diffraction inside the harbour and the influence of reflection outside the harbour

This chapter aims to provide an answer to sub-question 2a, referring to the influence of diffraction on the wave height changes in the main harbour basin. Moreover, the influence of reflection off the concrete harbour head walls in the area outside the harbour basin is also studied in detail. As discussed in Chapter 5 and 6, this wave process is expected to be dominant outside the harbour basin, even at locations outside the cone of influence based on the linear wave theory.

Section 7.1 presents the two-dimensional SWASH model created to demonstrate the influence of both phenomena. Subsequently, in Section 7.2 the trends in the measured water level time series are compared to the respective SWASH outputs. In Section 7.3 the incoming wave height at the output location in SWASH is compared to the respective measured value and to the incoming wave height generated by the wave maker, defined as input file in SWASH. Section 7.4 presents the change of the steady state wave height at the different output locations in the SWASH model. Furthermore, the steady state wave height values in the measurements and in the 2D SWASH model are compared in Section 7.5 . Lastly, Sections 7.6 and 7.7 summarise the conclusions and the remarks of the chapter respectively.

7.1   The simplified 2D SWASH model

To simulated only the influence of diffraction inside the harbour, the inner gravel slope and the concrete wall at the end of the harbour (Figure 1.1) are not included in the simplified 2D model. Moreover, the gravel slopes 2a and 2b as well as the gravel slopes 3a and 3b (Figure 1.1) are not included in the model domain to guarantee that only reflection off the harbour head walls will influence the area outside the harbour. The simplified 2D SWASH model includes only the side concrete walls and the head walls at the harbour basin entrance, as depicted in Figure 7.1. It is named 'simplified' 2D model to differentiate it from the full layout 2D SWASH model studied in Chapter 8.
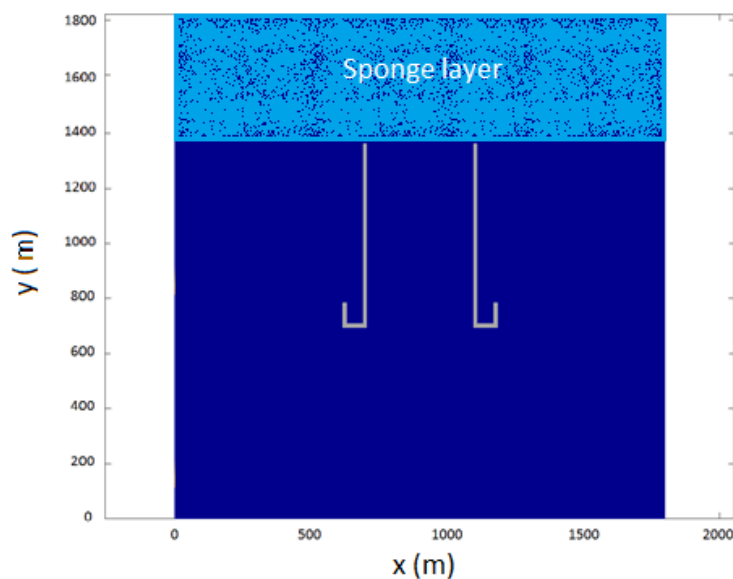
Figure 7.1 - Sketch of the simplified 2D SWASH model

According to Section 5.5 , the sponge layer with a length of 225m is proven efficient to absorb the wave energy behind the o outer gravel slope 2a. However, in this case the waves are not damped at a gravel slope before leaving the domain. Thus, the sponge layer length is doubled to guarantee the absorption of the waves. The sponge layer has a length of 450m. The number of waves that fit in the sponge layer for each test is included in Table 7.1.

Table 7.1 -The number of waves that fit in the sponge layer for all the selected tests.

Test	Wave length L (m)	Ratio $L_{sponge\ layer}/L$
T001	80.48	5.6
T002	120.74	3.7
T003	225.59	2.0
T010	39.38	11.4
T011	104.71	4.3
T012	197.05	2.3
T013	31.52	14.3

The model settings and the command file for SWASH in presented in Appendix F. As discussed in Section 6.1 , 2 vertical layers are used.

In Section 5.3 , it was observed that the wave amplitude at Point 1 calculated by the 1D SWASH model, simulating only reflection off the outer gravel slope 2a is significantly lower than the measured wave amplitude. It was hypothesised (Section 5.4) that the measured water level at wave gauge 1 is likely to be influenced more by reflected waves coming from the harbour head walls than by reflected waves coming from the outer gravel slopes.

In Figure 7.2, the theoretical cone of influence of the reflection is indicated by the red lines. Assuming linear theory, the reflected waves from the head walls are spread by an angle of 15° due to diffraction. To check if the area in front of the outer slope 2a is indeed influenced by reflected waves coming from reflection at the adjacent head walls, additional output locations have been defined. These are points 28, 29 and 31 to 35, specified with light blue colour in Figure 7.2 . Points 34 and 35 located in front of the head wall are expected to be mainly influenced by reflection. Points 31 and 32 are expected to be influenced due to diffraction of reflected waves. It needs to be verified if reflection off the head wall plays an important role at Points 1, 28, 29 and 33, located outside of the theoretical zone of influence.

To obtain an overview of the wave field in the harbour basin 23 extra points have been added inside the harbour. The purpose of these points is to check how the wave height differs at various locations in the harbour. The twelve wave gauges in the physical scale model (6-9, 11-16, 26 and 27 designed with purple colour in Figure 7.2) form a rectangular grid inside the basin. The additional points (40-62) are located on the vertices of a refinement of the existing grid. This results in 5 lines of output locations parallel to the basin length and 7 lines parallel to the basin width. The exact locations of all the additional points (29-35 and 40-62) can be found in the command file for the simplified 2D SWASH presented in Appendix L (Section L.2.1). Finally, Figure 7.3 shows the output locations in the 2D simplified SWASH model.
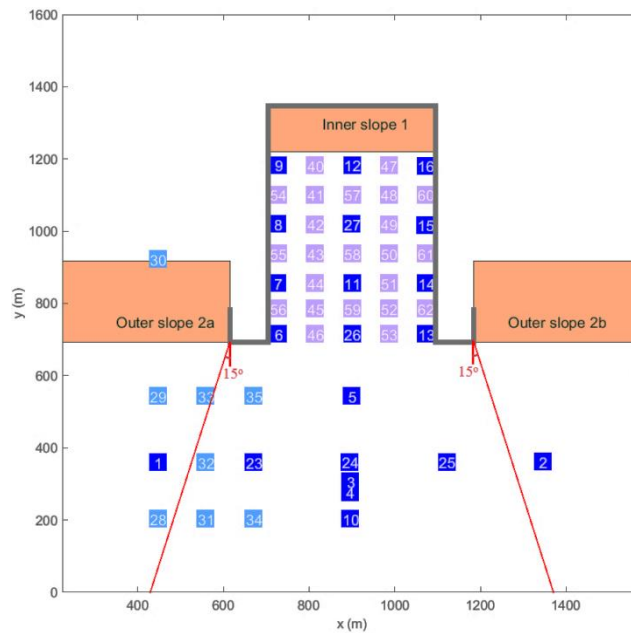
Figure 7.2 – Sketch of the full layout 1 with the output points in SWASH. The locations of wave gauges in the physical model are designed with blue colour. The extra points to check the influence of reflection at harbour head walls are designed with light blue colour. The additional output locations inside the harbour are designed with purple colour. The red line indicates the area influenced by the reflected waves from the harbour head walls.
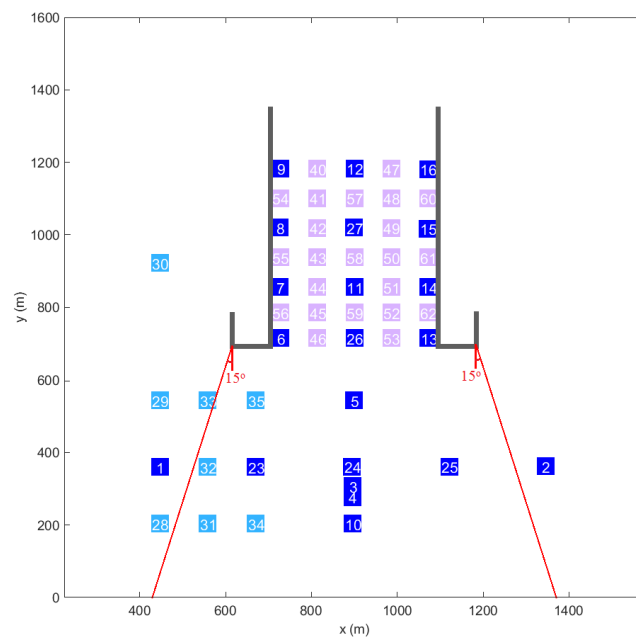
Figure 7.3 – The output locations in the 2D simplified SWASH model.

7.2   Comparison of the measured water levels to the SWASH outputs

The method described in Section 3.2.5 to calculate of the characteristic moments in time of the arrival of the incoming and the reflected waves at the wave gauges is also applied on the time series produced from the simplified 2D SWASH model. It should be noted that the method is applied for the 1st and the 2nd group of tests (Table 2.5 and Table 2.6) for which the wave celerity has been determined in Chapter 6. For the 3rd group (Table 2.7) of tests only the beginning and the end of the taper function is determined. After determining the first zero-down crossing (Moment 1b) in the water level time series at each point produced by SWASH the measurements and the SWASH outputs can be plotted in the same graphs and the two time series can be compared.

The output points outside the basin are expected to be influenced by reflection, while the points inside the basin are expected to be influenced by diffraction and not by reflection. The results of the aforementioned two groups of points are discussed separately. For a full overview of the water level time series for all the seven examined tests the reader is referred to Appendix J.

7.2.1 Output points outside of the harbour basin

The most important changes in terms of wave height occur from moment 2a until moment 2b (see for example Figure 7.4). These moments describe the arrival of the reflected waves from the head walls. The wave height increases or decreases depending on whether the incoming and the reflected wave enhance or cancel out each other. For all the points the water level changes are major for moments 2a and 2b. The second largest changes in the wave amplitudes occur in between moments 3a and 3b, which corresponds to the arrival of the re-reflected waves coming from the wave board.

Figure 7.4 – The water level time series generated by the 2D simplified SWASH model at Point 24 for test T002.

The graphs including the measures time series and respective SWASH time series are created by synchronising the Moment 1a in the measured signal with the Moment 1a determined in SWASH time series (see for example Figure 7.5 and Figure 7.6). As described in Section 3.2.5 Moment 2b represents the arrival of reflected waves from head walls, Moment 3b the arrival of the waves after the 2nd reflection at the wave board and Moment, 5b of the waves after the 3rd reflection on the head walls. The calculation of these moments depends on the wave celerity and on the head walls and wave board location. As the wave celerity in the measurements is equal to the celerity in SWASH (Section 6.6) and the geometry in the physical model and in the SWASH model are the same, the vertical lines 2b, 3b and 5b in the measurements and in SWASH coincide. Moreover, the SWASH outputs of the 1D model representing reflection at the harbour end are also included in the graph (see for example Figure 7.5 and Figure 7.6). By doing so, the influence of reflection off the harbour head walls (simulated by the simplified 2D model) and the influence of reflection off the harbour end (simulated by the 1D model) can be examined in comparison to the measurements.

When comparing the three time series in Figure 7.5, it follows that the observed changes in the measurements can better be explained by the time series of the 2D simplified model simulating reflections coming from the head wall than by the time series of the 1D SWASH model simulating reflections coming from the inner slope. According to Figure 7.5, the measured wave height and the wave height produced by the 2D simplified SWASH model increases after t-200s and then decreases until it reaches a constant state after Moment 5b. The wave height values in the "D SWASH time series are relatively lower than the measured values. However, the agreement between the measurements and the 2D simplified SWASH model output is much better than the agreement between the measurements and the 1D SWASH model simulating the reflection off the harbour end

(inner slope 1 and concrete wall). This observation indicates that the reflection at the harbour head walls plays a more important role in comparison to the reflection at the inner slope 1 at the wave gauges outside the basin in centreline AA'.
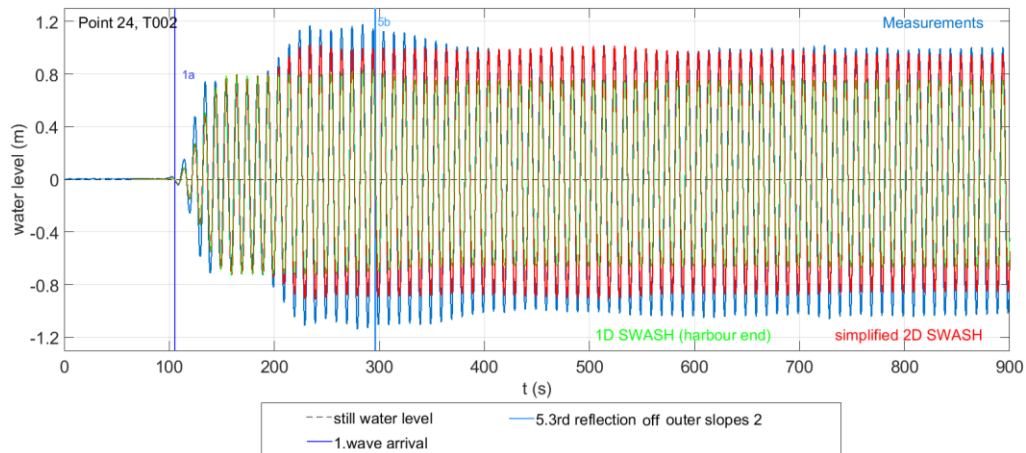
Figure 7.5 - T002, Point 24: Comparison of the measured water level time series to the simplified 2D SWASH outputs and also to the 1D SWASH (simulating reflection at the harbour end) model outputs.

Similar behaviour is observed for Point 5 (Figure 7.6). The 2D SWASH model time series follows the measured one, as it also decrease after Moment 2b and remains constant after Moment 5b. Again the agreement between the measurements and the 2D simplified model outputs is visibly better than the agreement between the measurements and the 1D model outputs
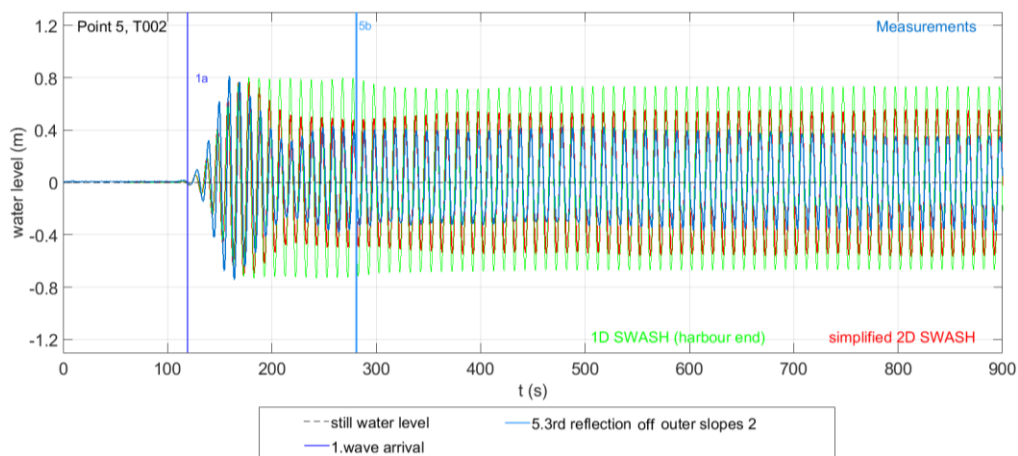
Figure 7.6 - T002, Point 5: Comparison of the measured water level time series to the simplified 2D SWASH outputs and also to the 1D SWASH (simulating reflection at the harbour end) model outputs .

A problem observed for the tests of the 3rd group (T010 and T013) is that the wave pattern does not remain constant at the end of the time series. For the rest of the tests after this moment a steady state is developed. However, this is not the case for T010 and T013. For example, for T010 and T013 at wave gauge 5, after approximately t=600s, the wave height starts to decrease (pictures A. and B. of Figure 7.7). This behaviour indicates that there is a numerical error in the calculation of the constant waves. The error of the next time step is added to the previous error. Therefore, the total error is increasing in time.
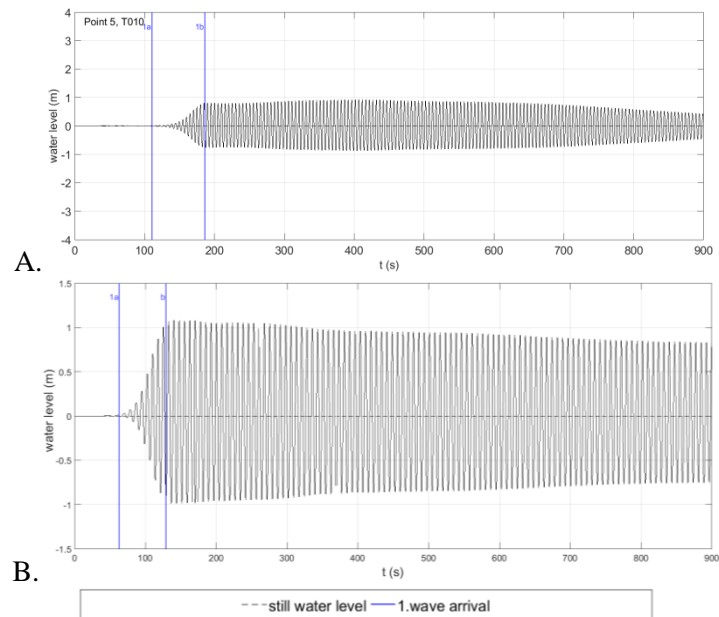
Figure 7.7 - The water level time series generated by the 2D simplified SWASH model at Point 5 for test T010 (picture A) and for T013 (picture B).

7.2.2   Output points inside the harbour basin

As in the simplified 2D SWASH model reflection does not influence the waves inside the harbour the characteristic vertical lines representing the arrival of reflected waves are not drawn in the SWASH time series. The only moments determined for points inside the harbour are moments 1a (start of taper function) and 1b (end of taper function). For most of the points examined for the seven different tests, the water level trends are similar to point 27, shown in in Figure 7.8. After Moment 1b the wave height increases, it remains constant for a few seconds (170< t <180s for Point 27) and then it drops slightly (180s<t<220s). From t=220s until t=500s the wave height increases slightly. After t=500s a steady state is reached.

The changes in the wave height before the steady state can be related to transversal reflections at the walls parallel to the basin length, when waves enter inside the harbour. Moreover, the water level inside the basin is also influenced by the head walls reflection: the incoming waves get first reflected at the head walls, and then there is a second reflection at the wave maker. This new re-reflected wave travels towards the harbour and influences the water level at wave gauges located inside the harbour.
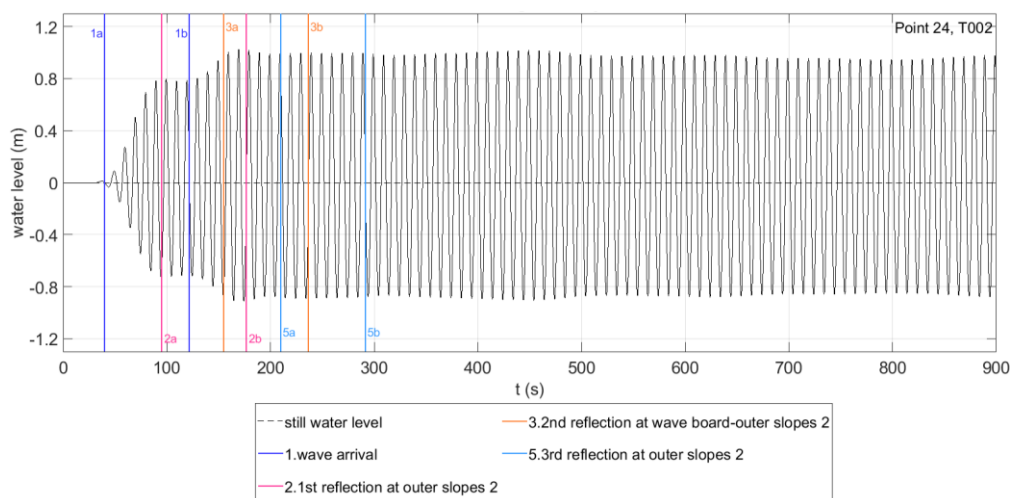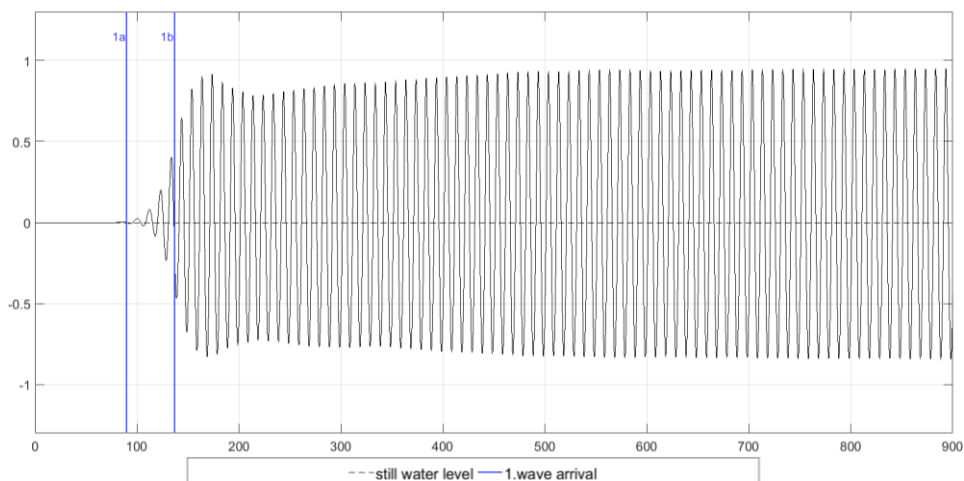

Figure 7.8 - The water level time series generated by the 2D simplified SWASH model at Point 27 for test T002.

As described in Section 7.2.1 , plots including the measured, the simplified 2D SWASH and the 1D model (modelling the harbour end) time series are created for all points and tests. Examples of such a plot are the pictures B of Figure 7.9 and Figure 7.10. Pictures A of the aforementioned figures include only the measurements signal and the 2D simplified SWASH model time series. In picture A of it is clear that the measured and the 2D SWASH time series are in very good agreement in terms of wave height from t=190s until t=290s. After t=290s the wave height in the 2D SWASH model does not decrease as observed in the measurements. The steady state wave height produced by the 2D simplified model is relatively higher than the measurement. However, as shown in picture B of Figure 7.9 the steady state wave height in the 1D SWASH model deviates slightly from the measured wave height.

A.

B.
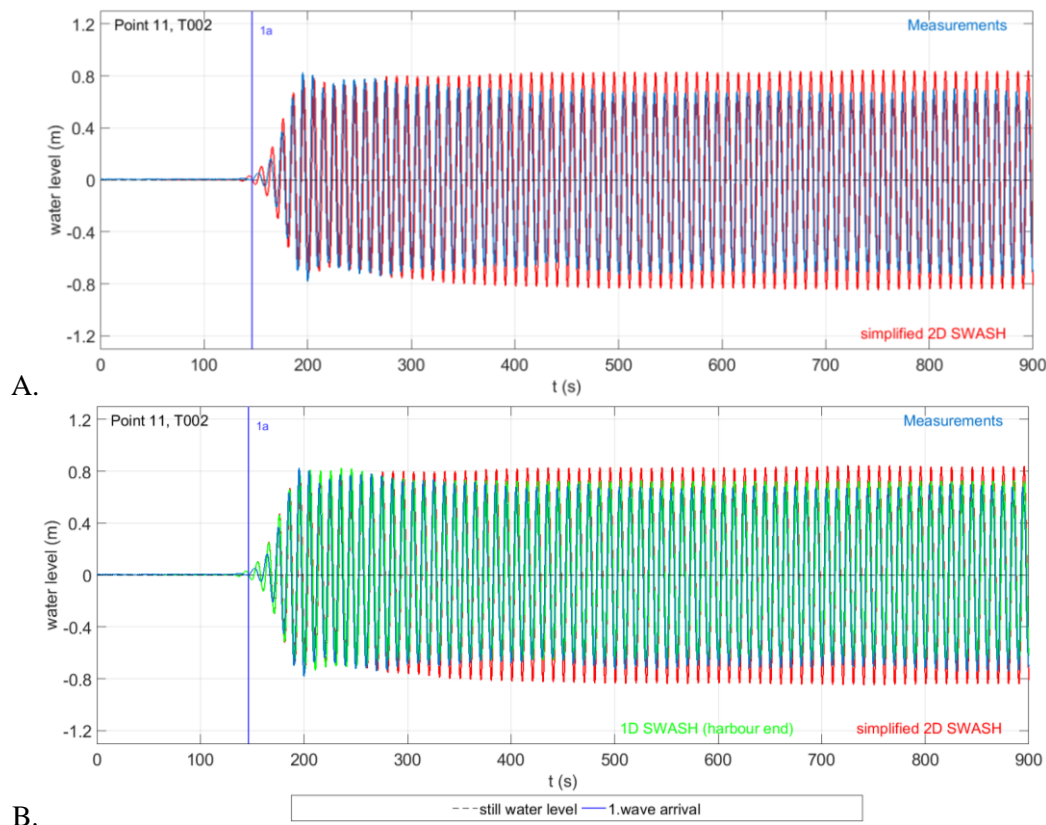
Figure 7.9 –T002, Point 11: Comparison of the measured water level time series to the simplified 2D SWASH outputs only (picture A) and also to the 1D SWASH (simulating reflection at the harbour end) model outputs (picture B).

From t=220s to t=350s in picture A of Figure 7.10 the time series produced by the simplified 2D SWASH model and the measured signal show the same trends: a decrease of the wave height until t=280s and then a small increase. However, the SWASH wave height is higher than the measured wave height. The same holds for the wave heights in the steady state. For Point 27 (picture B of Figure 7.10) the steady state wave height in the measurements is produced better in the 1D SWASH model than in the 2D model. This was also the case for Point 11.
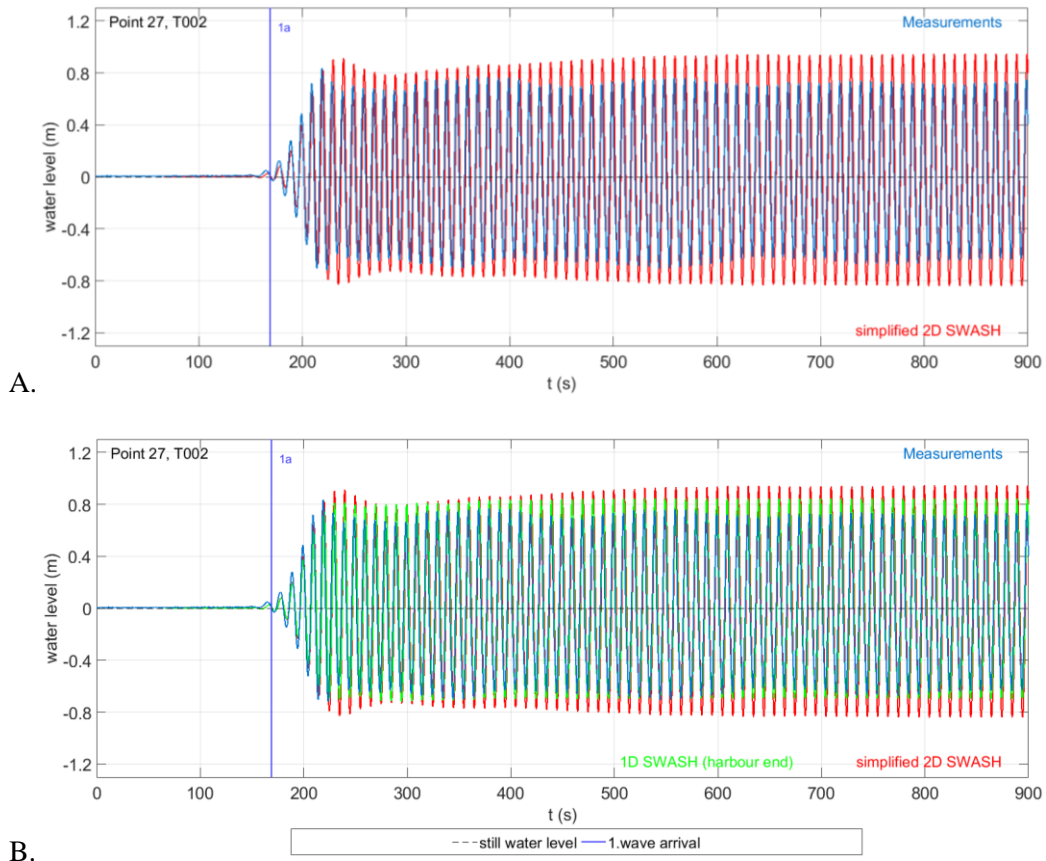
Figure 7.10-T002, Point 27: Comparison of the measured water level time series to the simplified 2D SWASH outputs only (picture A) and also to the 1D SWASH (simulating reflection at the harbour end) model outputs (picture B).

An important observation can be made for T010 and T013. As shown in pictures A and B of Figure 7.11, after t=500s approximately the wave height starts decreasing considerably. This behaviour is not realistic and can be attributed to numerical error. However, the causes of the error have not been further investigated in this thesis.
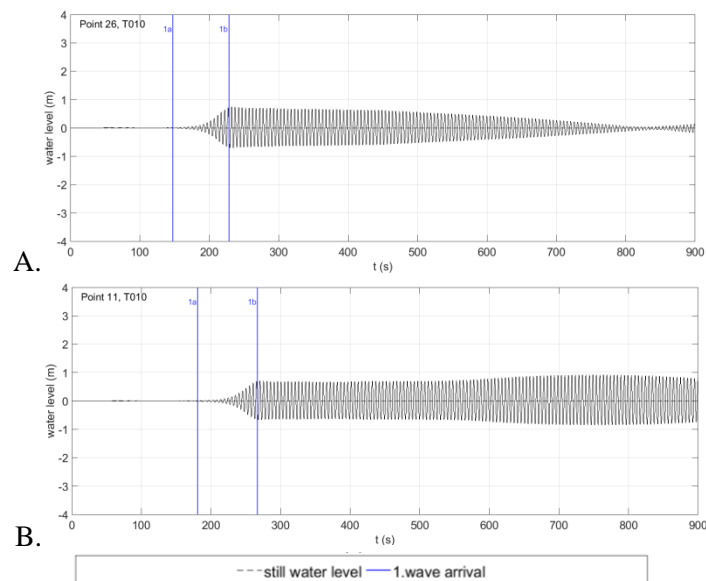
Figure 7.11 - The water level time series generated by the 2D simplified SWASH model at Point 26 (picture A) and 11 (picture B) for test T010.

7.3 Comparison of the fully developed incoming wave height in the measurements and in the simplified 2D SWASH model

In the 2D simplified SWASH model, the incoming wave height at the output points outside the harbour and along the model centreline (Figure 3.9) is calculated using the time interval from Moment 1b (end of the taper function) to Moment 2a (arrival of reflected waves from outer slopes 2). The results are shown in Table 7.2. The table also contains the standard deviation value for the incoming wave height at the five output points outside the harbour basin. The ratio in the last row of Table 7.2 expresses the difference of the mean measured incoming wave height and the mean incoming wave height computed with the simplified 2D SWASH model. The largest difference is observed for Test T010 in which the waves are breaking. For the rests of the tests the difference may vary from 3% to 6%. Taking into consideration the difficulty to describe numerically a monochromatic wave, the deviations between the measurements and the SWASH outputs are considered relatively small. Thus, SWASH is able to describe accurately the incoming wave height. It should be noticed that the differences between the measured incoming wave height and the respective SWASH results is smaller in the simplified 2D SWASH model than in the 1D model for reflection the harbour end (Section 6.3).

Table 7.3 shows the difference between the fully developed incoming wave height prescribed at the SWASH boundary that enters the SWASH domain and the measured incoming wave height calculated at the output locations. Again the highest difference is observed for test T010 (35%). For the remaining tests the differences range from 3 to 6% verifying the ability of SWASH to describe accurately the propagation of the simple monochromatic waves in the computational domain.

Table 7.2 - Comparison of the incoming wave height at the output locations outside the harbour basin in the simplified 2D SWASH model to the measurements.

|		T001	T002	T003	T010	T011	T012	T013
$H_{inc,SWASH}$ (m)	Point 10	1.06	1.51	2.46	2.15	3.16	2.83	2.05
	Point 4	1.06	1.50	2.44	2.01	3.15	2.84	2.05
	Point 3	1.06	1.50	2.45	1.87	3.15	-	2.04
	Point 24	1.01	1.46	2.35	1.67	3.13	-	2.04
	Point 5	-	-	-	-	-	-	-
$\overline{H}_{inc,SWASH}$ (m)		1.05	1.49	2.43	1.92	3.15	2.84	2.05
Std. deviation (m)		0.02	0.02	0.04	0.17	0.01	0.01	0.01
$H_{inc,measured}$ (m)		1.00	1.42	2.36	2.96	3.05	2.72	1.92
$\dfrac{\left\|\overline{H}_{inc,SWASH} - H_{inc,measured}\right\|}{H_{inc,measured}}$		4%	6%	3%	35%	3%	4%	6%

Table 7.3 - Comparison of the incoming wave height at the output locations outside the harbour basin in the simplified 2D SWASH model to the incoming wave height generated by the wave maker prescribed at the offshore SWASH boundary.

	T001	T002	T003	T010	T011	T012	T013
$\overline{H}_{mean,SWASH}$ (m)	1.05	1.50	2.48	1.92	3.16	2.85	2.05
$H_{inc,wave\ maker}$ (m)	0.99	1.44	2.39	2.97	3.02	2.75	1.94
$\dfrac{\left\|\overline{H}_{inc,SWASH} - H_{inc,wave\ maker}\right\|}{H_{inc,wave\ maker}}$	6%	4%	2%	35%	4%	3%	5%

7.4 Top view of the steady state average wave height at all the points

To demonstrate how the wave height differs at various locations it was decided to create a top view showing the steady state wave height at each output location. This graph shows the influence of diffraction on the wave height inside the harbour basin and the influence of reflection off the harbour head walls outside the basin.

For the points on the centreline line AA' a steady state is considered to be reaches after moment 5b until the end of the simulation (t=900s). For the rest of the point the beginning of the steady state part is calculated according to Section 3.4 . The constant steady state wave height is determined for all points. Subsequently, this value is divided by the incoming wave height for the specific test examined. As explained in Section 7.3 the incoming wave height generated by the wave maker travels inside the model domain and arrives at the output locations in the 2D SWASH model with an accuracy of 6% (excluding test T010). Hence, the wave maker incoming wave height is used for the calculation of the ratio $\bar{H}_{\text{steady state,diffracion model}}/H_{\text{incoming}}$ for all the seven tests. By dividing with the incoming wave height the results for all the seven tests examined can be compared.
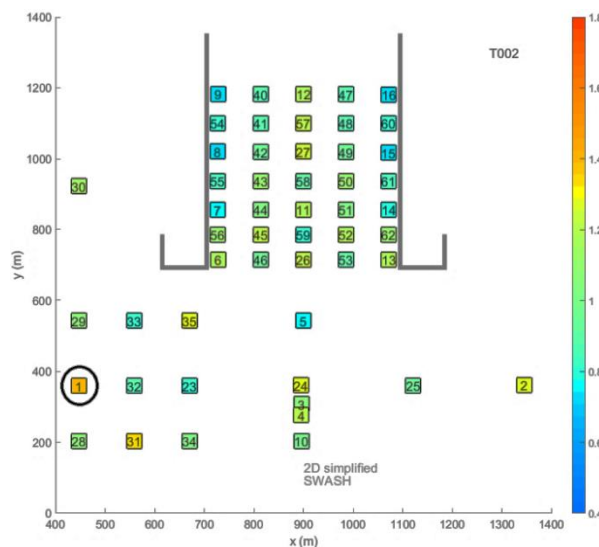
Figure 7.12 - The steady state wave height at all the output points calculated by the 2D simplified SWASH model for T002.

Figure 7.12 shows a top view plot, indicating with colours the value of the ratio at every point for T002. The plots and the exact values of the ratio for all the tests can be found in Appendix J. It is noted that the wave height changes inside the basin are mainly related to diffraction. For T002, the ratio $\bar{H}_{\text{steady state,diffracion model}}/H_{\text{incoming}}$ inside the harbour basin varies from 0.72 to 1.23. Last, according to Table 7.4, the ratio $\bar{H}_{\text{steady state,diffracion model}}/H_{\text{incoming}}$ inside the harbour basin varies from 0.58 to 1.34 among the tests indicating the important role diffraction plays inside the harbour. The tests of the 3rd group (T010 and T013) are not included in Table 7.4 due to the numerical instabilities observed (Section 7.3).

Table 7.4 – The variation of the ratio $\bar{H}_{\text{steady state,diffracion model}}/H_{\text{incoming}}$ inside the harbour basin and outside the cone of influence of reflection off the harbour head walls.

Test	H_{incoming} (m)	kd	group of test based on kd	$\bar{H}_{\text{steady state,diffracion model}}/H_{\text{incoming}}$			
				Inside the harbour		Outside the cone (Points 1,28,29)	
				Min	Max	Min	Max
T001	0.99	1.55	2nd-average kd	0.43	1.29	0.91	1.19
T002	1.44	1.03	2nd-average kd	0.72	1.23	1.07	1.41
T003	2.39	0.55	1st -low kd	0.83	1.18	0.67	1.23
T011	3.02	1.19	2nd-average kd	0.58	1.28	0.78	1.36
T012	2.75	0.63	1st-low kd	0.72	1.34	0.60	1.34

The changes in the wave height at the wave gauges outside the basin are related to reflections at the harbour head walls. For T002, the ratio $\overline{H}_{steady\ state,diffraction\ model}/H_{incoming}$ at wave gauge 1(marked with a circle in Figure 7.12) is equal to 1.41. This demonstrates that the water level at that location is highly influenced by the reflection at the head walls. This confirms the assumption made in Section 5.4 that another phenomenon apart from reflection at the outer gravel slope is influencing the wave record. Moreover, as the change of the wave height by 41 % is important, it can be supported that the wave height at wave gauge 1 is influenced more by the reflection off the head walls than the reflection at outer slope 2a. This conclusion is also supported by the variation of the ratio $\overline{H}_{steady\ state,diffraction\ model}/H_{incoming}$ at Points 1, 28, 29 located outside the cone of influence of reflection off the harbour head walls (Figure 7.12).

7.5 Compare to the measurements

As explained in Section 7.4 the ratio $\overline{H}_{steady\ state,}/H_{incoming}$ has been calculated based on simplified 2D SWASH model results at all output locations for the seven selected tests. The same ratio is calculated also for the measured time series and hence it is used to evaluate the SWASH results. In Figure 7.13 the ratio $\overline{H}_{steady\ state,}/H_{incoming}$ in the measurements and in the simplified 2D SWASH model are indicated by colours for test T002. The exact ratio values are presented in Table 7.5. The last column shows the in percentage the difference between the measured ratio and the ratio in SWASH (Equation 7.1). The graphs and the tables for the remaining six tests are presented in Appendix J.

$$Difference_{measurements-simplified} = \left| \frac{ratio_{measurements} - ratio_{simplified\ 2D\ SWASH\ model}}{ratio_{measurements}} \right| \qquad (7.1)$$

Where ratio $= \overline{H}_{steady\ state}/H_{incoming}$

Looking at the colour patterns of Figure 7.13 it can be supported that the agreement between the measurements and the simplified 2D SWASH model is good for test T002. In general, the values inside the basin deviate less from 1, in comparison to the ratios outside the basin. For test T002, at many output locations the agreement between the values of the ratio $H_{steady\ state}/H_{incoming}$ in the measurements and in SWASH is very good. For example, at Points 1,4,6,7,13,14,26 the difference between the measured values and the values calculated by SWASH is lower than 15%. On the contrary, at other locations, i.e. Point 5, 25, 9 the difference is larger than 40%. As mentioned in Section 5.3.2 , the resulting standing wave patterns in front of a concrete wall change within a short distance. This means that the steady state wave height in SWASH is highly depended on the exact location of the point. Therefore, the wave height values may change significantly at the area close to a specific point. This observation can explain the large differences spotted at a few output locations. The same observations hold for the remaining tests presented in Appendix J.
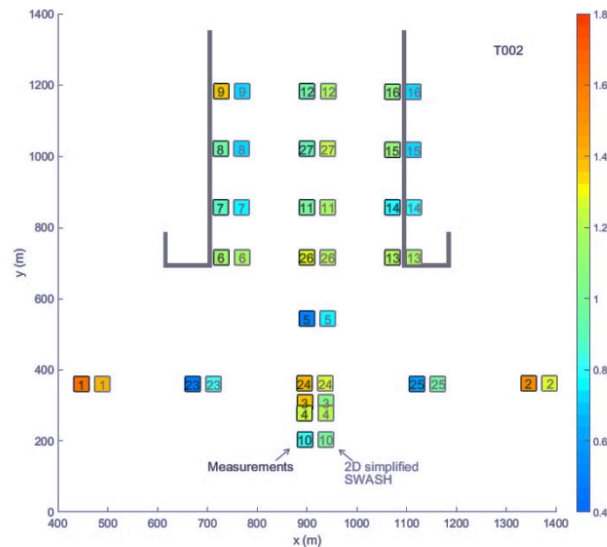
Figure 7.13 - Top view of the ratio H$_{steady\ state}$/H$_{incoming}$ at the wave gauges locations. The colours indicate the ratio values. At each location the left box shows the measurements result, while the right box shows the simplified 2D SWASH model results.

Table 7.5 - The exact values of ratio H$_{steady\ state}$/H$_{incoming}$ in the measurements and in the simplified 2D SWASH model.

Outside the harbour basin				Inside the harbour basin			
Wave Gauge	Measured H$_{steady\ state}$	2D simpl. H$_{steady\ state}$	Difference (%)	Wave Gauge	Measured H$_{steady\ state}$	2D simpl. H$_{steady\ state}$	Difference (%)
1	1.63	1.41	- 14	6	1.12	1.16	4
2	1.54	1.26	- 18	7	0.90	0.77	- 14
3	1.36	1.05	- 22	8	0.95	0.72	- 24
4	1.22	1.21	0	9	1.37	0.73	- 47
5	0.50	0.77	54	11	0.99	1.16	17
10	0.81	0.99	23	12	0.96	1.16	21
23	0.46	0.84	17	13	1.17	1.17	0
24	1.41	1.27	21	14	0.79	0.78	- 2
25	0.60	0.95	59	15	1.11	0.74	- 33
			|Max|= 59	16	1.06	0.74	- 30
				26	1.28	1.19	- 7
				27	0.94	1.23	30
							|Max|= 47

7.6   Conclusions

Chapter 7 focuses on providing an answer to research question 2 examining whether the wave phenomena of reflection and diffraction can be modelled accurately by SWASH. The simulation of reflection in SWASH was also treated in Chapters 5 and 6. Chapter 7 is the only chapter in which the role of diffraction is examined separately from the rests of the wave processes. To investigate the influence of diffraction inside the harbour and reflection off the harbour head walls a simplified 2D SWASH model was developed. The model included only the harbour head walls and the side concrete walls of the harbour. The harbour end was removed to avoid reflection of the waves. The most important information resulting from the work with this model is summarised in this section.

- For the points outside the basin, the changes in the water level after the arrival of reflected waves from the head walls are higher than the changes in the water level after the arrival of reflected waves from the inner slope 1, described in chapter 6. Therefore, for points outside the basin, reflection off the harbour head walls plays a more dominant role than the reflection from the inner

slope 1 inside the harbour. In addition, in Chapter 5 it was observed that the changes due to reflection off a wall are larger than the changes due to reflection off the outer gravel slopes. All in all, reflection off the harbour head walls is the dominant process outside the harbour basin.

- At the output points inside the basin, the initial changes in measured water level time series due to diffraction are reproduced in the simplified 2D SWASH model. This was not the case for the 1D SWASH model simulating reflection off the harbour end. However, in both the 2D model (diffraction) and the 1D model (reflection) the accuracy of the steady state wave height in comparison to the measurements is acceptable. This observation indicates that that both diffraction and reflection off the harbour end influence significantly the wave field inside the harbour and should be modelled accurately to reproduce the wave field in the measurements.

- From the comparison of the steady state wave height in the measurements and in the simplified SWASH model including the full layout 1, it follows that the general wave filed pattern is reproduced in SWASH. In many output points the difference between the measured wave height and the wave height in SWASH is relatively small. However, at other output location the agreement was not good showing that the final constant wave height in SWASH is sensitive to the standing wave patterns. For standing wave patterns that change within a short distance the wave height can vary significantly at the area close to a specific output point.

7.7   Remarks

The following remarks result from the work carried out in this chapter.

- For T010 and for T013 numerical instabilities are observed. At the output points the wave pattern does not remain constant after moment 5b. This behaviour indicates that there is a numerical error in the calculation of the constant waves. The total error is increasing in time, as the error of the next time step is added to the previous error. A critical view is required examining the results of the aforementioned tests.

- Wave gauge 1 in theory is located outside the cone of influence of reflection at the harbour head walls. However, it is proven that the water level at that location is highly influenced by the reflection of the head walls. This confirms the assumption made in Chapter 6. Despite the initial expectation, the wave height at wave gauge 1 is influenced more by the reflection off the head walls that the reflection off outer gravel slope 2a.

Chapter 8 Numerical simulation of wave penetration for the full layout 1

The objective of this chapter is to provide an answer to research question 3, referring to the performance of SWASH in simulating wave penetration in the full layout 1 (Figure 1.1). The ability of a two-dimensional SWASH model to describe the wave height changes (temporally and spatially) identified in the measured water level time series is examined. In Section 8.1 the bathymetry of the 2D SWASH model is introduced. The method of estimating the arrival of reflected waves presented in Section 3.3 is again applied and the plots are shown in Section 8.2. Moreover, the aforementioned section includes the graphs of the measured time series and the SWASH time series which are used to compare the wave height changes in time. Section 8.3 compares the incoming wave height in the final SWASH model simulating the full layout 1 first to the measured incoming wave height and then to the wave height prescribed at the SWASH boundary. Furthermore, in Section 8.4 the ratio of the steady state wave height in the final SWASH model divided by the incoming wave height is compared: first to the respective results for the simplified 2D SWASH model presented in Chapter 7 and later to the respective measured values. Furthermore, Section 8.5 highlights the knowledge obtained in Chapter 8 and answers to the research question 3. Finally, Section 8.6 points out the most important remarks regarding the SWASH performance resulting from the work discussed in this chapter.

8.1   The 2D SWASH model for the full layout 1

In this thesis wave penetration has been interpreted as a summation of physical processes. The wave processes studied separately in Chapters 5 to 7. Other than for the previous chapters, here it is aimed for to model all wave processes taking place in the experiments in SWASH simultaneously. For this purpose a 2D SWASH model representing the full layout 1 (Figure 1.1) is constructed. Figure 8.1 shows a sketch of the SWASH model.
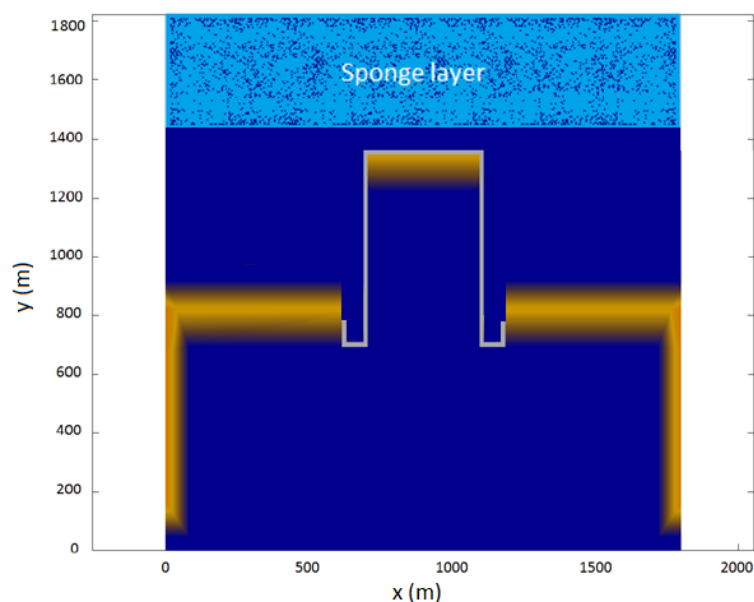
Figure 8.1-Sketch of the 2D SWASH model representing the complete layout 1

Details about the model set-up and the chosen settings, such as the use of 2 vertical layers are provided in Appendix L. The model output locations and the sponge layer length are specified as in the simplified 2D SWASH model presented in Section 7.1 .

8.2 Comparison of the measured water levels to the SWASH outputs

The method described in Section 3.2.5 for the calculation of the characteristic moments in time, when the incoming and the reflected waves arrive at the wave gauges, is also applied on the SWASH time series. After determining the first zero-down crossing (Moment 1a) the measured and the SWASH time series can be synchronised based on Moment 1a and then plotted at the same graph. As discussed in Section 7.2.1 , the characteristic moments in time depend on the wave celerity and on the physical model geometry. As the wave celerity in the measurements is equal to the celerity in SWASH (Section 6.6) and the physical model geometry is carefully reconstructed in SWASH, the vertical lines 2b, 3b, 4b, 5b, 6b and 7b in the measurements and in SWASH coincide.

As discussed in the previous chapters, the wave processes that influence the water level time series outside and inside the basin differ. Therefore, the results for the wave gauges outside and inside the basin are discussed separately. For a full overview of the water level time series for all the seven examined tests, the reader is referred to Appendix G.

8.2.1 Output points outside of the harbour basin

For the majority of the cases the time interval between Moments 1b and 2a that represents the constant fully developed incoming wave is sufficiently long to calculate the incoming wave height. The same holds for the measurements results, as discussed in Section 4.2. However, both in the measurements and in SWASH it is not possible to determine the constant incoming wave at wave gauge 5 for all the tests and at wave gauges 3 and 24 for T012, as the duration between the end of the taper function and the arrival of reflected waves is not long enough. The fully developed incoming wave height values in the measurements and in the 2D SWASH model of the full layout 1 are compared in Section 8.3

The water level trends at the output locations along the centreline AA' located out of the harbour basin show similar trends. In all the cases from Moment 1a the wave height increases until it reaches the fully developed wave height value (Moment 1b). From Moment 1b to 2a the wave height remains constant. For points outside the basin, the most important changes in terms of wave height occur from Moment 2b until Moment 3a (Figure 8.2), that represent the arrival of reflected waves from line y=693m, where the harbour head walls and the outer slopes are located (Figure 3.17). In this time interval, the wave height increases (Figure 8.2) or decreases (Figure 8.3) depending if the incoming and the reflected wave enhance or cancel each other. The wave height may still change slightly after Moments 6a and 6b (Figure 8.2 and Figure 8.3), but after Moment 7b it remains constant as a temporal steady state is developed (Figure 8.2 and Figure 8.3).

Figure 8.2 - The water level time series generated by the fully layout 1, 2D SWASH model at Point 24 for test T002.

Figure 8.3 - The water level time series generated by the full 2D SWASH model at Point 5 for test T002.

The water level time series obtained from SWASH should be compared to the respective measured time series. Two examples are presented here. The first example is for wave gauge 24 and T002 (H=1.44m, kd=1.03). The measured and the SWASH time series are synchronised on Moment 1a. The changes in the measured and the modelled water level are similar. The wave height remains constant before Moment 2b and then it increases until 3b. However, the increase is higher in the measured time series. In both time series the wave height remains constant until Moment 5b and then decreases slightly until 6b. Finally, in both cases a steady state is reached after moment 7b. The measured steady state wave height (1.41m) differs only by 2% from the steady state wave height in SWASH (1.44m). For T002, the steady state wave height in the measured signal and the SWASH time series is in good agreement at Points 10, 4 and 24, located outside the basin (see also Section 8.4.2 . On the contrary, this is not the case for Points 3 and 5 (Figure 8.5). It is worth mentioning that this observation holds about test T002 and that for the same points, but for different tests the agreement between measurements and SWASH may vary.

Figure 8.4 - T002, Point 24: Comparison of the measured water level time series to the full 2D SWASH outputs.

Figure 8.5 shows that at Point 5 SWASH is able to describe the decrease of the water level after Moment 2b, observed in the measurements. After Moment 5b for both time series the changes of the wave height are very small. However, the steady state wave height is SWASH (1.22m) is much larger than the wave height in the measurements (0.93m). The deviation between the measured and the SWASH steady state wave height can be related to the standing wave patterns. As discussed in

93

Section 5.3.2 , for a node-antinode pattern of the standing waves that changes within a short length it is possible that the measured wave height at a specific can be observed in the model at a different location, but close to point.
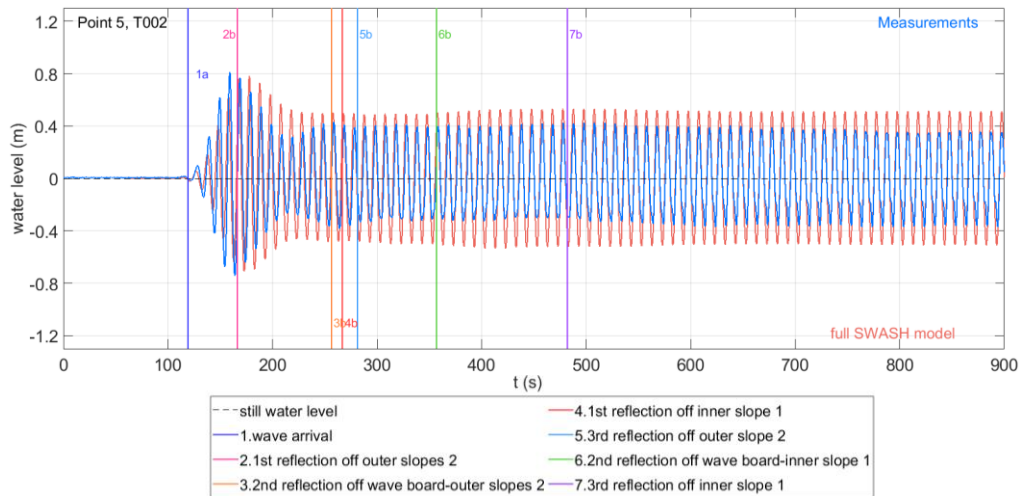
Figure 8.5 - T002, Point 5: Comparison of the measured water level time series to the full 2D SWASH outputs.

At the five output points outside the basin along the model centreline for test T010 (H=2.97m, kd =3.16, H/h=0.2, H/L =0.075) the wave pattern the final part of the time series from t=600s until t=900s does not remain constant. For instance, at Point 5 after approximately t=600s the wave height starts decreasing (Figure 8.7). For other points, such as Point 3, the wave height is increasing. A similar behaviour was also observed for T011 (H=3.015m, kd =1.19, H/h=0.2, H/L =0.029) as after moment 7b the wave height does not remain constant. For example, at Point 4 for T001 the wave height starts decreasing after t=600s (Figure 8.6). For the rest of the tests of the 1st and the 2nd group (Table 2.5 and Table 2.6) after this moment a steady state is developed.

This behaviour indicates that there is a numerical error in the calculation of the constant waves. The error of the next time step is added to the previous error. Therefore, the total error is increasing in time. It was attempted to solve the problem by adding more vertical layers which was expected to improve the accuracy of the calculations. As shown in Figure 8.8, by using 4 vertical layers instead of 2, the wave height reduction after t=600s is smaller. However, the wave height does not remain constant. At many of the points the increase of the vertical layers does not improve the results (i.e. Point 26 presented in Section 8.2.2).

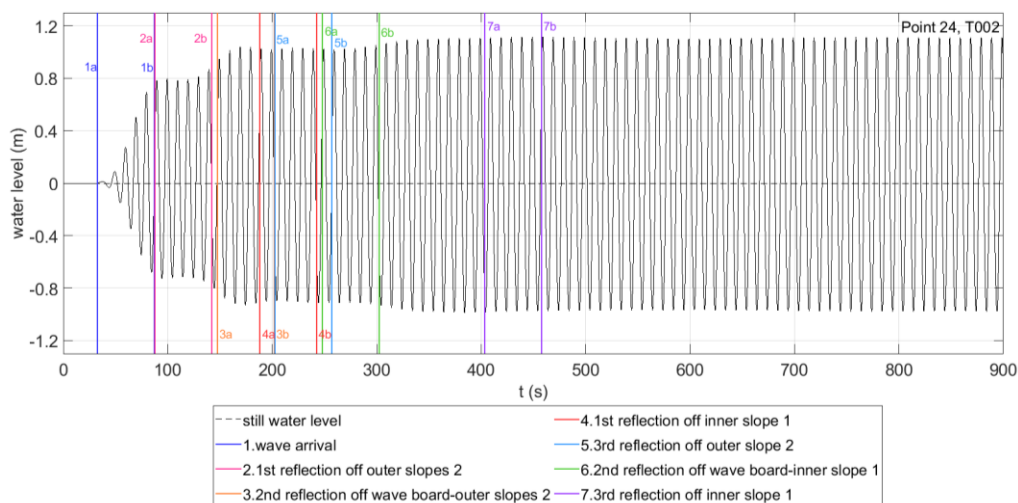**Figure 8.6 - The water level time series generated by the full 2D SWASH model at Point 4 for test T011.**

Figure 8.7 - The water level time series generated by the full 2D SWASH model at Point 5 for test T010.

Figure 8.8 - The water level time series generated by the full 2D SWASH model at Point 5 for test T010 using 4 vertical layers.

The numerical instabilities observed for T010 and T011 can be attributed to numerical dissipation. This means that the number of grid points per wave length is relatively low to describe well the propagation of waves. For T010 there are only 13 points per wave length, while for T011 there are 33 points per wave length (Appendix L). It is important to mention that the incoming wave height for tests T010 and T011 are the highest values among the seven selected tests. Thus, the values of the ratio of wave height to water depth H/h are also the highest. As the waves are relatively higher the number of grid point per wave length should be increased.

8.2.2   Output points inside the harbor basin

For the majority of the point for the 1ˢᵗ and the 2d group of test similar patterns are observed. A typical example is the water level time series at Point 11 for T002 (H=1.44m, kd=1.03), shown in Figure 8.9. The most important changes in the wave height occur from Moment 4a and until Moment 4b. After Moment 7b the water level remains constant.

For the points inside the basin, the duration of the wave record describing only the incoming wave height is not always long enough. For Point 12 in every test the reflected taper function wave arrives before the incoming wave can be fully developed. For the majority of the test cases at Point 27 there is no individual wave between the Moments 1b and 4a. This can be observed in Figure 8.10 which shows the water level time series at Point 27 for T002. The same observation holds also for the measured water level time series.

Figure 8.9 - The water level time series generated by the full 2D SWASH model at Point 11 for test T002.
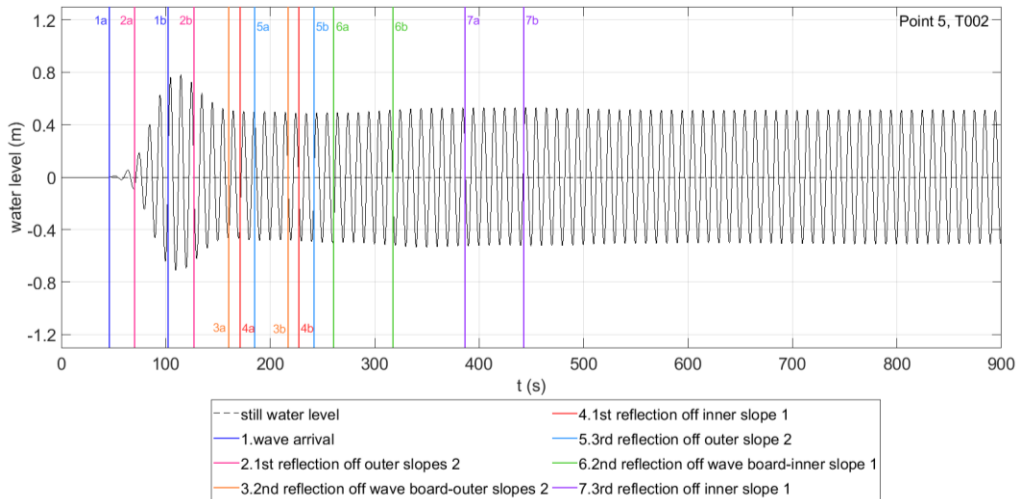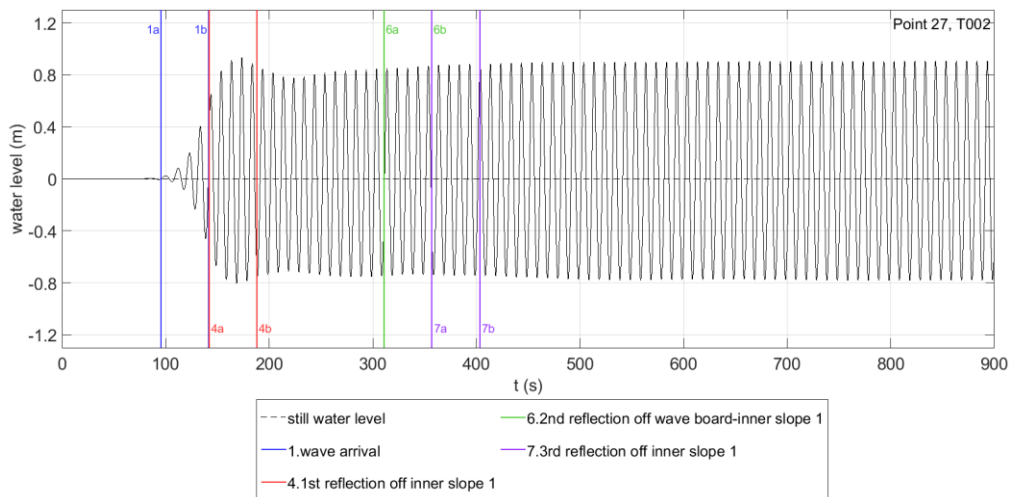

Figure 8.10 - The water level time series generated by the full 2D SWASH model at Point 27 for test T002.

The water level time series obtained from full 2D SWASH model are compared to the respective measured time series. Two examples are presented here. The first example (Figure 8.11) is for wave gauge 11 and T002 (H=1.44m, kd=1.03). The measured and the SWASH time series are in good agreement until Moment 4a. However, after this moment the wave height reduction observed in the measurements is not represented in the SWASH time series. The measured steady state wave height (after Moment 7b) is lower by 12.5% than the steady state wave height in SWASH.

The second example (Figure 8.12) is for wave gauge 27 and T002 (H=1.44m, kd=1.03). From Moment 4a to Moment 6b the time series produced by the full 2D SWASH model and the measured signal show the same trends: a decrease of the wave height until t=280s and then a small increase. However, the SWASH wave height is higher than the measured wave height. The same holds for the wave heights in the steady state (after Moment 7b). The measured steady state wave height (after Moment 7b) is lower by 23% than the steady state wave height in SWASH. The difference of the steady state wave height between the measurements and the SWASH results are discussed in Section 8.4.2 .
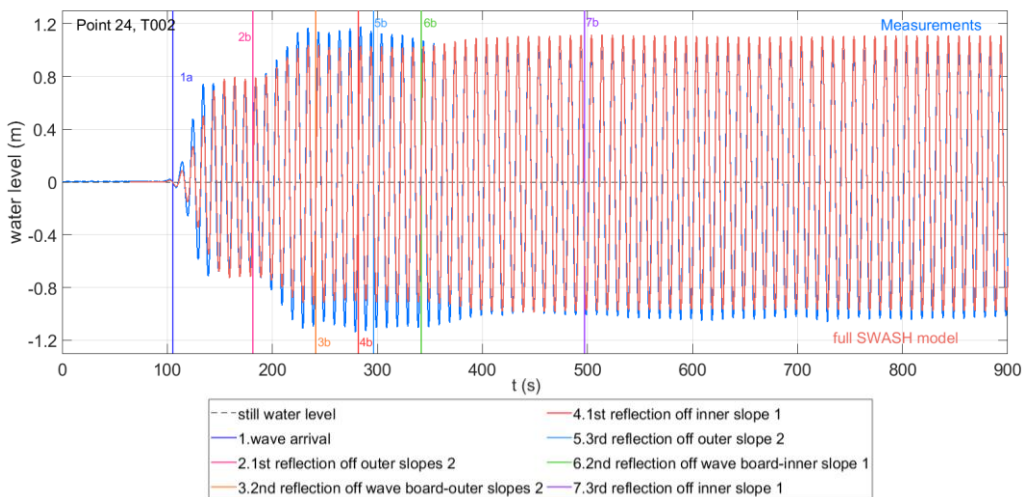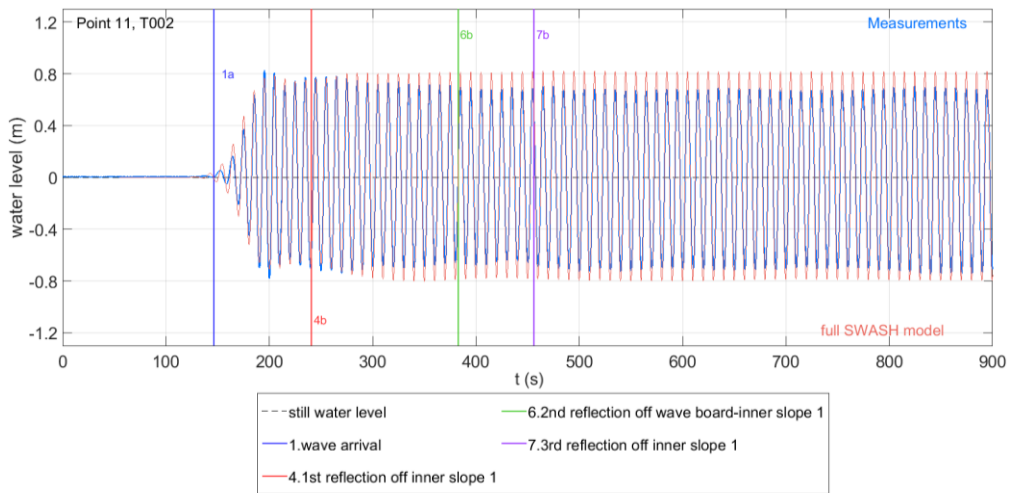
Figure 8.11 - T002, Point 11: Comparison of the measured water level time series to the full 2D SWASH outputs.
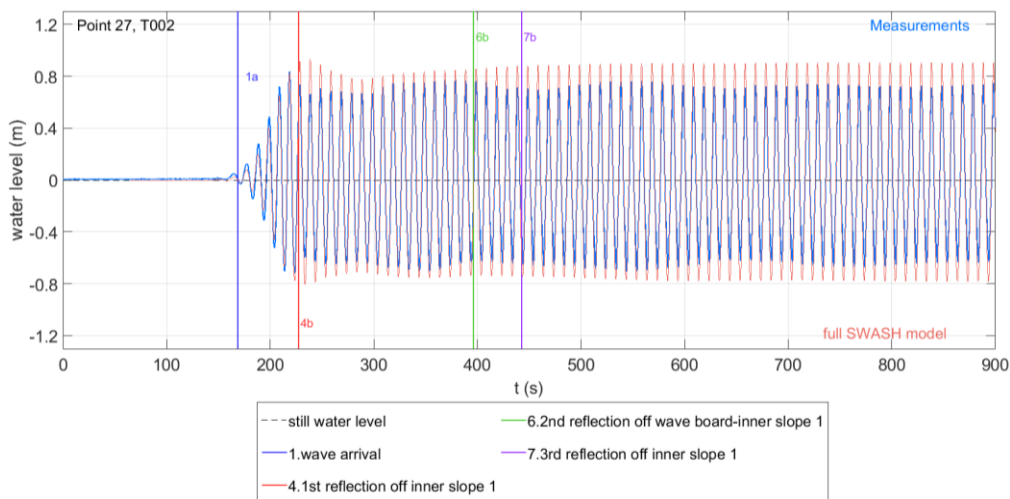
Figure 8.12 - T002, Point 27: Comparison of the measured water level time series to the full 2D SWASH outputs.

As discussed in Section 8.2.1 numerical instabilities are observed for the tests with the highest incoming wave height, T010 and T011. For example, this behaviour is obvious for T010 at Point 26, located inside the harbour basin (Figure 8.13). In Figure 8.14 it is clear that the problem is not solved by increasing the number of vertical layers from 2 to 4 in the SWASH model.
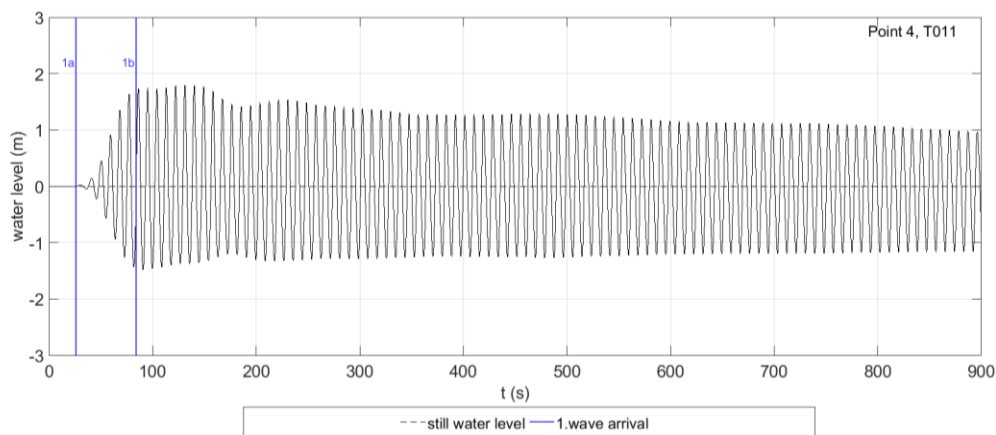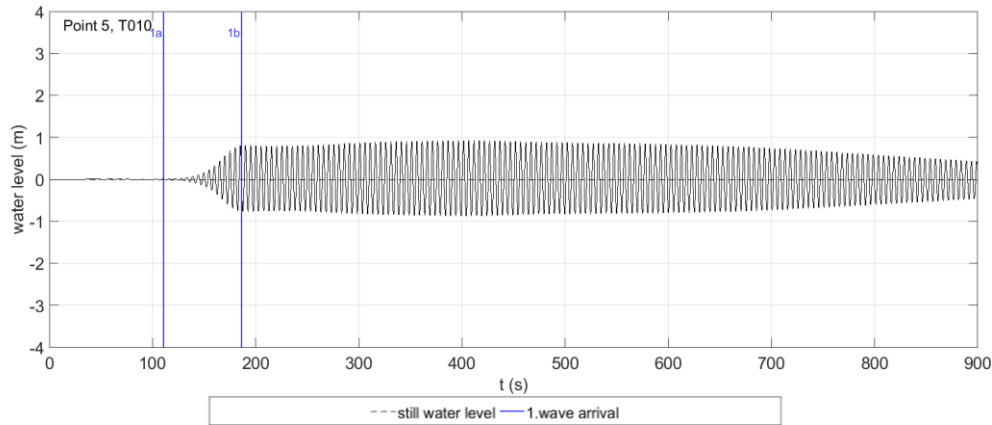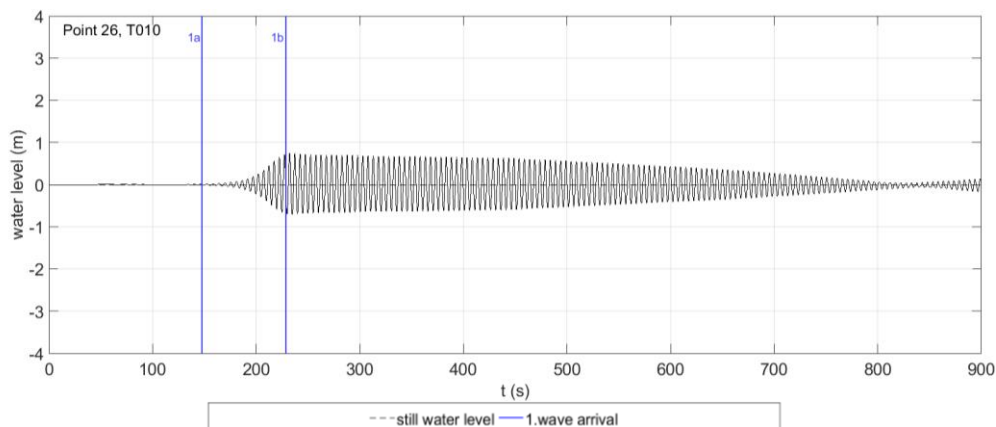

Figure 8.13- The water level time series generated by the full 2D SWASH model at Point 26 for test T010.

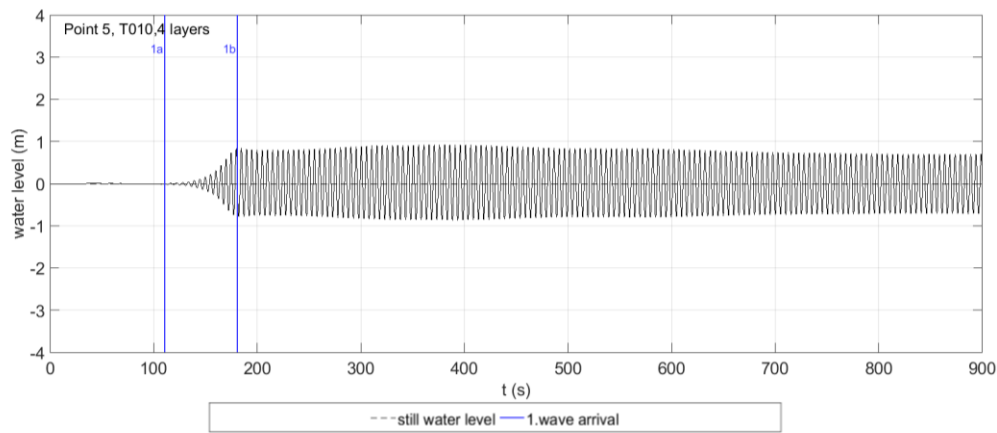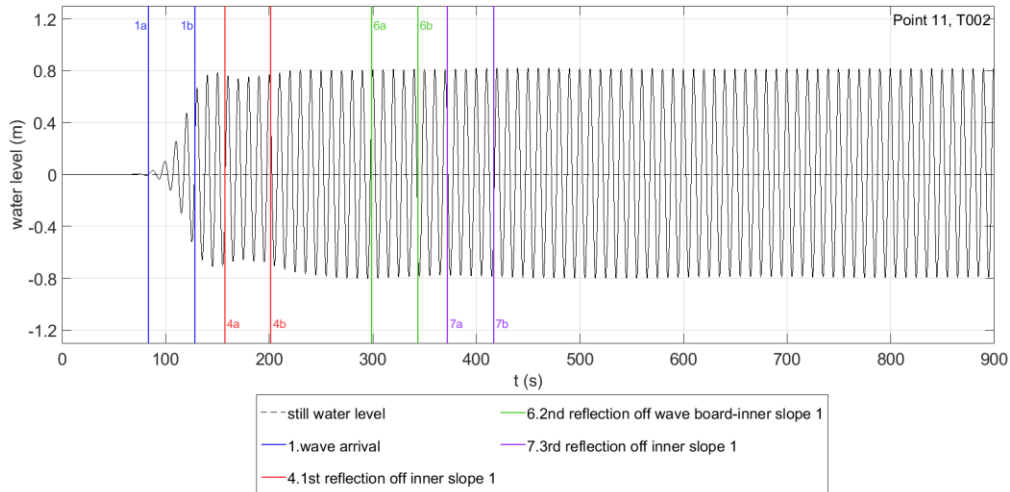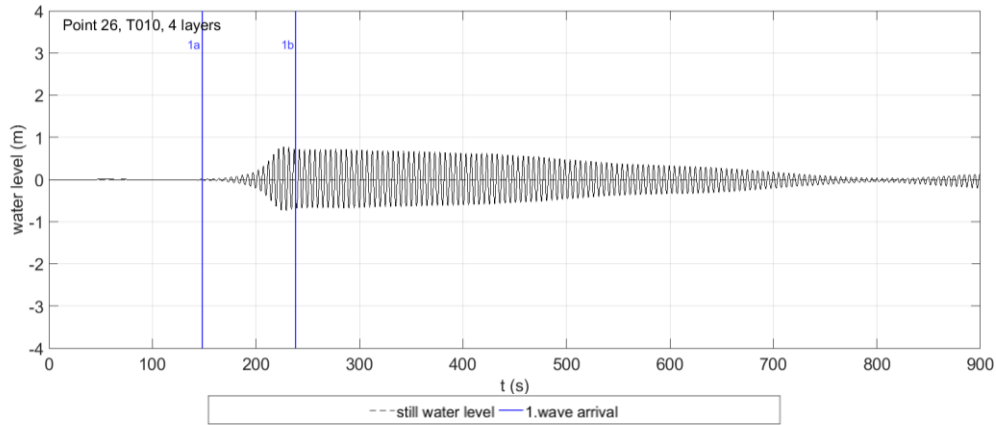**Figure 8.14 - The water level time series generated by the full 2D SWASH model at Point 26 for test T010 using 4 vertical layers.**

8.3 Comparison of the fully developed incoming wave height in the measurements and in the full 2D SWASH model

The time interval from Moment 1b (end of the taper function) to Moment 2a (arrival of reflected waves from outer slopes 2) is used to compute the incoming wave height in the full 2D SWASH model at the output points along the model centreline (Figure 3.9) outside the harbour. The incoming wave height at the five output points are presented in Table 8.1. As observed in the measurements (Section 4.2), at Point 5 for all tests and at Points 3 and 24 the time interval is not long enough to calculate a wave height value. Moreover, Table 8.1 includes the standard deviation value for the incoming wave height at the five output points outside the harbour basin for all the seven selected tests. The ratio in the last row of Table 8.1 shows the difference of the mean measured incoming wave height and the mean incoming wave height computed with the simplified 2D SWASH model. The results for tests T010 and T011 are not considered reliable as for those tests numerical instabilities occur (Section 8.2). For the rests of the tests the difference may vary from 4% to 6%. Due to the difficulty to simulate accurately monochromatic waves in a numerical model, the deviations between the measurements and the SWASH outputs are considered relatively small. Hence, SWASH is able to describe accurately the incoming wave height. It is worth mentioning that the differences between the measured incoming wave height and the respective full 2D SWASH model results differ by 0% to 2% from the simplified 2D SWASH model results. However, they differ by 1% to 3% from the values in the 1D model for reflection the harbour end (Section 6.3).This shows that the accuracy in terms of wave height is better in a 2D SWASH model rather than a 1D SWASH model.

Table 8.1 - Comparison of the incoming wave height at the output locations outside the harbour basin in the full 2D SWASH model to the measurements. For T010 and T011 numerical instabilities occur.

		T001	T002	T003	T010	T011	T012	T013
$H_{inc,SWASH}$ (m)	Point 10	1.06	1.48	2.50	2.15	3.15	2.86	2.06
	Point 4	1.05	1.52	2.47	2.01	3.20	2.85	2.06
	Point 3	1.04	1.49	2.45	1.87	3.18	-	2.04
	Point 24	1.03	1.48	2.50	1.67	3.11	-	2.04
	Point 5	-	-	-	-	-	-	
$\overline{H}_{inc,SWASH}$ (m)		1.05	1.50	2.48	1.92	3.16	2.85	2.05
Std. deviation (m)		0.01	0.01	0.03	0.20	0.04	< 0.01	0.01
$H_{inc,measured}$ (m)		1.00	1.42	2.36	2.96	3.05	2.72	1.92
$\left\| \dfrac{\overline{H}_{inc,SWASH} - H_{inc,measured}}{H_{inc,measured}} \right\|$		4%	6%	5%	35%	4%	5%	6%

98

Table 8.2 presents the difference between the fully developed incoming wave height prescribed at the SWASH boundary that enters the SWASH domain and the average measured incoming wave height computed at the output locations. As discusses, the results for T010 and T011 should not be taken into account due to the numerical instabilities observed (Section 8.2). For the remaining five tests the differences range from 4 to 6%.This shows the ability of SWASH to describe accurately the propagation of the simple monochromatic waves in the computational domain.

Table 8.2 - Comparison of the incoming wave height at the output locations outside the harbour basin in the full 2D SWASH model to the incoming wave height generated by the wave maker prescribed at the offshore SWASH boundary. For T010 and T011 numerical instabilities occur (columns with grey colour).

	T001	T002	T003	T010	T011	T012	T013
$\overline{H}_{mean,SWASH}$ (m)	1.05	1.50	2.48	1.92	3.16	2.85	2.05
$H_{inc,wave\ maker}$ (m)	0.99	1.44	2.385	2.97	3.015	2.745	1.935
$\dfrac{\overline{H}_{inc,SWASH} - H_{inc,wave\ maker}}{H_{inc,wave\ maker}}$	6%	4%	4%	35%	5%	4%	6%

8.4   The steady state wave height in the full 2D SWASH model

At points along the model centreline for both the measured time series and the time series calculated by SWASH a steady state is considered to be reached after Moment 7b (arrival of reflected waves experiencing their 3rd reflection at inner slope 1). The steady state wave height is the average value of the wave height of the individual waves for the time interval from Moment 7b until t=900s. For the rest of the output points the steady state wave height is determined using the final part of the time series until t=900s for which the wave height remains constant (difference smaller than 2%).

To compare the steady state wave height for all the tests, the ratio $H_{steady\ state}/H_{incoming}$ is calculated. The incoming wave height value used is the one produced by the wave maker ($H_{incoming,wave\ maker}$). As explained in Section 8.3 , the incoming wave height generated by the wave maker prescribed at the offshore SWASH boundary, travels inside the model domain and arrives at the output locations in the 2D SWASH model with an accuracy of 6%. This holds for the five selected tests as in T010 and T011 numerical instabilities occur.

The ratio $\overline{H}_{steady\ state,}/H_{incoming}$ is calculated for all the seven tests. By dividing with the incoming wave height, the results for all the seven tests examined can be compared. In Section 8.4.1 the ratio $\overline{H}_{steady\ state}/H_{incoming}$ at the different output points in the full 2D SWASH model are compared to the respective ratio in the simplified 2D SWASH model. Moreover, in Section 8.4.2 the ratio $\overline{H}_{steady\ state}/H_{incoming}$ at the different output points in the full 2D SWASH model are compared to the measurements.

8.4.1   Comparison of the steady state in the simplified 2D SWASH model to the full 2D SWASH model

The ratio $\overline{H}_{steady\ state,}/H_{incoming}$ at each output point in the full simplified 2D model is compared to the respective ratio in the simplified 2D model. The output points are shown in Figure 8.15. The only point which was excluded from this comparison was Point 30 which is located outside the physical model area and was only used to verify whether the waves are damped after passing though outer gravel slopes 2. This comparison between the two 2D SWASH models aims to validate how much the steady state wave height changes after the addition of the gravel slopes in the domain.
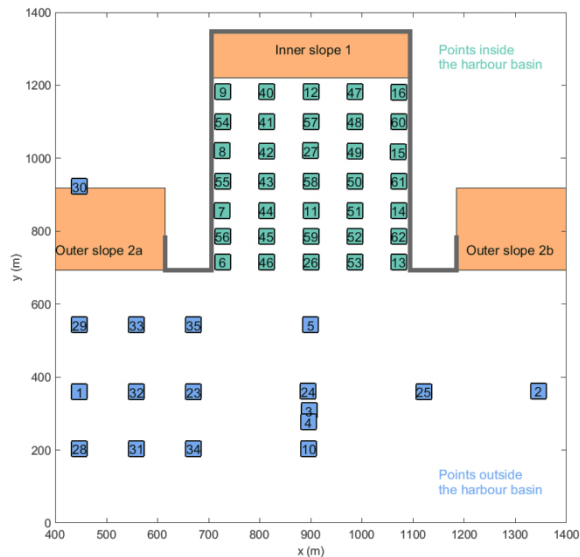
Figure 8.15 – The output locations outside and inside the harbour basin defined for both the full and the simplified 2D SWASH model.

The two 2D models are compared by the ratio Difference$_{full-simplified}$ which is calculated at each output point according to the following equation.

$$\text{Difference}_{full-simplified} = \left| \frac{(\overline{H}_{steady\ state,}/H_{incoming})_{full} - (\overline{H}_{steady\ state,}/H_{incoming})_{simplified}}{(\overline{H}_{steady\ state,}/H_{incoming})_{full}} \right| \tag{8.1}$$

The points outside the harbour basin are treated separately from the points inside the basin. The minimum, the average and the maximum value of the ratio Difference$_{full-simplified}$ are calculated for the points outside the basin outside the harbour. The results are shown in Table 8.3. Table 8.4 shows the same results for the point inside the harbour basin. The columns for T010 and T011 are marked with dark grey colour because they are excluded from the comparison due to the numerical instabilities observed at the results (Section 8.2).

Table 8.3 – The difference between the ratio $\overline{H}_{steady\ state,}/H_{incoming}$ at the output points outside the harbour basin in the full and the simplified 2D SWASH models for the seven selected tests. For T010 and T011 numerical instabilities occur (columns with grey colour).

Difference$_{full-simplified}$(%)	Output points outside the harbour basin						
	T001	T002	T003	T010	T011	T012	T013
Min	0	0	2	1	2	0	0
Average	4	5	17	10	6	7	4
Max	11	14	32	45	17	20	11

Table 8.4– The difference between the ratio $\overline{H}_{steady\ state,}/H_{incoming}$ at the output points outside the harbour basin in the full and the simplified 2D SWASH models for the seven selected tests. For T010 and T011 numerical instabilities occur (columns with grey colour).

Difference$_{full-simplified}$(%)	Output points inside the harbour basin						
	T001	T002	T003	T010	T011	T012	T013
Min	0	0	3	0	0	0	0
Average	2	3	11	11	4	7	2
Max	8	6	24	48	12	32	7

In both tables the values vary from 0% to 32%. This means that there are output locations for which the ratio does not change at all after adding the gravel slopes in the SWASH model. On the contrary, there are a few locations where the difference between the ratios is significant. Overall, the percentages outside and inside the basin vary within the same limits. As the average percentages are relatively small, varying from, 2 to 17% it can be claimed that the differences between the full and the simplified 2D SWASH model are relatively small. The reflections from the gravel slopes do not alter significantly the steady state wave heights. This means that inside the basin diffraction is the process which influences more the steady state wave height results in SWASH. Moreover, reflection off the harbour head walls is the process which influences more the steady state wave height results in SWASH.

8.4.2 Comparison of the steady state in the measurements and in the full 2D SWASH model

For each test, a graph is created visualising the ratio $\bar{H}_{steady\ state,}/H_{incoming}$ in the measurements and the 2D full SWASH model results. Each graph is accompanied with a table showing the exact values of the ratio. The graphs and the tables for all the tests are included in Appendix K. In this section only the results for T002 (Figure 8.16 and Table 8.5) are discussed.

For test T002, it can be observed that the values of the ratio $H_{steady\ state}/H_{incoming}$ for the measurements and for SWASH are in very good agreement at various output locations. For many points, i.e. Point 4, 10, 24, 6, 13, 14, 26, the difference between the measured values and the values calculated by SWASH is lower than 10%. However, at other locations, i.e. Point 5, 23, 25, 9 the difference is larger than 40%. These large differences can be related to fact that the SWASH wave height values are quite sensitive to the exact location of the point. As discussed in Section 5.3.2 , the resulting standing wave patterns changes within a short distance. Therefore, the wave height values may a change significantly at the region close to a specific point. This means that the measured wave height at a certain point can be found in SWASH at a location close to the exact location of the point. In general, the spatial wave pattern as indicated by the colours in Figure 8.16 is in good agreement between the measurements and the SWASH outputs. It can also be observed that the wave heights inside the basin are relatively lower than outside the harbour.

For T002, the values of the ratio for SWASH are constantly lower or higher than the measured values (Table 8.5). Additionally, from the comparison of the graphs for the different test it is observed that the wave height is not underestimated or overestimated at a specific wave gauge or for a certain group of point (e.g. inside or outside the harbour basin).
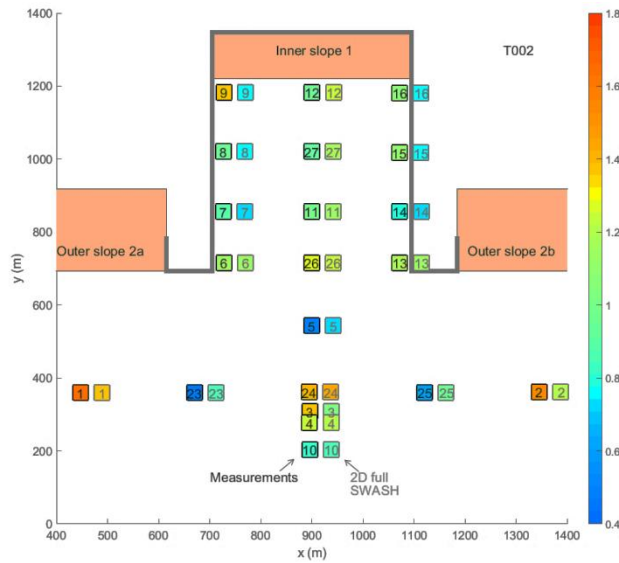
Figure 8.16 –2D full model results for T002: Top view of the ratio $H_{steady\ state}/H_{incoming}$ at the output locations included in the measurements. The colours indicate the ratio values.

Table 8.5 - 2D full model results for T002: The exact values of ratio $H_{steady\ state}/H_{incoming}$ at the output locations included in the measurements.

Outside the harbour basin				Inside the harbour basin			
Wave Gauge	Measured $H_{steady\ state}$ / H_{inc}	2D full $H_{steady\ state}$ / H_{inc}	Difference (%)	Wave Gauge	Measured $H_{steady\ state}$ / H_{inc}	2D full $H_{steady\ state}$ / H_{inc}	Difference (%)
1	1.63	1.36	-16	6	1.12	1.13	2
2	1.54	1.19	-23	7	0.90	0.73	-19
3	1.36	1.02	-25	8	0.95	0.76	-20
4	1.22	1.20	-2	9	1.37	0.76	-45
5	0.50	0.71	44	11	0.99	1.12	13
10	0.81	0.87	8	12	0.96	1.22	27
23	0.46	0.87	90	13	1.17	1.14	-3
24	1.41	1.45	2	14	0.79	0.74	-7
25	0.60	0.95	59	15	1.11	0.77	-30
	|Max|= 1.63	|Max|= 1.45	|Max|= 90	16	1.06	0.77	-28
				26	1.28	1.23	-4
				27	0.94	1.16	23
					|Max|= 1.37	|Max|= 1.23	|Max|= 45

8.5   Conclusions

This chapter addresses research question 3. Question 3 examines the ability of a 2D SWASH model representing the full geometry of the physical scale model to describe the wave height changes (temporally and spatially) in the measured water level time. The conclusions regarding this question are pinpointed in this section.

- The most important temporal trends observed in the measured water level time series can also be observed in the water level time series of the two-dimensional SWASH model representing the full layout 1. Firstly, the incoming wave height measured by the wave gauges is reproduced at the output locations in SWASH with an error lower than 6%. Moreover, after plotting the measured water level time series and the respective SWASH time series in the same graphs it was confirmed that the wave height changes due to reflection and diffraction can be identified qualitatively in SWASH. Finally, both in the measured signal and in SWASH a steady state is developed in most tests, except for tests T010 and T011 in which SWASH did not reach a steady state. For the rest of the tests the wave height remains constant during this final, steady state, part of the time series.

- From the comparison of the steady state wave height in the measurements and in the SWASH model including the full layout 1, it can be concluded that the overall spatial wave field pattern is in agreement. At many output locations the exact wave height in the measurements is accurately reproduced in SWASH. The difference between the measured wave height and the wave height calculated by the 2D full SWASH model was lower than 10% and thus sufficiently small. However, at a few output locations the exact wave height values were not described so well by SWASH, as the measured and the modelled wave height deviated more than 40%. These large deviations were attributed to the fact that the standing wave patterns change fast within a short horizontal distance and thus the wave height can vary significantly in the area close to a specific output point. It may be possible that the measured wave height at a specific point can be identified in SWASH in the region close to the exact point coordinates.

- At the output points for tests T010 and T011, in which the wave height to water-depth ratio is higher than 0.2, numerical instabilities were observed. At the end part of the time series the wave height instead of being constant, increases or decreases gradually, or initially decreases and then increases. This behaviour is not realistic and can be attributed to numerical error. An increase of the number of vertical layers used in SWASH does not solve the problem. It is assumed that the numerical instabilities can be attributed to the relatively low number of grid cells per wave length. In cases where the amount of cells per wave length is low, it is not possible for SWASH to capture accurately the wave shape and the numerical dissipation starts to influence the results. However, this assumption has not been verified within this study.

8.6   Remarks

Apart from the results referring to research question 3 (Section 8.5) in this chapter additional knowledge was obtained regarding the performance of SWASH. The most important information obtained after studying in detail the outputs of the two-dimensional SWASH model for the full layout 1 are summarised.

- The incoming wave height at the output locations along the model centreline differ less than 2% from the incoming wave height generated by the wave maker prescribed at the offshore model boundary. The only exception is T010 in which energy dissipation due to wave breaking leads to lower incoming wave height values compared to the value imposed at the boundary.

- The steady state wave height for the SWASH model including only the harbour head walls and the vertical walls off the harbour basin to the SWASH model including the full layout 1 is

compared. After the comparison, it can be supported that diffraction inside the harbour basin and reflection at the harbour head walls are two phenomena that mainly influence the final wave field in SWASH.

Chapter 9 Conclusions & Recommendations

This thesis examines the ability of SWASH to simulate the wave processes contributing to wave penetration separately and combined. As wave penetration is a summation of physical processes, each process should be modelled accurately by SWASH. To validate the numerical model, seven tests (Table 1.2) from a dataset of a physical scale model of schematic port layouts (Deltares, 2016) were studied. To reduce the amount of wave processes involved, the simplest port layout was chosen. This is layout 1 presented in Figure 1.1. Monochromatic wave conditions were analysed as in this case wave penetration becomes less complex and differences between the measurements and the computational results were most easily identified. Subsequently, simplified models including one or two wave processes were examined. Lastly, a SWASH model including all the wave processes influencing wave penetration in layout 1 was studied.

This chapter highlights the scientific contributions of this study and presents the main outcomes in the content of answers to the research questions and sub-questions formulated in Sections 1.4 and 1.5 . Additionally, recommendations for future research are outlined.

9.1   Conclusions

The main findings of the three primary research questions which guided this study are summarized in this section.

Question 1:   How accurate can SWASH model wave propagation, the incoming wave height and the wave celerity of individual waves?

- In the physical scale model, the incoming wave height that is prescribed to the wave maker is measured by the wave gauges. Also in SWASH the incoming wave height simulated inside the domain matches the waves prescribed as boundary condition. Thus, no unexpected phenomena are taking place during the propagation of the waves from the wave maker (in the physical model) and the model boundary (in SWASH) towards the harbour.

- For kd values lower than 3 and wave height to wave length ratio lower than the breaking limit, it can be confirmed that the wave celerity in the measurements and the wave celerity in SWASH are in agreement and they are both equal to the wave celerity calculated according to the linear wave theory. For kd values higher than 3 and non-breaking waves, the agreement between the wave celerity in the measurements and the wave celerity calculated by SWASH celerity is sufficiently good, even though the linear theory does not hold. Finally, for kd values higher than 3 and breaking waves the wave celerity in SWASH is significantly lower than the measured celerity.

- The wave amplitude of the first waves generated by the wave maker is smoothly increasing from zero to the full prescribed wave height. In this initial part of the wave maker signal a taper function is applied. Both in the measurements and in SWASH simulations it was observed that the taper function signal behaves different than the fully developed incoming wave part. Firstly, the taper function part travels faster than the wave celerity of the fully developed part, which matches to linear wave theory. Secondly, as the distance from the wave maker increases, the wave height of the taper function part decreases. All in all, the behaviour of taper function part of the waves is non-linear. In SWASH the same features were observed: the wave celerity of the taper

function part is higher than the fully developed part and the wave height of the taper function part decreases for an increasing distance from the offshore boundary representing the wave maker. However, the agreement between the taper function part in the measurements and in SWASH was not examined in detail in this thesis.

Question 2: Can wave reflection and diffraction be modelled accurately by SWASH?

Sub question 2a. : Is it possible to accurately reproduce the correct amount of reflection in SWASH, using the porosity and stone values from the scale model?

- An increase or decrease of the porosity of a gravel slope by 10% does not influence to a large extend the water level in front of the slope. The same holds for changes of the stone size by 10%, which result in lower constant wave height than in the measurements. It was proven that the measured signal in front of the outer gravel slope was also influenced by the reflections off the harbour concrete head walls. This means that there is no wave gauge measured signal which is only influenced by the reflections off the gravel slope and can be used to calibrate the porosity and stone size values in SWASH. Therefore, it was decided to use in SWASH simulations the porosity and stone size values as described for the experiments, converted to prototype scale.

- The arrival of reflected waves is visible both in measurements and in SWASH at every observation point, as the wave height changes slightly or significantly depending on the location of the observation point. The most important trends due to reflection are reproduced qualitatively in the SWASH model. However, large deviations in the wave heights can be found.

- For the points outside the harbour basin, the steady state wave height in the measurements and in SWASH differ significantly, indicating that reflection off the harbour end does not play a dominant role in the area outside the basin.

- For the points along the centreline of layout 1 located inside the harbour basin, the difference between the steady state wave height in the measurements and in SWASH varies from 12 to 40%. This means that the reflection phenomenon explains a significant part of the total steady state wave height. It can be concluded that reflection off the harbour end plays an important role in the wave field inside the harbour basin.

Sub question 2b. : Is it possible to accurately reproduce the diffraction of wave energy into a harbor basin in SWASH?

- Information about the influence of diffraction on the wave height changes in the main harbour basin cannot be derived from the measurements, as the time interval between the arrival of the incoming and the reflected waves from the end of the harbour is not long enough.

- In SWASH the effect of diffraction can be studied by removing the harbour end to avoid reflection of the waves. From the comparison of the steady state wave height influenced only by diffraction to the respective measured value it can be concluded that the wave penetration inside the harbour basin is determined significantly influenced by diffraction. However, as discussed in sub-question 2a, reflection off the harbour end is the dominant process inside the harbour. It should be clarified that both processes, reflection off the harbour end and diffraction play an important role in the wave penetration inside the harbour basin and none of them can be ignored.

- Although information about diffraction in the measurements is rather limited, the initial trends observed were compared to the SWASH outputs. From this comparison, it follows that the initial

part of the SWASH time series as waves enter the basin is in good agreement with the part of the measurements only influenced by diffraction.

- The wave reflection off the harbour head walls is the phenomenon with the most important influence on the wave field outside the harbour basin, even at locations outside the cone of influence calculated according to the linear wave theory. The most important trends due to reflection off the head walls can be identified in the resulting water level signals in SWASH.

All in all, it can be concluded that the accuracy of SWASH in modelling the wave processes of reflection and diffraction is sufficiently well for engineering purposes.

Question 3: Can a two-dimensional SWASH model representing the full layout 1 describe the wave height changes (temporally and spatially) in the measured water level time series?

- The most important temporal trends observed in the measured water level time series can also be observed in the water level time series of the two-dimensional SWASH model representing the full layout 1. Firstly, the incoming wave height measured by the wave gauges is reproduced at the output locations in SWASH with an error lower than 6%. Moreover, after plotting the measured water level time series and the respective SWASH time series in the same graphs it was confirmed that the wave height changes due to reflection and diffraction can be identified qualitatively in SWASH. Finally, both in the measured signal and in SWASH a steady state is developed in most tests, except for tests T010 and T011 in which SWASH did not reach a steady state. For the rest of the tests the wave height remains constant during this final, steady state, part of the time series.

- From the comparison of the steady state wave height in the measurements and in the SWASH model including the full layout 1, it can be concluded that the overall spatial wave field pattern is in agreement. At many output locations the exact wave height in the measurements is accurately reproduced in SWASH. The difference between the measured steady state wave height and the steady state wave height calculated by the 2D full SWASH model was lower than 10% and thus sufficiently small. However, at a few output locations the exact wave height values were not described so well by SWASH, as the measured and the modelled wave height deviated more than 40%. This observation is related to the method used in this thesis, comparing local values. The large deviations can be explained by the fact that the standing wave patterns change fast within a short horizontal distance and thus the wave height can vary significantly in the area close to a specific output point. It may be possible that the measured wave height at a specific point can be identified in SWASH in the region close to the exact point coordinates.

- In all the examined measured water level time series a steady state is developed. In the majority of SWASH water level time series also a steady state is developed. However, for some tests in which the wave height to water-depth ratio is higher than 0.2 (tests T010, T011) the wave pattern does not remain constant as numerical instabilities are observed. The total error was increasing in time. An increase of the number of vertical layers in SWASH was not proven capable to solve the problem. It is assumed that the numerical instabilities can be attributed to the relatively low number of grid cells per wave length. In cases where the amount of cells per wave length is low, it is not possible for SWASH to capture accurately the wave shape and the numerical dissipation starts to influence the results. However, this assumption has not been verified within this study.

9.2   Recommendations

During the course of this study several points of interest for further research were detected. These topics are discussed in this section, which is divided in two parts. The first part exhibits recommendations regarding the improvement of the approach and the methods applied in thesis. The second part focuses on applying the existing methodology in different cases and other conditions.

To begin with, the numerical instabilities observed in two of the seven examined tests should be further investigated. Their origin as well as appropriate prevention measures should be identified. It is postulated that they are probably a consequence of the low number of cells per wave length for the specific tests. Hence, the grid resolution should be decreased. It would be a nice idea to adapt the grid size for each test based on the number of cells per wave length. However, this may be time consuming as new input files and a new SWASH command files will have to be created for every case. Alternatively, a researcher can select 3 different grid sizes and use the more suitable depending on the wave height and wave length of the monochromatic waves examined. The wave height relatively to the water depth influences the grid size as the number of cells per wave length in SWASH should be increased for higher waves.

SWASH results for the standing wave patterns suggest that the wave height value may change significantly within a short horizontal distance. This holds especially in front of a concrete wall as in this case the reflection is higher. Therefore, it can be studied whether the wave height values measured at a specific wave gauge can be identified within a short distance from the respective output point in SWASH. As the standing waves height varies horizontally according to the wave length, the distance from the output location can be a fraction of the wave length.

In this study, the celerity of monochromatic waves in the measurements as well as in SWASH was determined as follows: Initially the celerity is estimated assuming that linear wave theory holds and then the water level time series are shifted at a specific point. Subsequently, the agreement of the water level time series in terms of the wave height and times shift is visually inspected to verify whether the initially assumed celerity was correct. However, it was proven that this method cannot be applied for kd values higher than 3 as for this cases non-linear effects start becoming important. It is important to tackle this issue by improving the existing method. An alternative approach would be to assume for higher kd values that a high order Stoke theory applies and then make an initial assumption for the wave celerity. Moreover, as visual inspection can be depended on the judgement of the engineer it will be useful to try to quantify when the agreement can be considered good, average or not good. This can be done by setting limits for the wave height and the time shift variations.

This study examined how accurately the main wave processes influencing wave penetration are modelled in SWASH. These wave processes were examined separately and combined on simple wave and layout conditions which form the basis for most complex cases. As the conclusions of these research show generic trends, it is expected that they can be applied in other conditions. In other words, this thesis approach can be applied for example for different angle of incoming waves inside the basin, for more complex wave conditions (e.g. bi-chromatic, JONWSAP spectrum) and for more complex layouts (layout 2 and 3 in Table 1.1). Finally, it would provide further insight about wave penetration modelling with SWASH, to reproduce the results of this thesis using physical model scale and examine whether this choice improves or not the agreement between the measurements and the SWASH results.

Bibliography

Allsop, N.W.H. (1998), *Coastlines, structures and breakwaters*, Published by: Thomas Telford, Chapter 11.

Al Saady, M.(2014), *Numerical study of regular and irregular wave interaction with vertical breakwaters*, MSc thesis, Delft University of Technology (repository.tudelft.nl)

Battjes, J.A. (1974), "Surf similarity." *Proc. 14th Conf.Coastal Eng*. Copenhagen: ASCE, New York, pp.466-480

Berkhoff, J.C.W. (1972), Computation of combined refraction-diffraction, *13th Int. Conf. Coastal Eng.*, pp. 471-490.

Berkhoff, J.C.W. (1976), *Mathematical models for simple harmonic linear water waves, wave diffraction and refraction*, Delft Hydraulics Publication No. 163.

Borsboom, M.J.A., N.Doorn, J.Groeneweg, and M.R.A. van Gent (2000), A Boussinesq-type model that conserves both mass and momentum, *27th Int. Conf. on Coastal Eng.*, ASCE, Sydney, 148-161

Boshek, M. R. (2009), *Reflection and Diffraction Around breakwaters*, MSc thesis, Delft University of Technology (repository.tudelft.nl)

De Jong, M.P.C., S.P. Reijmerink, A. Capel and A.J. van der Hout (2015), *Combining numerical wave models for efficient design of port layouts and entrance channels*, PIANC-COPEDEC IX, Rio de Janeiro, Brazil.

Deltares (2016), *Benchmark tests of wave penetration in harbours-Measurement report*, Deltares Technical Report, author: P.P.D. Van der Ven, reference 1209490-000-HYE-0001

Deltares (2013), *PHAROS - User & Technical Manual - Version 9.11.19731 - 11 May 2013,* Delft

Deltares (2008), *Triton 1.0 - User and technical manual version 1.0.,* Delft

DHI. (2007). *MIKE 21 bw User guide.*

Frostick L.E., McLelland S.J. and Mercer T.G. (2011), *Users Guide to Physical Modelling and Experimentation: Experience of the HYDRALAB Network*, CRC Press/Balkema

Hasselmann K., T.P. Barnett, E. Bouws, H. Carlson, D.E. Cartwright, K. Enke, J.A. Ewing, H. Gienapp, D.E. Hasselmann, P. Kruseman, A. Meerburg, P. Müller, D.J. Olbers, K. Richter, W. Sell, H. Walden (1973), *Measurements of Wind-Wave Grothw and Sweel Decay during the Joint North Sea Wave Project (JONSWAP)*, Deutsches Hydrographisches Institut Hamburg

Holthuijsen, L.H. (2007), *Waves in Oceanic and Coastal Waters*, Cambridge University Press

Monteban, D. (2016), *Numerical modelling of wave agitation in ports and access channels- A comparison study between SWASH and MIKE 21bw*, MSc thesis, Delft University of Technology (repository.tudelft.nl)

Rabinovich, A. B. (2009). Seiches and Harbour Oscillations. In: Y.C Kim (Ed.), *Handbook of Coastal and Ocean Engineering*, Singapore: World Scientific.

Roelvink, D., A.J.H.M. Reniers, A. van Dongeren, J. Van Thiel de Vries, J. Lescinski, and R. McCall (2015), *XBeach model description and manual.* Unesco-IHE Institute for Water Education, Deltares and Delft University of Technology.

The SWASH Team (2016), *SWASH User Manual-SWASH version 3.14*. Retrieved from http://SWASH.sourceforge.net

Thompson, E., Chen, H., and Hadley, L. (1996), Validation of Numerical Model for Wind Waves and Swell in Harbours. *J.Waterway, Port, Coastal, Ocean Eng.,* 122(5), 245-257.

United States (2008), *Coastal engineering manual*. Washington, D.C.: U.S. Army Corps of Engineers. http://coastalengineeringmanual.tpub.com/

Van der Ven, P.P.D., S.P. Reijmerink, A.J. van der Hout and M.P.C. de Jong (2018), *Open benchmark datasets for validating numerical wave penetration models*, PIANC World Congress Panama City, Panama 2018

Van Mierlo, F.A.J.M. (2014), *Numerical modelling of wave penetration in ports*, MSc thesis, Delft University of Technology (repository.tudelft.nl)

Wong, A.L.Z. (2016), *Wave hydrodynamics in ports, Numerical model assessment of XBeach*, MSc thesis, Delft University of Technology (repository.tudelft.nl)

Zijlema, M. and Stelling, G., and Smit, P. (2011), SWASH: An operational public domain code for simulating wave fields and rapidly varied flows in coastal waters. *Coastal Engineering, 58*(10),992-1012

Appendix A   Wave processes related to wave propagation in ports

Shoaling

Shoaling is the variation of the amplitude of the waves in their direction of propagation due to depth-induced changes of the group velocity in that direction. As the wave propagates into shallower water, the group velocity is initially increasing and then decreasing. In stationary conditions the energy flux, which is equal to the product of the wave group velocity and the wave energy per horizontal surface area, must remain constant along the wave rays. Therefore, the wave amplitude is initially decreasing and then increasing, over a flat sloping bottom. According to the energy flux balance, the wave amplitude theoretically goes to infinity, as the group velocity approaches zero at the waterline. It is obvious that the linear wave theory cannot longer be applied here and non-linear effects (e.g. wave breaking) play a dominant role.

As the waves approach the coast the wave spectrum changes due to shoaling. The lower frequencies are enhanced more than the higher frequencies and there is a slight shift of the spectrum towards lower frequencies. Moreover, the peak of the spectrum and the significant weight height will be higher. Typically the water depth inside the harbour is significantly smaller than the offshore water depth and shoaling occurs. Shoaling is also relevant in case of a non-uniform bottom depth in the harbour.

Refraction

Another phenomenon induced by the variations of water depth is refraction. Refraction is the turning of waves towards shallower water due to depth-induced or current-induced changes of the phase speed in the lateral direction, along the wave crests. Horizontal variations in water depth along the wave crest correspond to phase speed variation along the crest.

$$c = \sqrt{\frac{g}{k} \tanh(kd)} \qquad\qquad \textbf{(A. 1)}$$

According to Equation A.1 the crest moves faster in deeper water than in shallow water. Therefore, for a given time interval, the crest moves over a larger distance in deeper water than in shallower water. This results to the wave turning towards the shallower region with the lower propagation speed.

If due to refraction the wave rays converge, the wave amplitude increases. On the contrary, for diverging wave rays there is a reduction of the wave amplitude. The local bathymetry determines if the wave rays will converge or diverge.

Large scale refraction is related to sub-marine canyons or shoals. Small scale refraction occurs in the outer area of a port, as is related to small-scale features such as shoals and channels that can be found in coastal regions. The phenomenon of refraction can be important inside the harbour area if the bottom depth is non-uniform.

Refraction plays an important role for ports with approach channels. An approach channel is designed to be wide and deep enough for large ships to enter inside the harbour area. Based on the linear refraction theory the waves can cross the channel if their approach angle is larger than a critical angle, otherwise they will be reflected or transmitted. The critical angle can be determined by the Snell's law. Short waves can easily cross a channel, because their critical angles are very low. The longer the wave, the higher the critical angle (capped at a certain angle), the faster a long wave will be caught in a channel. For a more detailed description about processes involved in wave propagation in navigation channels the reader is referred to De Jong et al. (2016).

Reflection and transmission

When waves hit a structure or a coast, part of the wave energy will be reflected, dissipated or transmitted. The balance between the three phenomena depends on the incoming wave characteristics and the structure's material, geometry and permeability.

Transmission refers to amount of water that passes through the structure as well as the overtopping water quantity. The transmitted waves might have smaller wave heights and different wave periods from the incident waves.

The reflection coefficient k_r shows the percentage of the wave height that is reflected.

$$k_r = \frac{H_r}{H_i} \tag{A. 2}$$

where H_r is the reflected wave height and H_i is the incoming wave height.

The reflection coefficient ranges from 100% to 0%. For example, a vertical cliff or wall may reflect almost the whole amount of the incoming wave energy. On the other hand, for relatively short waves, there is almost no reflection on a gentle beach and the total amount of wave energy is dissipated. The amount of reflected wave energy depends on the characteristics of the incoming wave: height, length and direction. For example, the reflection is less when waves approach the obstacle under an angle.

The properties of the surface to which the waves collide also influence the amount of energy reflected. The structure permeability, the geometry and the roughness are factors that play an important role. Thompson et al. (1996) created a table including reflection coefficients for different structures. The values varied significantly for different structure type, but also for each structure the range of the reflection coefficient was relatively broad. In general, steeper slopes are related to higher reflection coefficients.

In a harbour the waves will reflect at the breakwaters and the quay walls resulting in fully or partially standing waves. At each point in front of the reflecting boundary, the wave motion will be the sum two waves: the incident wave, propagating towards the wall and the reflected wave, propagating away from the wall. At the antinodes the wave height may be twice the incoming wave height in case of fully reflected waves. This may lead to unacceptable wave heights for sailing ships or for moored ships at a berth.

A dimensionless parameter helpful to understand and predict the amount of energy reflected is the Irribaren number or the surf similarity parameter (Battjes, 1974). It is applied to waves travelling perpendicular towards a smooth structure and it is given by the following equation.

$$\xi_o = \frac{\tan a}{\sqrt{H_{m0}/L_o}} \tag{A. 3}$$

where ξ_o is the Irribaren number, a is the bottom slope, H_{m0} is the incident wave height and L_o is the deep-water wave length ($L_o = \frac{g \, T_{m-1,0}^2}{2\pi}$, where $T_{m-1,0}$ is the wave period)

The Iribbaren number is the ratio of the slope steepness to the wave steepness and can be used to predict the type of wave breaking, the amount of energy dissipation and also the reflection coefficient.

Diffraction

Diffraction is the turning of waves towards areas with lower amplitudes due to amplitude changes along the wave crest. Due to diffraction the waves travel into the shadow zone of an obstacle resulting to changes in wave direction and wave height. The phenomenon of diffraction has strong effects along

the geometric shadow line of obstacles such as islands, headlands and breakwaters. In ports diffraction occurs at a breakwater tip or at an entrance of a basin and so wave energy penetrates in their shadow area.

The effect of diffraction on long waves (low-frequency waves) is stronger than on short waves (high-frequency waves). For example, long waves diffract more around the breakwater tip and a larger amount of energy is distributed in the sheltered area behind the breakwater. Therefore, a shift of energy density towards the lower frequencies is observed in the energy spectrum in the shadow zone area. This results to a lower mean wave period in the sheltered region.

Diffraction may turn initially unidirectional, long-crested waves into different directions and areas. Cross-seas occur in the regions where waves meet again. The wave height in these areas will be the sum of harmonic waves from different direction and information about the phases is necessary.

Wave breaking

A non-linear process affecting waves in coastal waves is depth-induced wave breaking. Wave break is also called surf breaking and it is still poorly understood and difficult to be modelled accurately. When waves approach the shore the wave amplitude increases mainly due to shoaling. The ratio of wave height to the to the water depth H/h the waves is becoming higher. The wave height cannot any longer be considered small compared to the water depth. The water column under the wave front is equal to h+H/2, while under the though it is equal to h-H/2. Thus the wave front propagates faster than the trough and eventually the wave breaks. The process of breaking limits the wave height in shallow water and is the main source of energy dissipation in the surf zone. For harbour designs including beach areas wave breaking is relevant.

White-capping is the phenomenon of wave breaking when the ratio of wave height to the wave length H/L exceeds a certain limit, i.e. the waves become too steep. As white capping mainly occurs in deep water it is less relevant for the area close or in a harbour.

Low-frequency waves[1]

Low-frequency waves or infragravity waves (timescales roughly between 25 and 250s) are motions generated by variations in wave height in time and space in wave groups of wind generated short waves. They are called infragravity waves as they have lower frequencies than the short waves that are free surface gravity waves. They are also called bound low frequency waves as they travel with the wave group speed and their length is equal to the length of the wave group. Bound low frequency waves occur when two high-frequency waves with similar or almost equal wave frequencies interact. Low-frequency waves do not necessarily have to be bound but can also be free waves after breaking of the short carrier waves and reflecting at the coast.The infragravity waves should always be taken into consideration for a port design as they are related to resonance. When the length of low frequency waves coincides with the harbour basin length, in other words, the infragravity wave frequency is slightly different from the eigenfrequency of the basin, resonance may occur. Additionally, The low-frequency waves could also lead to large vessel motions when the frequency coincides with or is almost equal to one of the natural periods of a (moored) vessel.

The simplest example of bound long wave is for a wave group of bi-chromatic waves. A bi-chromatic wave consists of two regular waves. If these two waves have a small difference-frequency a group signal emerges. The surface elevation consists of a fast oscillating part based on the average radial frequency of the two components and a slowly oscillating part, of which the timescale is based on the difference between the frequencies of the two components. If the two components radial frequencies are very close to each other the slow timescale can become very large.

A Bi-chromatic short wave field generates 1 long wave. In reality however we have a full spectrum of waves of different frequencies. All the possible multiplications between 2 components in this

---

[1] Low frequency waves due to earthquake or land slide are not considered here.

spectrum can interact and create a long wave. The full long surface elevation is going to be the superposition of all these possible components, the total incoming bound long wave field.

In the nearshore there is an energy transfer from short wave frequencies to the lower frequencies. As wave groups enter the surf zone, their groupiness is reduced by breaking. Therefore the forcing mechanism, i.e. the variations in wave energy is weaker and the bound long waves can become decoupled from the wave groups. The bound long waves are released and become freely propagating long waves with speed given by the dispersion relationship.

Harbour oscillations

The eigenmodes of a harbour basin are determined by basins' geometry and depth. When the wave periods coincide with the eigenperiods (typical values between 0.5 to 30 minutes) of the basin resonance could occur. This is most typical for low frequency waves. Inside the basin area standing wave pattern can be developed. This means that in some locations the wave height will be amplified, which may be a limiting factor for the port operations. As the wave height is maximum at antinodes and minimum at nodes, strong horizontal currents arise, which might be unsafe for sailing or moored vessels.

The lowest frequency mode in a harbour is of major importance and is referred as the Helmholtz mode (Rabinovich, 2009). For this mode the wave length will be four times the basin length. In an ideal open-ended rectangular basin there will be a node at the entrance and an anti-node at the closed boundary.

Harbour oscillations are similar to the seiches in enclosed basins, such as lakes. Seiches can be understood as a water body swaying back and forth. The main difference between the two phenomena is that harbour is not fully closed, but partially, so the wave energy radiates out of the harbour. On the contrary, in a closed basin energy dissipation is governing. Moreover, seiches are generated due to external forcing mechanisms such as wind or atmospheric pressure.

Dispersion

Frequency dispersion, or simply wave dispersion, describes the phenomenon that wave celerity is a function of the wave frequency and /or the wave amplitude. Equation A.4 is the linear dispersion relationship and can be rewritten as in Equation A.5, as the phase velocity c is equal to the ratio ω/k.

$$\omega^2 = gk \tanh kd \tag{A.4}$$

$$\text{or } c^2 = \frac{g}{k} \tanh kd \tag{A.5}$$

where ω is the angular frequency ($\omega = \frac{2\pi}{T}$, where T is the wave period), k is the wave number ($k = \frac{2\pi}{L}$, where L is the wave length), d is the water depth and g the gravitational acceleration.

According to wave dispersion the longer waves (low frequency waves) propagate faster than the short waves (high frequency waves). This is valid in deep water where the depth is much larger than the wave length and the wave height. For large values of d the term tanh(kd) in the equation A.5 is equal to 1 and the phase velocity is not influenced by the depth, but from the wave length. In deep water the individual waves with different frequencies travel in groups. The group celerity in deep water differs from the individual phase speed.

As the waves approach the shallow water the water depth is small compared to the wave length and the wave amplitude. The term tanh(kd) will be approximately equal to kd. This means that the water depth determines the phase speed value and not the frequency. The waves become non-dispersive as the phase celerity does not depend anymore on the frequency. The group celerity in shallow water is equal to the individual phase speed.

Waves are generated offshore during a storm and consist of a large range of frequencies. Due to frequency dispersion, the lower frequency/longer waves propagate faster towards the coast or a harbour. This filtering effect becomes stronger for high directional spreading. Wind generated waves will travel to different directions, only part of the wave energy will reach a specific area. As the waves travel away from the storm, they become gradually more long-crested.

In shallow water high amplitude waves propagate faster than low amplitude waves. This nonlinear effect is known as amplitude dispersion. As explained above in shallow water the celerity is highly dependent on the water depth, which is relatively small compared to the wave amplitude. Amplitude dispersion also is related to the wave steepness. In coastal areas and harbour regions both amplitude and frequency dispersion should be taken into account.

Non-linear wave-wave interactions

If four wave components fulfil the resonance condition, energy transfer between them will occur. These resonant interactions are called quadruplet wave-wave interactions and are relevant for deep water, where they stabilize the wave spectrum shape.

Triad wave-wave interactions refer to the energy transfer and phase-coupling when three wave components fulfil the resonance conditions. This requires that the sums of frequencies and wave number vector of two freely propagating wave components are equal to the frequency and wave number, respectively, of a third freely propagating wave component. The same holds for four wave components. In addition, in case the sum of frequencies of three wave components may equal or almost equal to the frequency of the fourth component, resonance occurs and energy transfers between the waves. This phenomenon takes place in extremely shallow water, where the waves are non-dispersive. (Holthuijsen, 2007)

Due to triad wave-wave interactions there is energy transfer to frequencies multiple times higher than the peak frequency and to very low frequencies. This is presented in Figure A.1. The energy transfer is enhanced as the wave steepness and amplitude increase and the waves become non-linear. The wave-wave interactions may create an additional high frequency peak in the spectrum under fully developed shallow water conditions and near the outer edge of the surf zone.
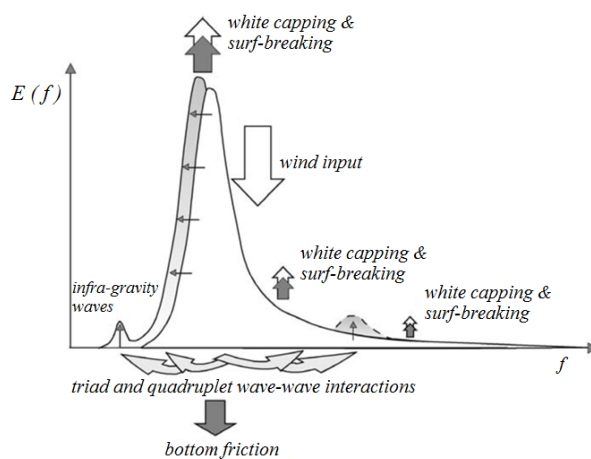

Figure A.1 -The energy flow through the spectrum in shallow water (Holthuijsen, 2007).

As the non-linear wave-wave interaction can significantly alter the shape of the spectrum it, should be taken into account when waves propagate towards a harbour and especially when the non-linearity of the waves is important. In case that the port has an entrance channel not including the non-linear wave interactions in the model can lead to underestimating the wave energy passing through the channel. When waves enter water that is so shallow that the linear wave theory no longer holds, the non-linear Boussinesq models (e.g. TRITON) and multilayer models (e.g. SWASH) can be used. These models include shoaling, refraction, diffraction and reflections and also nonlinear wave-wave interactions.

116

Appendix B   Physical scale model data

This appendix contains information about the physical scale model of the open benchmark dataset of schematic port layouts (Deltares, 2016). Section B.1 presents the wave conditions for all the examined tests in prototype scale. Section B.2 includes the coordinates of the harbour layout. The coordinated of the measurement locations are provided in Section B.3.

B.1 List of wave conditions for all the layouts in prototype scale

Table B.1 – Wave conditions in prototype scale (scale 1:45).

Test	Layout	Type	H[m], Hmo[m]	T[s], Tp[s]	Angle cartesian	Directional spreading	Steering file duration [s]
T001	1	Monochromatic	0.99	7.51	90	(n.a.)	3515
T002	1	Monochromatic	1.44	10.00	90	(n.a.)	4012
T003	1	Monochromatic	2.39	16.97	90	(n.a.)	5414
T004	1	Monochromatic	1.04	7.51	110	(n.a.)	3515
T005	1	Monochromatic	1.49	10.00	110	(n.a.)	4012
T006	1	Bi-chromatic	1.44	8.25	90	(n.a.)	5313
			1.44	11.74	90	(n.a.)	
T007	1	Bi-chromatic	1.44	9.06	90	(n.a.)	5635
			1.44	10.93	90	(n.a.)	
T008	1	Bi-chromatic	1.08	10.73	105	(n.a.)	6292
			1.08	9.39	75	(n.a.)	
T009	1	Bi-chromatic	1.08	10.73	95	(n.a.)	6292
			1.08	9.39	75	(n.a.)	
T010	1	Monochromatic	2.97	5.03	90	(n.a.)	3012
T011	1	Monochromatic	3.02	8.99	90	(n.a.)	3810
T012	1	Monochromatic	2.75	15.03	90	(n.a.)	5011
T013	1	Monochromatic	1.94	4.49	90	(n.a.)	2911
T014	1	JONSWAP	1.44	10.00	90	(n.a.)	12014
T015	1	Bi-chromatic	2.57	10.06	90	(n.a.)	8318
			2.57	15.76	90	(n.a.)	
T016	1	Bi-chromatic	2.61	10.06	90	(n.a.)	6842
			2.61	12.07	90	(n.a.)	
T021	2	Monochromatic	0.99	7.51	90	(n.a.)	3515
T022	2	Monochromatic	1.44	10.00	90	(n.a.)	4012
T023	2	Monochromatic	2.39	16.97	90	(n.a.)	5414
T025	2	Monochromatic	1.49	10.00	110	(n.a.)	4012
T026	2	Monochromatic	1.49	10.00	70	(n.a.)	4012
T027	2	Monochromatic	2.97	5.03	90	(n.a.)	3012
T028	2	Monochromatic	3.02	8.99	90	(n.a.)	3810
T030	2	Monochromatic	1.8	4.49	90	(n.a.)	2911
T031	2	Bi-chromatic	2.57	15.76	90	(n.a.)	8318

			2.57	10.06	90	(n.a.)	
T032	2	Bi-chromatic	2.61	12.07	90	(n.a.)	6842
			2.61	10.06	90	(n.a.)	
T035	2	JONSWAP	4.77	10.00	90	(n.a.)	12014
T036	2	JONSWAP	7.16	10.00	90	(n.a.)	12014
T038	2	JONSWAP	2.21	10.00	90	cos-2s with s=4	12014
T039	2	JONSWAP	2.39	10.00	70	(n.a.)	12014
T040	2	JONSWAP	2.39	10.00	110	(n.a.)	12014
T046	2	JONSWAP	2.34	10.00	90	(n.a.)	12014
T052	3	Monochromatic	1.44	10.00	90	(n.a.)	4012
T053	3	Monochromatic	2.39	16.97	90	(n.a.)	5414
T055	3	Monochromatic	1.49	10.00	110	(n.a.)	4012
T056	3	Monochromatic	1.49	10.00	70	(n.a.)	4012
T057	3	Monochromatic	2.97	5.03	90	(n.a.)	3012
T058	3	Monochromatic	5.99	8.99	90	(n.a.)	3810
T059	3	Monochromatic	6.80	15.03	90	(n.a.)	5011
T060	3	Monochromatic	1.8	4.49	90	(n.a.)	2911
T061	3	Bi-chromatic	2.57	15.76	90	(n.a.)	8318
			2.57	10.06	90	(n.a.)	
T062	3	Bi-chromatic	2.61	12.07	90	(n.a.)	6842
			2.61	10.06	90	(n.a.)	
T063	3	Sea monochromatic	2.48	6.98	110	(n.a.)	6212
		Swell monochromatic	0.54	15.03	70	(n.a.)	
T064	3	Sea JONSWAP	4.82	6.98	110	(n.a.)	9009
		Swell monochromatic	0.54	15.03	70	(n.a.)	
T068	3	JONSWAP	2.21	10.00	90	cos-2s with s=4	12014
T069	3	JONSWAP	2.39	10.00	70	(n.a.)	12014
T070	3	JONSWAP	2.39	10.00	110	(n.a.)	12014
T076	3	JONSWAP	2.34	10.00	90	(n.a.)	12014
T078	3	JONSWAP	4.46	10.00	90	cos-2s with s=20	12014
T079	3	JONSWAP	4.77	10.00	90	(n.a.)	12014
T080	3	JONSWAP	7.16	10.00	90	(n.a.)	12014
T081	3	JONSWAP	9.63	10.00	90	(n.a.)	12014
T083	3	Monochromatic	4.73	5.03	90	(n.a.)	3012
T084	3	JONSWAP	4.77	6.98	90	(n.a.)	9009
T085	3	JONSWAP	4.55	15.03	90	(n.a.)	17012
T086	3	Sea JONSWAP	4.77	6.98	110	(n.a.)	9009
		Swell PM-spectrum	1.71	15.03	70	(n.a.)	

B.2 Harbour layout

The following table contains the x and y coordinates of the corners (measured from within the harbour) of the concrete walls that form the harbour layout. The harbour layout itself and its location in the wave basin are displayed in the following figure.

Table B.2 – Coordinates of the harbour layout.

Harbour corner	x (m)	y(m)
A	615.15	783.00
B	615.15	693.00
C	705.15	693.00
D	705.15	1346.85
E	1094.85	1346.85
F	1094.85	693.00
G	1184.85	693.00
H	1184.85	783.00
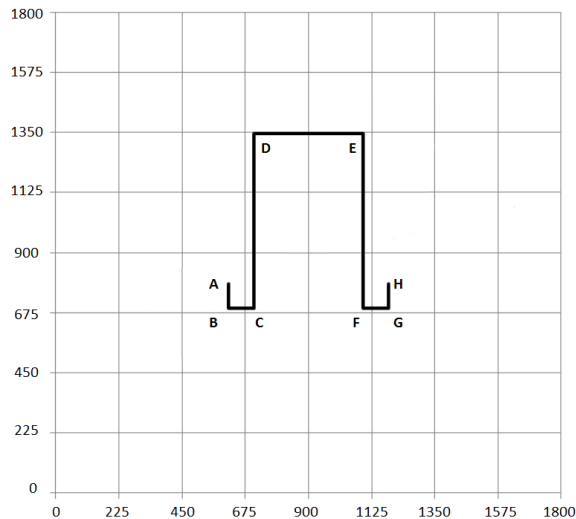
Figure B.1 – Harbour contour.

B.3 Locations of wave gauges

The measurement set up for layout 1 is presented in Figure B.2. The exact locations of the wave gauges in layout 1 are provided in the Table B.3.

Table B.3 – Measurement locations coordinates.

Wave gauge	x(m)	y(m)
1	447.075	359.505
2	1345.635	361.755
3	896.400	307.575
4	895.455	277.065
5	899.685	543.600
6	811.485	743.940
7	726.435	856.305
8	726.660	1020.645
9	728.190	1183.095
10	896.175	203.715
11	900.000	856.350
12	900.360	1183.275
13	1072.350	715.500
14	1072.350	856.350
15	1071.315	1017.045
16	1072.080	1181.340
23	670.365	359.730
24	894.825	360.945
25	1121.175	360.450
26	900.000	715.500
27	899.775	1020.510

Figure B.2 – Measurement locations.

119

Appendix C   Zero crossing analysis

Zero crossing analysis is performed to determine the individual waves. According to Holthuijsen (2007) in a surface elevation record, a wave is the profile of the surface elevation between two successive downward zero-crossings of the elevation. The definition with the downward crossings is preferred instead of the up-crossing definition, because in visual estimates the height of the crest relative to the preceding trough is normally considered to be the wave height. In addition, in a breaking wave, the (steep) front, which is most relevant for the breaking process, is included in the definition with downward crossings.

To find the wave characteristics based on a wave record requires averaging all of the individual wave heights and periods in the record. For this purpose the duration of the record has to be short enough to be stationary and at the same time long enough to obtain reasonably reliable averages. A typically used duration is at sea is 15–30 min. For controlled conditions in laboratory and especially for constant monochromatic waves, this time interval can be reduced. In Figure B.1 the zero crossings are presented by stars. An individual wave is defined between the first and the following star. The wave height H is defined as the vertical distance between the highest and the lowest surface elevation in a wave. The period T of a wave is defined as the time interval between the start and the end of the wave (the interval between one zero-down crossing and the next). Since this wave period is defined with zero-crossings, it is called the zero-crossing period, T_0 (Holthuijsen, 2007).
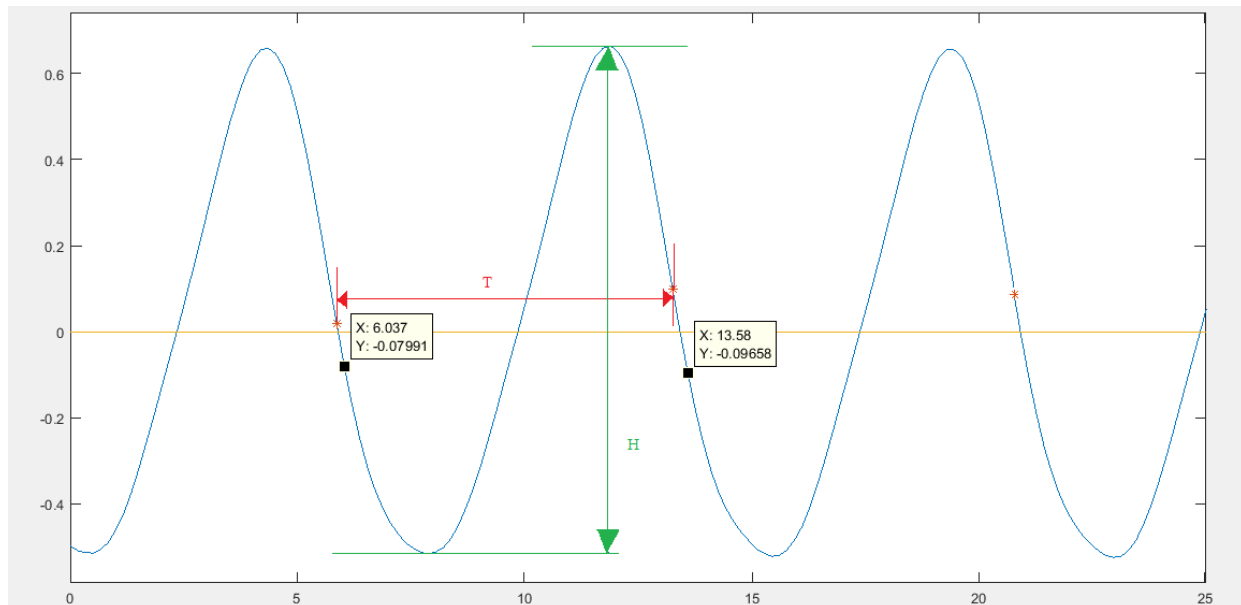
Figure C.1- Definition of an individual wave by zero-crossing analysis at point 10 for T001. The wave height and wave period are indicated. Horizontal axis: t(s), Vertical axis: water level (m).

After performing the zero crossing analysis and identifying the individual waves, the wave characteristics at each measurement location can be determined. For each test at all measurement locations the mean wave height and the mean wave period can be calculated. In a wave record with N waves, the mean wave height $\overline{H}$ is defined as

$$\overline{H} = \frac{1}{N} \sum_{i=1}^{N} H_i \tag{B.1}$$

where i is the sequence number of the wave in the record (i.e., i=1 is the first wave in the record, i=2 is the second wave, etc.).

The zero crossing analysis was applied for the following simple sinusoidal wave (Equation B.2) using the same time step as in the measurements (in prototype scale). It was shown that the error in the wave height was equal to 0.03% (Equation B.3) and thus sufficiently small for the calculations of the wave height.

$$\textbf{water level} = 1 * \sin\left(\frac{2\pi}{10} * t\right), \textbf{with } \Delta t = 0.1342$$

(B-2)

$$\textbf{error} = \frac{H - H_{\text{zero crossing}}}{H} = \frac{2 - 1.9995}{2} = 0.03\% \qquad \text{(B-3)}$$

Appendix D   Theoretical comparison of the different wave model types

To select the models with the most accurate and efficient performance in modelling wave penetration Van Mierlo (2014) compared different numerical models types. To be considered as capable to predict waves in harbours, the models should include the most relevant wave processes such as reflection, diffraction, shoaling and harbour oscillations. The different model types and their advantages and disadvantages regarding the application of wave penetration are briefly described in the following paragraphs. For a more analytical description the reader is referred to Van Mierlo (2014).

A. Spectral wave models

The governing equations in a spectral wave model are the energy balance equations of the energy transported by waves. The wave energy can be transferred in space, but also within the energy density spectrum. They are developed to be efficient in deep ocean applications as they can describe wave propagation over large distances. However, as they do not resolve individual waves, accurate model of diffraction is as the phases of the individual waves are not calculated. Moreover, as energy spectra are used, the generation of infragravity waves cannot be included. Therefore, this type of models is not appropriate for wave penetration simulations.

B. Shallow water models, forced on primary wave group scale

This type of models solves the shallow water equations. This means that hydrostatic pressure is assumed and this is an obstacle in modelling frequency-dispersive waves. Although this type of models can accurately model the propagation of infragravity waves are not recommended to model waves in a harbour area.

C. Mild-slope models

The mild-slope equation is derived from the potential flow theory by linearization. As it is an elliptic partial differential equation it can be solved in the frequency domain. This wave model type can approximate the wave spectra by adding waves with different frequencies and from different directions based on the superposition principle. In the mild-slope models there is no limitation in the maximum kd value and short waves propagating in deep water can be modelled accurately. As it is a linear model type it cannot model non-linear waves and non-linear wave interactions. Due to the mild-slope assumption there are restrictions in terms of wave amplitude, wave steepness and bottom slopes.

This type of models can very well be used to model wave penetration into harbour basins, because it takes into account the most relevant wave processes and it is numerically very efficient. A large range of conditions can be tested in a relatively short time period, whereas much more time is needed for more complete and computationally demanding wave models. The accuracy of mild slope models is often more than adequate for consultancy projects and the stages of projects in which wave penetration modelling is performed. For additional information about the mild-slope models, the reader is referred to De Jong et al, 2015.

D. Boussinesq-type models

Boussinesq-type equations are also derived by the potential flow theory. The vertical dimension is eliminated for example with a perturbation series expansion of the velocity at the bottom. It is worth mentioning that the free surface boundary conditions are not necessarily linearized. This class of wave models can describe non-linear interactions. Boussinesq-type models are time demanding. Moreover, there is a limitation of the maximum kd-value in the models, which usually can be up to 3 or 4. This model class is suitable for simulating wave penetration in harbours.

E. Non-hydrostatic models

The non-hydrostatic models solve the shallow water equations in combination with a vertical momentum equation. By adding a term for the non-hydrostatic pressure in the horizontal momentum equation it is possible to accurately take into account the vertical structure of the flow. The water depth is divided in the vertical direction. A different number of vertical layers correspond to different maximum kd-value. This is a computationally demanding class of models. Moreover, non-linear wave interactions can be taken into account.

F. Full free-surface Navier-Stokes models

This type of models is able to model nonlinear phenomena and wave breaking in particular, but it is computationally demanding and has not been used in harbour applications.

Van Mierlo (2014) concluded that the wave model types which provide more reliable results about wave penetration are mild slope models, Boussinesq type models and non-hydrostatic models. The three model classes are presented in Table D.1. The second column of the table includes some examples of operational wave models for each wave model class.

Table D.1 -The optimal classes of models for simulating wave penetration. The second column contains the operational wave model chosen to be studied in detail by F. Van Mierlo (2014).

Type of wave model	Wave model
Mild-slope	PHAROS
Boussinesq type models	TRITON
Non-hydrostatic models	SWASH

Appendix E   Measured water level time series and steady state wave height

E.1 Measured water level time series

This appendix presents the measured water level time series for the seven tests including the characteristic moments in time determined in Section 3.3. The points are presented according to their position in line AA'. The first point is Point 10, which is the closest to wave maker. The last point is Point 27 for which the distance from the wave maker is the maximum.
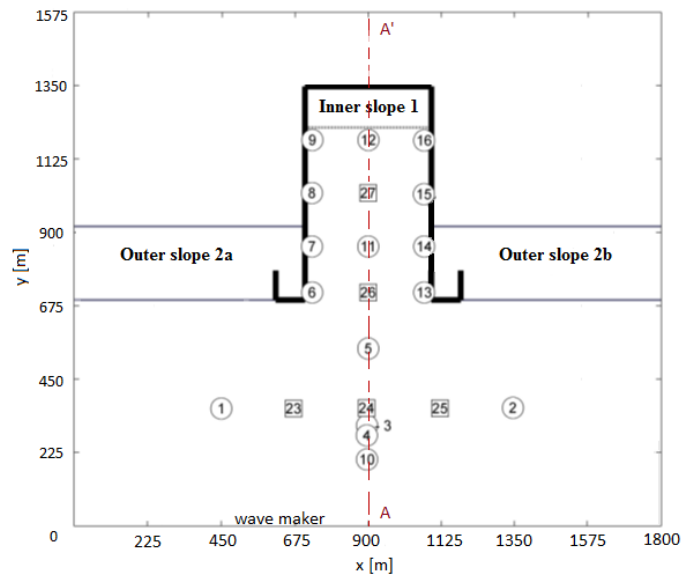
Figure E.1 - Model centre line (AA') is located in the middle of the basin in terms of width. This figure is a repetition of Figure 3.9.
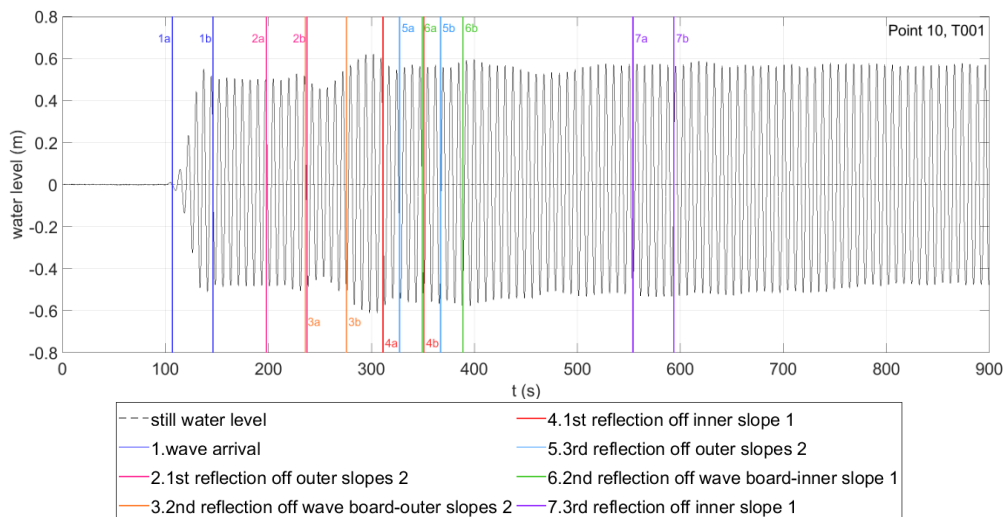
Figure E.2 – Measured water level time series for T001 at Point 10.
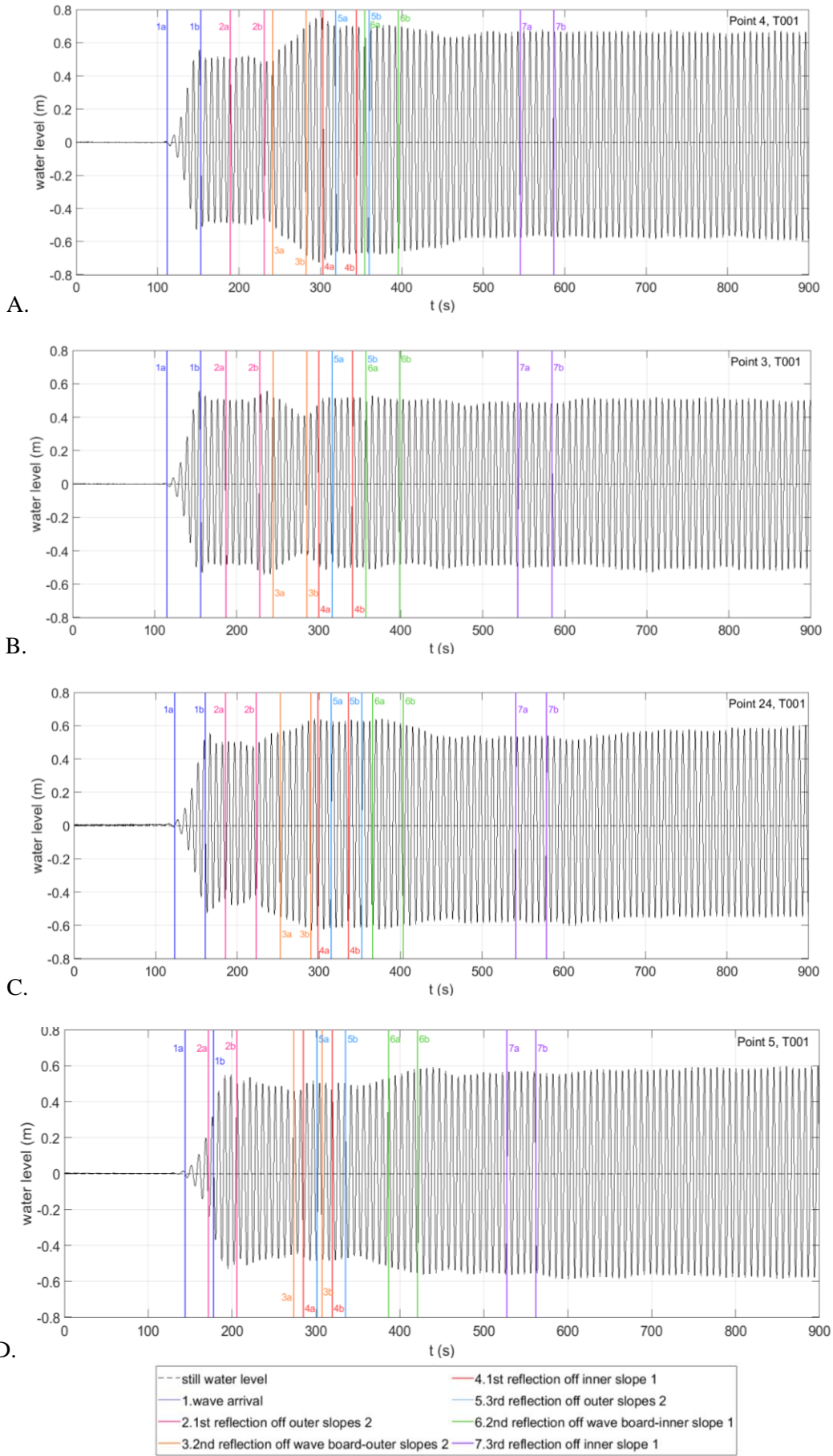
Figure E.1-Measured water level time series for T001 at Points 4, 3, 24 and 5.
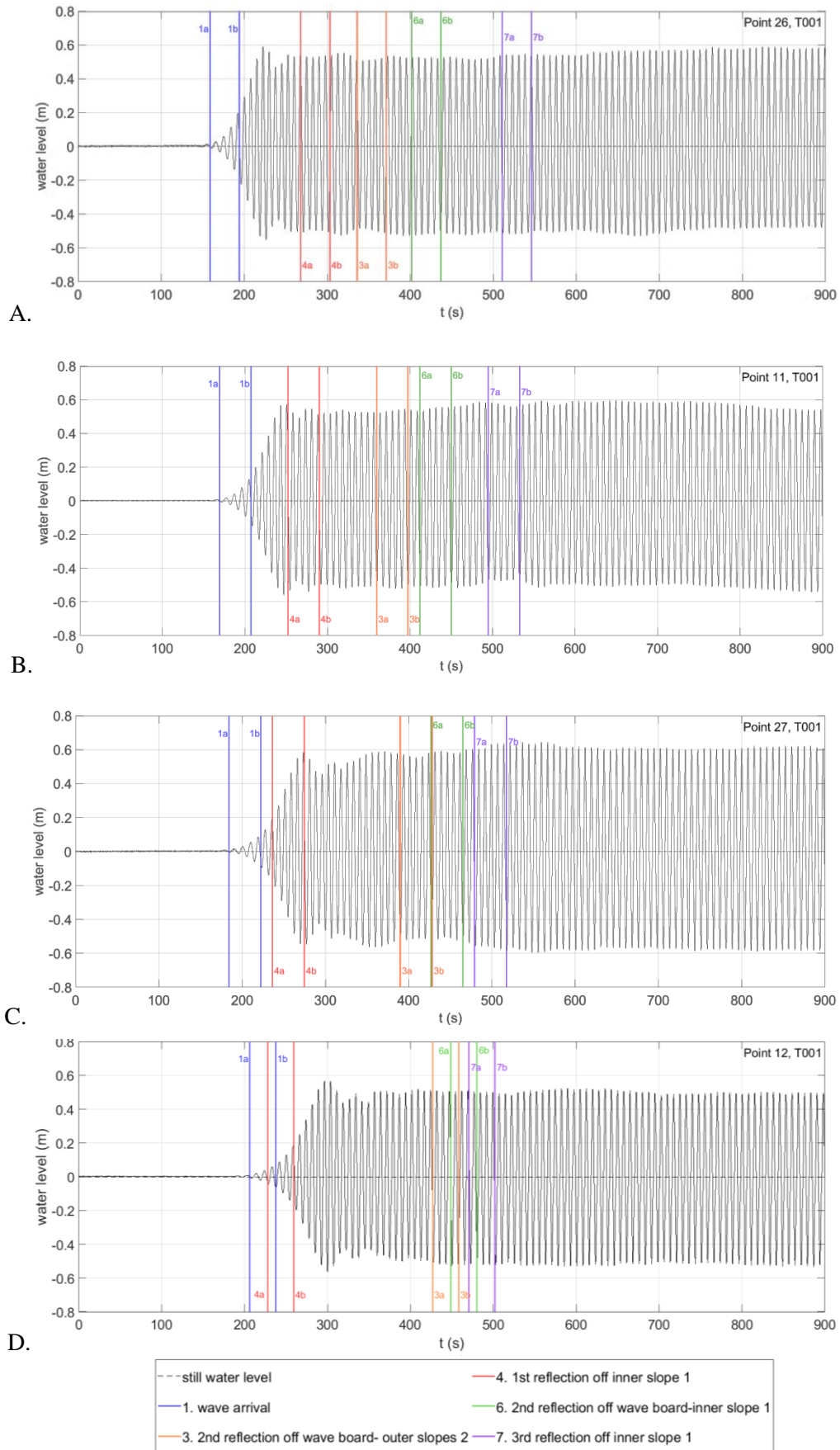
Figure E.2 –Measured water level time series for T001 at Point 26 (A), 11 (B), 27 (C) and 12 (D).
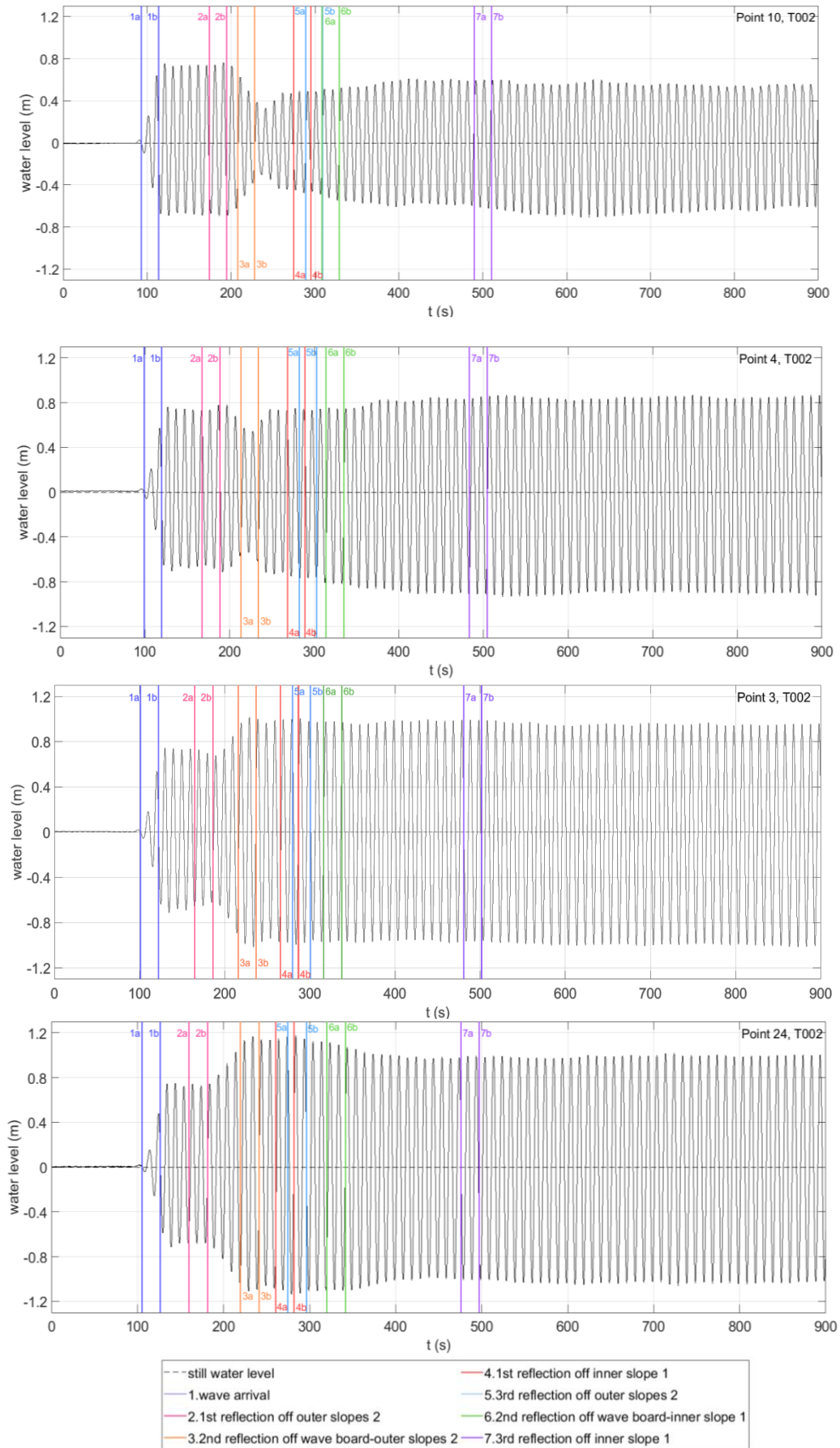
Figure E.3 – Measured water level time series for T002 at Point 10 (A), 4 (B), 3 (C) and 24 (D).
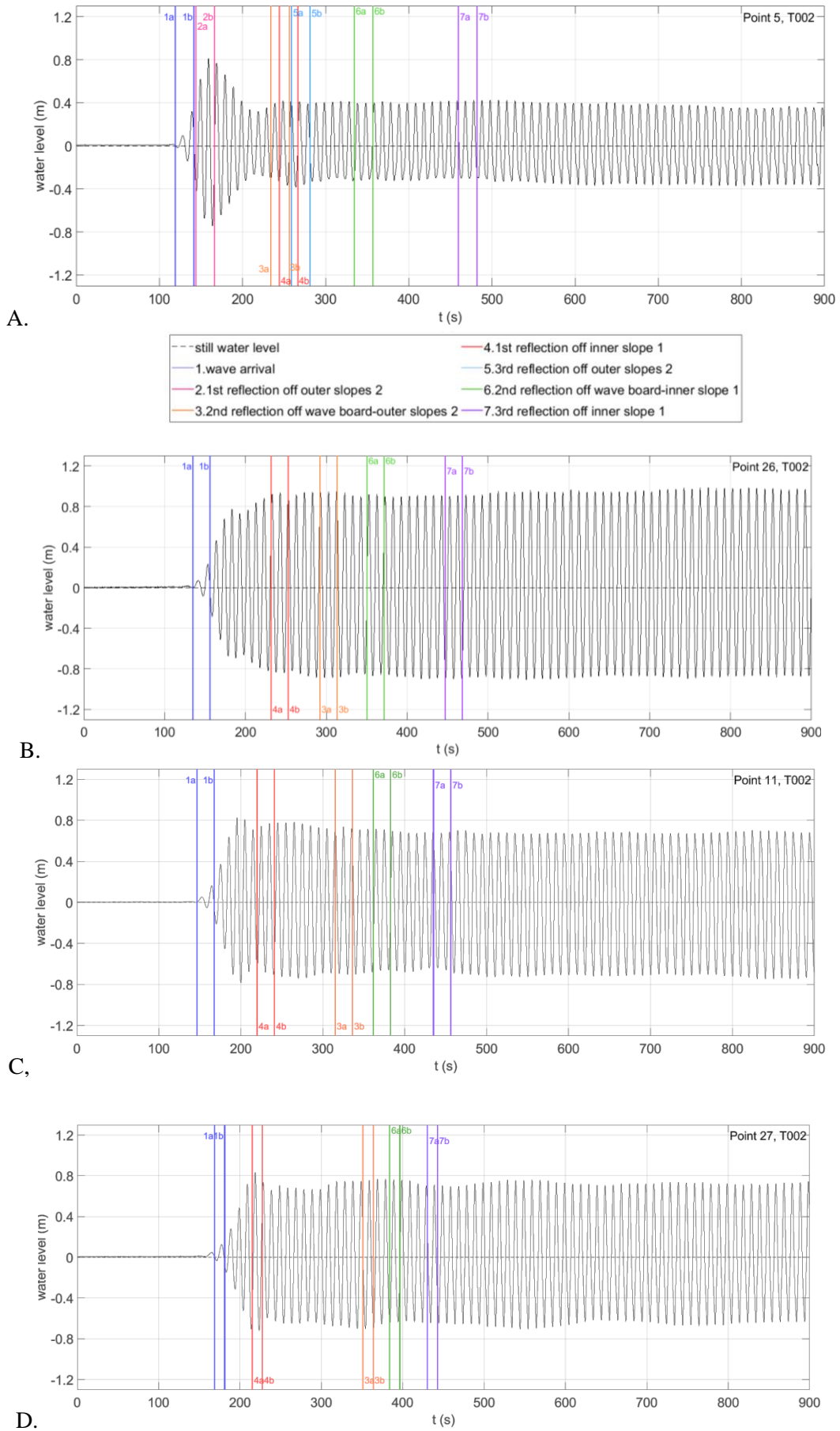
Figure E.4 – Measured water level time series for T002 at Point 5 (A), 26 (B), 11 (C) and 27 (D).
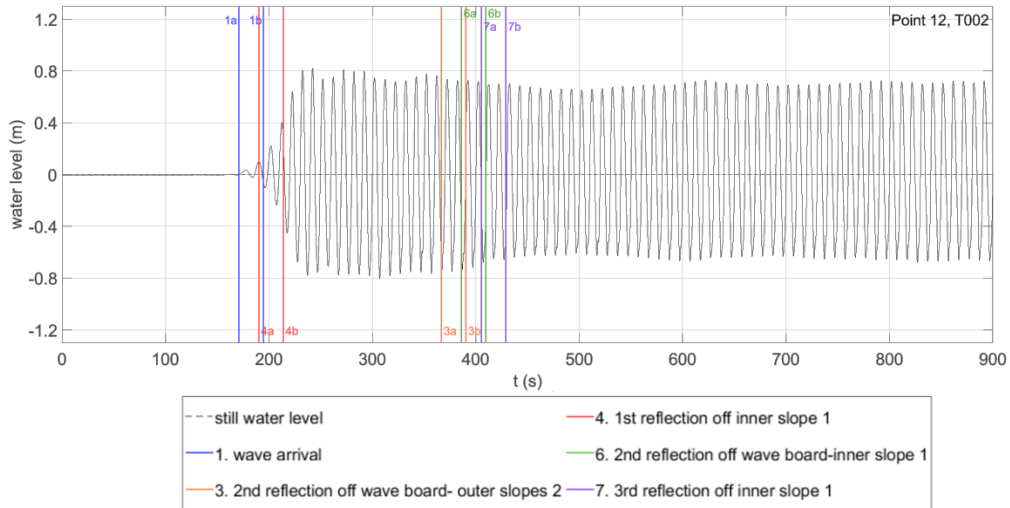
Figure E.5 – Measured water level time series for T002 at Point 12.
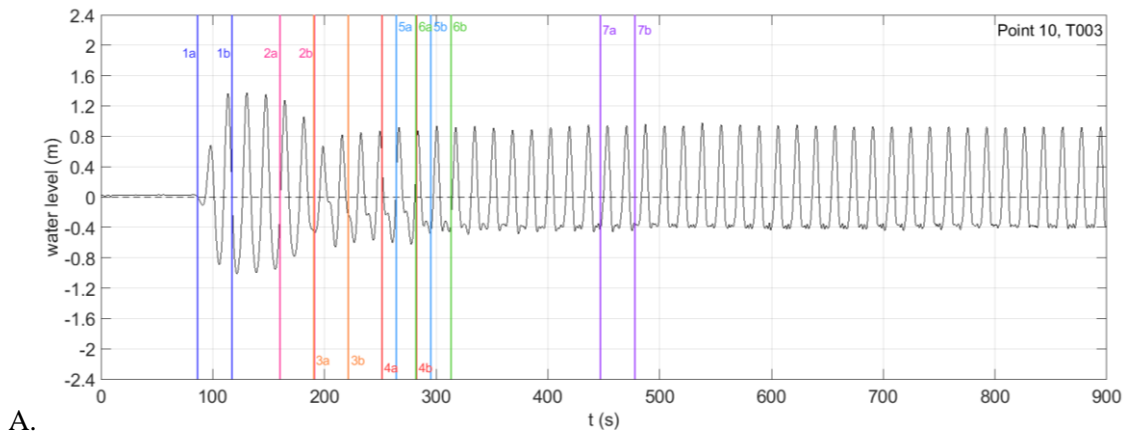
A.
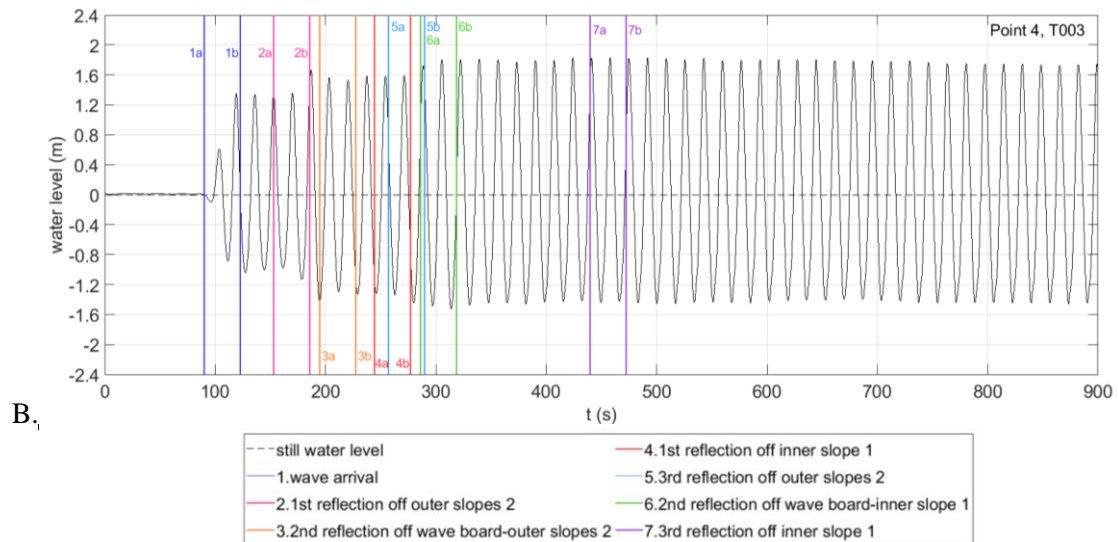
B.

Figure E.6 - Measured water level time series for T003 at Point 10(picture A) and Point 4 (picture B).
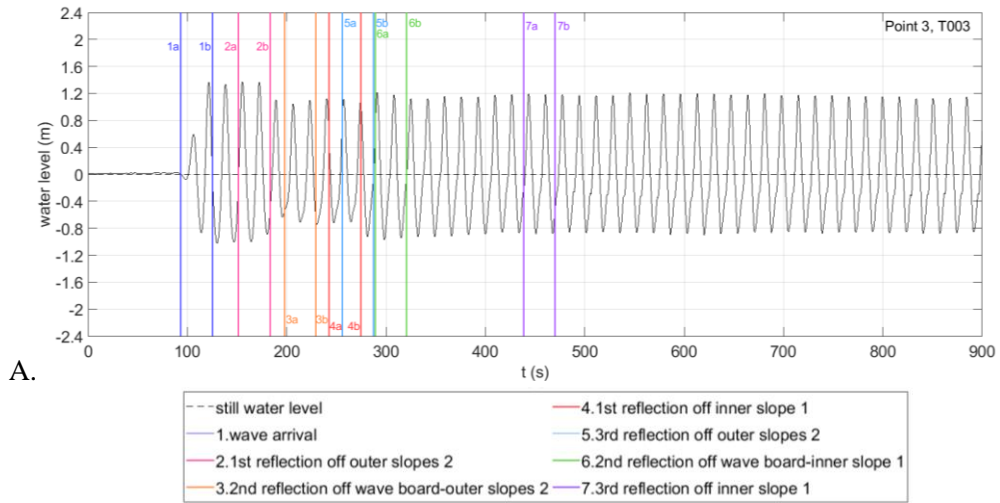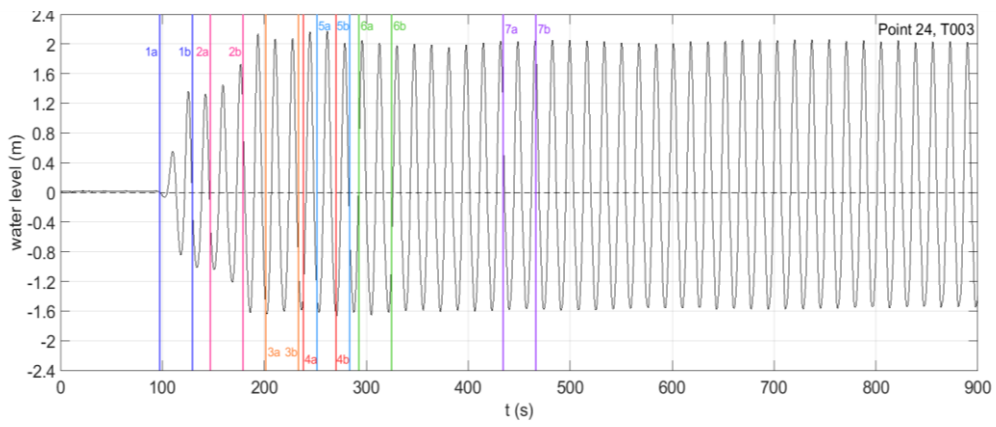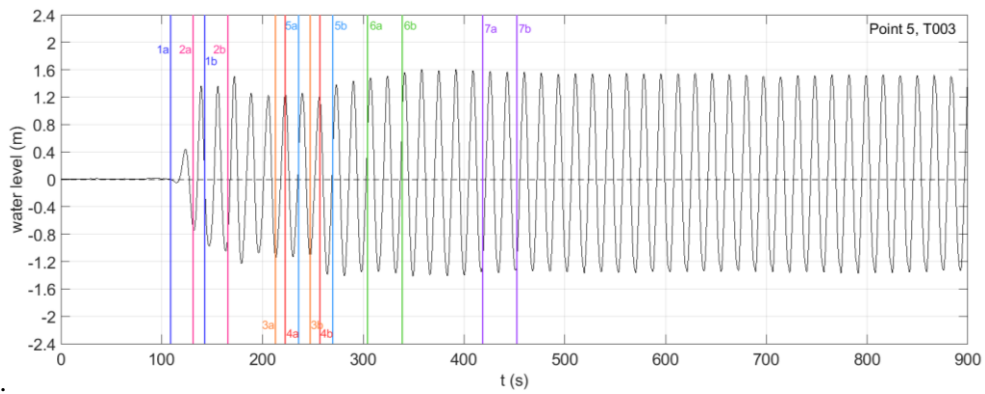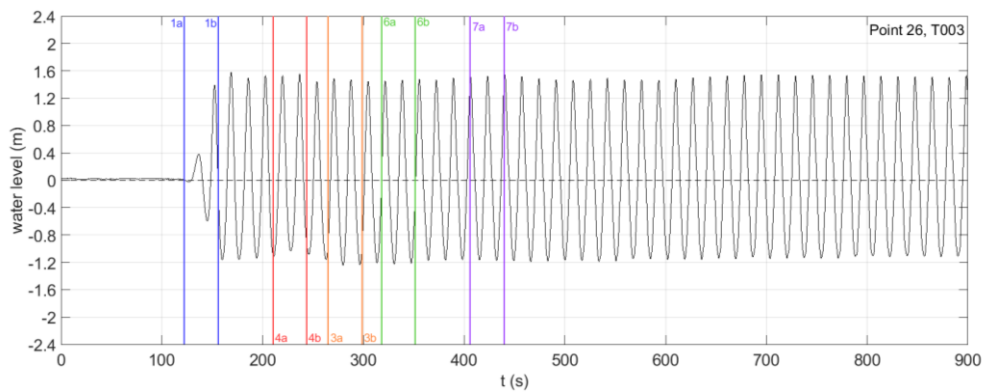
Figure E.7 - Measured water level time series for T003 at Point 3 (A), 24 (B), 5 (C) and 26 (D).
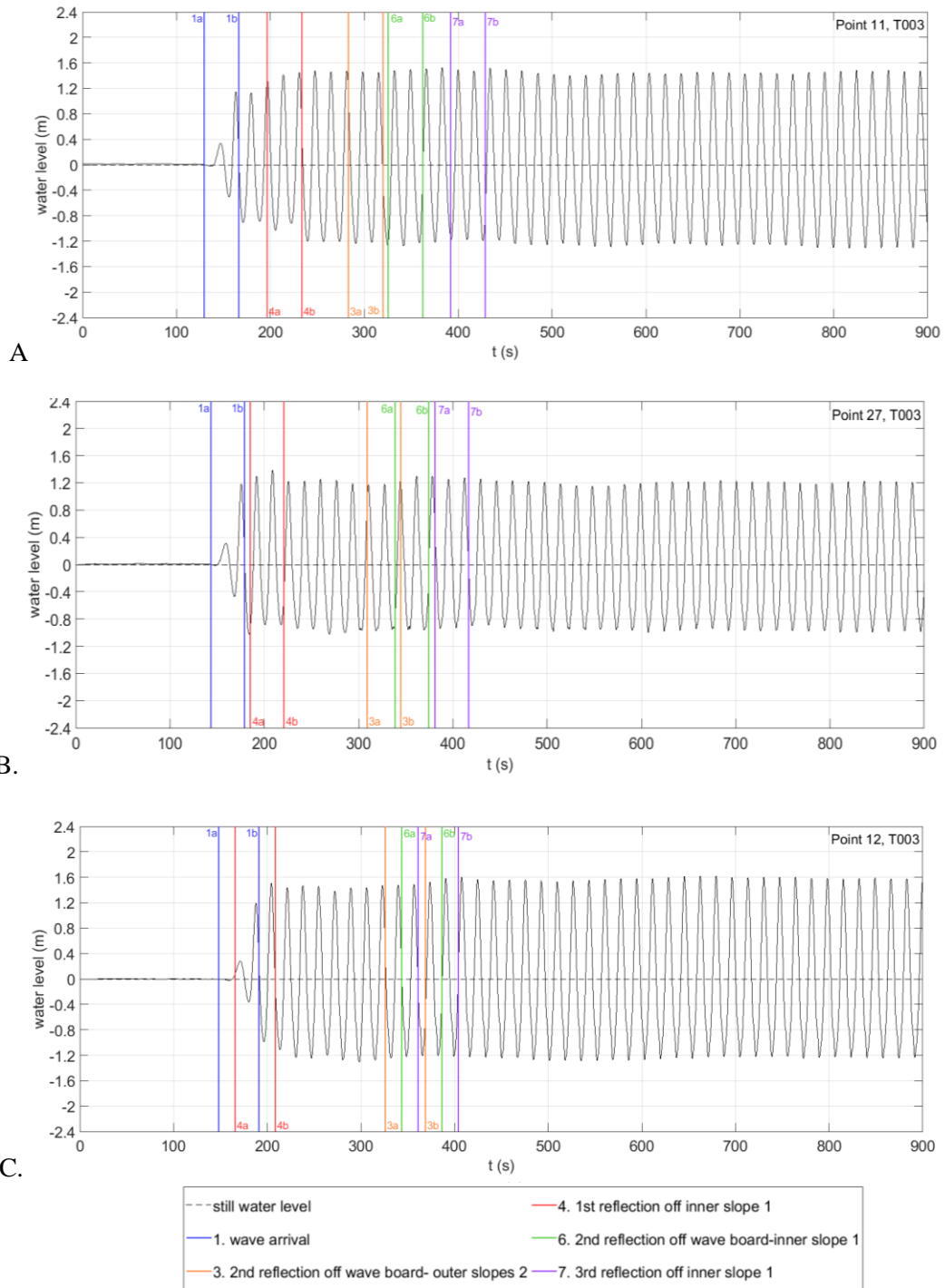
Figure E.8 - Measured water level time series for T003 at Point 11 (picture A), at Point 27 (picture B) and at Point 12 (picture C).
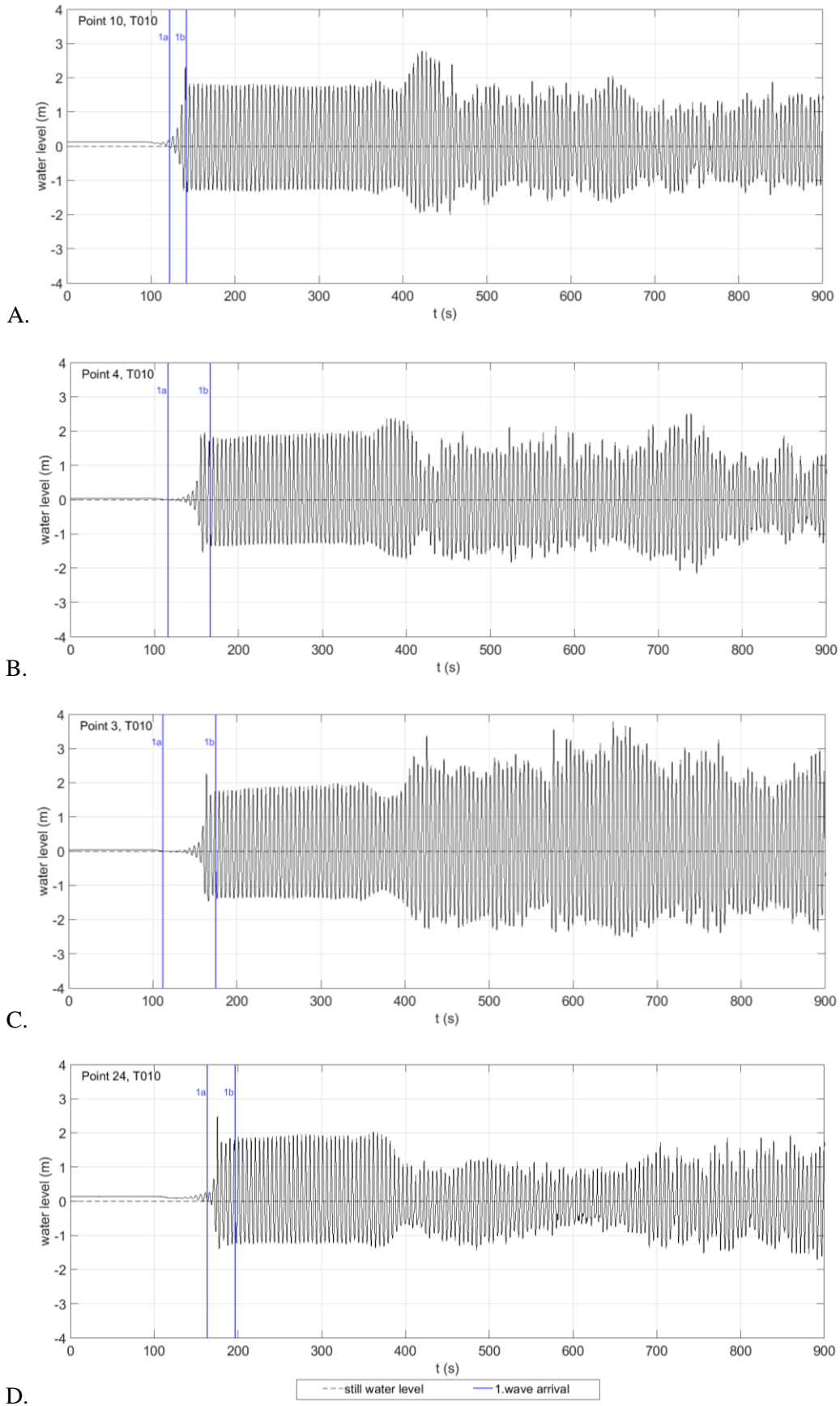
Figure E.9 - Measured water level time series for T010 at Point 10 (picture A), at Point 4 (picture B), at Point 3 (picture C) and at Point 24 (picture D).
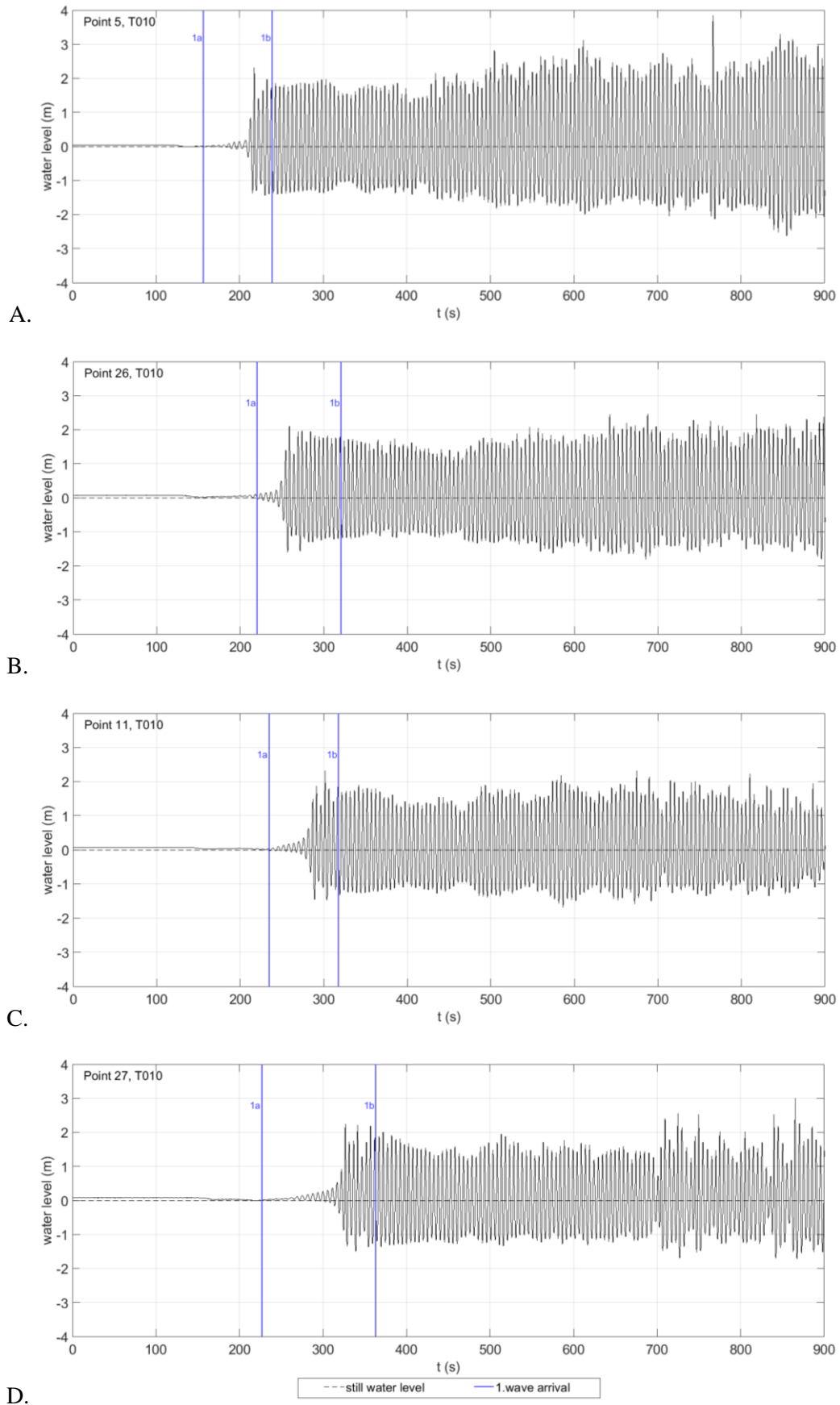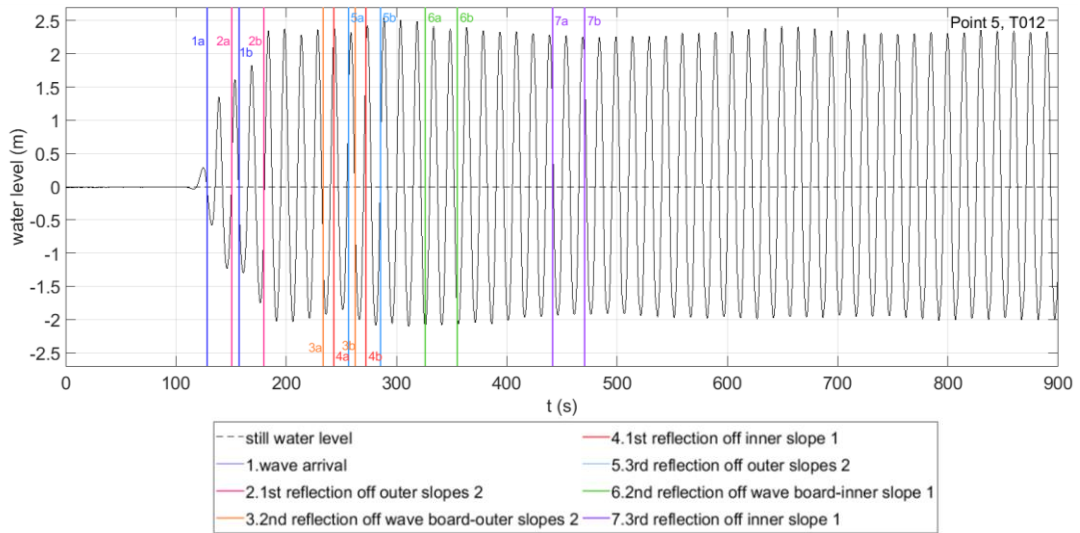
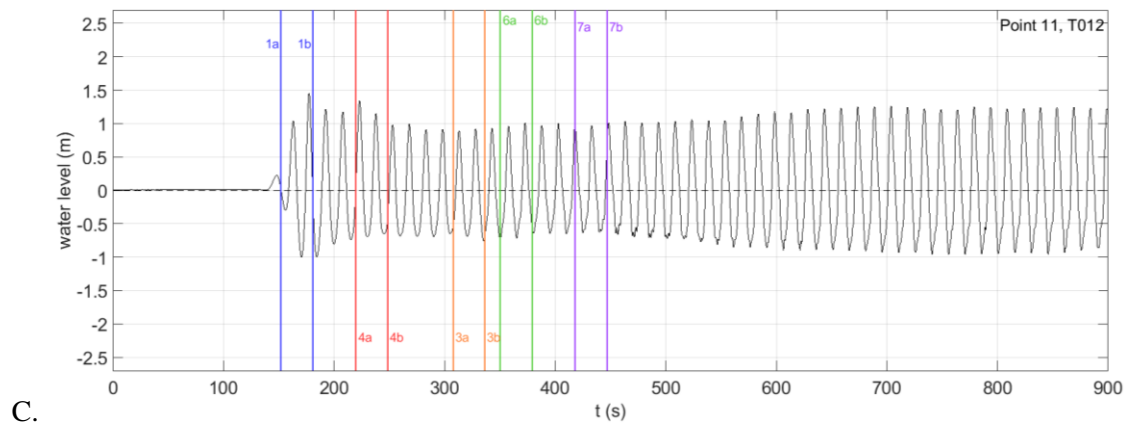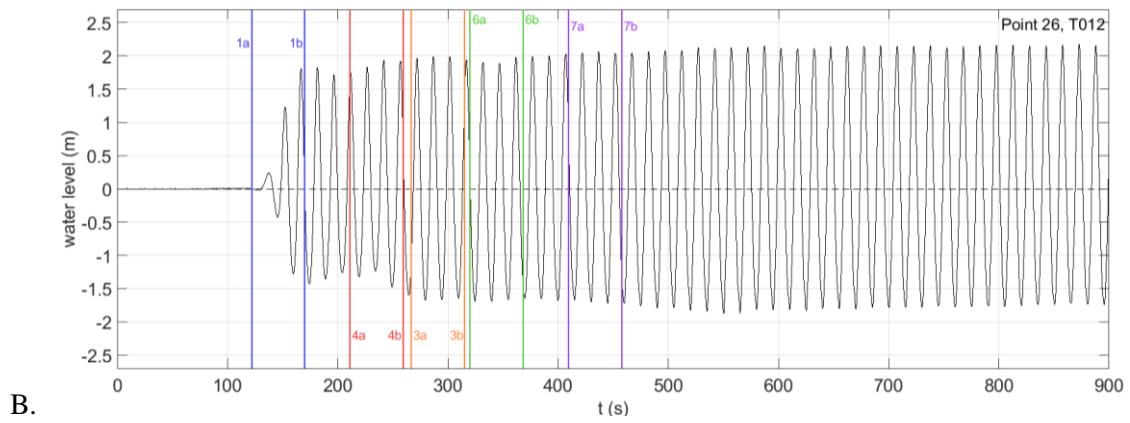**Figure E.10 - Measured water level time series for T010 at Point 5(picture A), at Point 26 (picture B), at Point 11 (picture C) and at Point 27 (picture D).**
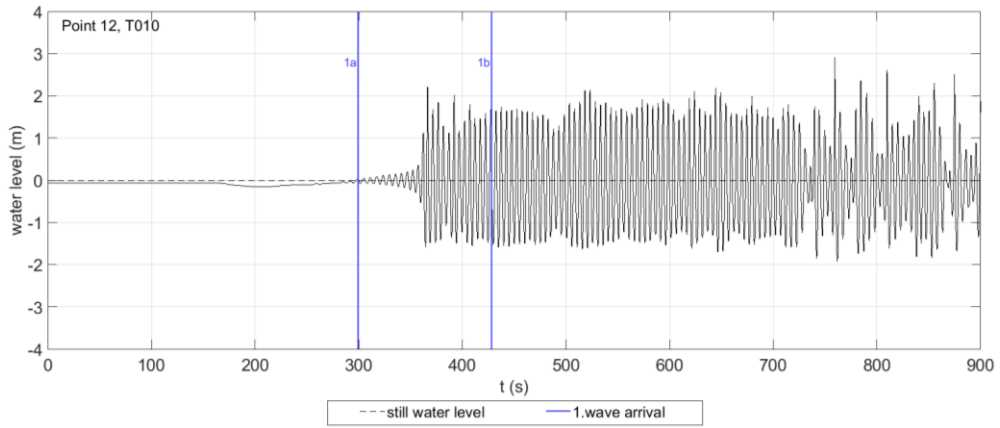
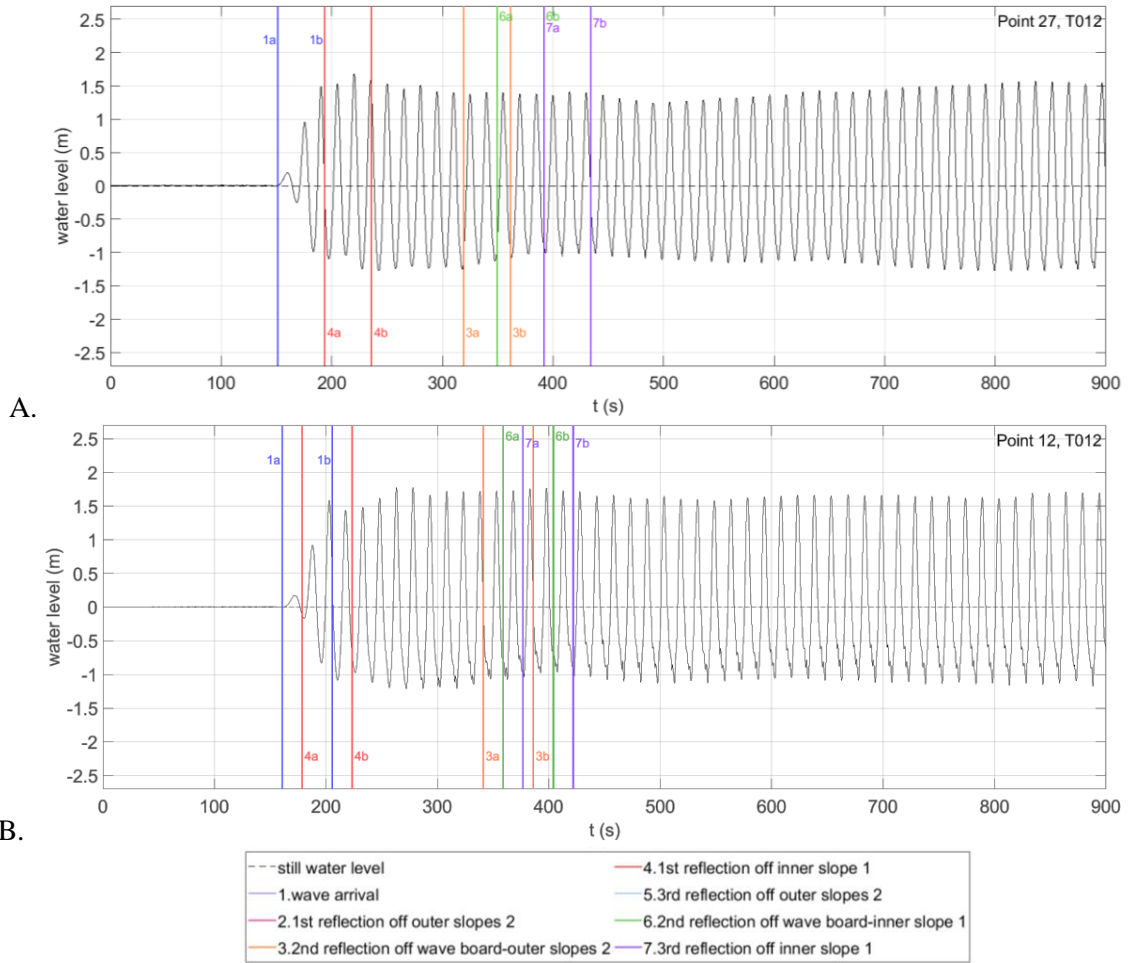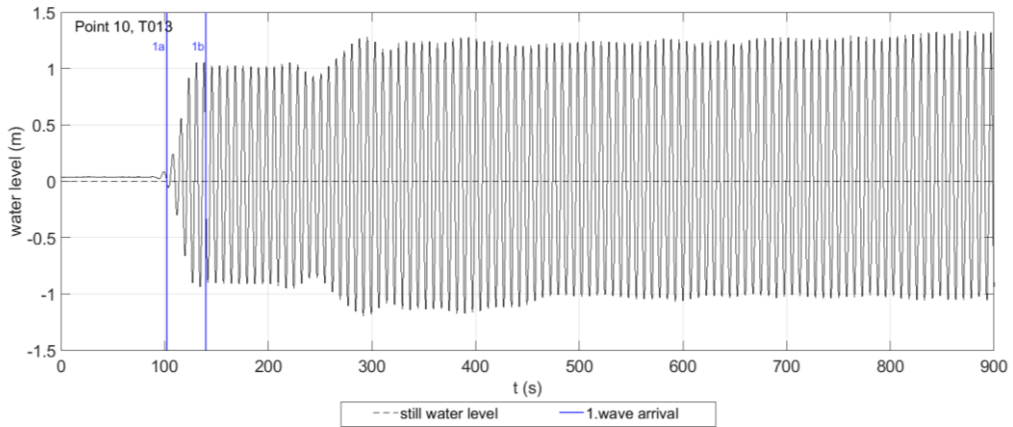**Figure E.11 - Measured water level time series for T010 at Point 12.**
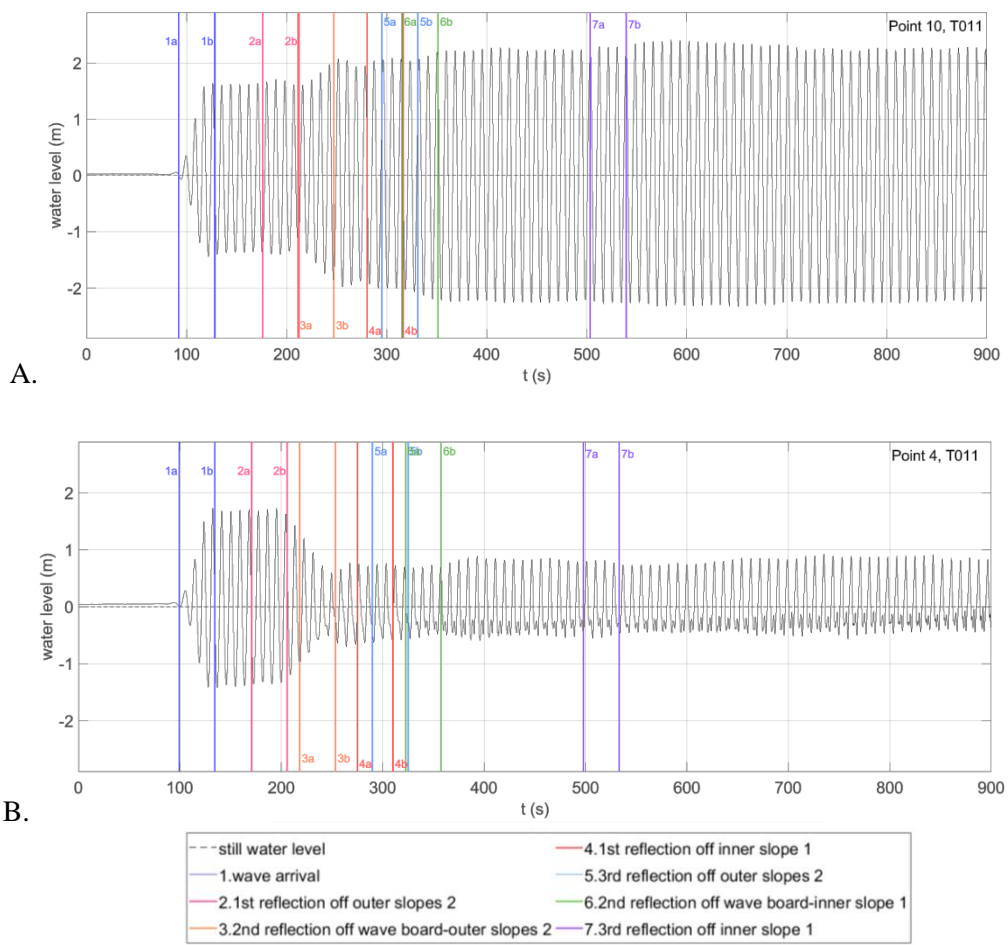
Figure E.12 - Measured water level time series for T011 at Point 10 (picture A) and at Point 4 (picture B).
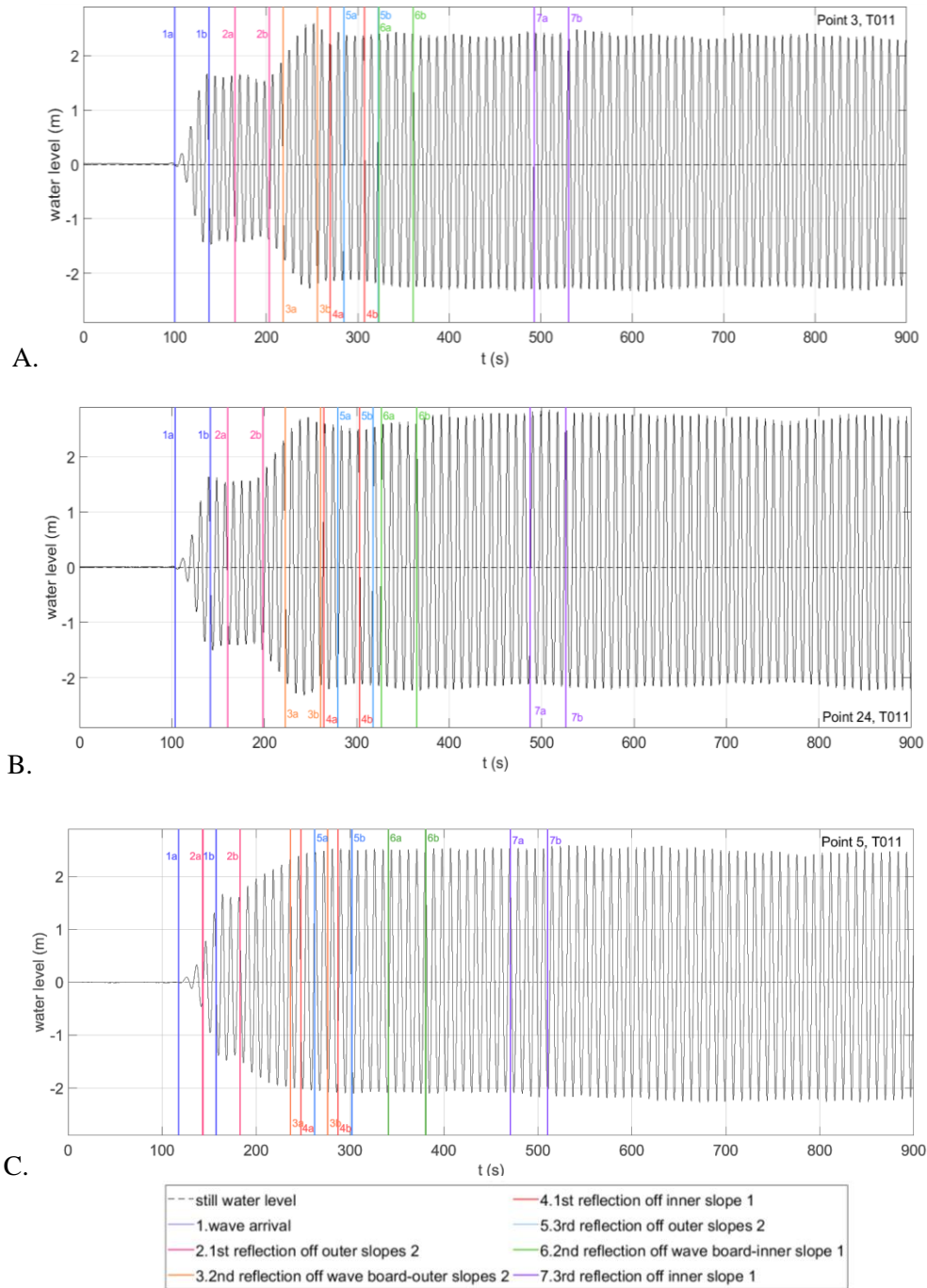
Figure E.13 - Measured water level time series for T011 at Point 3 (picture A), at Point 24 (picture B) and at Point 5 (picture C).
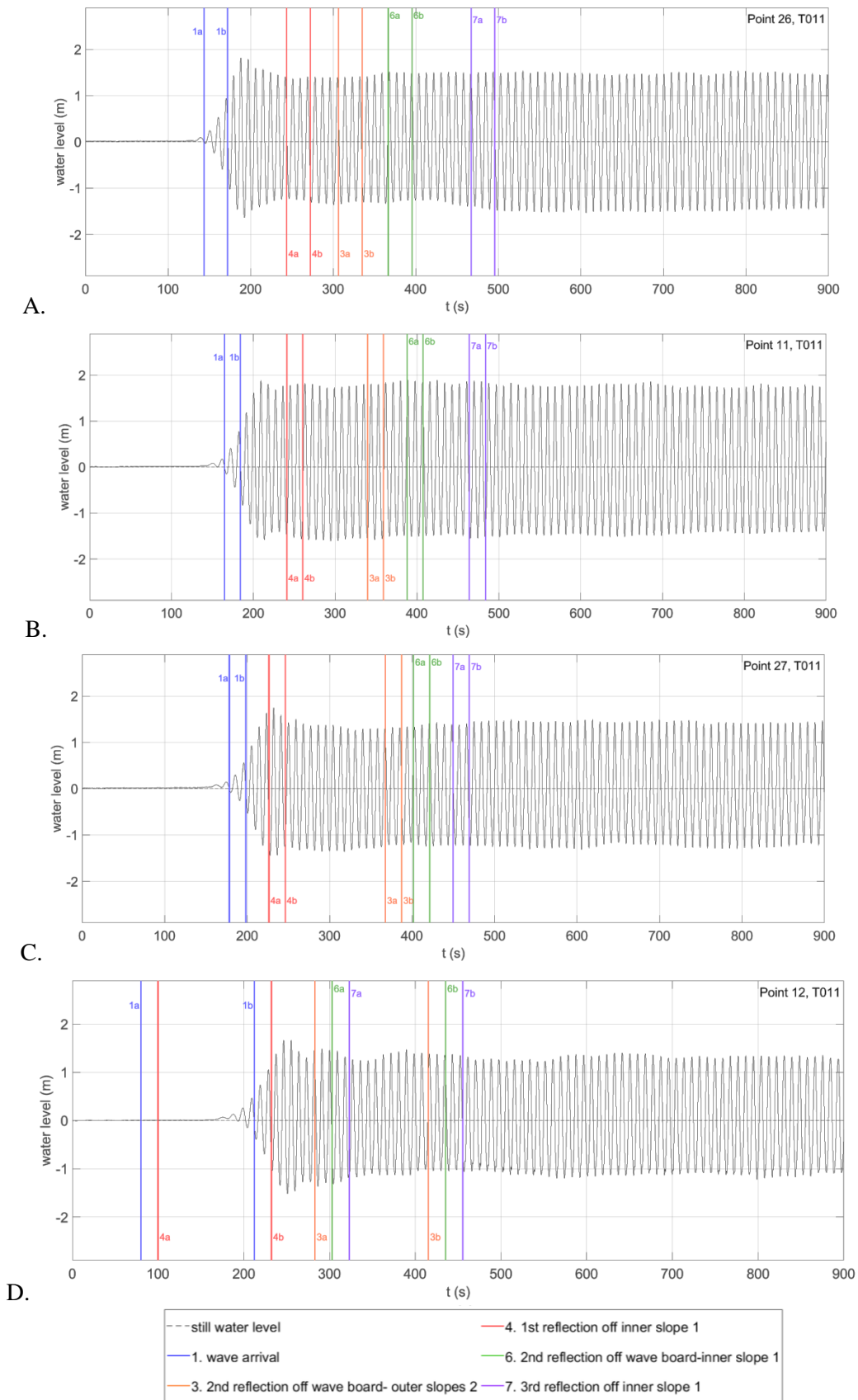
Figure E.14 - Measured water level time series for T011 at Point 26 (picture A), at Point 11 (picture B), at Point 27 (picture C) and at Point 12 (picture D).
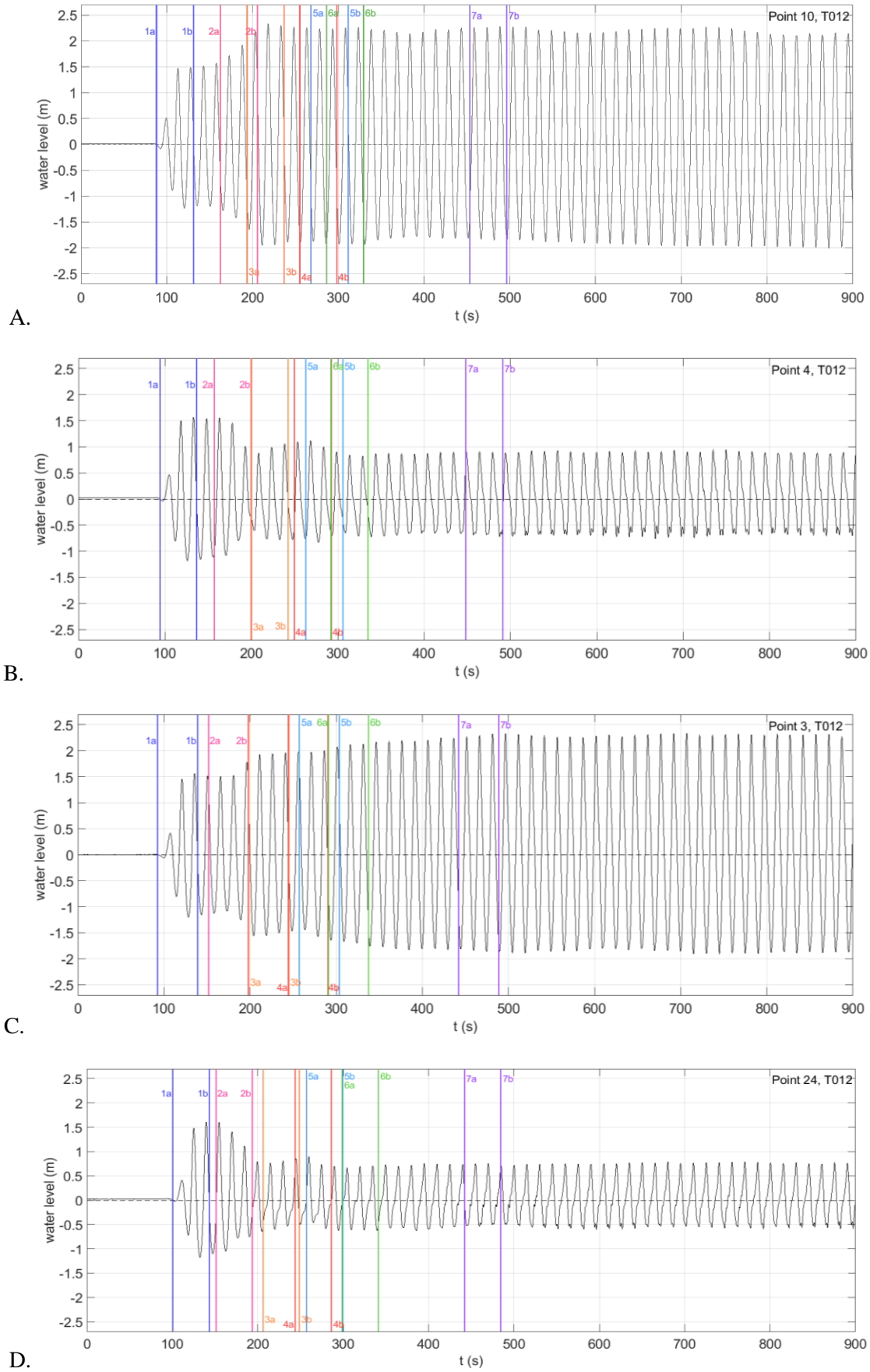
Figure E.15 - Measured water level time series for T012 at Point 26 (picture A), at Point 11 (picture B), at Point 27 (picture C) and at Point 12 (picture D).

Figure E.16 - Measured water level time series for T012 at Point 5.

B.

C.

Figure E.17 - Measured water level time series for T012 at Point 26 (picture A) and at Point 11 (picture B).

Figure E.18 - Measured water level time series for T012 at Point 27 (picture A) and at Point 12 (picture B).

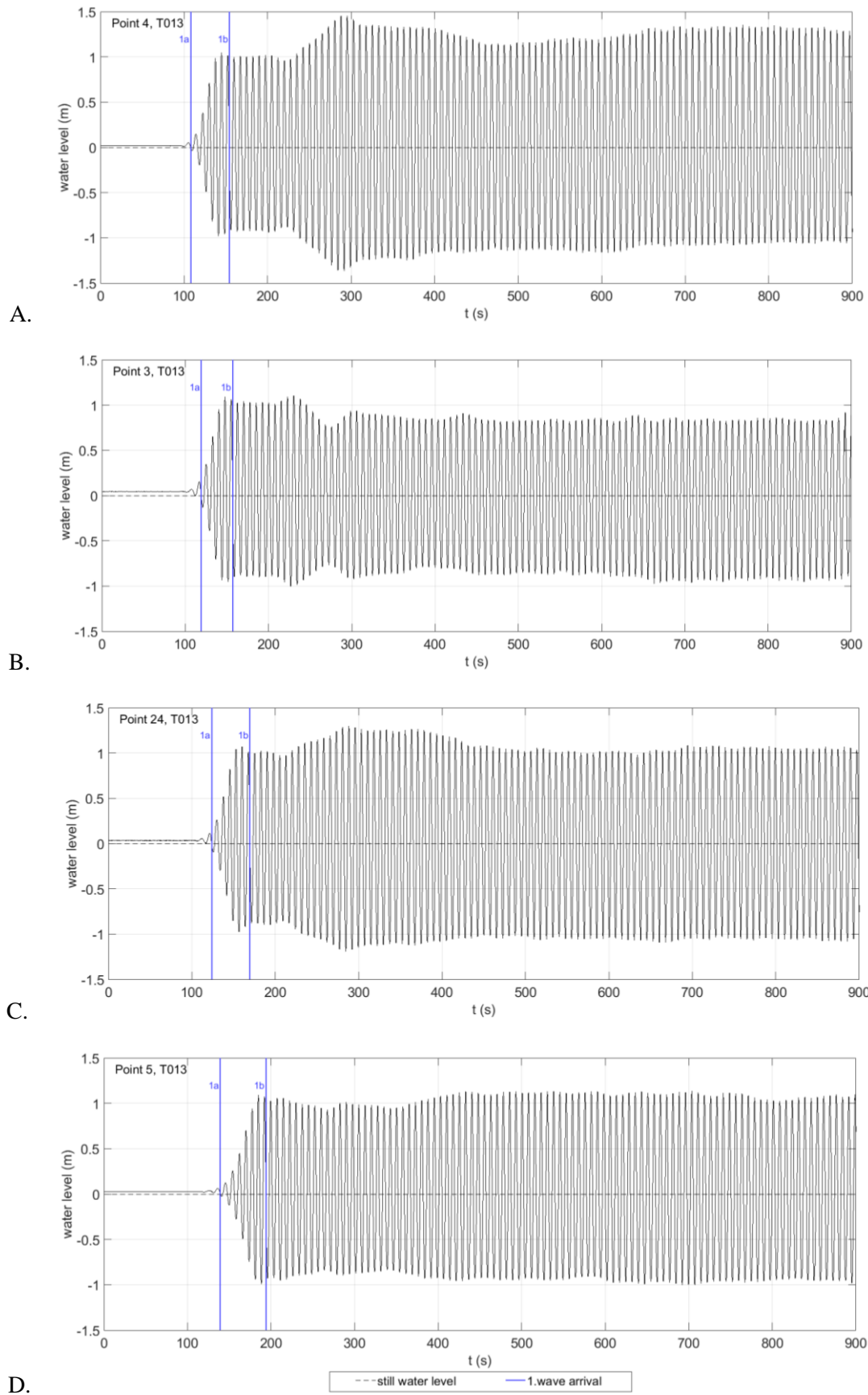**Figure E.19 - Measured water level time series for T013 at Point 10.**

Figure E.20 - Measured water level time series for T012 at Point 4 (picture A), at Point 3 (picture 3), at Point 24 (picture C) and at Point 5 (picture D).
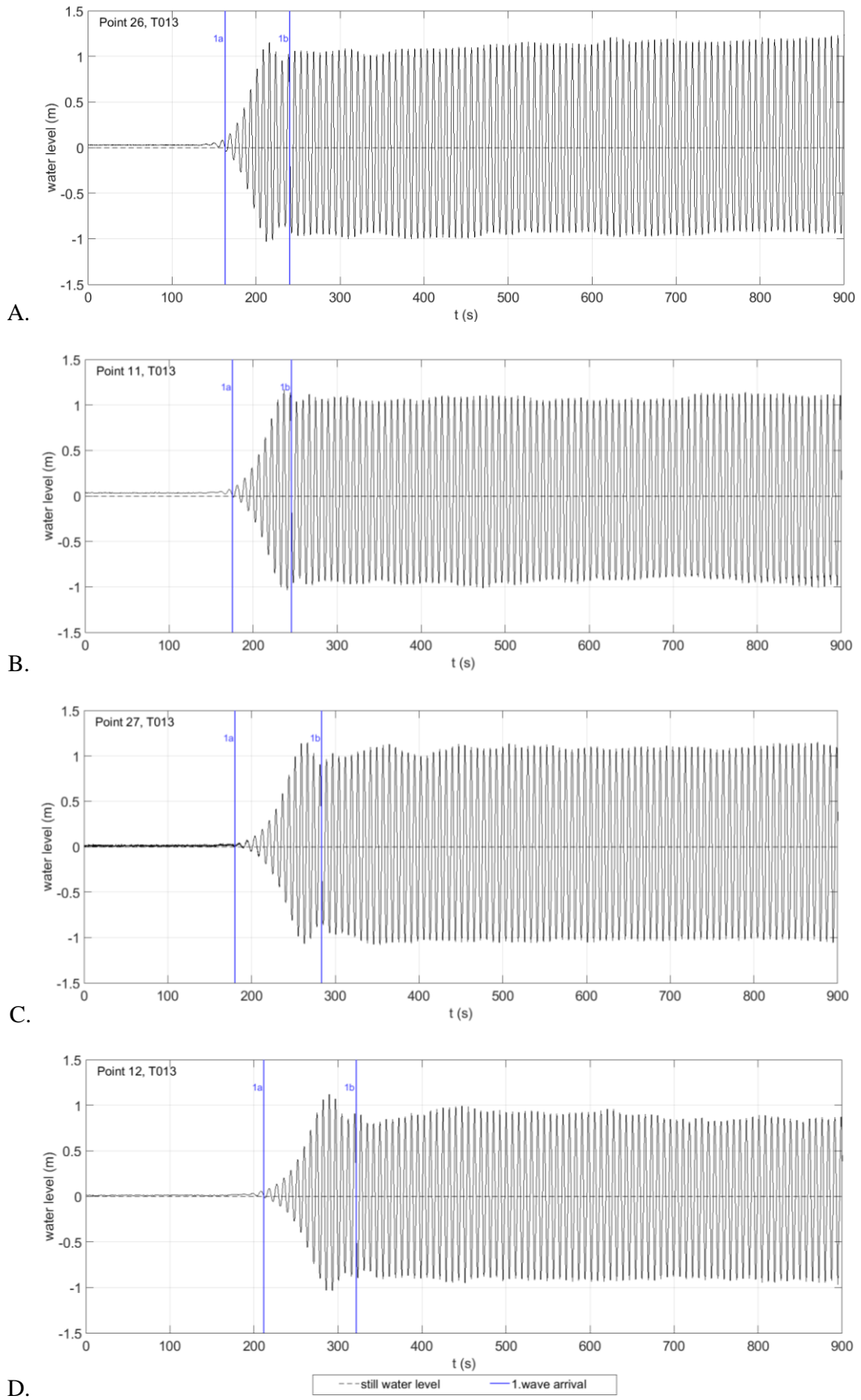
Figure E.21 - Measured water level time series for T012 at Point 27 (picture A) and at Point 12 (picture B).

E.2 Measured steady state wave height

The ratio $\overline{H}_{\text{steady state,diffraction model}}/H_{\text{incoming}}$ is calculated for all the seven tests. By dividing with the incoming wave height the results for all the seven tests examined can be compared. To demonstrate how the wave height differs at various locations it was decided to create a top view showing the steady sate at each output location. For each test a top view is shown in which the value of the ratio at every point is indicated by colours. The exact values of the ratio are presented in accompanying tables. The results for T001 are presented in the main text in Section 3.4.
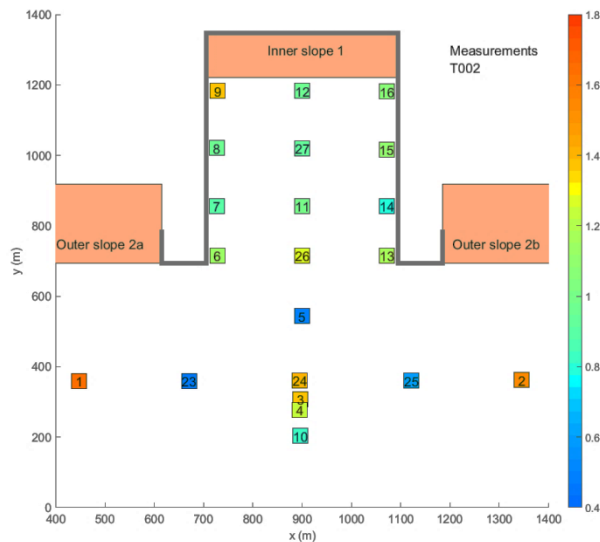

Figure E.24– Top view of the ratio $\overline{H}_{\text{steady state}}/H_{\text{incoming}}$ in the measurements for T002.

Table E.1 - The exact values of the ratio $\overline{H}_{\text{steady state}}/H_{\text{incoming}}$ in the measurements for T002.

Outside the harbour basin			
Wave Gauge	Measured $H_{\text{steady state}}$	Wave Gauge	Measured $H_{\text{steady state}}$
1	1.63	10	0.81
2	1.54	23	0.46
3	1.36	24	1.41
4	1.22	25	0.60
5	0.50		

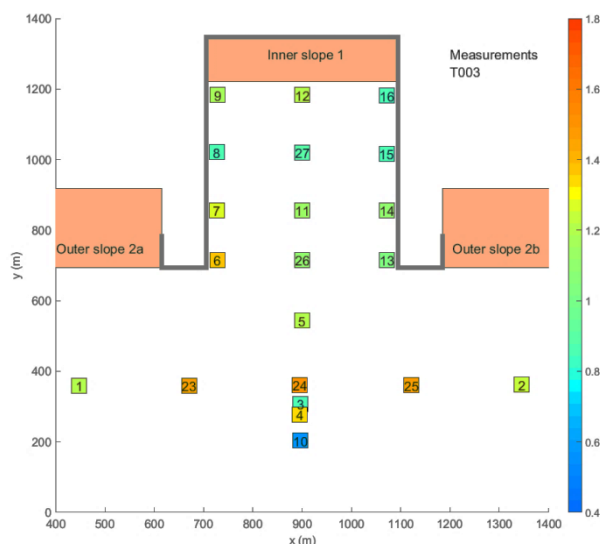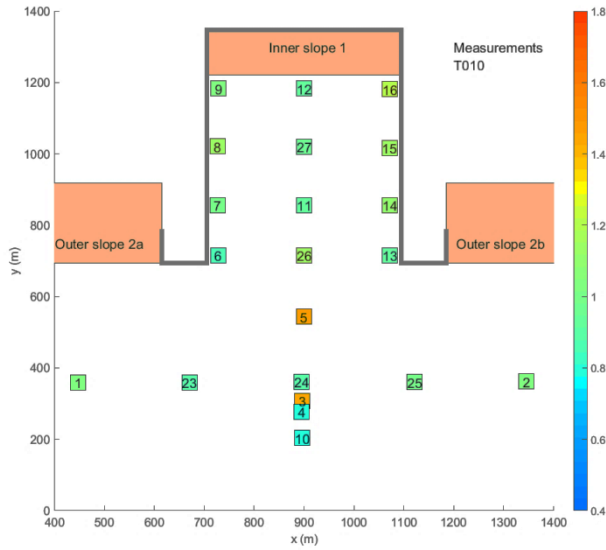| Inside the harbour basin			
Wave Gauge	Measured $H_{\text{steady state}}$	Wave Gauge	Measured $H_{\text{steady state}}$
6	1.12	13	1.17
7	0.90	14	0.79
8	0.95	15	1.11
9	1.37	16	1.06
11	0.99	26	1.28
12	0.96	27	0.94

Figure E.25– Top view of the ratio $\overline{H}_{\text{steady state}}/H_{\text{incoming}}$ in the measurements for T003.

Table E.2 - The exact values of the ratio $\overline{H}_{\text{steady state}}/H_{\text{incoming}}$ in the measurements for T003.

Outside the harbour basin			
Wave Gauge	Measured $H_{\text{steady state}}$	Wave Gauge	Measured $H_{\text{steady state}}$
1	1.19	10	0.57
2	1.23	23	1.48
3	0.85	24	1.51
4	1.35	25	1.46
5	1.21		

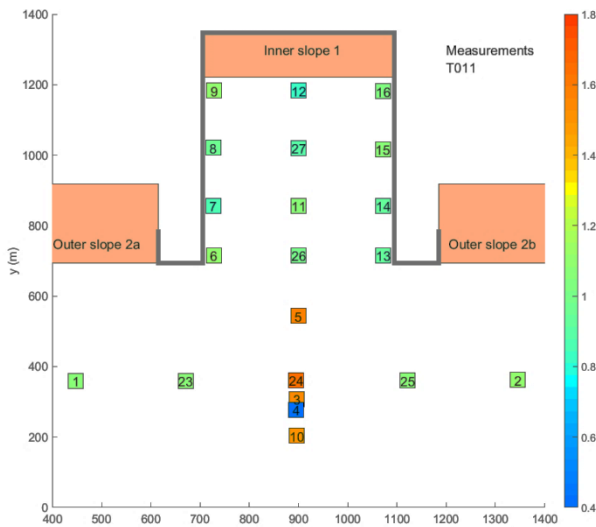| Inside the harbour basin			
Wave Gauge	Measured $H_{\text{steady state}}$	Wave Gauge	Measured $H_{\text{steady state}}$
6	1.39	13	1.03
7	1.27	14	1.11
8	0.86	15	0.85
9	1.16	16	0.87
11	1.14	26	1.11
12	1.19	27	0.91

Figure E.26– Top view of the ratio $\bar{H}_{steady\ state}/H_{incoming}$ in the measurements for T010.

Table E.3 - The exact values of the ratio $\bar{H}_{steady\ state}/H_{incoming}$ in the measurements for T010.

Outside the harbour basin			
Wave Gauge	Measured $H_{steady\ state}$	Wave Gauge	Measured $H_{steady\ state}$
1	1.03	10	0.80
2	1.04	23	0.89
3	1.43	24	0.88
4	0.79	25	0.99
5	1.47		

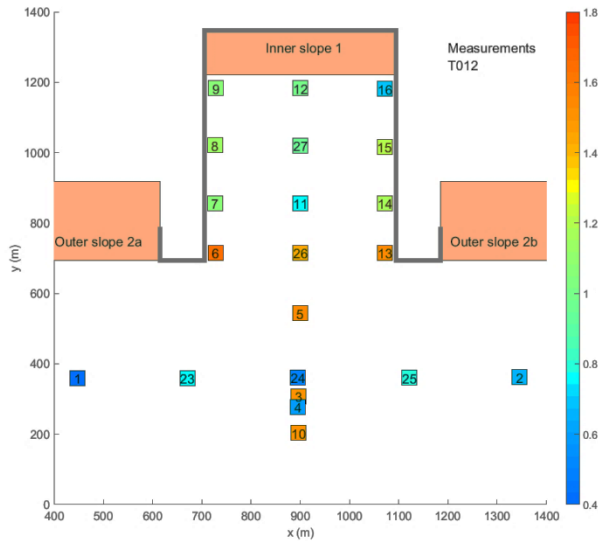| Inside the harbour basin			
Wave Gauge	Measured $H_{steady\ state}$	Wave Gauge	Measured $H_{steady\ state}$
6	0.85	13	0.93
7	1.00	14	1.09
8	1.15	15	1.15
9	1.02	16	1.19
11	0.93	26	1.12
12	0.92	27	0.95

Figure E.27– Top view of the ratio $\bar{H}_{steady\ state}/H_{incoming}$ in the measurements for T011.

Table E.4 - The exact values of the ratio $\bar{H}_{steady\ state}/H_{incoming}$ in the measurements for T011.

Outside the harbour basin			
Wave Gauge	Measured $H_{steady\ state}$	Wave Gauge	Measured $H_{steady\ state}$
1	1.05	10	1.52
2	1.10	23	1.05
3	1.54	24	1.63
4	0.43	25	1.07
5	1.57		

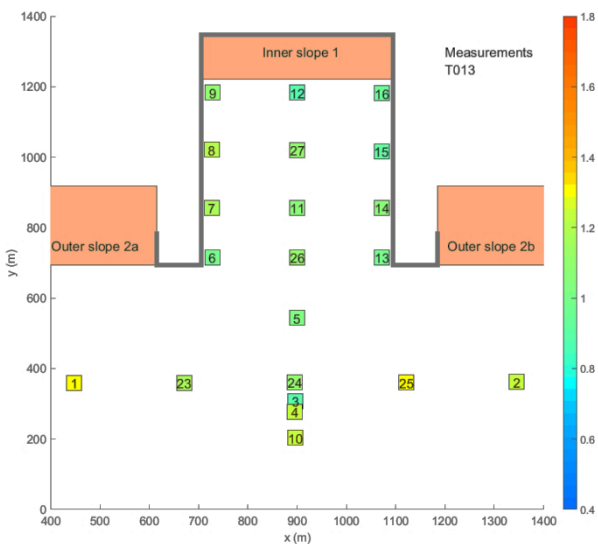| Inside the harbour basin			
Wave Gauge	Measured $H_{steady\ state}$	Wave Gauge	Measured $H_{steady\ state}$
6	1.10	13	0.93
7	0.85	14	0.93
8	0.98	15	1.06
9	1.09	16	1.03
11	1.07	26	0.99
12	0.81	27	0.89

143

Figure E.28– Top view of the ratio $\bar{H}_{steady\ state}/H_{incoming}$ in the measurements for T012.

Table E.5 - The exact values of the ratio $\bar{H}_{steady\ state}/H_{incoming}$ in the measurements for T012.

Outside the harbour basin			
Wave Gauge	Measured $H_{steady\ state}$	Wave Gauge	Measured $H_{steady\ state}$
1	0.33	10	1.51
2	0.67	23	0.77
3	1.52	24	0.47
4	0.59	25	0.79
5	1.56		

Inside the harbour basin			
Wave Gauge	Measured $H_{steady\ state}$	Wave Gauge	Measured $H_{steady\ state}$
6	1.63	13	1.53
7	1.06	14	1.16
8	1.15	15	1.21
9	1.05	16	0.69
11	0.75	26	1.43
12	1.00	27	0.95

Figure E.29– Top view of the ratio $\bar{H}_{steady\ state}/H_{incoming}$ in the measurements for T013.

Table E.6 - The exact values of the ratio $\bar{H}_{steady\ state}/H_{incoming}$ in the measurements for T013.

Outside the harbour basin			
Wave Gauge	Measured $H_{steady\ state}$	Wave Gauge	Measured $H_{steady\ state}$
1	1.32	10	1.22
2	1.22	23	1.18
3	0.88	24	1.09
4	1.22	25	1.29
5	1.04		

Inside the harbour basin			
Wave Gauge	Measured $H_{steady\ state}$	Wave Gauge	Measured $H_{steady\ state}$
6	0.99	13	1.01
7	1.17	14	1.06
8	1.20	15	0.94
9	1.11	16	0.97
11	1.07	26	1.10
12	0.91	27	1.10

Appendix F   Wave maker signal

This Appendix includes the figures of the wave signal generated by wave maker motion for T002, T003, T010, T011, T012 and T013. As discussed in Section 2.2, these water surface elevation time series are computed using the wave maker displacements in the physical model. The figures can be helpful in understanding the shape of the water level time series, especially the parts of the series undisturbed by reflection or diffraction. It is worth mentioning that the time axis in the following graphs differs from axis in the wave records for the respective test.
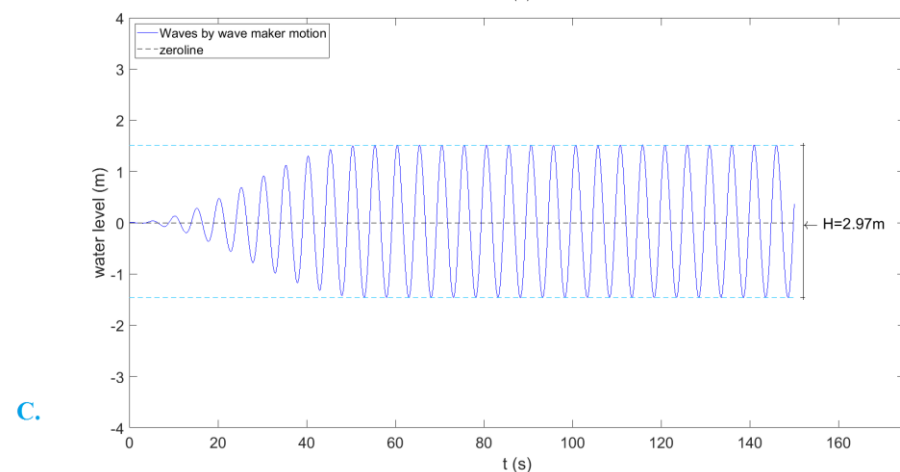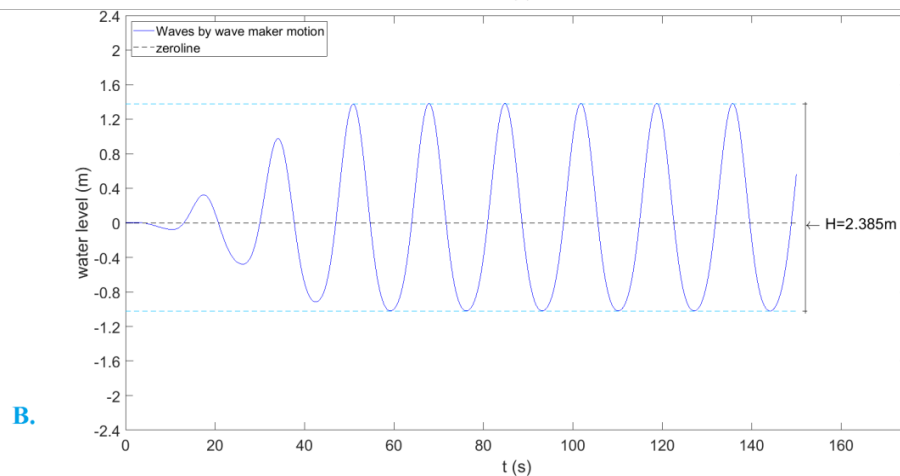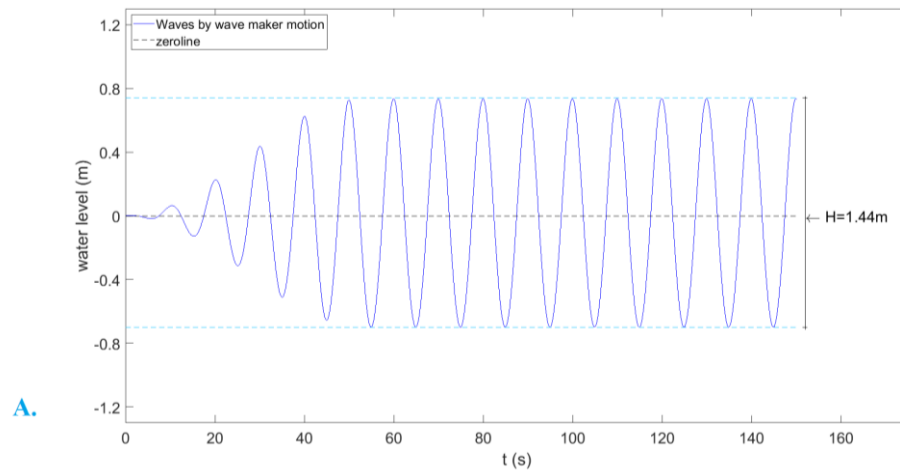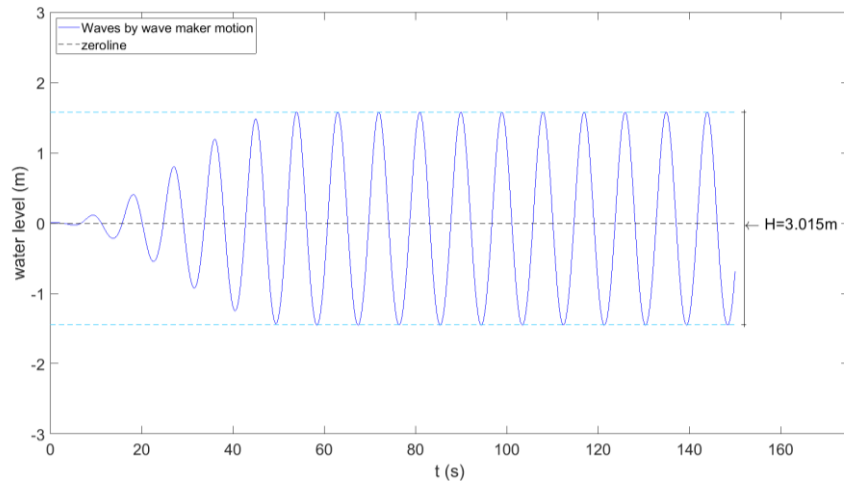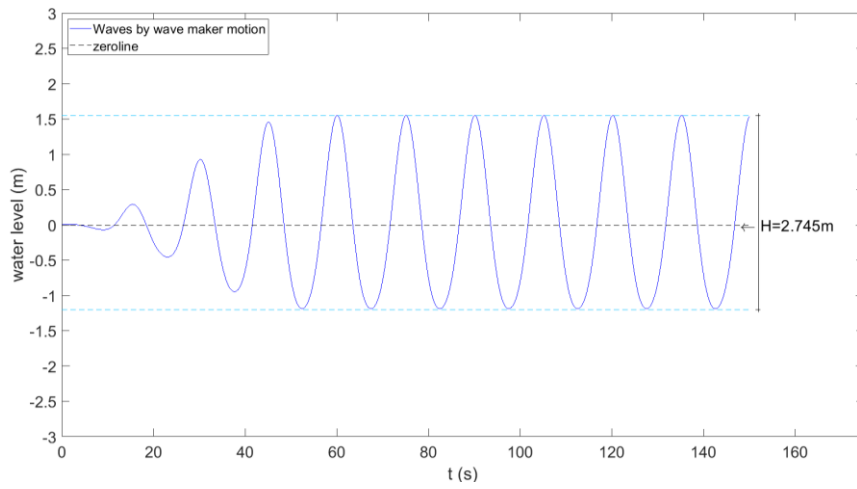

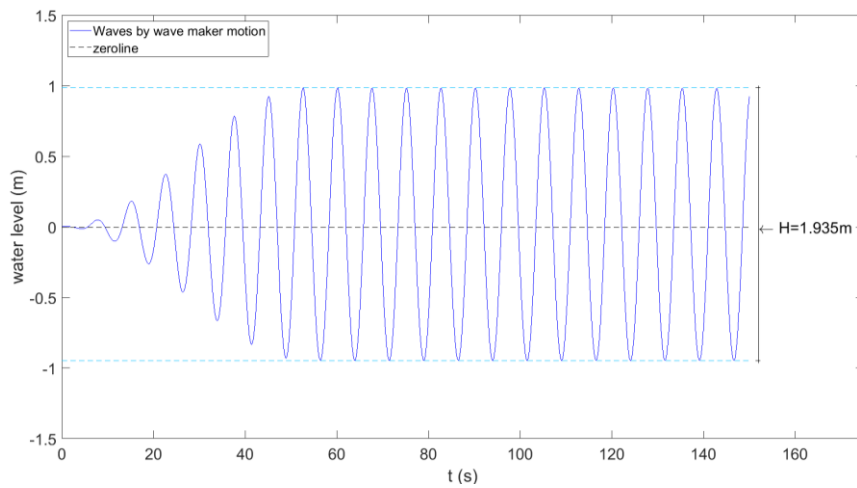Figure F.1 - Wave machine incoming signal for test T002 (graph A.), T003 (graph B) and T010 (graph C).

Figure F.2 - Wave machine incoming signal for test T011 (graph D.), T012 (graph E) and T013 (graph F).

Appendix G   Results of the 1D model for reflection off outer gravel slope 2a

This Appendix contains additional information for Chapter 6. The water level time series at Point 1 and the water level envelopes for runs 2 to 9 are presented.
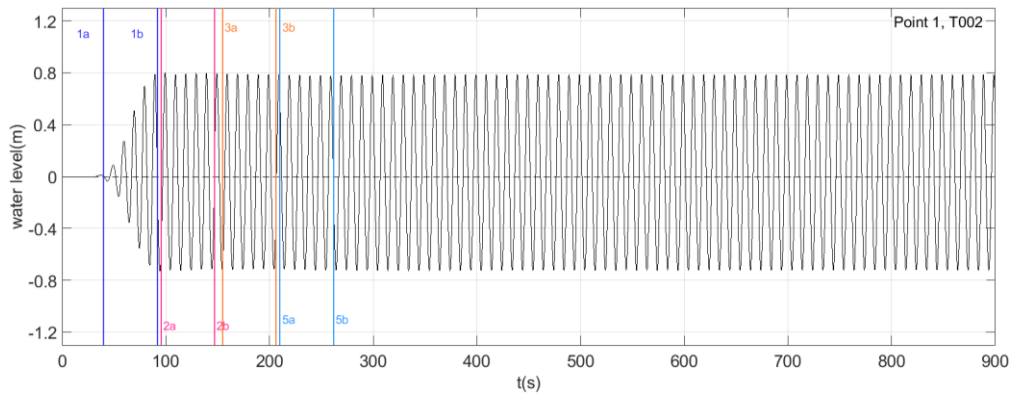

Figure G.1 - Run 2, water level in time at Point 1 generated by SWASH for T002.
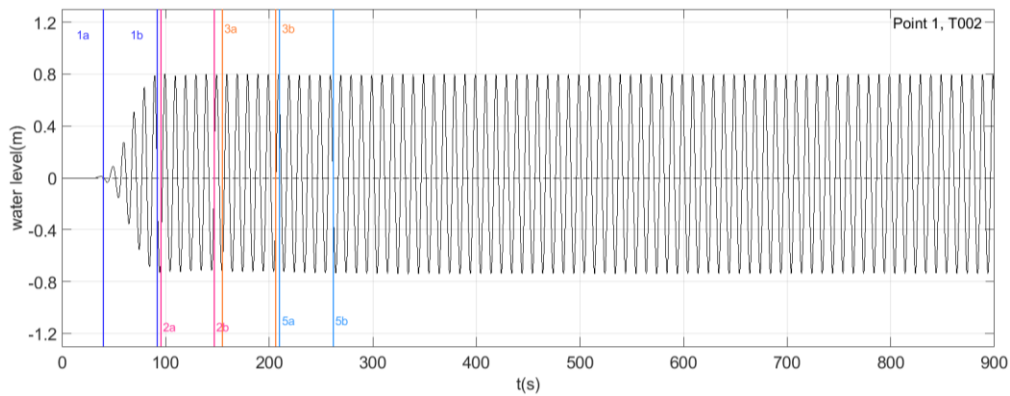

Figure G.2 - Run 3, water level in time at Point 1 generated by SWASH for T002.

Figure G.3 - Run 4, water level in time at Point 1 generated by SWASH for T002.

Figure G.4 - Run 5, water level in time at Point 1 generated by SWASH for T002.

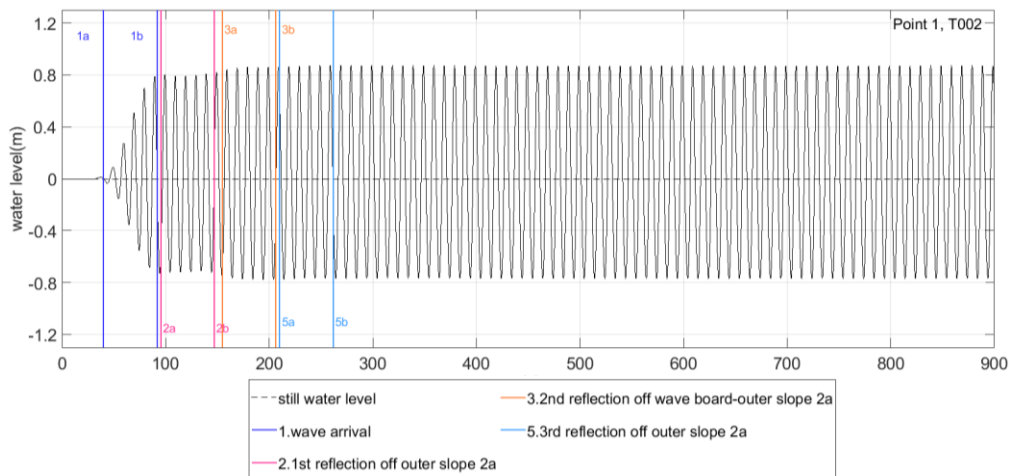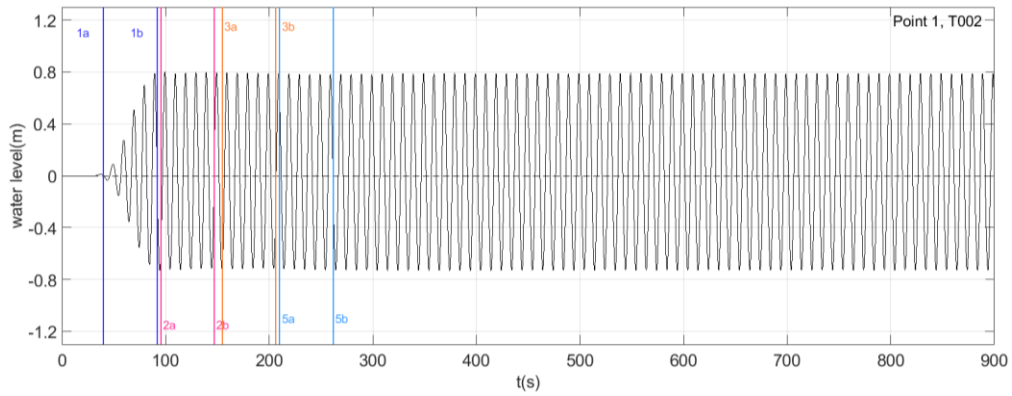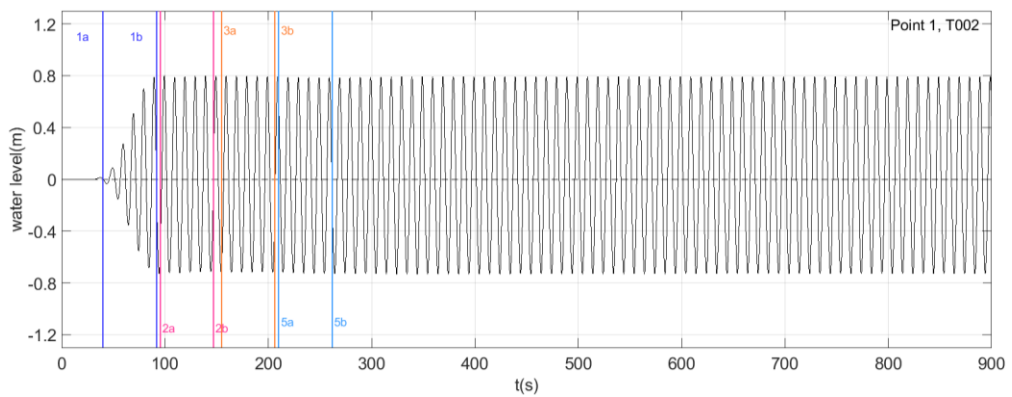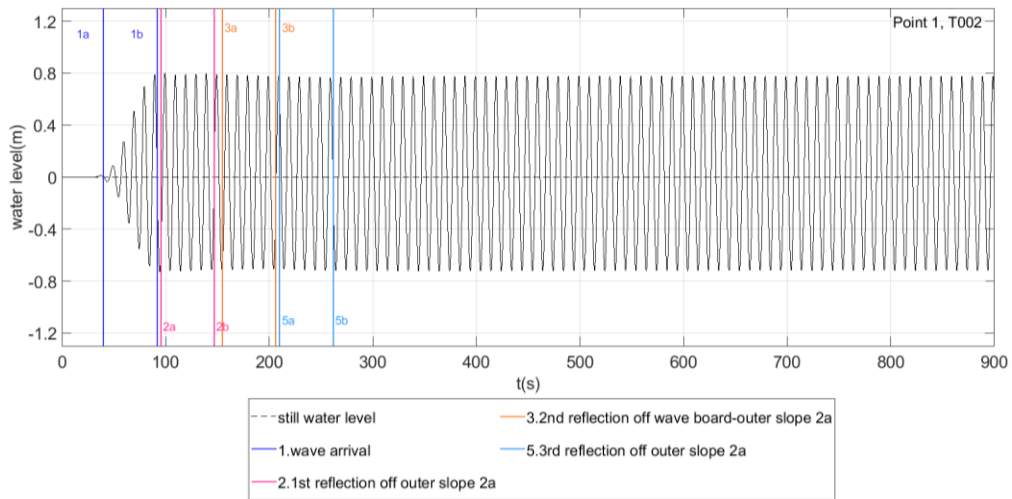**Figure G.5 - Run 6, water level in time at Point 1 generated by SWASH for T002.**

Figure G.6 - Run 7, water level in time at Point 1 generated by SWASH for T002.
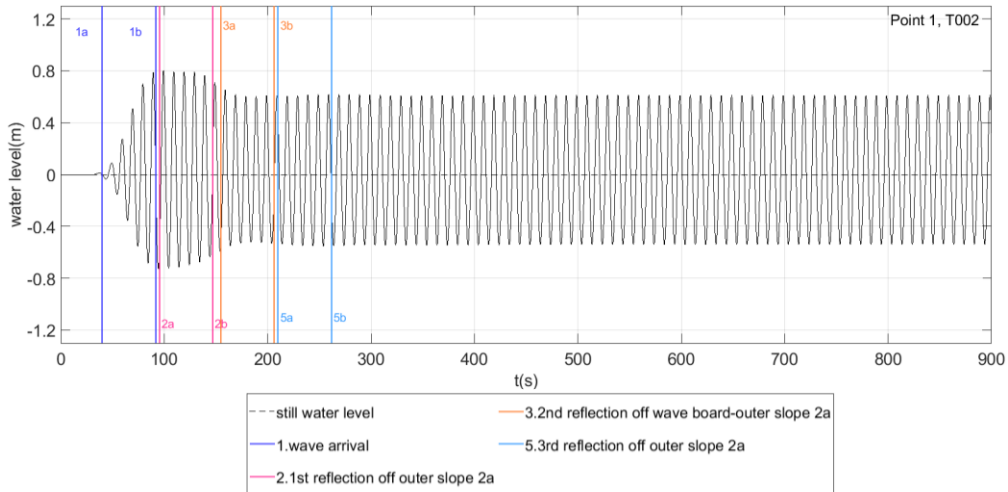
148

Figure G.7- Run 8, water level in time at Point 1 generated by SWASH for T002.

In the experiments the incoming monochromatic wave travels inside the basin and gets reflected at the gravel slope. Therefore, the water surface elevation measured at the wave gauges 1 is the summation of the incoming and the reflected wave. In other words, inside the basin standing waves occur. For 100% reflection at a wall, there are some locations where the surface elevation is equal to zero (nodes) and locations where the surface elevation reaches a maximum value (antinodes). It is reasonable that at a measurement location close to an antinode the wave height will be larger than the wave height at a location close to a node. In a real case where waves get damped at the slope and also transmitted through it, there is a slight motion at the "nodes" locations. Still at the locations where nodes are located for the same wave with full reflection, the envelope of the surface elevation has the minimum amplitude. At the locations where antinodes are for the full reflection case, the envelope of the surface elevation will have the maximum amplitude (Figure G.8)
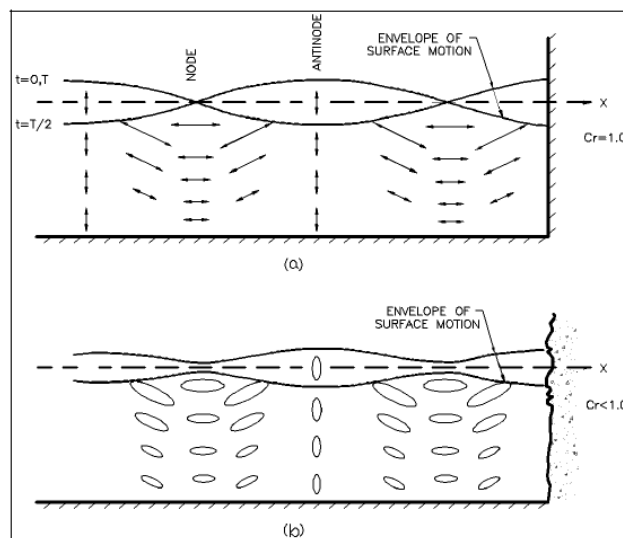

Figure G.8 - a. Complete reflection b. Partial reflection, United States (2008).

The wave envelopes during the stationary part of the runs are shown in the following figure.
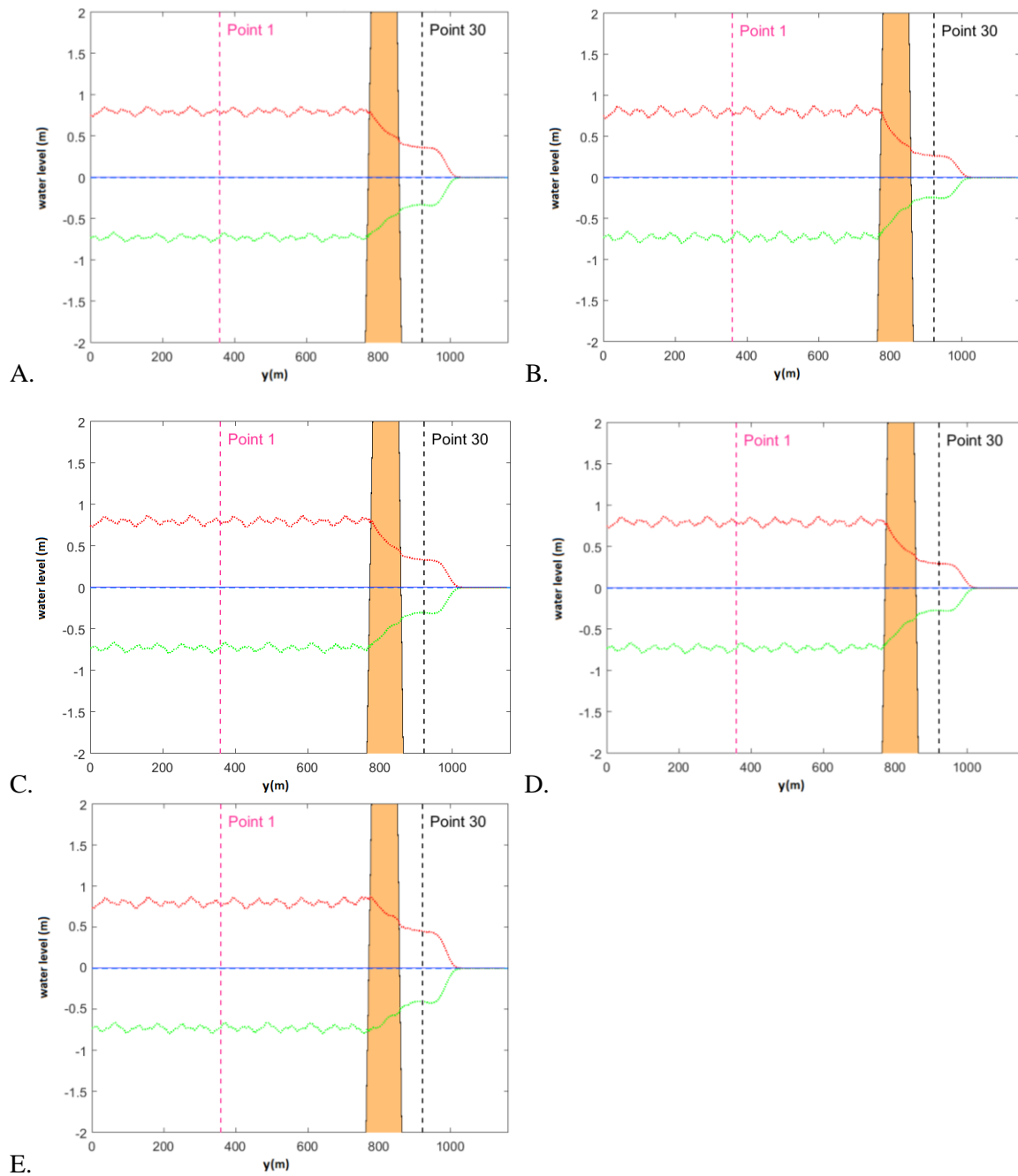

Figure G.9 – The envelope of the water level during the steady state part for run 2 (picture A), run 3 (picture B), run 5 (picture C), run 6 (wall case, picture D) and run 7 (picture E).

Appendix H 1D SWASH MODELS SETTINGS

H.1 The models set-up

The settings applied in the 1D SWASH models are described here. The various settings are discussed in order of appearance in the command files presented in section H.2. For additional information about the selected model set-up and possible alternative settings the reader is referred to the SWASH user manual (The SWASH Team, 2016). As explained in Section 2.6.3, the SWASH models are in prototype scale.

Initially, it is defined that the run will be one-dimensional, as the default option is two dimensional. As a one dimensional model is less computationally demanding than a two dimensional case, a small grid size (Δx=0.9m) can be chosen is chosen to obtain accurate results. According to the SWASH manual for low waves, i.e. H/h<<1 (with H a characteristic wave height and h the still water depth) it is sufficient to take 50 grid cells per wave length. On the contrary, for relatively high waves it is better to take at least 100 grid cells per wave length. However, this high amount of grid cells results in a high computational time. A practical rule of thumb is to choose at least 30 cells per wave length. The following table summarises the grid cells per wave length for the chosen grid resolution.

Table H.1 – The ratio wave height to water depth H/h and the number of grid cells per wave length for each of the 7 selected tests.

Test	H (m)	h (m)	H/h (m)	L (m)	Δx (m)	Cells per wave length
T001	0.99	19.8	0.1	80.48	0.9	89
T002	1.44	19.8	0.1	120.74	0.9	134
T003	2.385	19.8	0.1	225.59	0.9	251
T010	2.97	19.8	0.2	39.38	0.9	44
T011	3.015	19.8	0.2	104.71	0.9	116
T012	2.745	19.8	0.1	197.05	0.9	219
T013	1.935	19.8	0.1	31.52	0.9	35

The runs were in multi-layered mode and two equidistant vertical layers were used. The number of layers is determined by linear wave dispersion for primary waves indicated by the kd value. The higher the value of kd, the more vertical layers needed. According to the SWASH user manual (The SWASH Team, 2016), for kd≤7.7, two vertical layers are required to keep the relative error in the normalized wave celerity (=c/$\sqrt{gh}$) lower than 1%. This error is acceptable for the application of wave penetration examined in this thesis.

The model geometry and the structures properties are defined in 4 input files. The bathymetry file has a constant depth value (19.8m) at all cells. The hydraulic structure file contains the values of the height of each structure in the physical model. The geometry shown in Figure 2.2 and Table 2.2 is carefully reconstructed. The structures and the water properties in the model are defined by using porous layers. The concrete walls are modelled with a porosity of 0.001 and a stone size of 0.045m. A porosity of 0.4 and a stone size of 0.675m are used to define the gravel slopes in the original run (Table 5.2). The water is modelled with a porosity of 1 and a stone size of 0m. The transition from the gravel slope to the concrete wall is done using three layers of 2 cells each. The layer next to the gravel slope has a porosity of 0.3 and a stone size of 5.06m.The second layer has a porosity of 0.2 and a stone size of 3.38m. The last layer has a porosity of 0.1 and a stone size of 1.69m.This means that the wall is shifted by 6 cells (0.12cm) from the end of the gravel slope. This is done to guarantee the

stability of the model. The same technique was also applied in the 2D model in every transition from a gravel slope to a concrete harbour wall.

The incoming wave height generated by the wave maker in the physical scale model is prescribed at the offshore boundary of the model .The boundary behind the gravel slopes is defined as a closed boundary.

Both the initial water level and velocity components are set to zero. Moreover, the non-hydrostatic pressure is included in the shallow water equations. Using the default settings, the Keller-box scheme is applied for the time integration of the non-hydrostatic vertical pressure gradient. SWASH always accounts for energy dissipation due to wave breaking and no special command has to be specified. Furthermore, the spatial discretisation employed for u/v and w momentum equations is specified. Instead of the upwind scheme, in this application the standard central difference scheme is used.

In the 1D model simulating the reflection in front of outer gravel slope 2a a sponge layer is defined behind the gravel slope and in front of the end of the domain. More details about the sponge layer length defined in front of the model end boundary can be found in Section 5.2. However, in the 1D model simulating the reflection at the harbour end, there is a concrete wall at the end of the harbour basin and thus a sponge layer at the end of the domain is not required.

In SWASH the first order implicit Euler scheme is used for the time integration. Hence, a CFL condition is required to guarantee numerical stability. According to the SWASH user manual (The SWASH Team, 2016) the CFL condition for a 2 dimensional case is described by the following equation. The one dimensional case is a simplified version of the aforementioned equation. . Due to the restriction of the CFL condition and time step is again equal to $\Delta t=0.020s$.

$$Cr = \Delta t \left(\sqrt{gd} + \sqrt{u^2 + v^2}\right) \sqrt{\frac{1}{\Delta x^2} + \frac{1}{\Delta y^2}} \le 1$$

where: Cr: Courant number
          Δt: time step
          Δx, Δυ grid size in x- and y- direction
          u,v: velocity components in x- and y- direction
          d: water depth

The default range of the Courant number is 0.4 to 0.8. However, in case of wave interaction with complex structures such as quay walls a maximum Courant number of 0.5 is recommend. In the SWASH command file the Courant number is restricted within the range 0.2 to 0.5. As the time step is controlled by the CFL limits, it might change over the simulation time.

Finally, as discussed in section 3.1, the total simulation time is 900 s (i.e. 15min). Each computation took approximately 20 minutes on a 64-bit Linux cluster node with an Intel Xeon E3-1276 CPU @ 3.6GHz and 32 GB RAM.

To obtain the water level time series at the output points of interest, text files of the water level values every 0.10 s are requested as output. To create the envelope of the water level values, another output file that has to be defined is the water level at all grid cells every 0.60 s.

H.2 The SWASH command files

H.2.1 Command file for the 1D model for reflection off outer gravel slope 2a

The SWASH command file for the 1D SWASH model simulating reflection off the outer gravel slope 2a discussed in Chapter 5 is the following.

```
!*****************HEADING*******************************************
PROJ 'model1D' '1'
!*****************MODEL INPUT***************************************
MODE DYN ONED
CGRID REGULAR 0.00 0.0 0.0 1152.0 0.0 1280 0
VERTICAL 2
!
INPGRID BOT REG 0.00 0.0 0.0 1280 0 0.9 1
READINP BOTTOM 45. 'S2_1DmodelTM.bot' 1 0 FREE
INPGRID POROSITY REG 0.00 0.0 0.0 1280 0 0.9 1
READINP POROSITY 1. 'S2_1DmodelTM.por' 1 0 FREE
INPGRID PSIZE REG 0.00 0.0 0.0 1280 0 0.9 1
READINP PSIZE 45. 'S2_1DmodelTM.psiz' 1 0 FREE
INPGRID HSTRUCTURE REG 0.00 0.0 0.0 1280 0 0.9 1
READINP HSTRUCTURE 45. 'S2_1DmodelTM.hstr' 1 0 FREE
!
INITIAL ZERO
BOU SIDE W BTYPE WEAK SMOO 1 SEC UNIFORM SERIES 'Paddle45_5_96_T002.tms'
BOU SIDE E BTYPE WEAK SMOO 1 SEC UNIFORM FOURIER 0 0 0 0
SPON E 225.0
NONHYDROSTATIC
!
DISCRET UPW NONE
DISCRET CORRDEP NONE
!
TIMEI 0.2 0.5
! *******************OUTPUT REQUESTS**********************************
POINTS 'punt1'          359.50500000    0.00000000
POINTS 'punt2'          361.75500000    0.00000000
POINTS 'punt30' 922.50000000    0.00000000
FRAME 'frame1'  0.00 0.0 0.0 1152.0 0.0 1280 0
!
QUANTITY WATLEV 'WATLEV' 'WATLEV' -10 10 -999
QUANTITY HS 'HS' 'HS' 0 10 -999 0 25 MIN
!
TABLE  'punt1' HEAD '1Dmodel_p1.tbl' TSEC XP YP WATL OUTPUT 000000.000 0.10 SEC
TABLE  'punt30' HEAD '1Dmodel_p30.tbl' TSEC XP YP WATL OUTPUT 000000.000 0.10 SEC
!
TABLE 'frame1' HEAD '1Dmodel_hs.fr' TSEC XP YP HS
TABLE 'frame1' HEAD '1Dmodel_wl.fr' TSEC XP YP WATL VKSI VETA OUTPUT 000000.000
0.60 SEC
!
COMPUTE 000000.000 0.020 SEC 001500.000
!
STOP
```

H.2.1 Command file for the 1D model for reflection off the harbour end

The SWASH command file for the 1D SWASH model simulating reflection off the harbor end, discussed in Chapter 6 is the following.

```
!*****************HEADING*******************************************
PROJ 'model1D' '1'
!*****************MODEL INPUT***************************************
MODE DYN ONED
```

CGRID REGULAR 0.45 0.0 0.0 1360.8 0.0 1512 0
! CGRID REGULAR 0.01 0.0 0.0 30.24 0.0 1512 0 dx=0.02
VERTICAL 2
!
INPGRID BOT REG 0.45 0.0 0.0 1512 0 0.9 1
READINP BOTTOM 45. '1DmodelTM.bot' 1 0 FREE
INPGRID POROSITY REG 0.45 0.0 0.0 1512 0 0.9 1
READINP POROSITY 1. '1DmodelTM.por' 1 0 FREE
INPGRID PSIZE REG 0.45 0.0 0.0 1512 0 0.9 1
READINP PSIZE 45. '1DmodelTM.psiz' 1 0 FREE
INPGRID HSTRUCTURE REG 0.45 0.0 0.0 1512 0 0.9 1
READINP HSTRUCTURE 45. '1DmodelTM.hstr' 1 0 FREE
!
INITIAL ZERO!
BOU SIDE W BTYPE WEAK SMOO 1 SEC UNIFORM SERIES 'Paddle45_5_96_T002.tms'!
NONHYDROSTATIC
!
DISCRET UPW NONE
DISCRET CORRDEP NONE
!
TIMEI 0.2 0.5
! ********************OUTPUT REQUESTS********************************
POINTS 'punt3'   307.57500000   0.00000000
POINTS 'punt4'   277.06500000   0.00000000
POINTS 'punt5'   543.60000000   0.00000000
POINTS 'punt10'   203.71500000   0.00000000
POINTS 'punt11'   856.35000000   0.00000000
POINTS 'punt12'   1183.28000000 0.00000000
POINTS 'punt24'   360.94500000   0.00000000
POINTS 'punt26'   715.50000000   0.00000000
POINTS 'punt27'   1020.51000000 0.00000000
!
FRAME 'frame1' 0.45 0.0 0.0 1360.8 0.0 1512 0
QUANTITY WATLEV 'WATLEV' 'WATLEV' -10 10 -999
QUANTITY HS 'HS' 'HS' 0 10 -999 0 25 MIN
!
TABLE 'punt3' HEAD '1Dmodel_p3.tbl' TSEC XP YP WATL OUTPUT 000000.000 0.10 SEC
TABLE 'punt4' HEAD '1Dmodel_p4.tbl' TSEC XP YP WATL OUTPUT 000000.000 0.10 SEC
TABLE 'punt5' HEAD '1Dmodel_p5.tbl' TSEC XP YP WATL OUTPUT 000000.000 0.10 SEC
TABLE 'punt10' HEAD '1Dmodel_p10.tbl' TSEC XP YP WATL OUTPUT 000000.000 0.10 SEC
TABLE 'punt11' HEAD '1Dmodel_p11.tbl' TSEC XP YP WATL OUTPUT 000000.000 0.10 SEC
TABLE 'punt12' HEAD '1Dmodel_p12.tbl' TSEC XP YP WATL OUTPUT 000000.000 0.10 SEC
TABLE 'punt24' HEAD '1Dmodel_p24.tbl' TSEC XP YP WATL OUTPUT 000000.000 0.10 SEC
TABLE 'punt26' HEAD '1Dmodel_p26.tbl' TSEC XP YP WATL OUTPUT 000000.000 0.10 SEC
TABLE 'punt27' HEAD '1Dmodel_p27.tbl' TSEC XP YP WATL OUTPUT 000000.000 0.10 SEC
!
TABLE 'frame1' HEAD '1Dmodel_hs.fr' TSEC XP YP HS
TABLE 'frame1' HEAD '1Dmodel_wl.fr' TSEC XP YP WATL VKSI VETA OUTPUT 000000.000
0.60 SEC
!
COMPUTE 000000.000 0.020 SEC 001500.000
!
STOP

Appendix I   Results of the 1D SWASH model simulating reflection off the harbour end

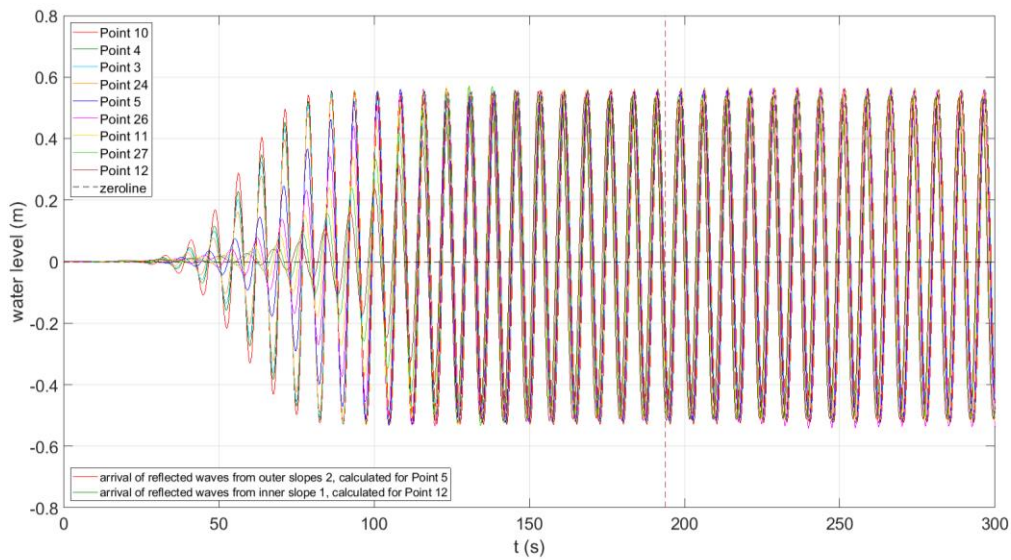## I.1 Wave celerity in the 1D SWASH model simulating reflection off the harbour end

Figure I.1 - Time series of all points along Line AA' shifted earlier in time to match with Point 10, for T001.
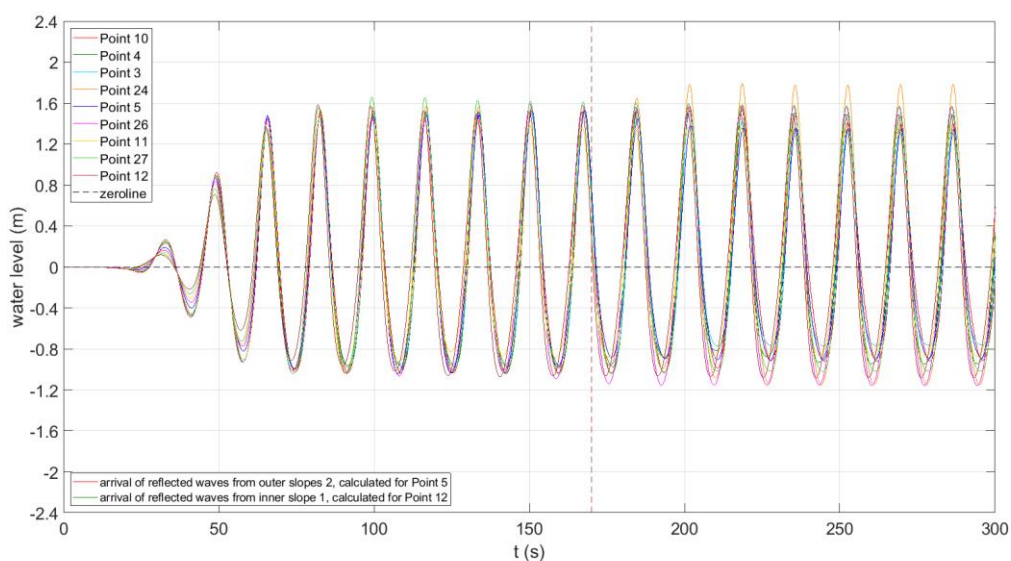

Figure I.2 - Time series of all points along Line AA' shifted earlier in time to match with Point 10, for T003.
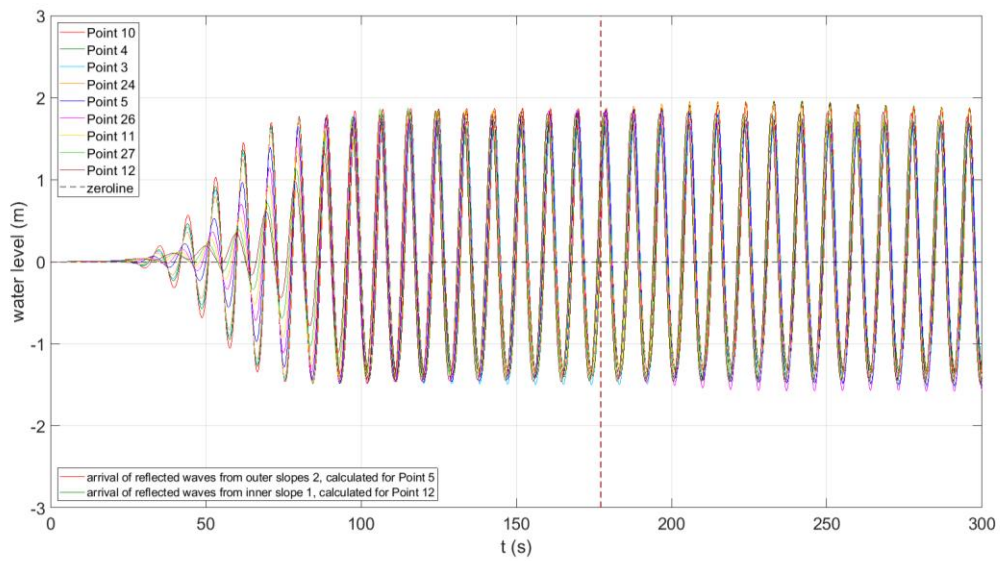
Figure I.3 - Time series of all points along Line AA' shifted earlier in time to match with Point 10, for T011.
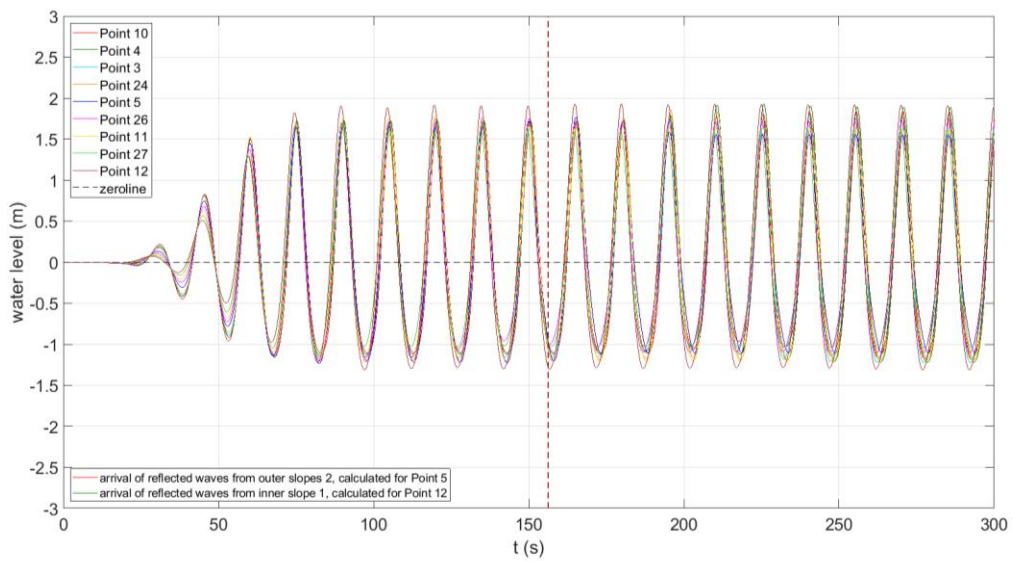

Figure I.4 - Time series of all points along Line AA' shifted earlier in time to match with Point 10, for T012.

I.2 Comparison of the measured water level times series to the outputs of the 1D SWASH model simulating reflection off the harbour end

The first group of tests for low kd values is presented in Table I.1. The graphs comparing the measured water level time series to the SWASH outputs are shown only for test T003, as it is a representative test of the group.

Table I.1 – The first group of tests for low kd values. This table is a repetition of Table 2.5.

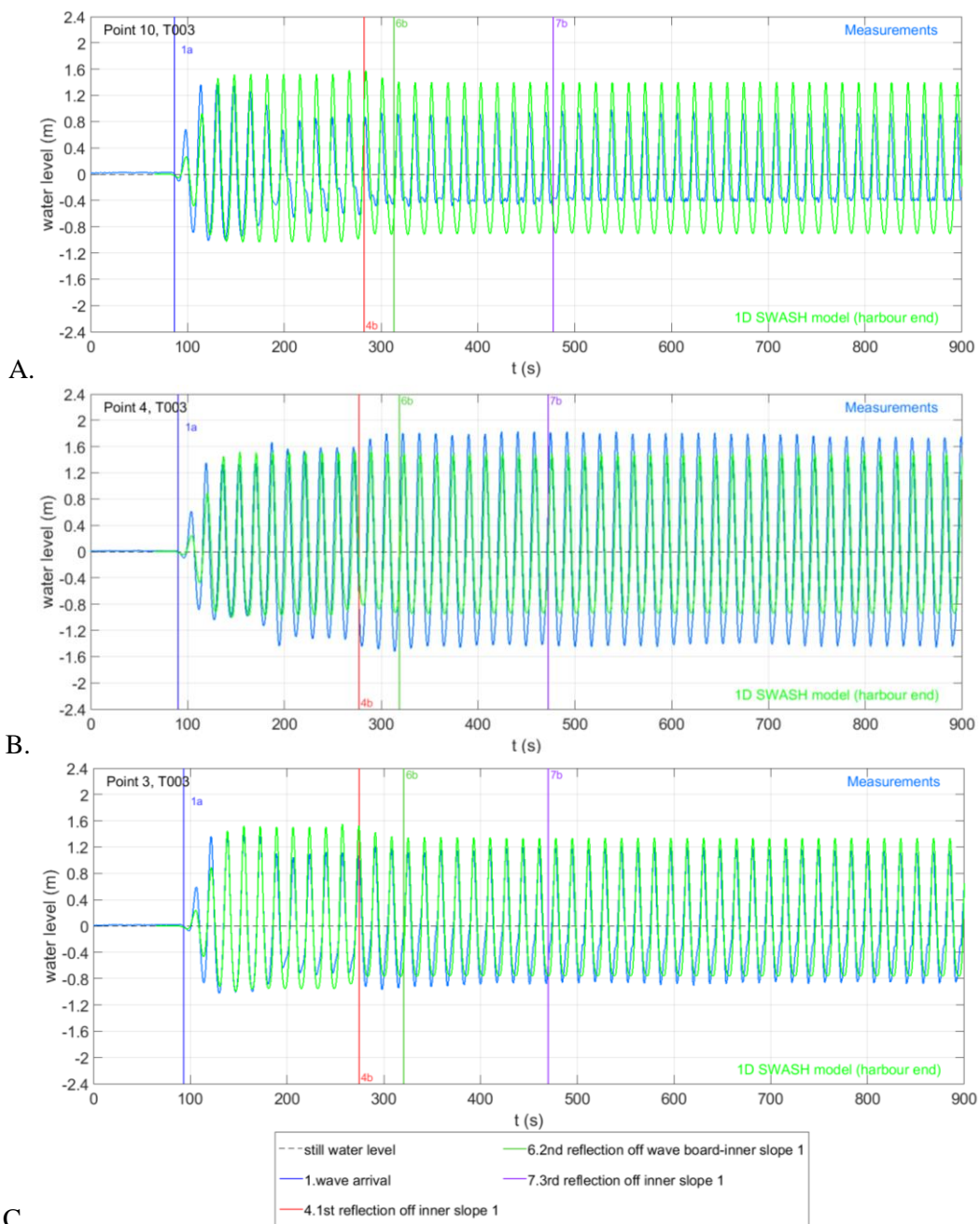| Test	L [m]	kd	Wave conditions	H/L	Wave breaking
T003	225.59	0.55	Intermediate/shallow water	0.011	-
T012	197.05	0.63	Intermediate/shallow water	0.014	-

A.

B.

C.

Figure I.5 – T003, The measured water level time series and the time series generated by the 1D SWASH model simulating reflection off the harbour end for Point 10 (picture A), Point 4 (picture B) and Point 3 (picture C).
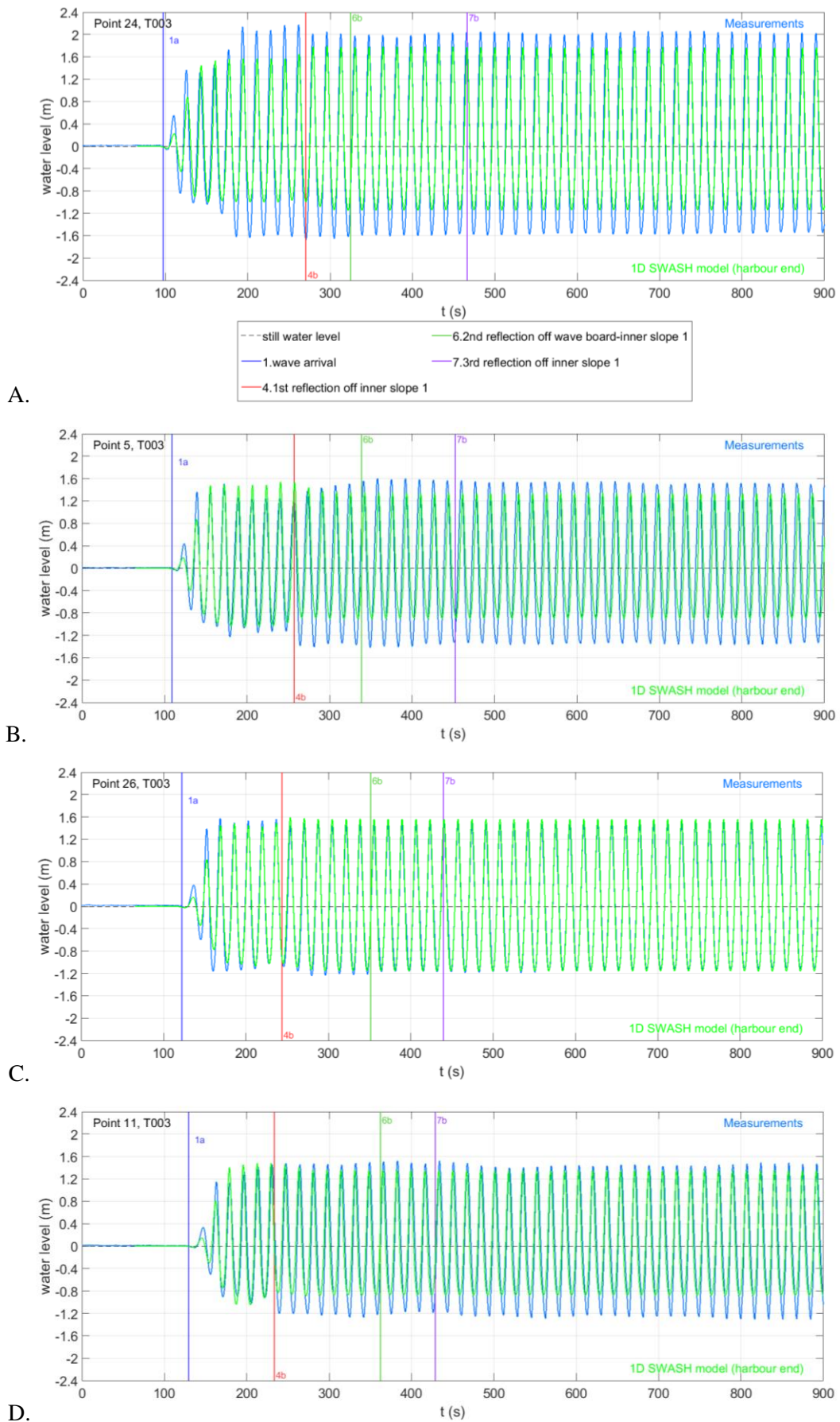
Figure I.6 – T003, The measured water level time series and the time series generated by the 1D SWASH model simulating reflection off the harbour end for Point 24 (picture A), 5(pict. B), 26(pict. C) and Point 11(pict. D).
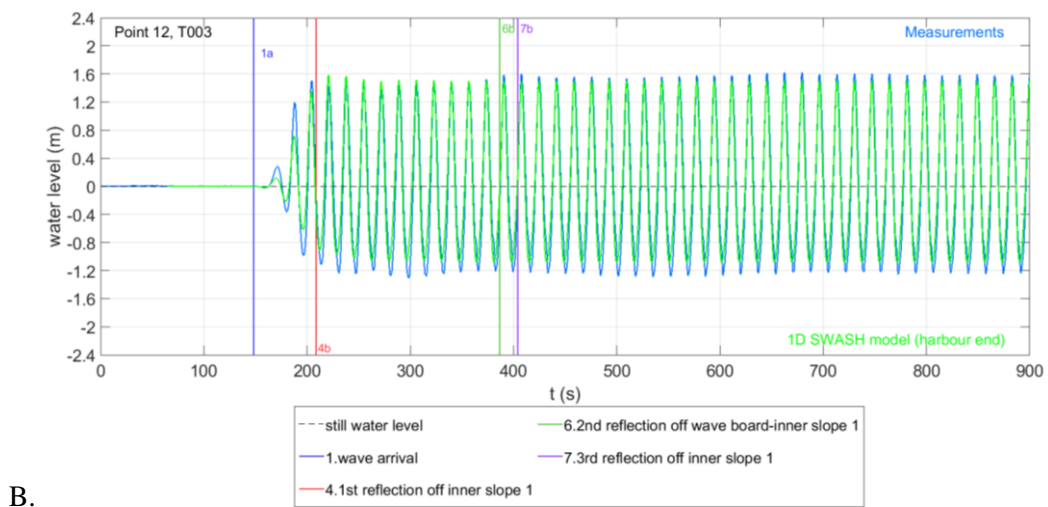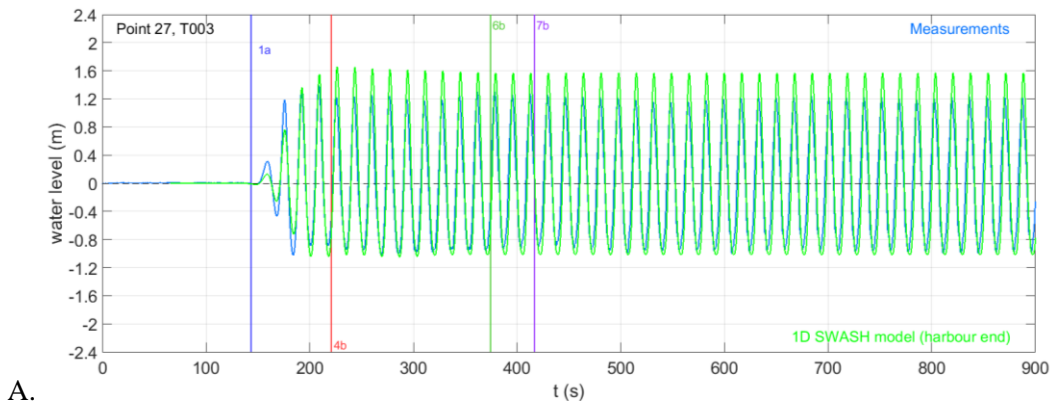
Figure I.7 – T003, The measured water level time series and the time series generated by the 1D SWASH model simulating reflection off the harbour end for Point 27 (picture A) and Point 12(picture B).

The second group of tests for average kd values is presented in Table I.2. The graphs comparing the measured water level time series to the SWASH outputs are shown only for test T002, as it is a representative test of the group.

Table I.2 – The second group of tests for average kd values. This table is a repetition of Table 2.6.

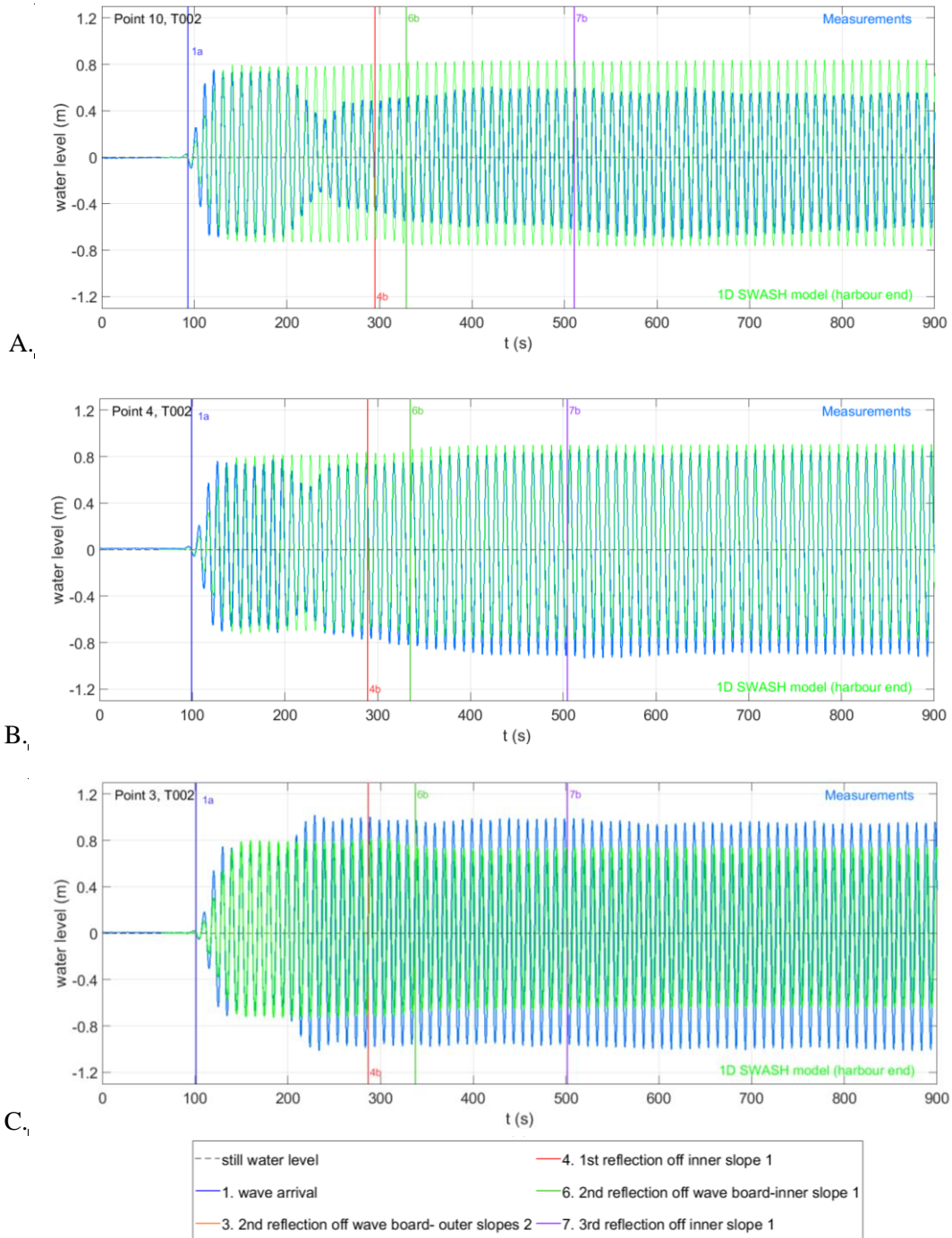| Test	L [m]	kd	Wave conditions	H/L	Wave breaking
T001	80.48	1.55	Intermediate water	0.001	-
T002	120.74	1.03	Intermediate water	0.012	-
T011	104.71	1.19	Intermediate water	0.029	-

A.

B.

C.

Figure I.8 – T002, The measured water level time series and the time series generated by the 1D SWASH model simulating reflection off the harbour end for Point 10 (picture A), Point 4 (picture B) and Point 3 (picture C).
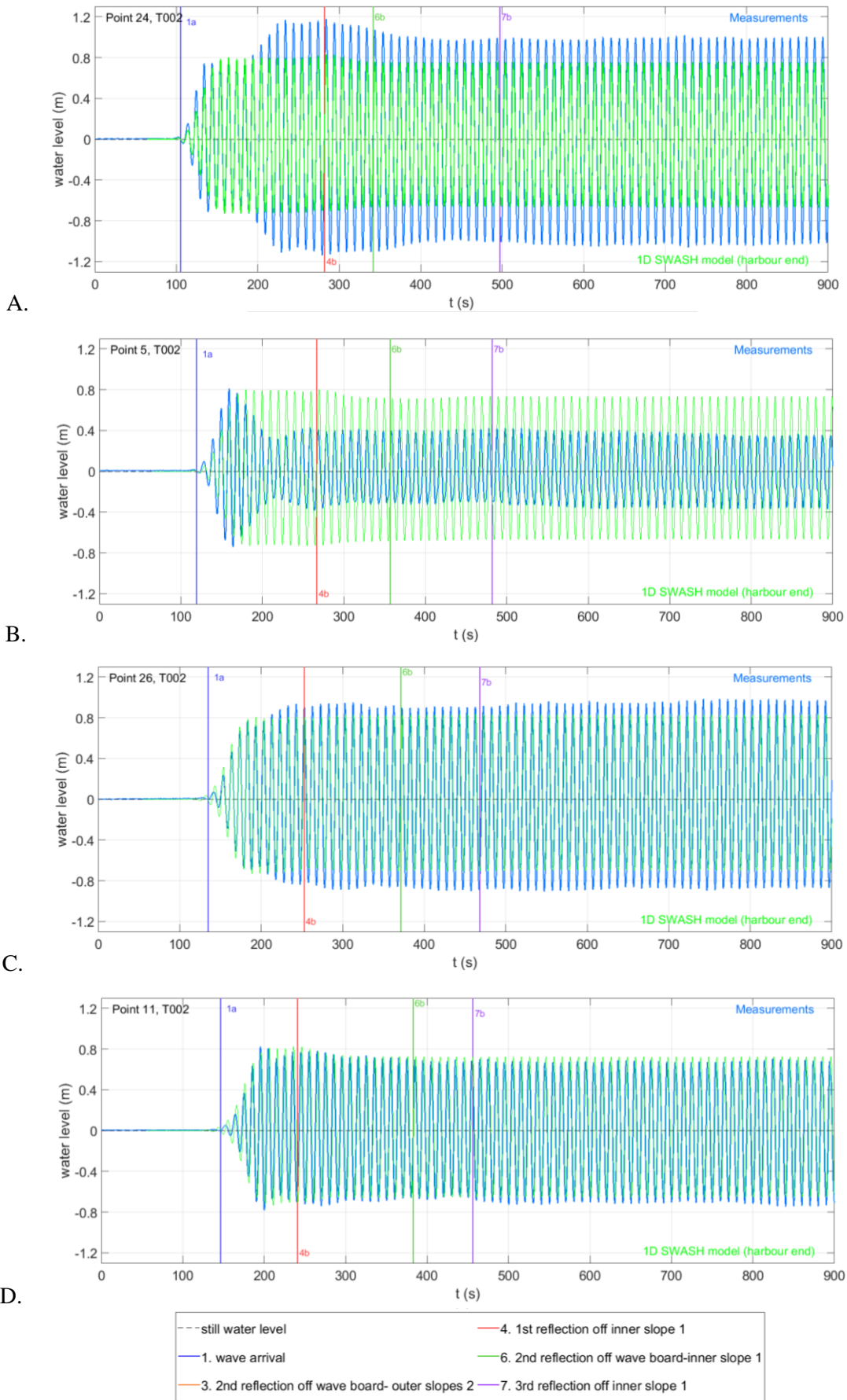
Figure I.9 – T002, The measured water level time series and the time series generated by the 1D SWASH model simulating reflection off the harbour end for Point 24 (picture A), 5(pict. B), 26(pict. C) and 11(pict. D).
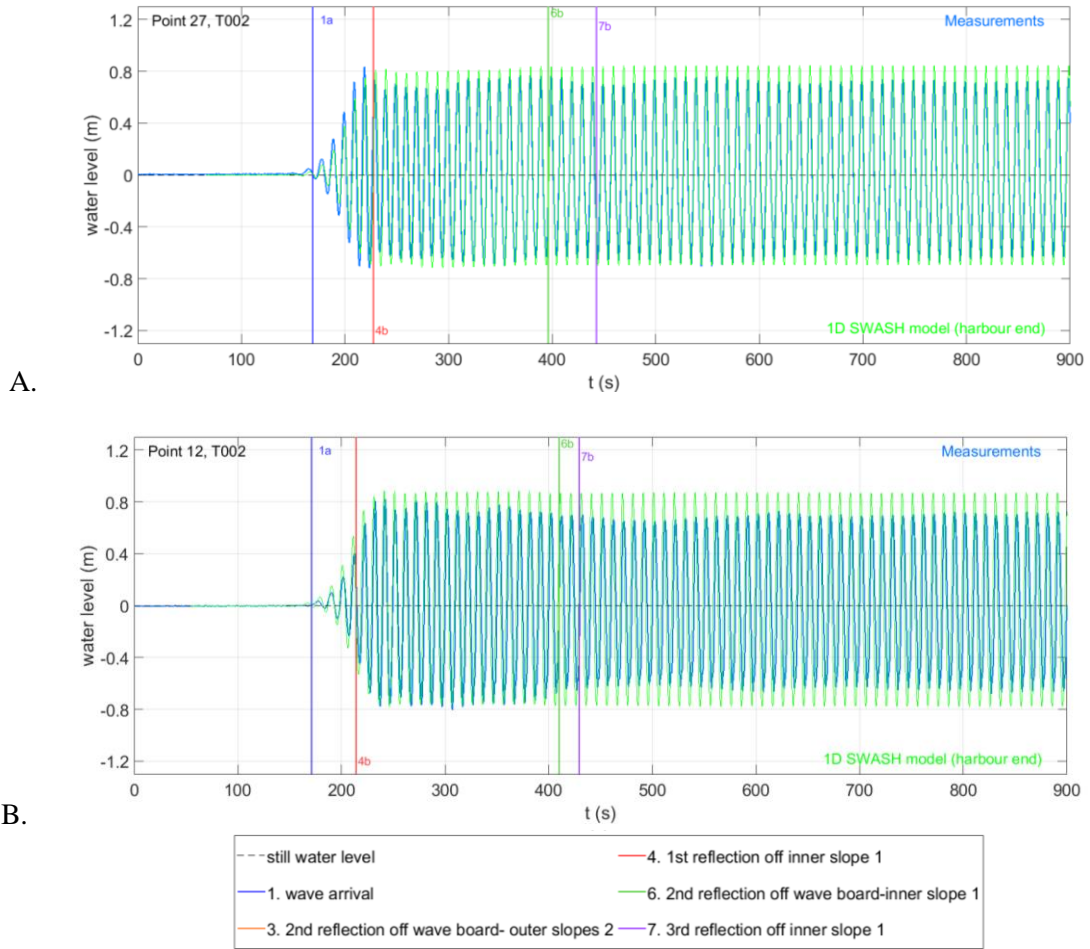
Figure I.10 – T002, The measured water level time series and the time series generated by the 1D SWASH model simulating reflection off the harbour end for Point 27 (picture A) and Point 12(picture B).

The third group of tests for high kd values is presented in Table I.3. The graphs comparing the measured water level time series to the SWASH outputs are shown for test T010 and test T013, as it in the first case wave breaking occurs, while in the second the waves do not break.

Table I.3 – The third group of tests for high kd values. This table is a repetition of Table 2.7.

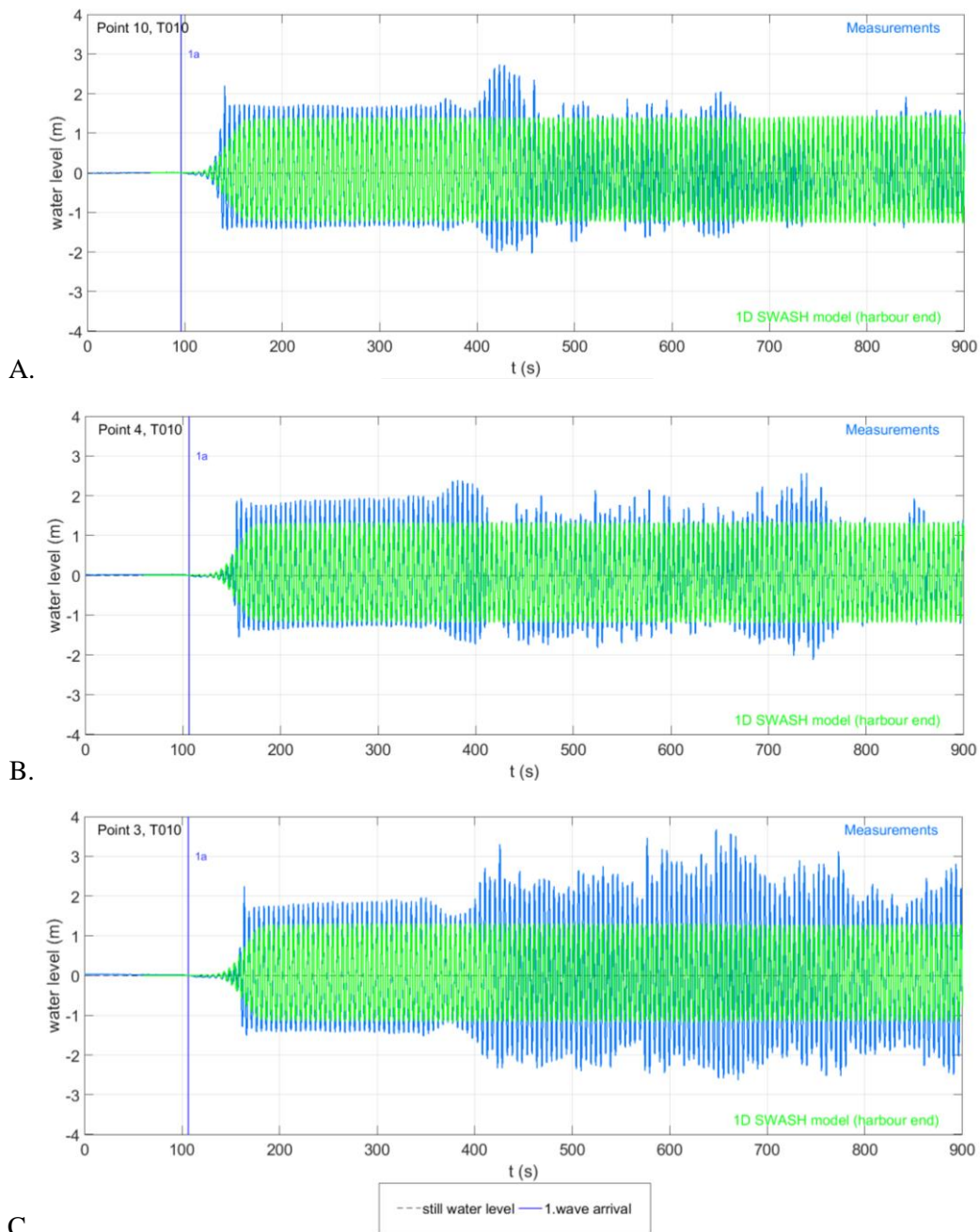| Test	L [m]	kd	Wave conditions	H/L	Wave breaking
T010	39.38	3.16	Deep/Intermediate water	0.075	yes
T013	31.52	3.95	Deep water	0.061	close to the breaking limit

A.

B.

C.

Figure I.11 – T010, The measured water level time series and the time series generated by the 1D SWASH model simulating reflection off the harbour end for Point 10 (picture A), Point 4 (picture B) and Point 3 (picture C).
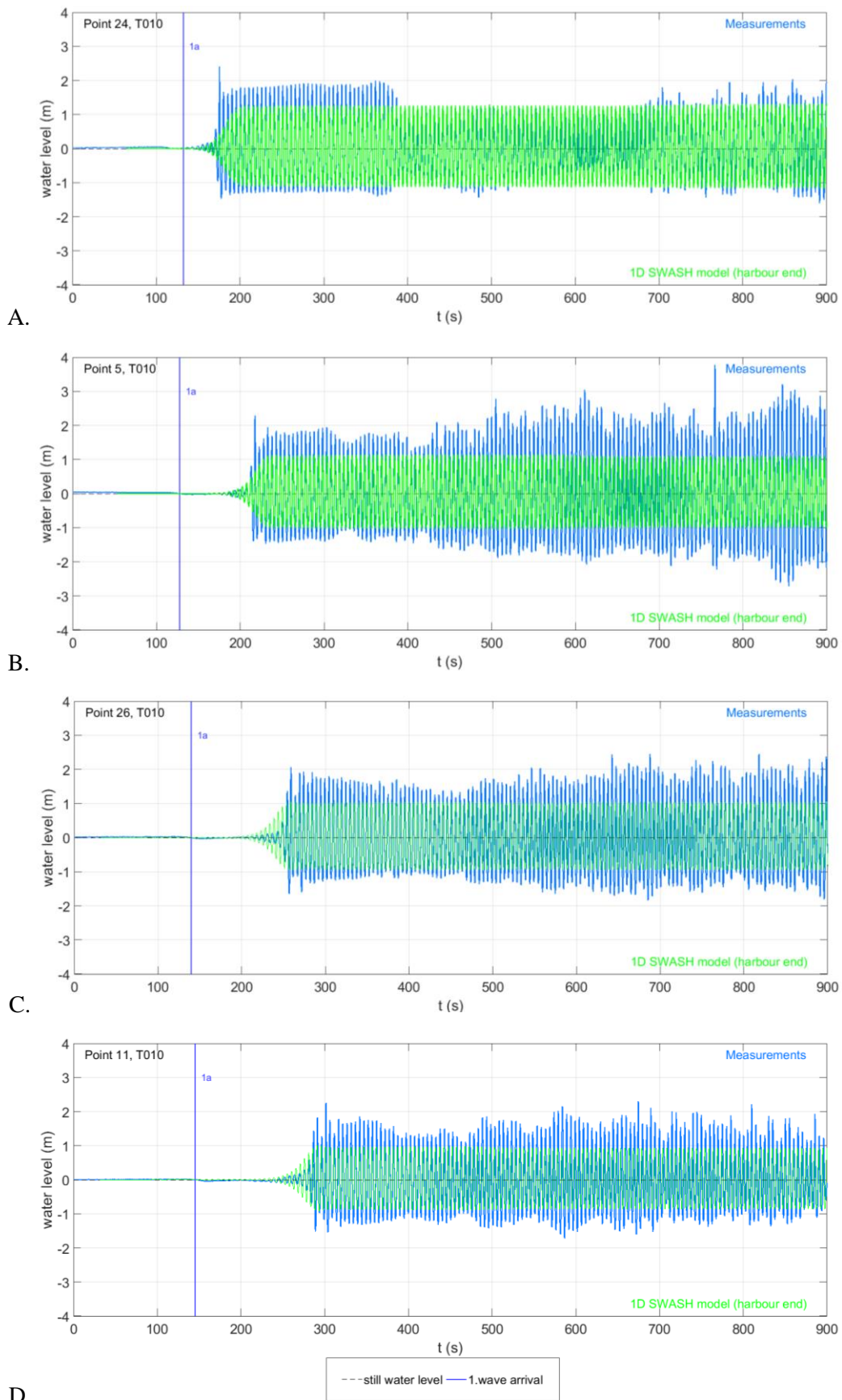
163

Figure I.12 – T010, The measured water level time series and the time series generated by the 1D SWASH model simulating reflection off the harbour end for Point 24 (picture A), 5(pict. B), 26(pict. C) and Point 11(pict. D).
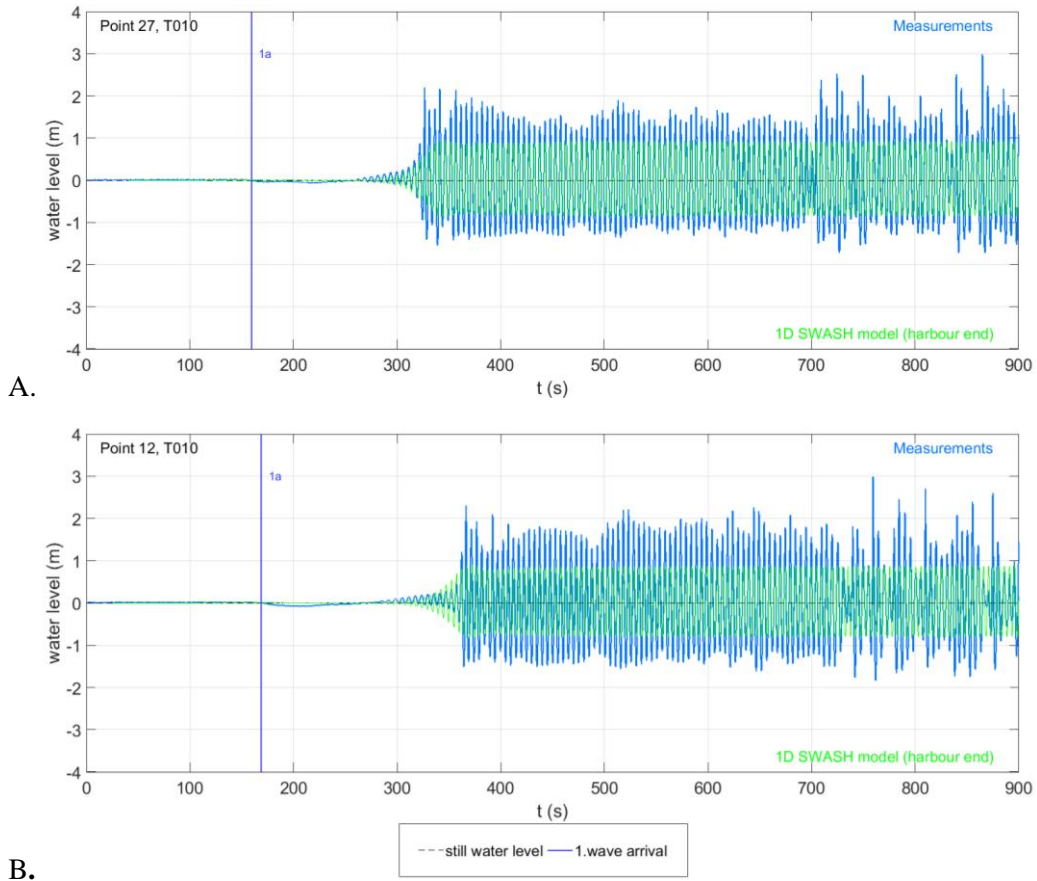
Figure I.13 – T010, The measured water level time series and the time series generated by the 1D SWASH model simulating reflection off the harbour end for Point 27 (picture A) and Point 12(picture B).

Figure I.14 – T013, The measured water level time series and the time series generated by the 1D SWASH model simulating reflection off the harbour end for Point 10 (picture A) and Point 4 (picture B).

Figure I.15 – T013, The measured water level time series and the time series generated by the 1D SWASH model simulating reflection off the harbour end for Point 3 (picture A), 24 (picture B), 5(picture C) and Point 26(picture D).
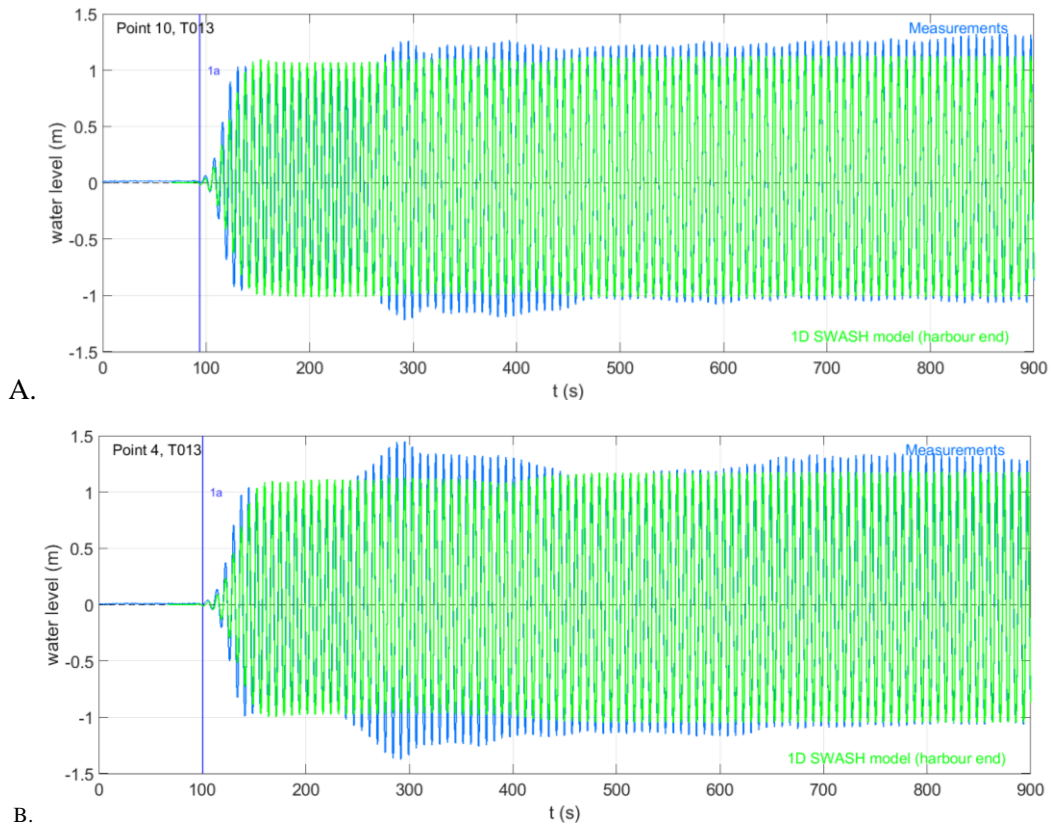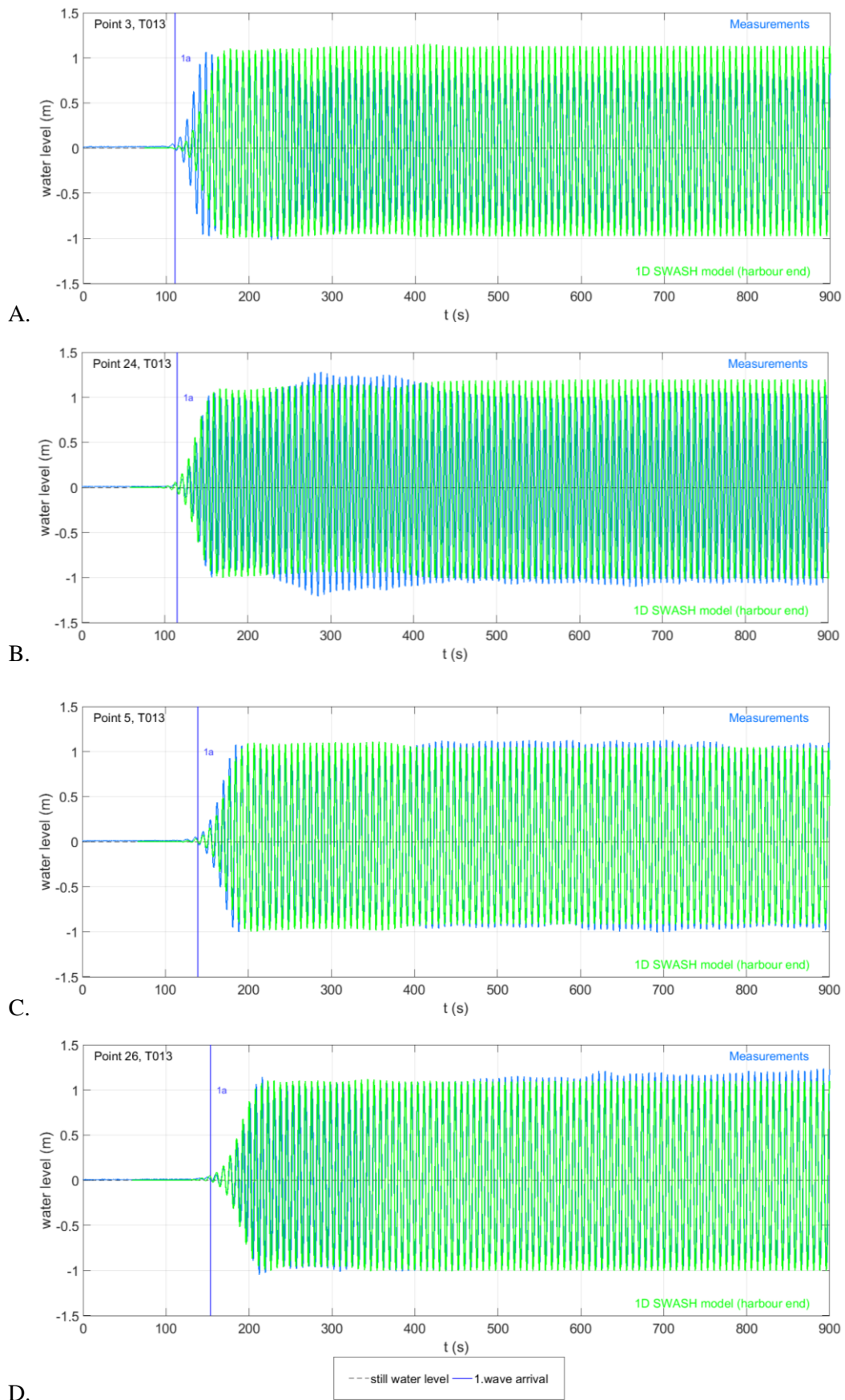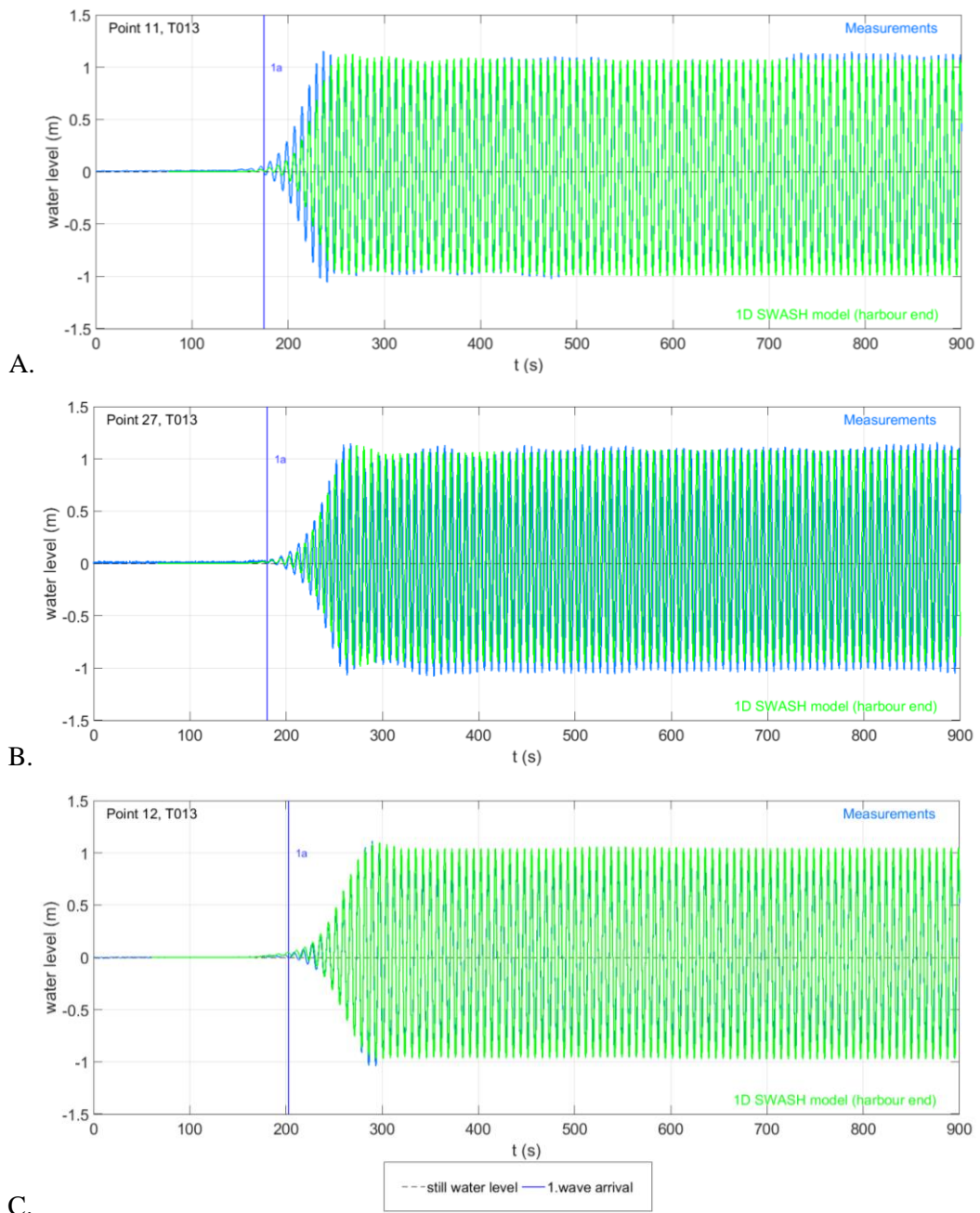
Figure I.16 – T013, The measured water level time series and the time series generated by the 1D SWASH model simulating reflection off the harbour end for Point 11 (picture A), Point 27 (picture B) and Point 12(picture C).

Appendix J   Results of the simplified 2D SWASH model

J.1 Comparison of the measured water level times series to the simplified 2D SWASH model outputs and to the 1D SWASH model about reflection at the harbour end

The first group of tests for low kd values, presented in Table I.1, includes tests T003 and T012. The graphs comparing the measured water level time series to the SWASH outputs are shown only for test T003, as it is a representative test of the group.

A.

B.

Figure J.1 - T003, Point 10 (picture A) and Point 4 (picture B): Comparison of the measured water level time series to the simplified 2D SWASH outputs only and also to the 1D SWASH (simulating reflection at the harbour end) model outputs.

Figure J.2 - T003, Point 3 (picture A), Point 24 (picture B) and Point 5 (picture C): Comparison of the measured water level time series to the simplified 2D SWASH outputs only and also to the 1D SWASH (simulating reflection at the harbour end) model outputs.

A.1

A.2

B.

C.

Figure J.3 - T003, Point 26 (pictures A.1 and A.2), Point 11 (picture B) and Point 27 (picture C): Comparison of the measured water level time series to the simplified 2D SWASH outputs only and also to the 1D SWASH (simulating reflection at the harbour end) model outputs.

Figure J.4 - T003, Point 12: Comparison of the measured water level time series to the simplified 2D SWASH outputs only and also to the 1D SWASH (simulating reflection at the harbour end) model outputs.

The second group of tests for average kd values, presented in Table I.2, includes tests T001, T002 and T011. The graphs comparing the measured water level time series to the SWASH outputs are shown only for test T002, as it is a representative test of the group.
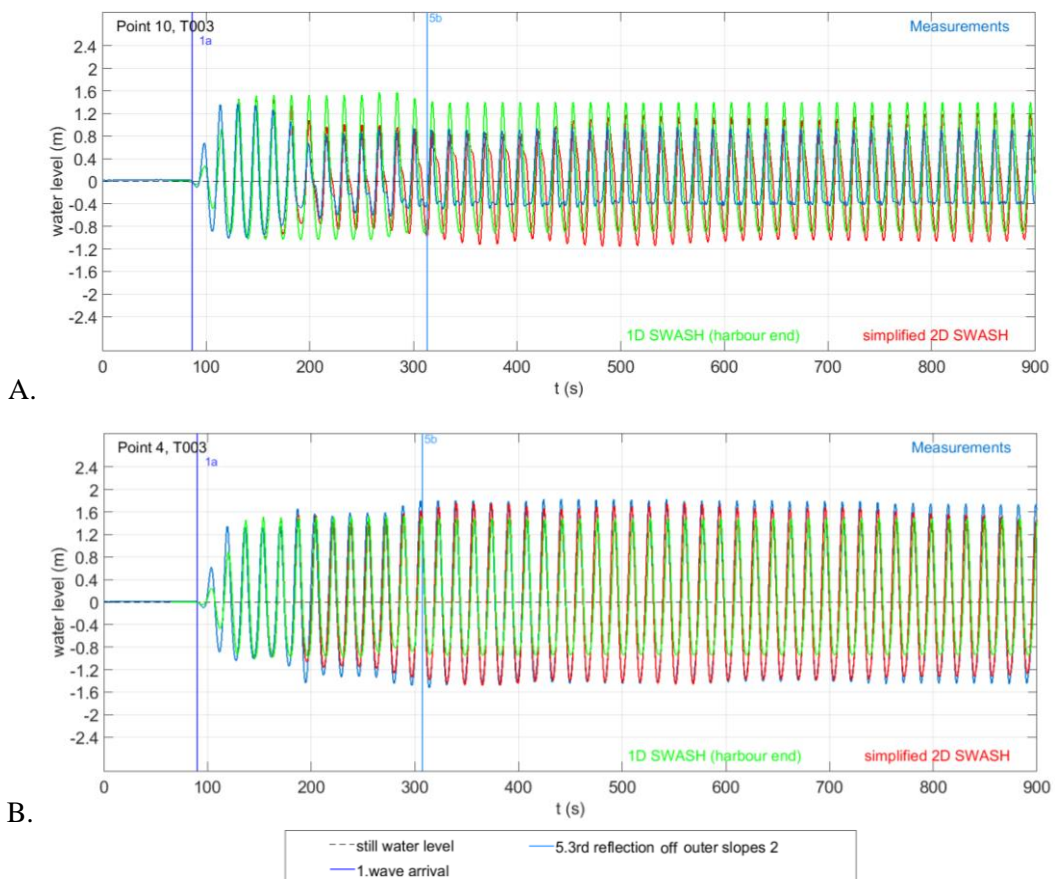

A.

B.

Figure J.5 - T002, Point 10 (picture A) and Point 4 (picture B): Comparison of the measured water level time series to the simplified 2D SWASH outputs only and also to the 1D SWASH (simulating reflection at the harbour end) model outputs.
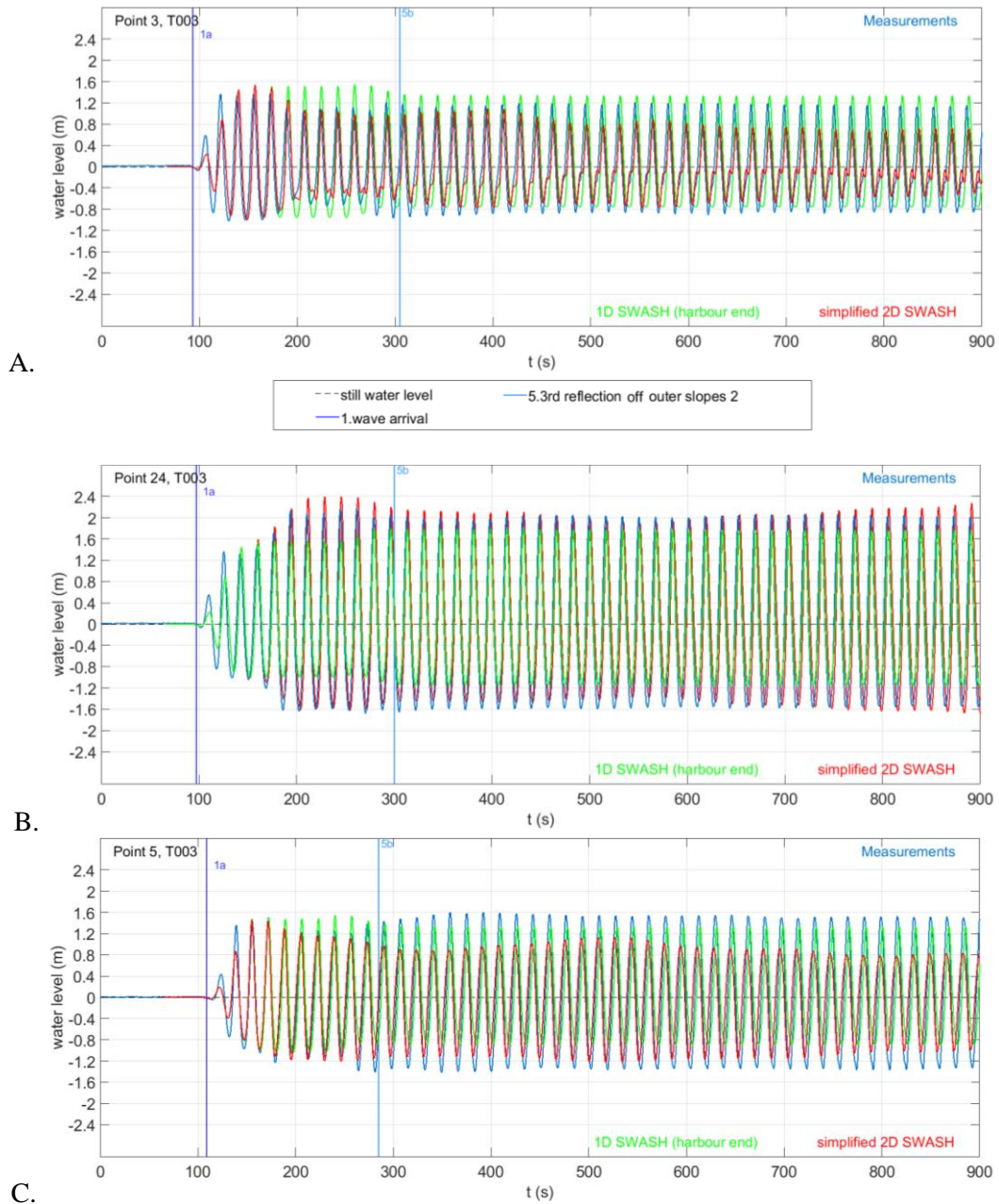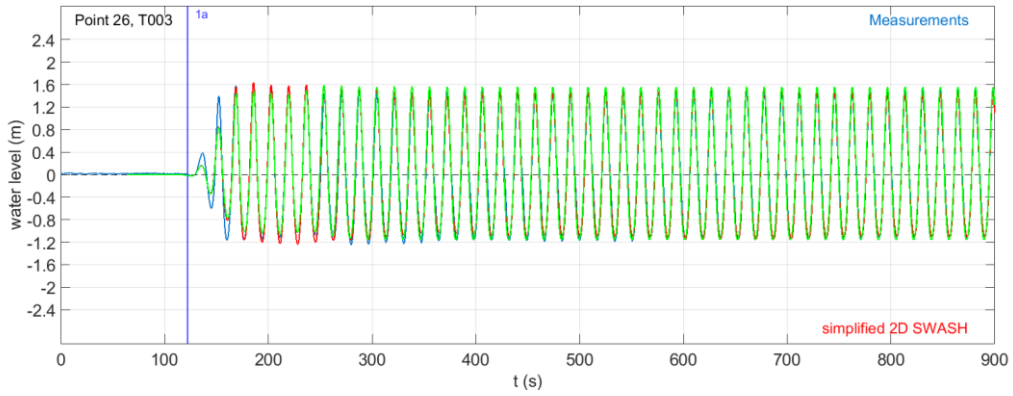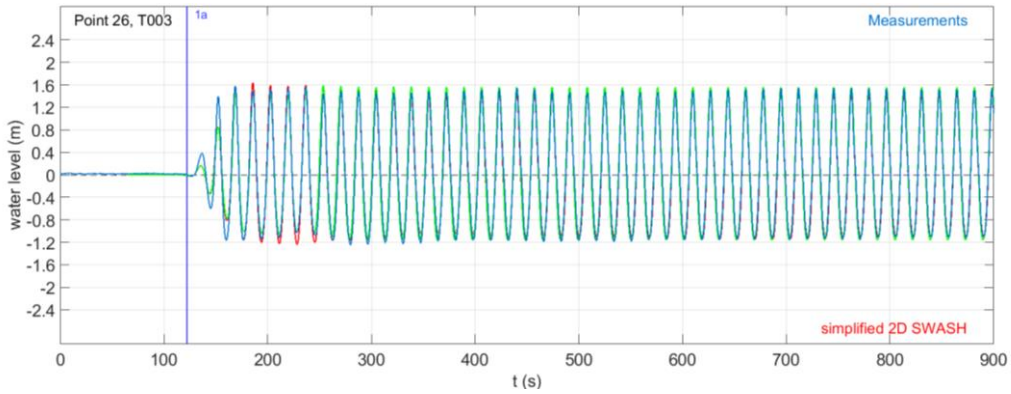
Figure J.6 - T002, Point 3 (picture A), Point 24 (picture B), Point 5 (picture C) and Point 26 (picture D): Comparison of the measured water level time series to the simplified 2D SWASH outputs only and also to the 1D SWASH (simulating reflection at the harbour end) model outputs.
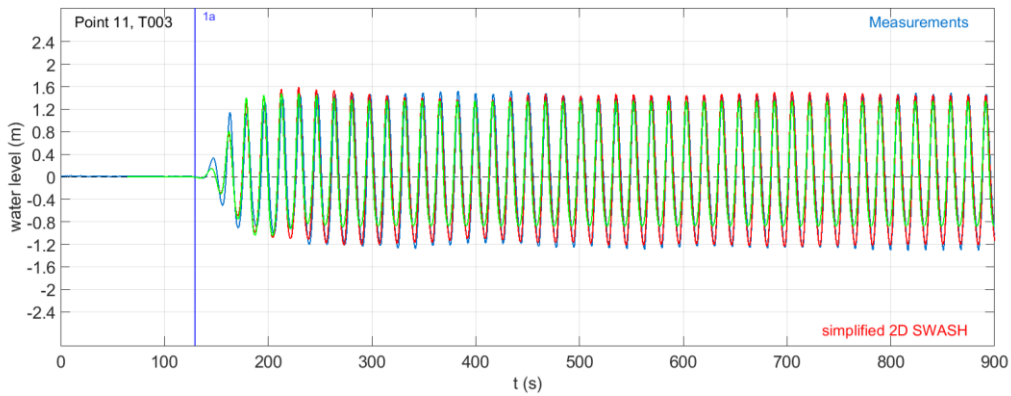
Figure J.7 - T002, Point 27 (picture A) and Point 12 (picture B): Comparison of the measured water level time series to the simplified 2D SWASH outputs only and also to the 1D SWASH (simulating reflection at the harbour end) model outputs.
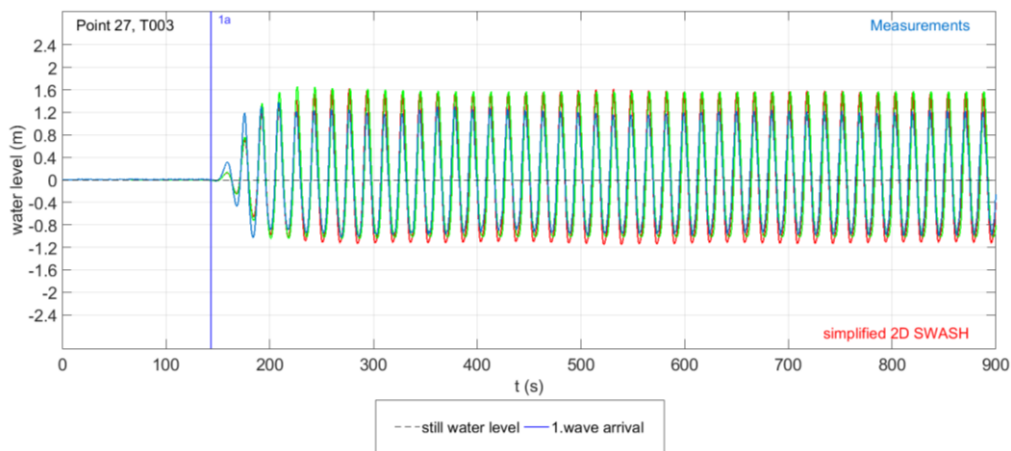
The third group of tests for high kd values, presented in Table I.3, includes tests T010 and T013. The graphs comparing the measured water level time series to the SWASH outputs are shown for both tests, as in T010 wave breaking occurs, while in T013 the waves do not break.

Figure J.8 - T010, Point 10 (picture A.1 and A.2), Point 4 (picture B) and Point 3 (picture C): Comparison of the measured water level time series to the simplified 2D SWASH outputs only and also to the 1D SWASH (simulating reflection at the harbour end) model outputs.
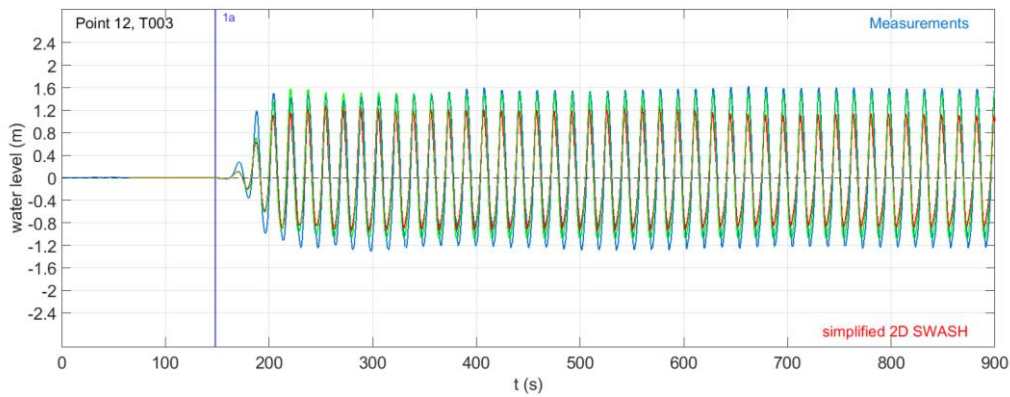
Figure J.9 - T010, Point 24 (picture A), Point 5 (picture B), Point 26 (picture C) and Point 11 (picture D): Comparison of the measured water level time series to the simplified 2D SWASH outputs only and also to the 1D SWASH (simulating reflection at the harbour end) model outputs.
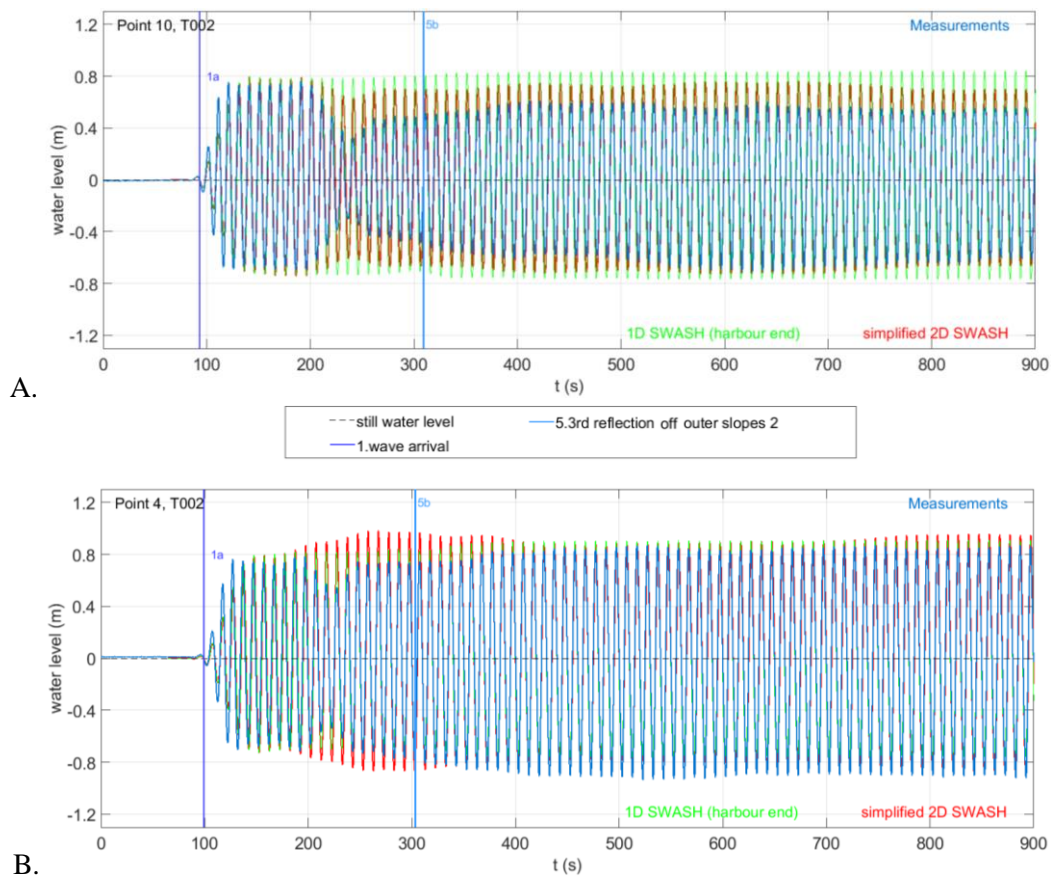
Figure J.10 - T010, Point 27 (picture A) and Point 11 (picture B): Comparison of the measured water level time series to the simplified 2D SWASH outputs only and also to the 1D SWASH (simulating reflection at the harbour end) model outputs.
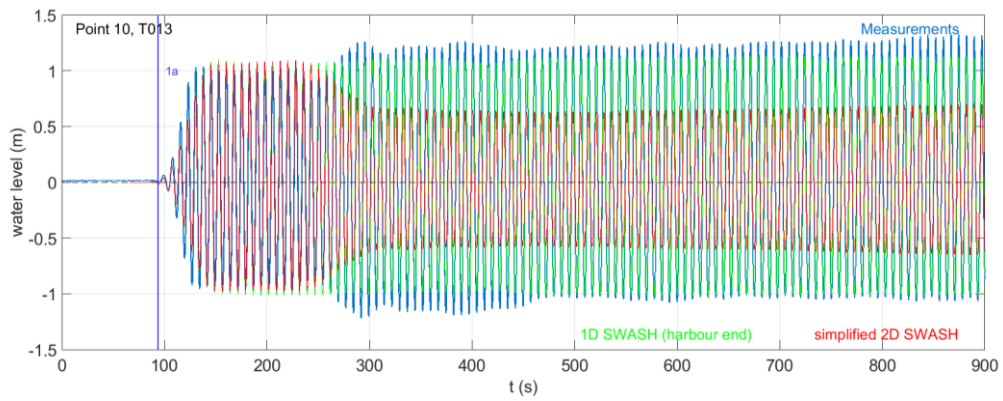
Figure J.11 - T013, Point 10: Comparison of the measured water level time series to the simplified 2D SWASH outputs only and also to the 1D SWASH (simulating reflection at the harbour end) model outputs.

176
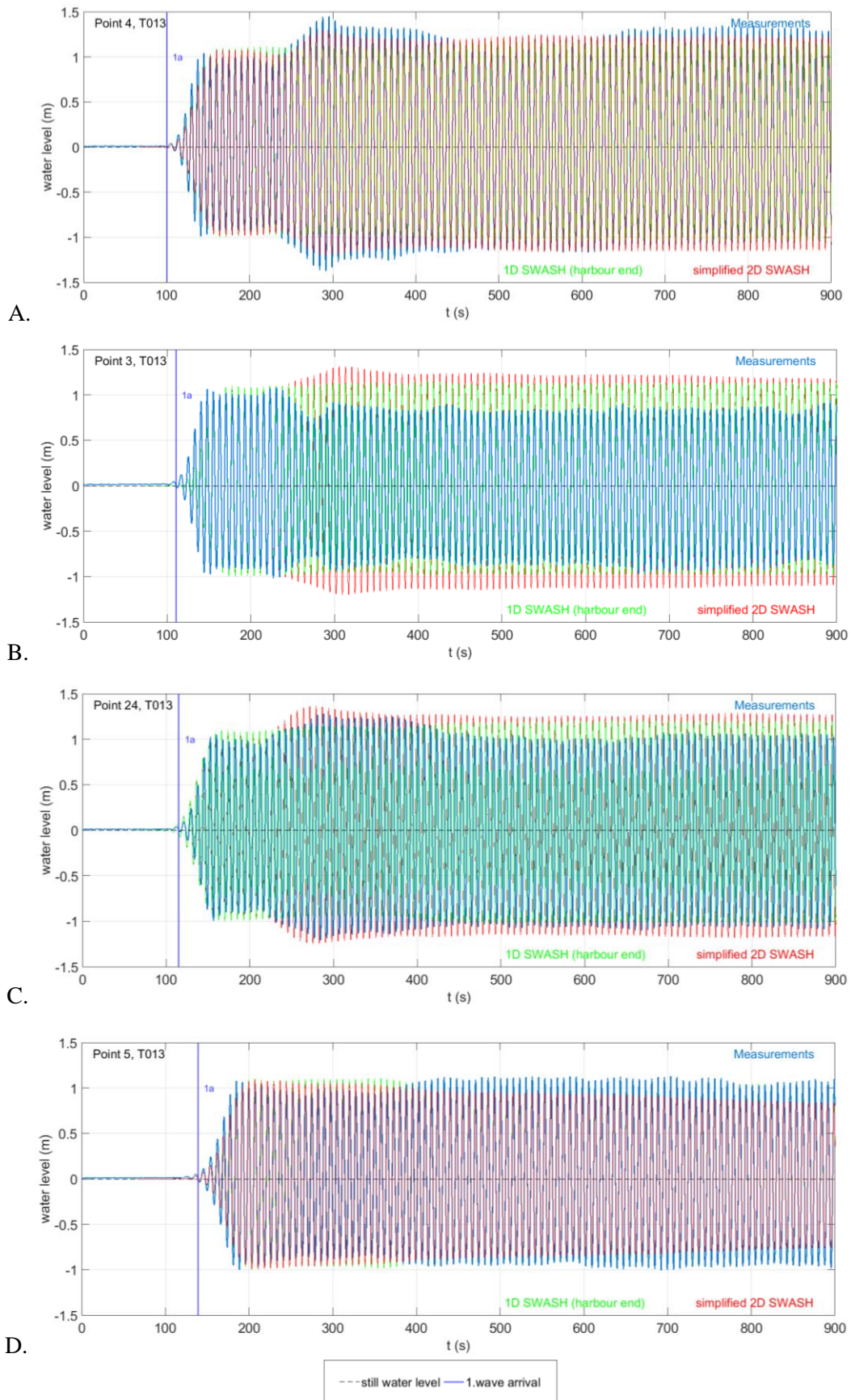
Figure J.12 - T013, Point 4 (picture A) and Point 4 (picture B): Comparison of the measured water level time series to the simplified 2D SWASH outputs only and also to the 1D SWASH (simulating reflection at the harbour end) model outputs.
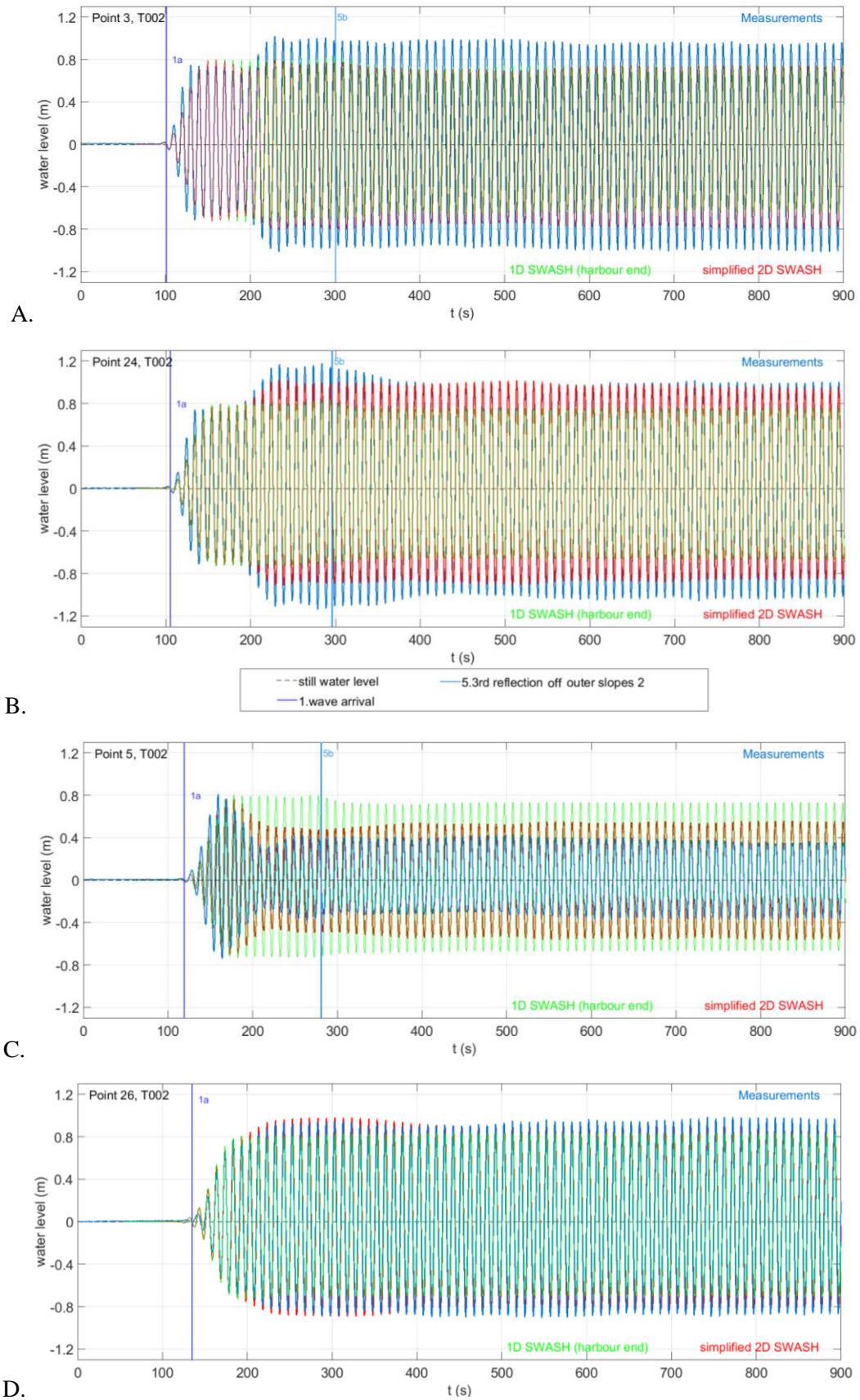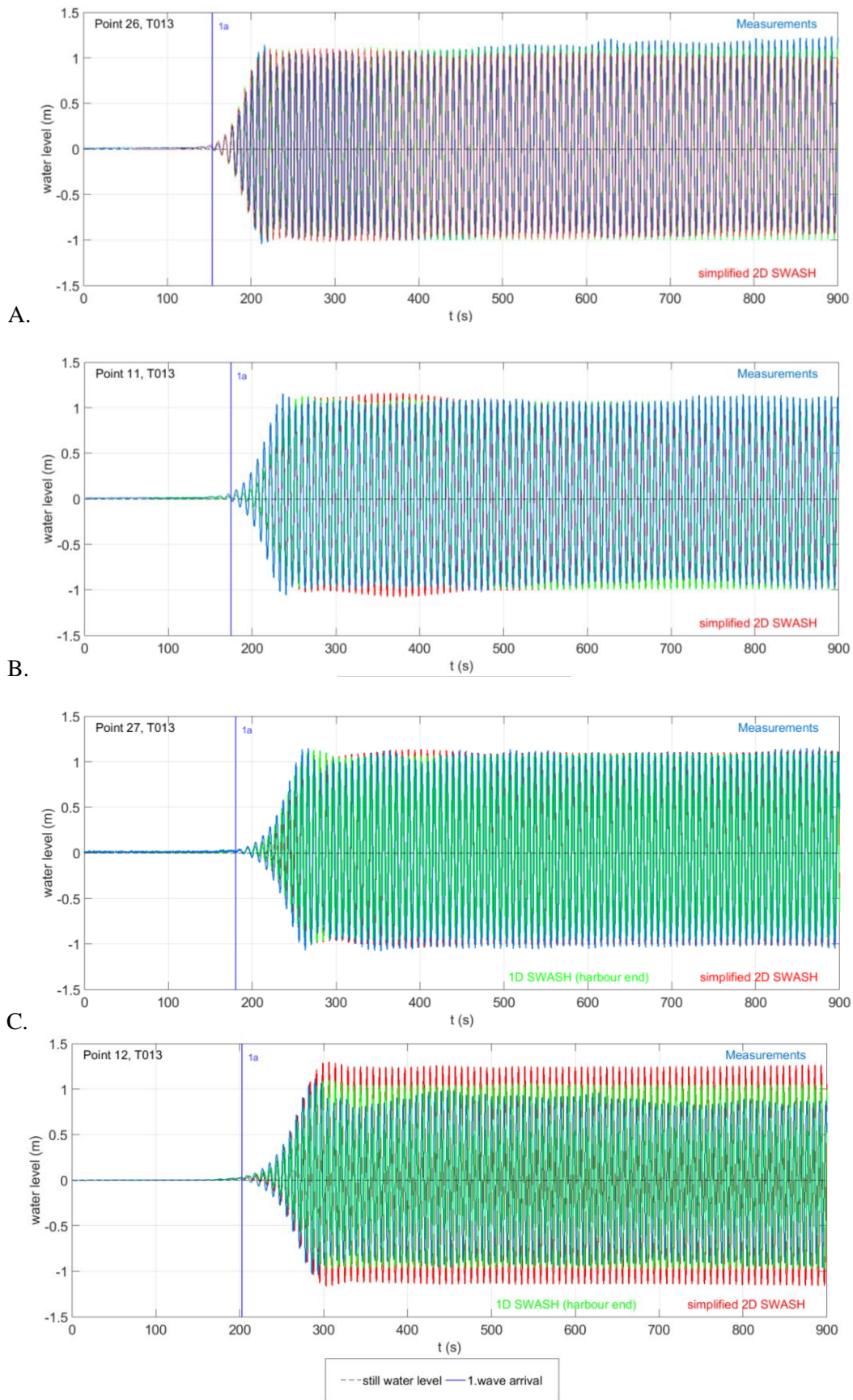
**Figure J.13 - T013, Point 26 (picture A), Point 11 (picture B), Point 27 (picture C) and Point 12 (picture D):
Comparison of the measured water level time series to the simplified 2D SWASH outputs only and also to the 1D
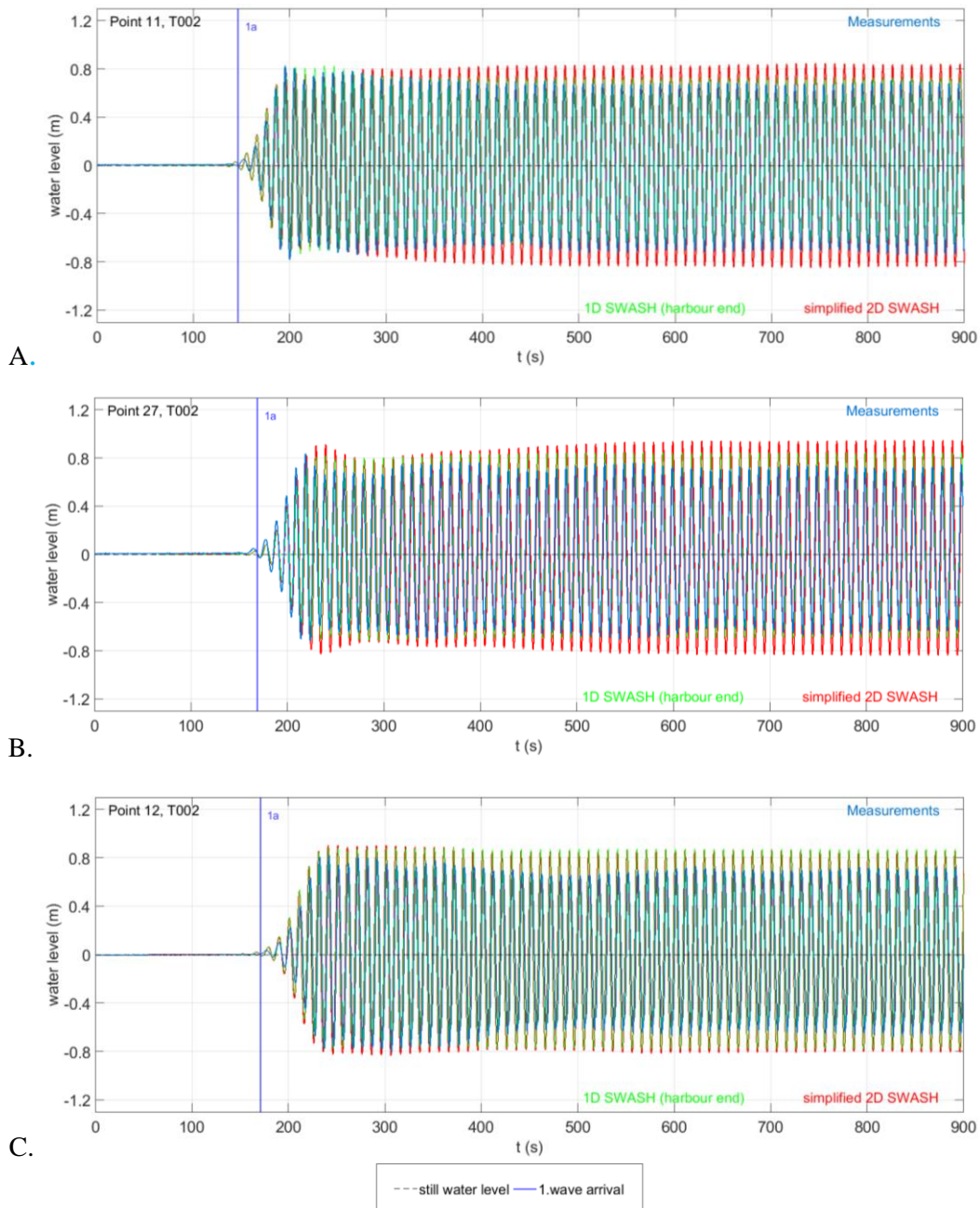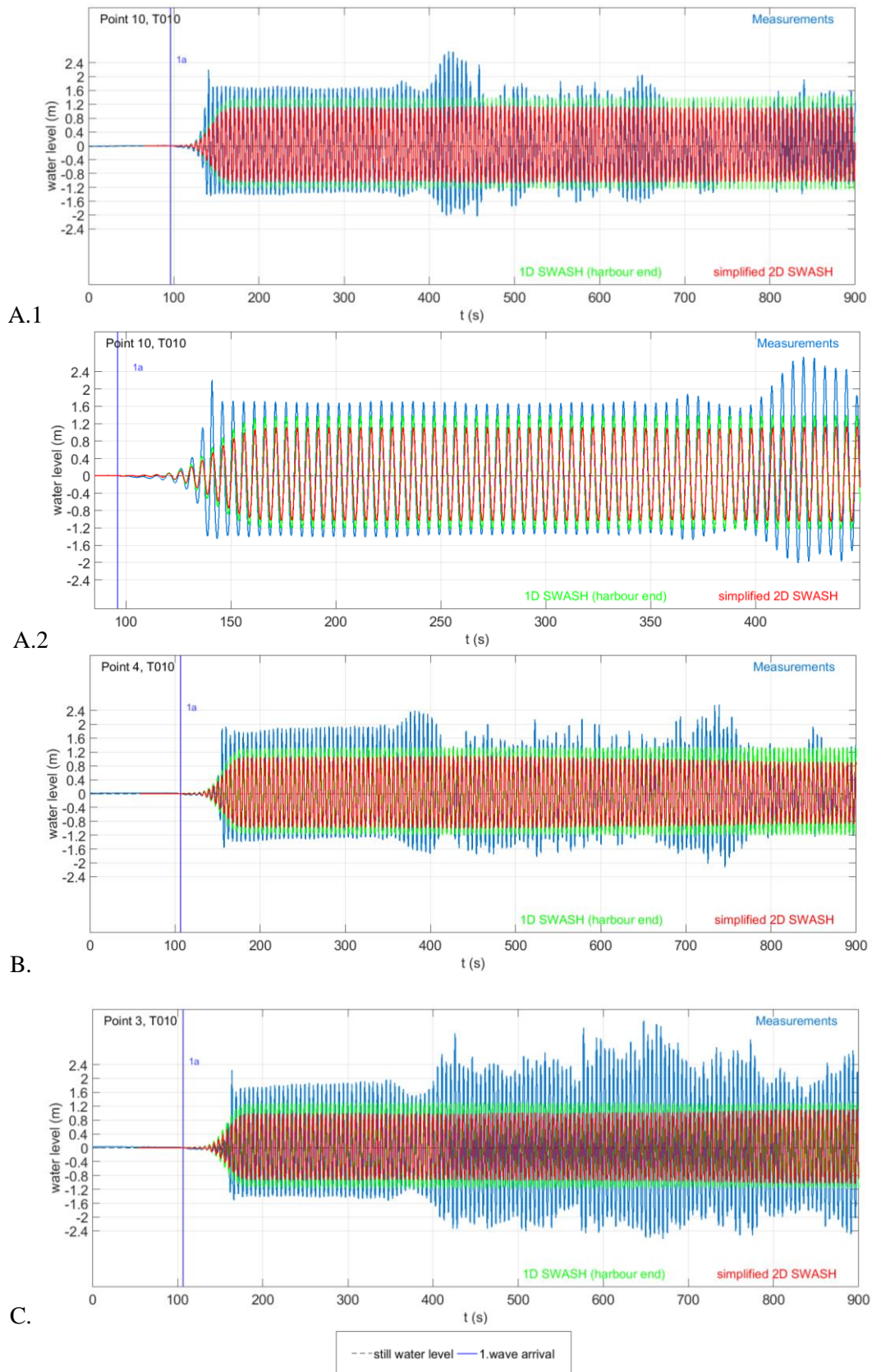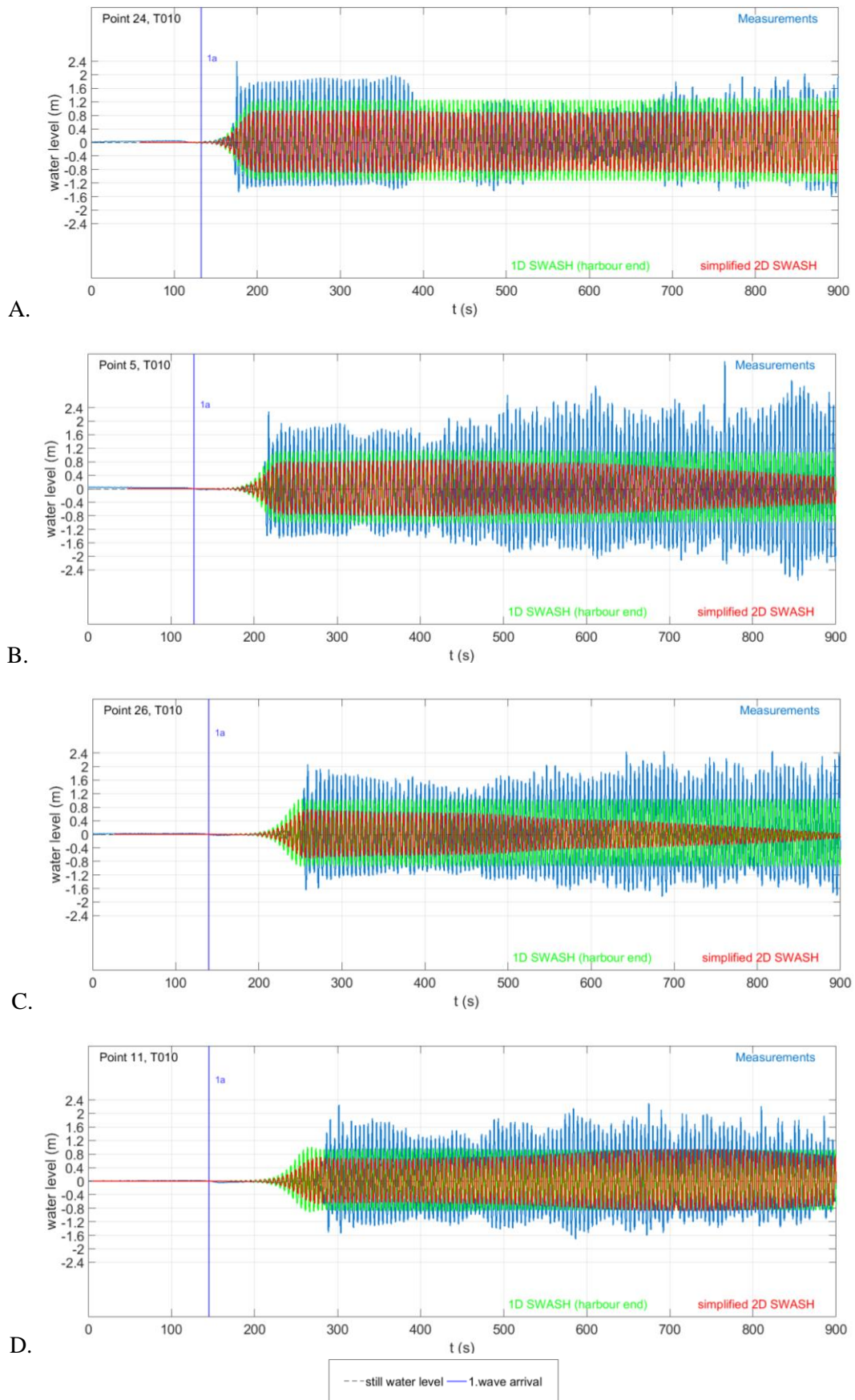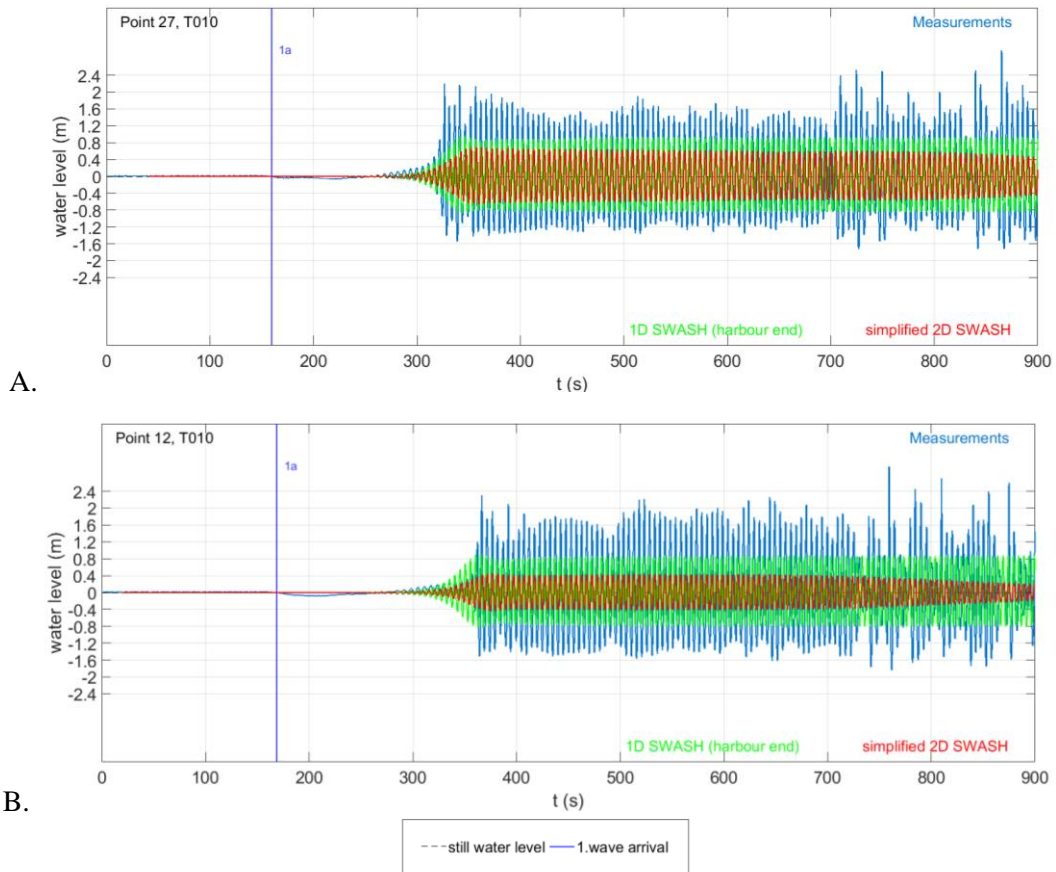SWASH (simulating reflection at the harbour end) model outputs.**

J.2 Comparison of the steady state in the measurements to the simplified 2D SWASH model outputs

Figure J.14 – T001, Top view of the ratio $H_{steady\ state}/H_{incoming}$ at the wave gauges locations. The colours indicate the ratio values. At each location the left box shows the measurements result, while the right box shows the simplified 2D SWASH model results.

Table J.1 – T001, The exact values of ratio $H_{steady\ state}/H_{incoming}$ in the measurements and in the simplified 2D SWASH model.

Outside the harbour basin				Inside the harbour basin			
Wave Gauge	Measured $H_{steady\ state}/H_{inc}$	2D simpl. $H_{steady\ state}/H_{inc}$	Difference (%)	Wave Gauge	Measured $H_{steady\ state}/H_{inc}$	2D simpl. $H_{steady\ state}/H_{inc}$	Difference (%)
1	1.20	1.19	-1	6	1.00	1.09	9
2	1.18	1.03	-13	7	1.27	0.69	-45
3	1.03	1.23	20	8	1.21	0.53	-57
4	1.26	1.20	- 4	9	1.15	0.44	-61
5	1.17	0.96	-17	11	1.10	1.09	0
10	1.08	0.67	-38	12	1.03	1.29	25
23	1.28	1.45	13	13	1.07	1.04	- 3
24	1.14	1.27	11	14	0.94	0.68	-28
25	1.32	1.40	6	15	0.87	0.54	-38
			|Max|= 38	16	0.98	0.43	-57
				26	1.07	1.09	1
				27	1.20	1.13	-7
							|Max|= 61

Figure J.15 – T002, Top view of the ratio $H_{steady\ state}/H_{incoming}$ at the wave gauges locations. The colours indicate the ratio values. At each location the left box shows the measurements result, while the right box shows the simplified 2D SWASH model results.

Table J.2 – T002, The exact values of ratio $H_{steady\ state}/H_{incoming}$ in the measurements and in the simplified 2D SWASH model.

Outside the harbour basin				Inside the harbour basin			
Wave Gauge	Measured $H_{steady\ state}/H_{inc}$	2D simpl. $H_{steady\ state}/H_{inc}$	Difference (%)	Wave Gauge	Measured $H_{steady\ state}/H_{inc}$	2D simpl. $H_{steady\ state}/H_{inc}$	Difference (%)
1	1.63	1.41	- 14	6	1.12	1.16	4
2	1.54	1.26	- 18	7	0.90	0.77	- 14
3	1.36	1.05	- 22	8	0.95	0.72	- 24
4	1.22	1.21	0	9	1.37	0.73	- 47
5	0.50	0.77	54	11	0.99	1.16	17
10	0.81	0.99	23	12	0.96	1.16	21
23	0.46	0.84	17	13	1.17	1.17	0
24	1.41	1.27	21	14	0.79	0.78	- 2
25	0.60	0.95	0	15	1.11	0.74	- 33
			|Max|= 54	16	1.06	0.74	- 30
				26	1.28	1.19	- 7
				27	0.94	1.23	30
							|Max|= 47

180

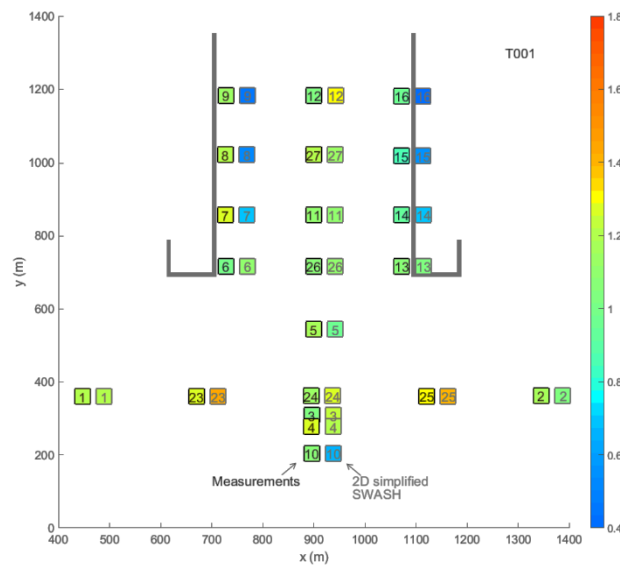**Figure J.16 – T003, Top view of the ratio $H_{steady\ state}/H_{incoming}$ at the wave gauges locations. The colours indicate the ratio values. At each location the left box shows the measurements result, while the right box shows the simplified 2D SWASH model results.**

Table J.3 – T003, The exact values of ratio $H_{steady\ state}/H_{incoming}$ in the measurements and in the simplified 2D SWASH model.

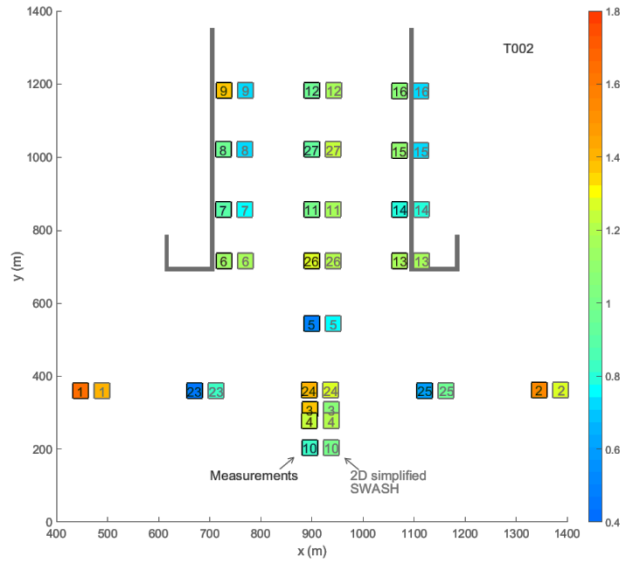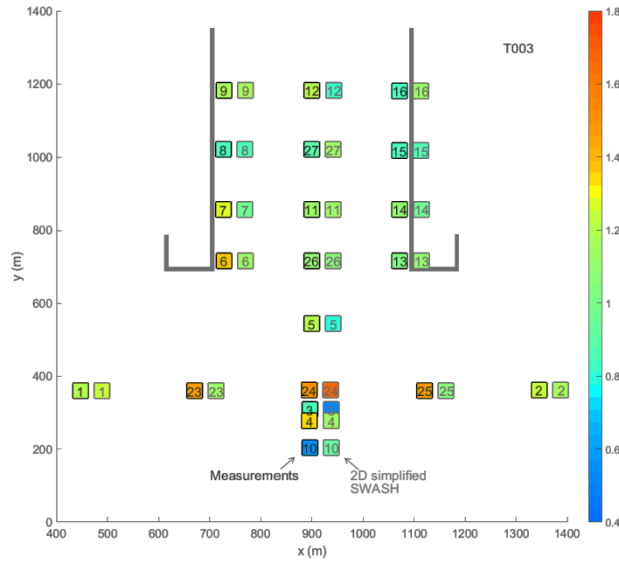| Outside the harbour basin				Inside the harbour basin			
Wave Gauge	Measured $H_{steady\ state}/H_{inc}$	2D simpl. $H_{steady\ state}/H_{inc}$	Difference (%)	Wave Gauge	Measured $H_{steady\ state}/H_{inc}$	2D simpl. $H_{steady\ state}/H_{inc}$	Difference (%)
1	1.19	1.23	4	6	1.39	1.13	-19
2	1.23	1.17	-5	7	1.27	0.95	-26
3	0.85	0.51	-40	8	0.86	0.87	1
4	1.35	1.12	-17	9	1.16	1.18	2
5	1.21	0.78	-36	11	1.14	1.12	-1
10	0.57	0.92	62	12	1.19	0.83	-30
23	1.48	1.14	-23	13	1.03	1.11	8
24	1.51	1.69	12	14	1.11	0.96	-14
25	1.46	1.07	-27	15	0.85	0.87	3
			|Max|= 82	16	0.87	1.15	32
				26	1.11	1.06	-5
				27	0.91	1.13	24
							|Max|= 47

Figure J.17 – T010, Top view of the ratio H$_{\text{steady state}}$/H$_{\text{incoming}}$ at the wave gauges locations. The colours indicate the ratio values. At each location the left box shows the measurements result, while the right box shows the simplified 2D SWASH model results.

Table J.4 – T010, The exact values of ratio H$_{\text{steady state}}$/H$_{\text{incoming}}$ in the measurements and in the simplified 2D SWASH model.

Outside the harbour basin				Inside the harbour basin			
Wave Gauge	Measured H$_{\text{steady state}}$ / H$_{\text{inc}}$	2D simpl. H$_{\text{steady state}}$ / H$_{\text{inc}}$	Difference (%)	Wave Gauge	Measured H$_{\text{steady state}}$ / H$_{\text{inc}}$	2D simpl. H$_{\text{steady state}}$ / H$_{\text{inc}}$	Difference (%)
1	1.03	0.85	-18	6	0.85	0.52	-40
2	1.04	0.59	-43	7	1.00	0.31	-68
3	1.43	0.68	-52	8	1.15	0.13	-88
4	0.79	0.66	-17	9	1.02	0.17	-84
5	1.47	0.26	-82	11	0.93	0.52	-44
10	0.80	0.72	-10	12	0.92	0.19	-79
23	0.89	0.71	-20	13	0.93	0.61	-34
24	0.88	0.61	-31	14	1.09	0.19	-82
25	0.99	0.80	-20	15	1.15	0.34	-71
			|Max|= 82	16	1.19	0.19	-84
				26	1.12	0.16	-86
				27	0.95	0.31	-67
							|Max|= 88

Figure J.18 – T011, Top view of the ratio $H_{steady\ state}/H_{incoming}$ at the wave gauges locations. The colours indicate the ratio values. At each location the left box shows the measurements result, while the right box shows the simplified 2D SWASH model results.

Table J.5 – T011, The exact values of ratio $H_{steady\ state}/H_{incoming}$ in the measurements and in the simplified 2D SWASH model.

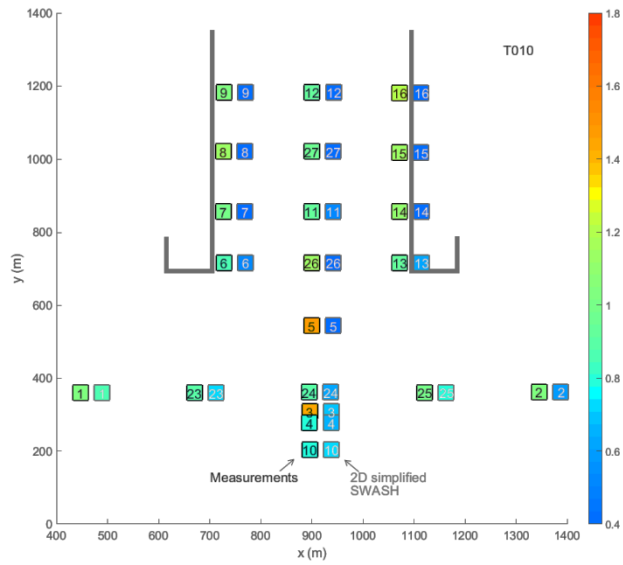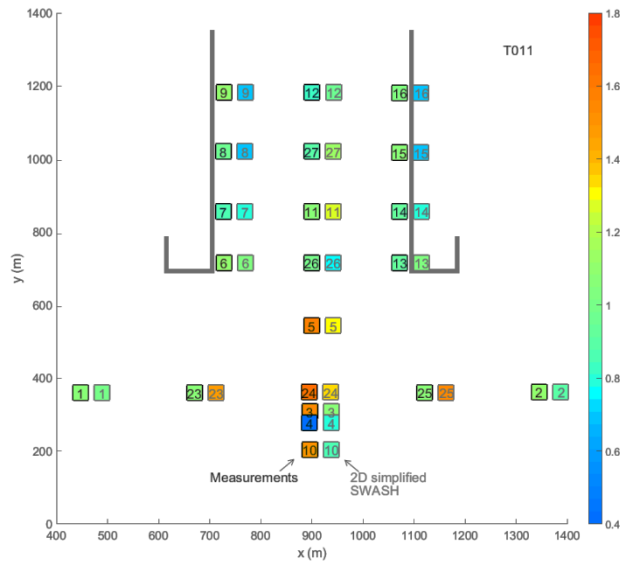| Outside the harbour basin				Inside the harbour basin			
Wave Gauge	Measured $H_{steady\ state}/H_{inc}$	2D simpl. $H_{steady\ state}/H_{inc}$	Difference (%)	Wave Gauge	Measured $H_{steady\ state}/H_{inc}$	2D simpl. $H_{steady\ state}/H_{inc}$	Difference (%)
1	1.05	1.00	- 4	6	1.10	1.04	-5
2	1.10	0.91	- 17	7	0.85	0.78	-8
3	1.54	1.06	- 31	8	0.98	0.69	-29
4	0.43	0.78	83	9	1.09	0.70	-36
5	1.57	1.30	- 17	11	1.07	1.28	20
10	1.52	0.87	- 42	12	0.81	0.98	21
23	1.05	1.49	20	13	0.93	1.04	11
24	1.63	1.35	21	14	0.93	0.80	-15
25	1.07	1.55	11	15	1.06	0.70	-34
			|Max|= 83	16	1.03	0.70	-32
				26	0.99	0.76	-23
				27	0.89	1.12	25
							|Max|= 36

Figure J.19 – T012, Top view of the ratio $H_{steady\ state}/H_{incoming}$ **at the wave gauges locations. The colours indicate the ratio values. At each location the left box shows the measurements result, while the right box shows the simplified 2D SWASH model results.**

Table J.6 – T012, The exact values of ratio $H_{steady\ state}/H_{incoming}$ **in the measurements and in the simplified 2D SWASH model.**

Outside the harbour basin				Inside the harbour basin			
Wave Gauge	Measured $H_{steady\ state}/H_{inc}$	2D simpl. $H_{steady\ state}/H_{inc}$	Difference (%)	Wave Gauge	Measured $H_{steady\ state}/H_{inc}$	2D simpl. $H_{steady\ state}/H_{inc}$	Difference (%)
1	0.33	0.60	80	6	1.63	1.32	- 19
2	0.67	0.67	0	7	1.06	1.20	14
3	1.52	1.72	14	8	1.15	1.10	- 4
4	0.59	0.99	69	9	1.05	0.91	- 13
5	1.56	1.73	11	11	0.75	1.02	37
10	1.51	1.50	0	12	1.00	0.93	- 8
23	0.77	1.09	41	13	1.53	1.34	- 12
24	0.47	0.72	55	14	1.16	1.18	2
25	0.79	1.19	51	15	1.21	1.10	- 9
			|Max|= 69	16	0.69	0.93	34
				26	1.43	1.21	- 16
				27	0.95	0.97	2
							|Max|= 37

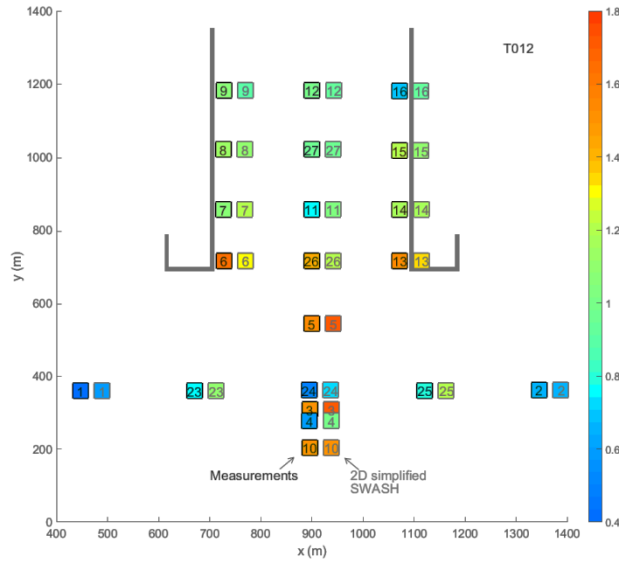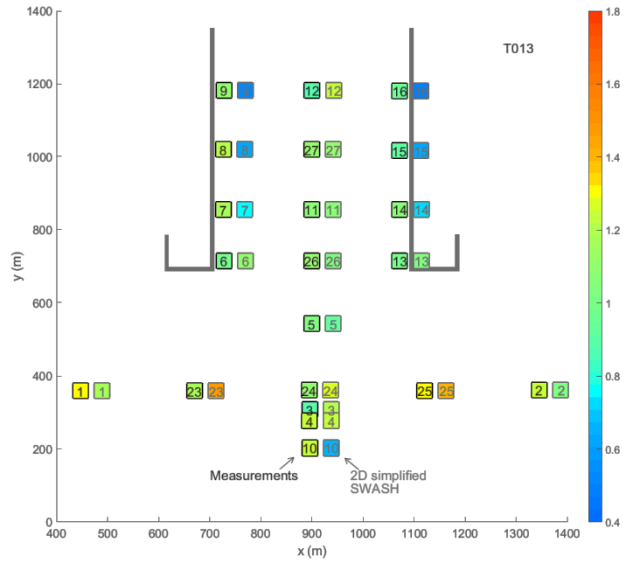**Figure J.20 – T013, Top view of the ratio H_{steady state}/H_{incoming} at the wave gauges locations. The colours indicate the ratio values. At each location the left box shows the measurements result, while the right box shows the simplified 2D SWASH model results.**

Table J.7 – T013, The exact values of ratio H_{steady state}/H_{incoming} in the measurements and in the simplified 2D SWASH model.

Outside the harbour basin				Inside the harbour basin			
Wave Gauge	Measured $H_{steady\ state} / H_{inc}$	2D simpl. $H_{steady\ state} / H_{inc}$	Difference (%)	Wave Gauge	Measured $H_{steady\ state} / H_{inc}$	2D simpl. $H_{steady\ state} / H_{inc}$	Difference (%)
1	1.32	1.18	-10	6	0.99	1.09	10
2	1.22	1.02	-16	7	1.17	0.76	-36
3	0.88	1.21	37	8	1.20	0.62	-49
4	1.22	1.22	0	9	1.11	0.52	-53
5	1.04	0.93	-10	11	1.07	1.07	0
10	1.22	0.66	-46	12	0.91	1.24	36
23	1.18	1.46	23	13	1.01	1.04	3
24	1.09	1.26	16	14	1.06	0.74	-30
25	1.29	1.40	8	15	0.94	0.62	-34
			|Max|= 46	16	0.97	0.50	-48
				26	1.10	1.04	-5
				27	1.10	1.09	-1
							|Max|= 53

Appendix K Results of the 2D SWASH model representing the full layout 1

K.1 Comparison of the measured water level times series to the outputs of the 2D SWASH model representing the full layout 1

The first group of tests for low kd values, presented in Table I.1, includes tests T003 and T012. The graphs comparing the measured water level time series to the SWASH outputs are shown only for test T003, as it is a representative test of the group.

A.

B.

Figure K.1 - T003, Point 10 (picture A) and Point 4 (picture B): Comparison of the measured water level time series to the full 2D SWASH outputs.

Figure K.2 - T003, Point 3 (picture A), Point 24 (picture B), Point 5 (picture C) and Point 26 (picture D): Comparison of the measured water level time series to the full 2D SWASH outputs.

Figure K.3 - T003, Point 11 (picture A), Point 27 (picture B) and Point 12 (picture C): Comparison of the measured water level time series to the full 2D SWASH outputs.

The second group of tests for average kd values, presented in Table I.2, includes tests T001, T002 and T011. The graphs comparing the measured water level time series to the SWASH outputs are shown only for test T002, as it is a representative test of the group.
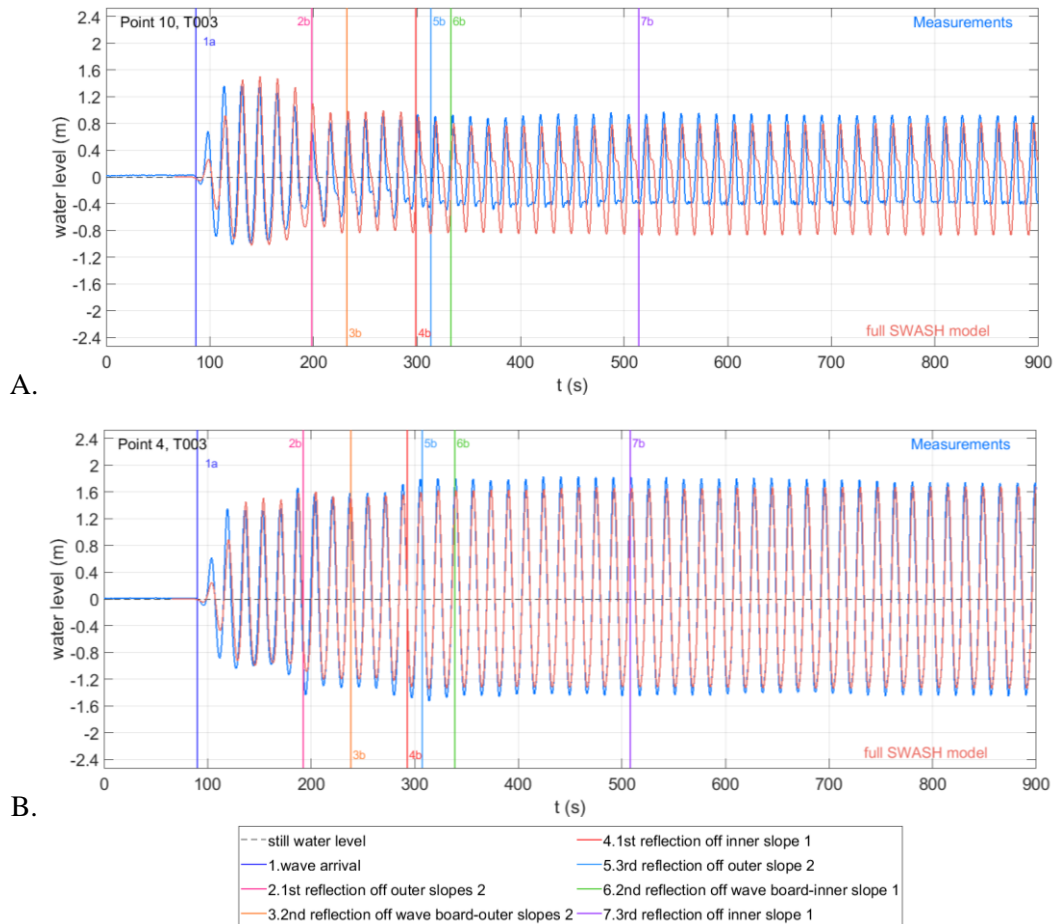

A.

B.

C.

Figure K.4 - T002, Point 10 (picture A), Point 4 (picture B) and Point 3 (picture C): Comparison of the measured water level time series to the full 2D SWASH outputs.

Figure K.5 - T002, Point 24 (picture A), Point 5 (picture B), Point 26 (picture C) and Point 11 (picture D): Comparison of the measured water level time series to the full 2D SWASH outputs.
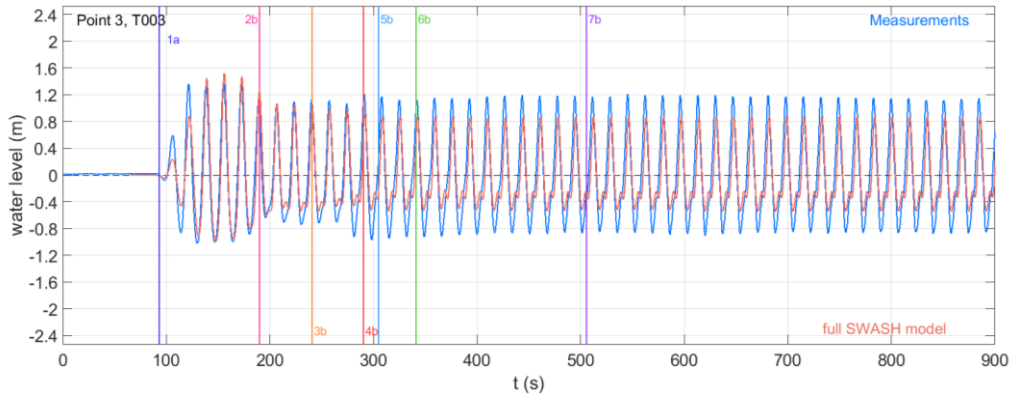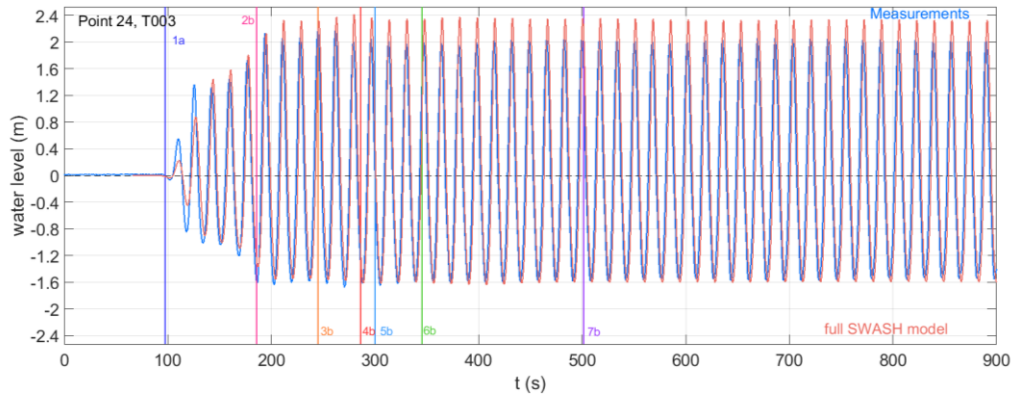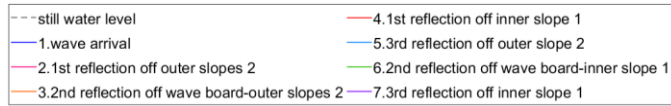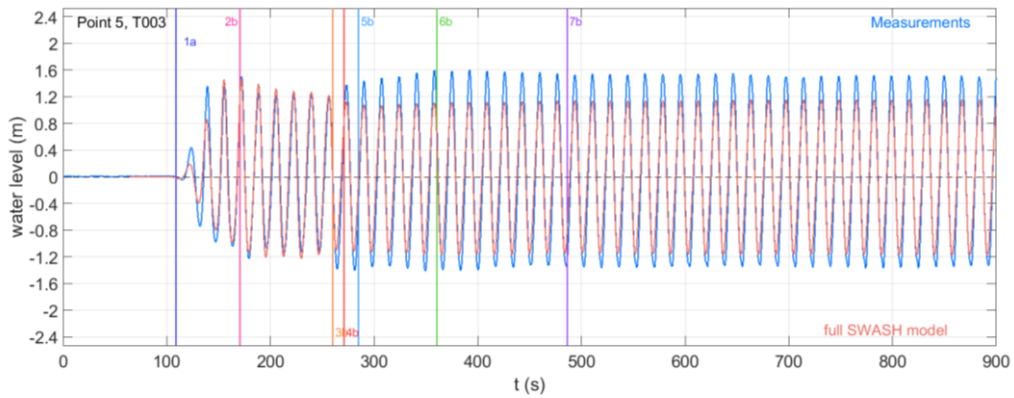
Figure K.6 - T002, Point 27 (picture A) and Point 12 (picture B): Comparison of the measured water level time series to the full 2D SWASH outputs.

The third group of tests for high kd values, presented in Table I.3, includes tests T010 and T013. The graphs comparing the measured water level time series to the SWASH outputs are shown for both tests, as in T010 wave breaking occurs, while in T013 the waves do not break.
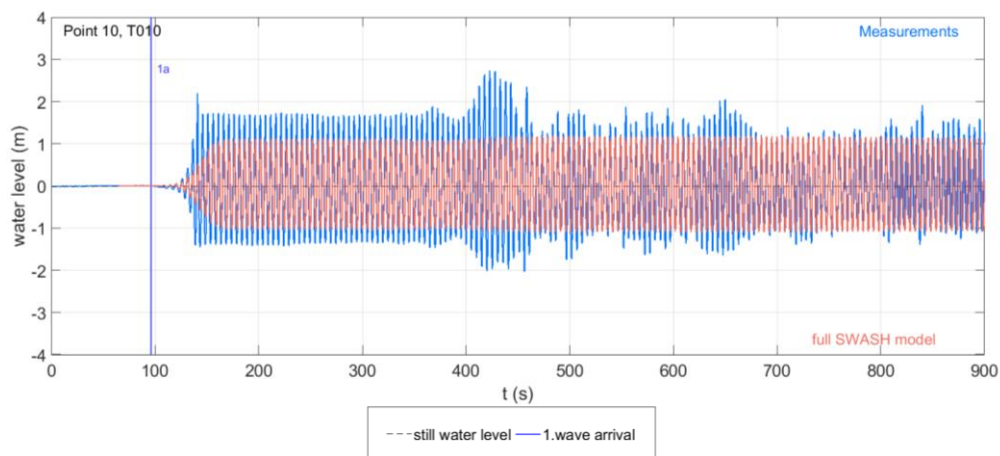
Figure K.7 - T010, Point 10: Comparison of the measured water level time series to the full 2D SWASH outputs.
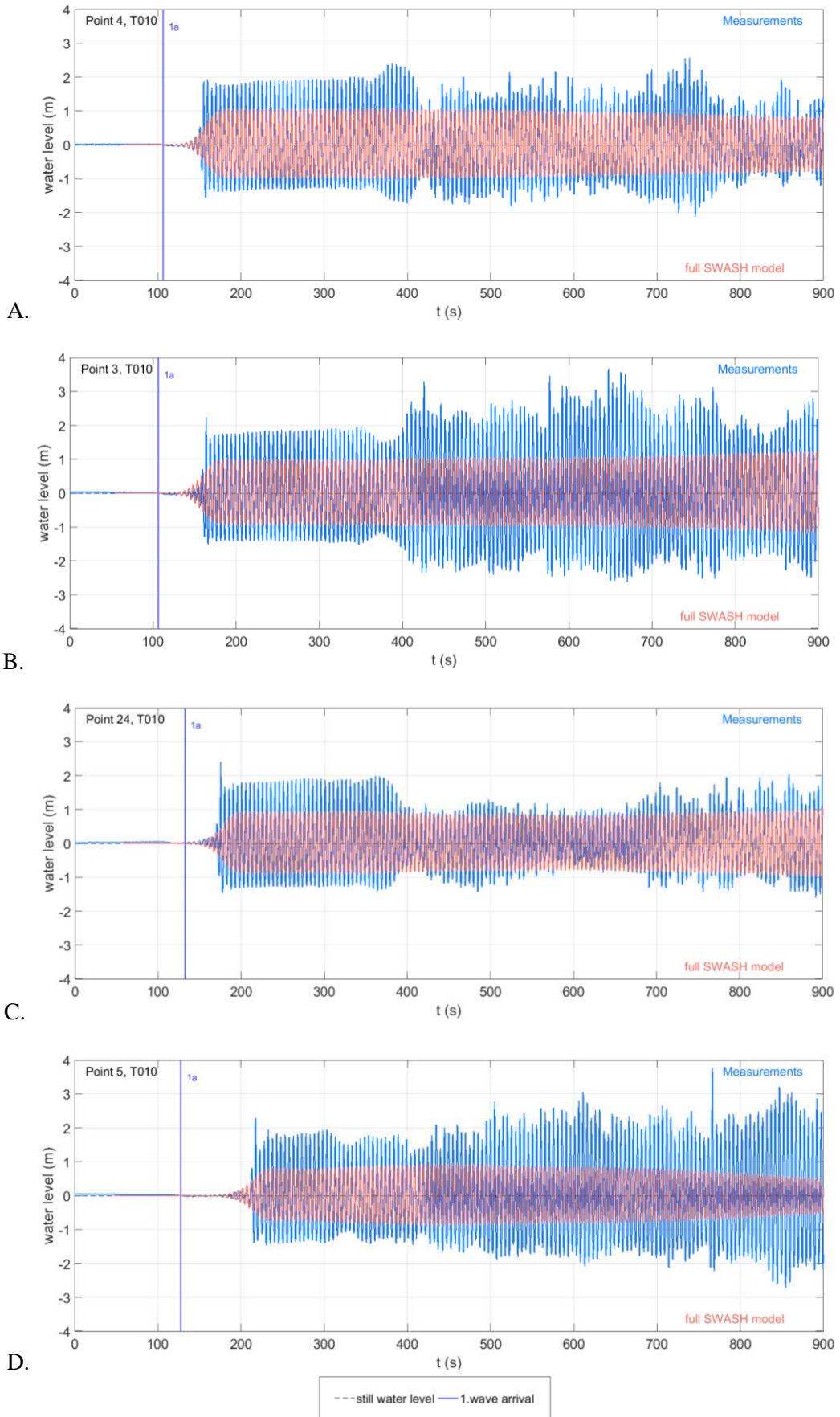
Figure K.8 - T010, Point 4 (picture A), Point 3 (picture B), Point 24 (picture C) and Point 5 (picture D): Comparison of the measured water level time series to the full 2D SWASH outputs.
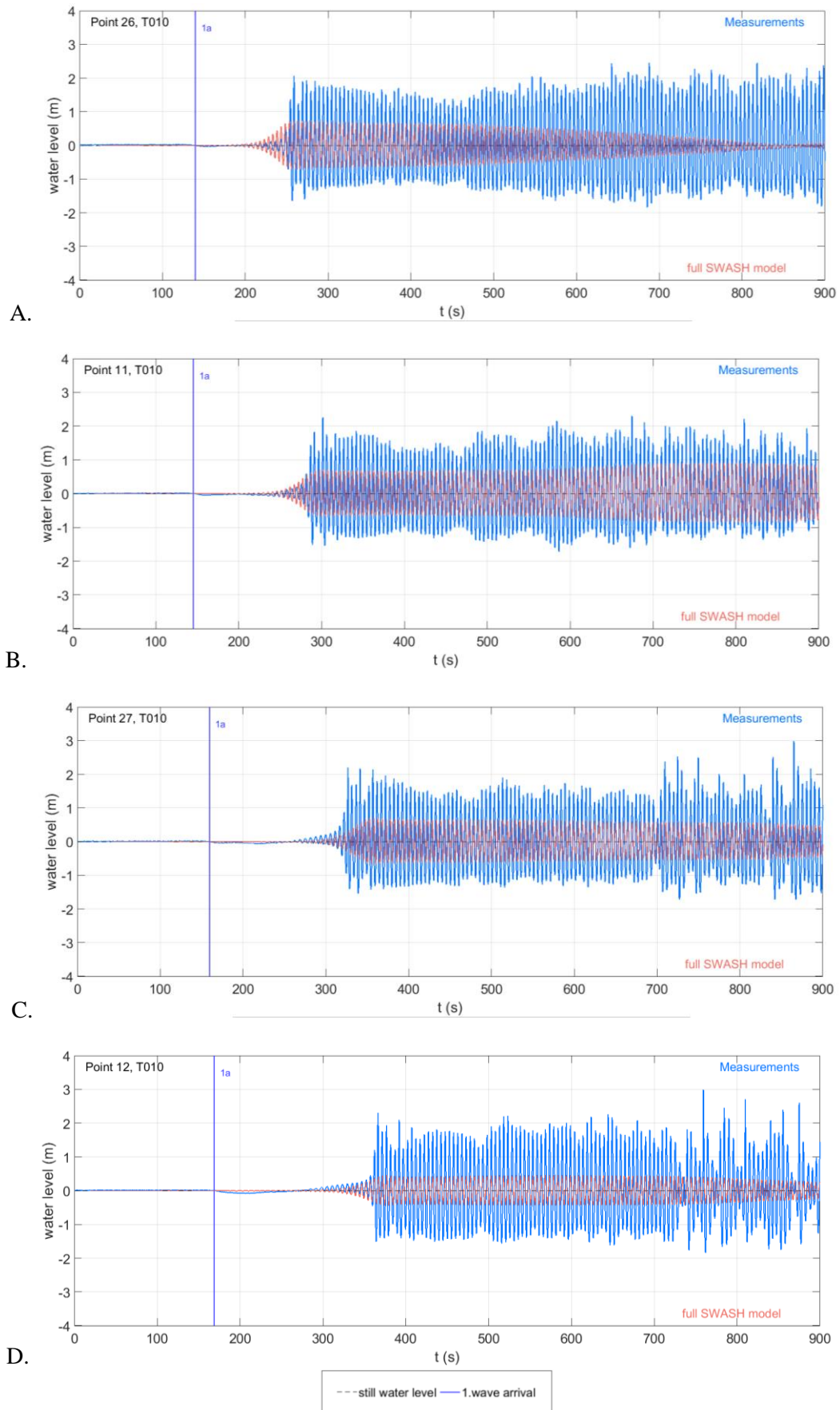
Figure K.9 - T010, Point 26 (picture A), Point 11 (picture B), Point 27 (picture C) and Point 12 (picture D): Comparison of the measured water level time series to the full 2D SWASH outputs.
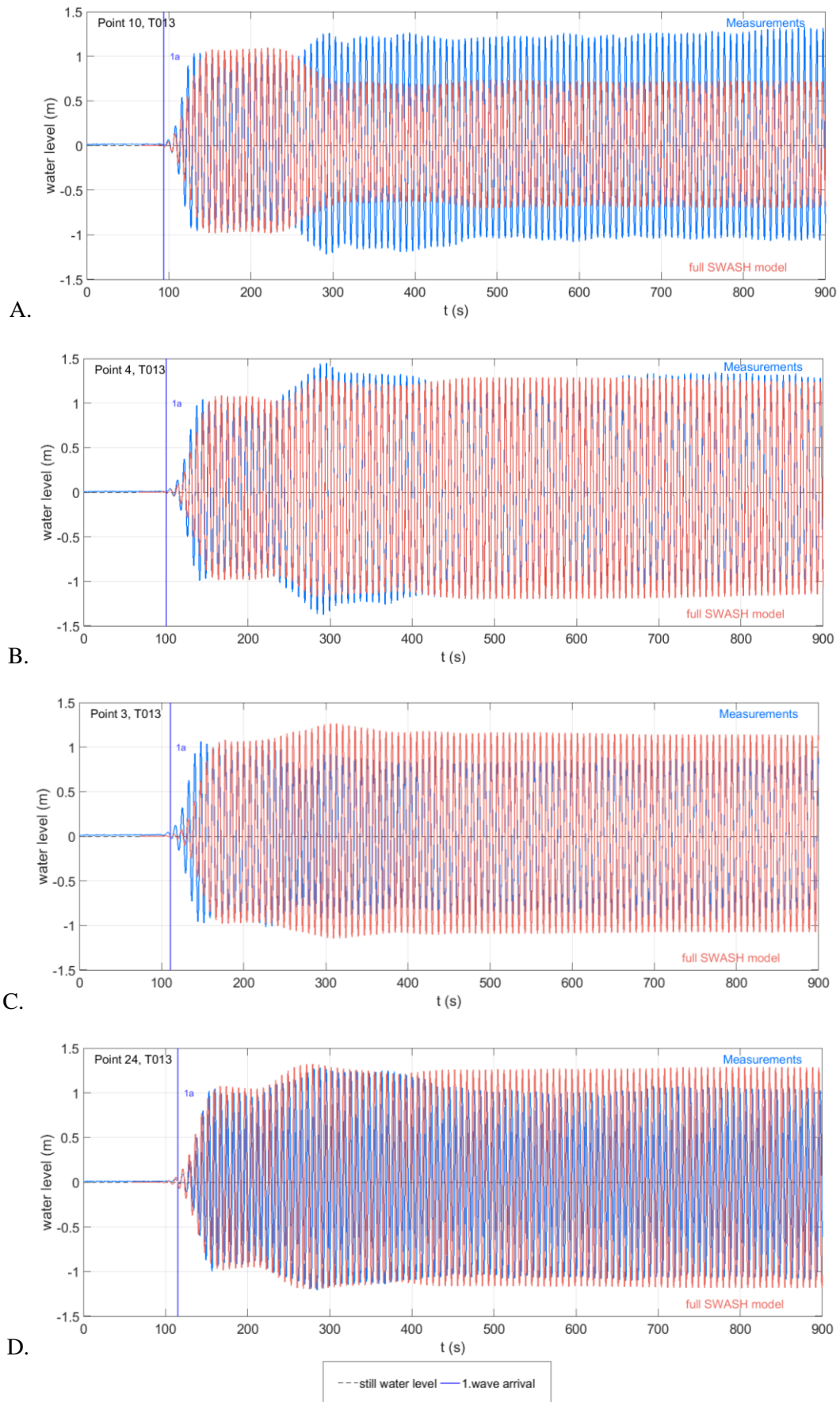
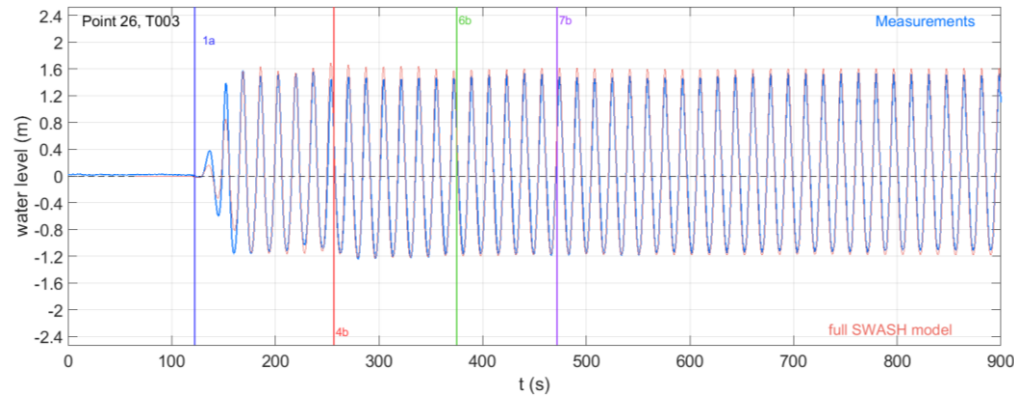**Figure K.10 - T013, Point 10 (picture A), Point 4 (picture B), Point 3 (picture C) and Point 24(picture D): Comparison of the measured water level time series to the full 2D SWASH outputs.**

195
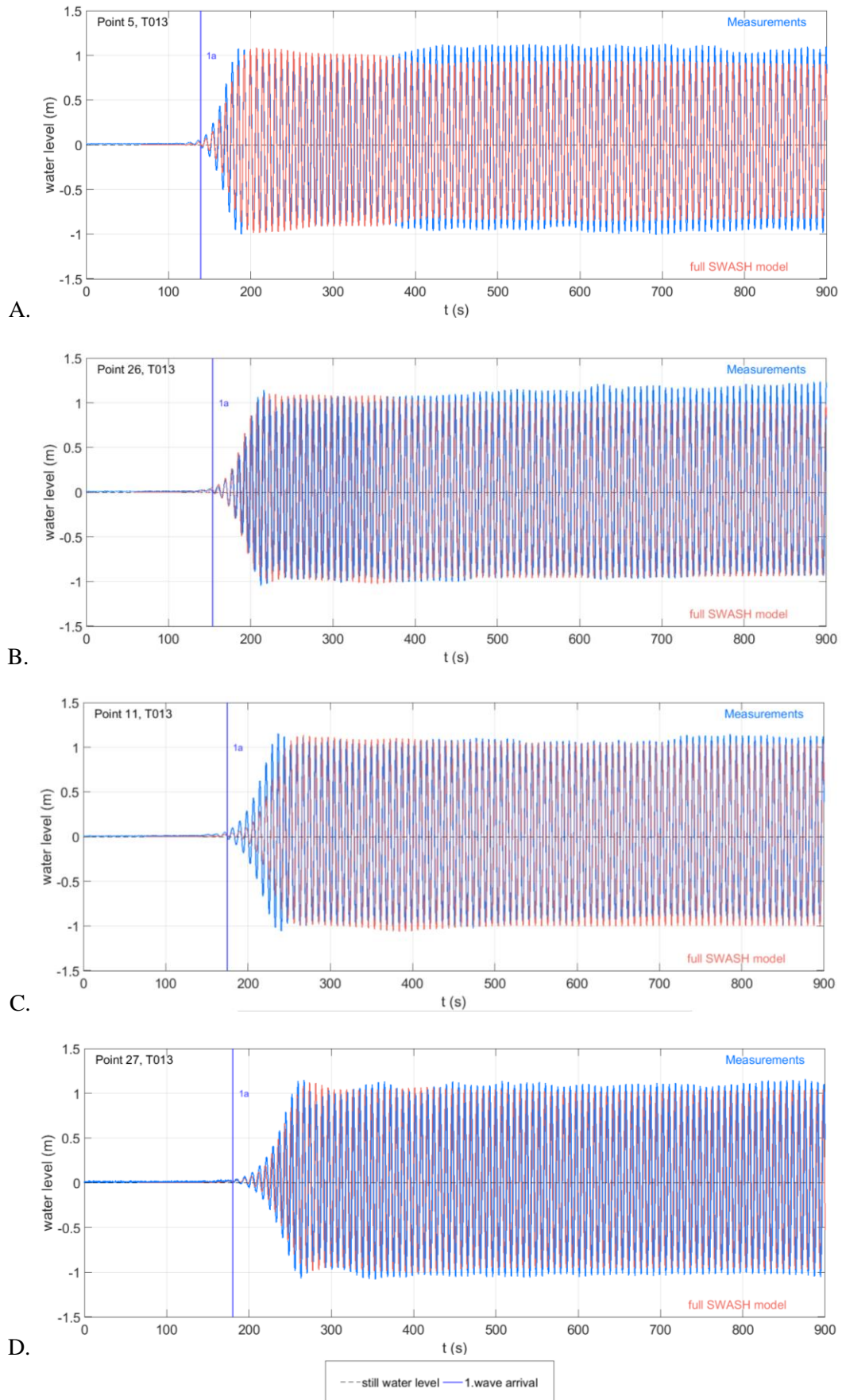
Figure K.11 - T013, Point 5 (picture A), Point 26 (picture B), Point 11 (picture C) and Point 27(picture D): Comparison of the measured water level time series to the full 2D SWASH outputs.
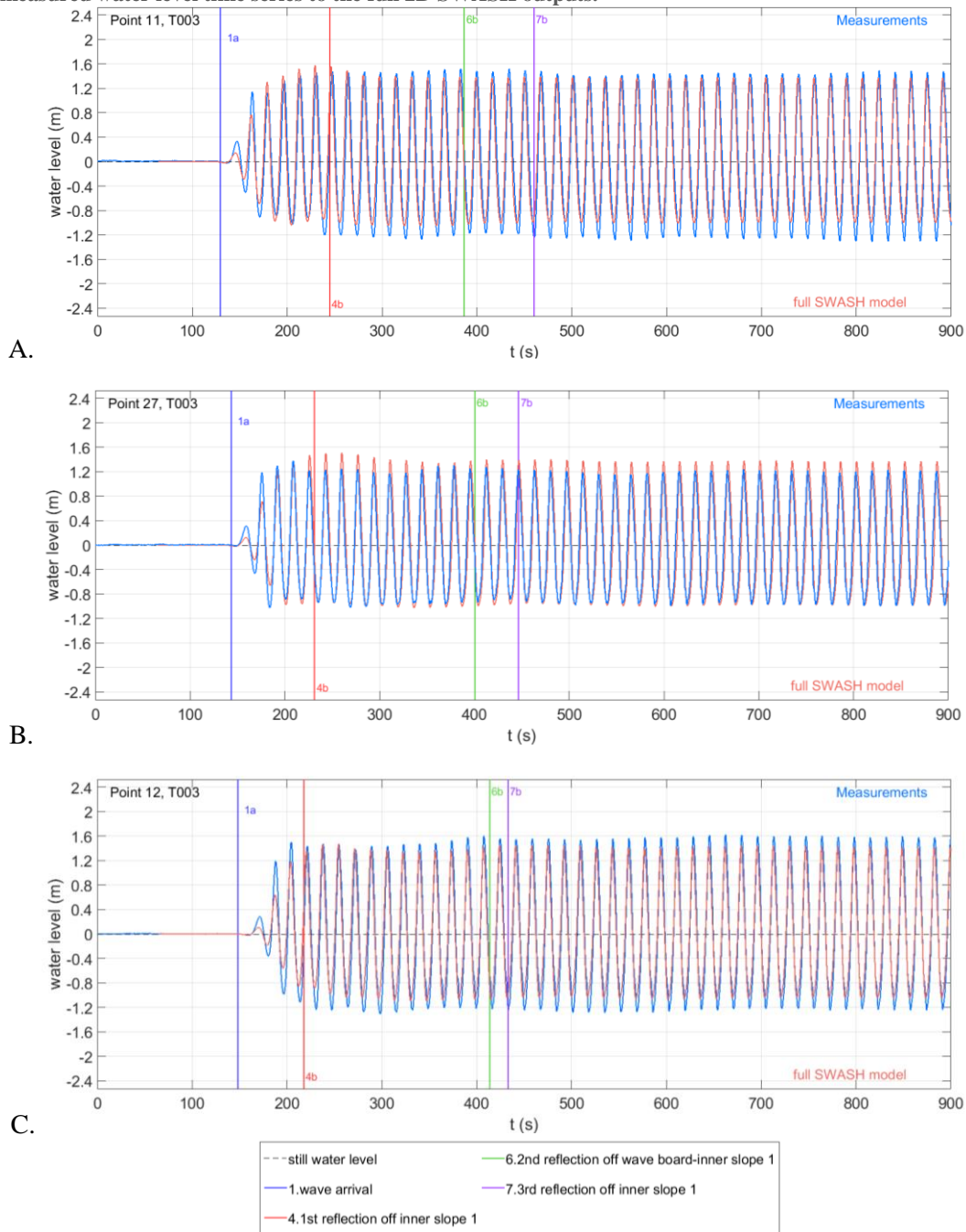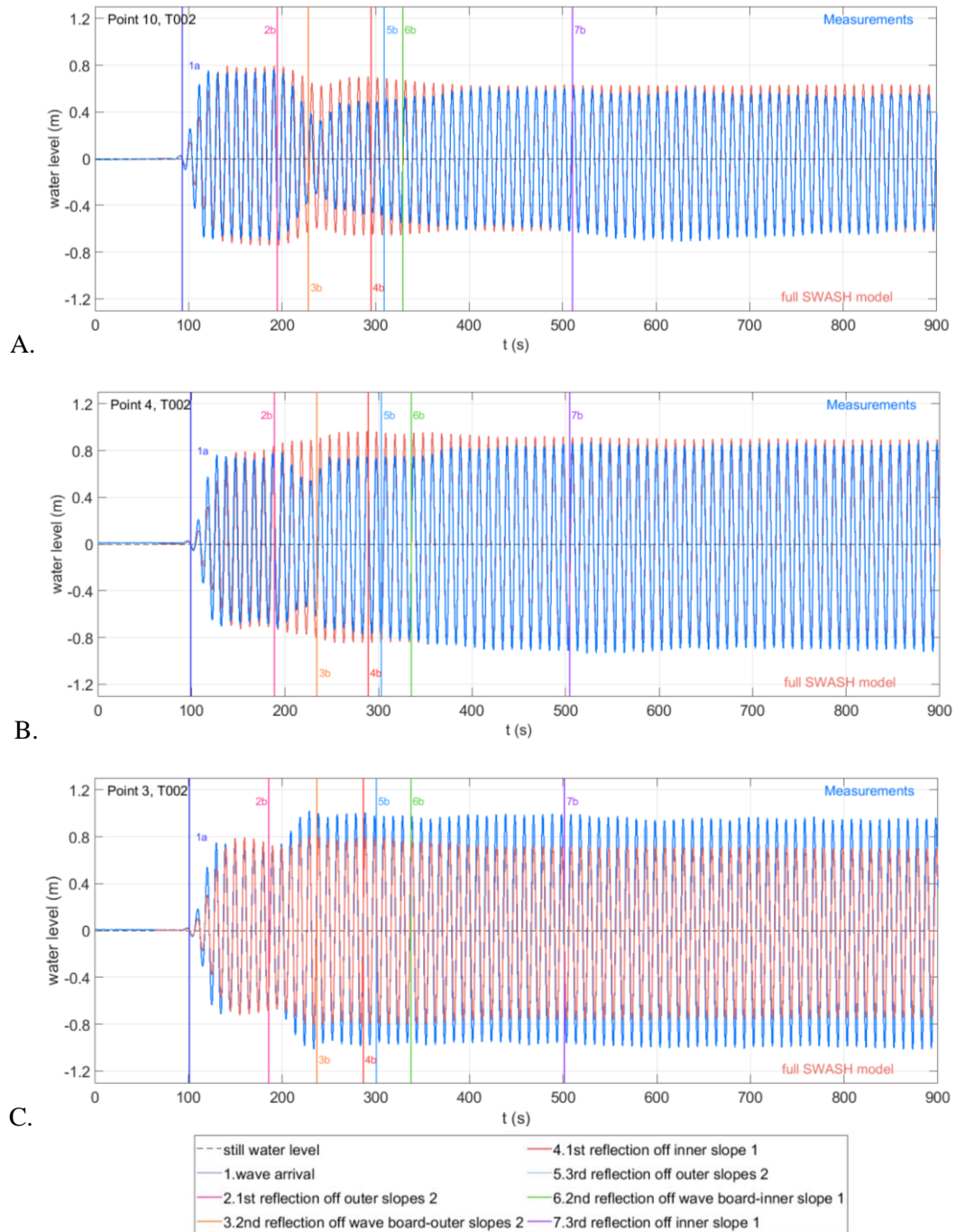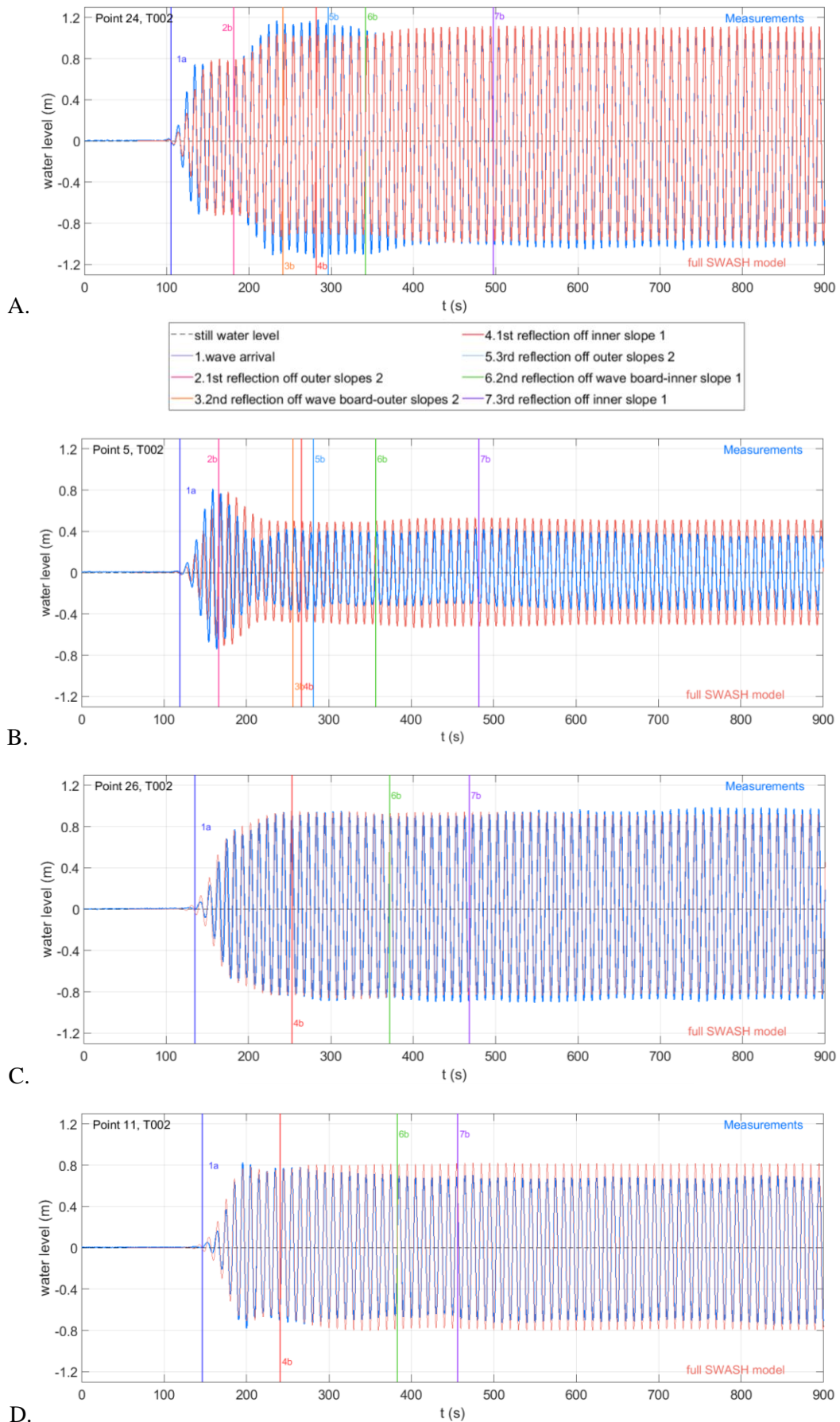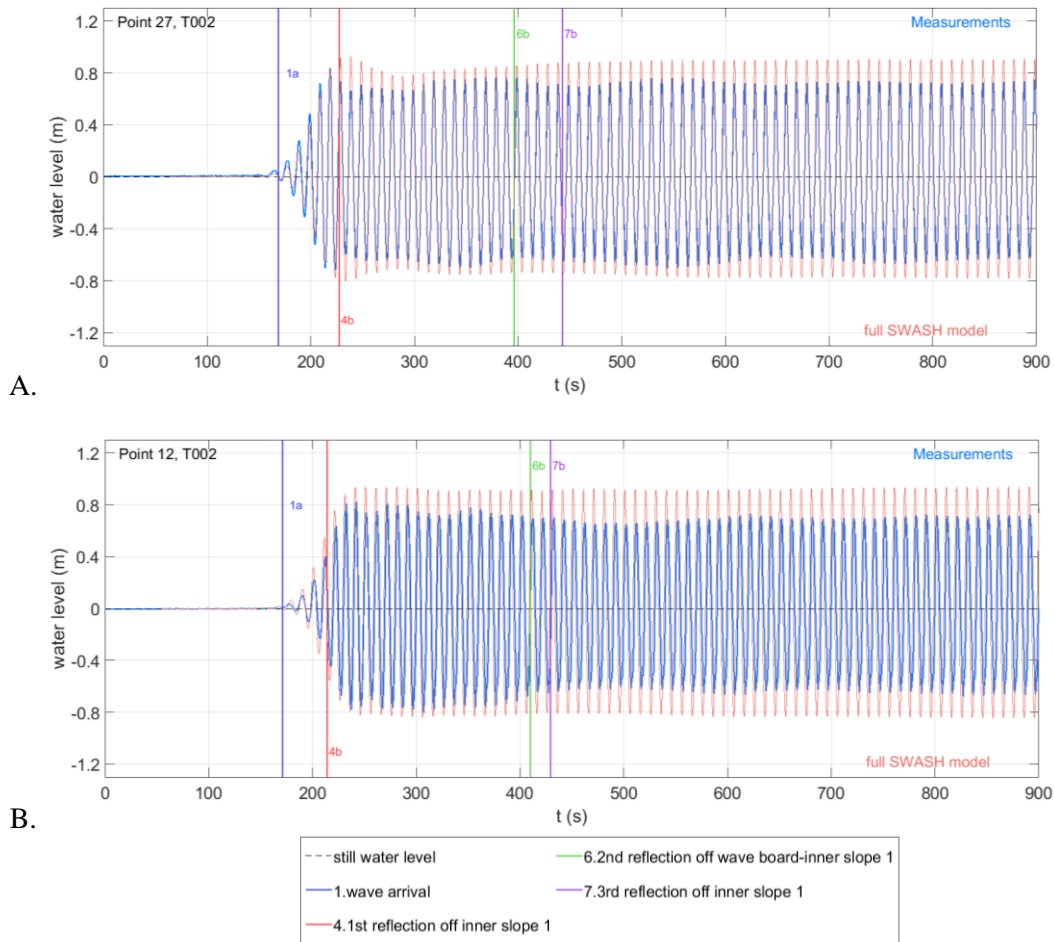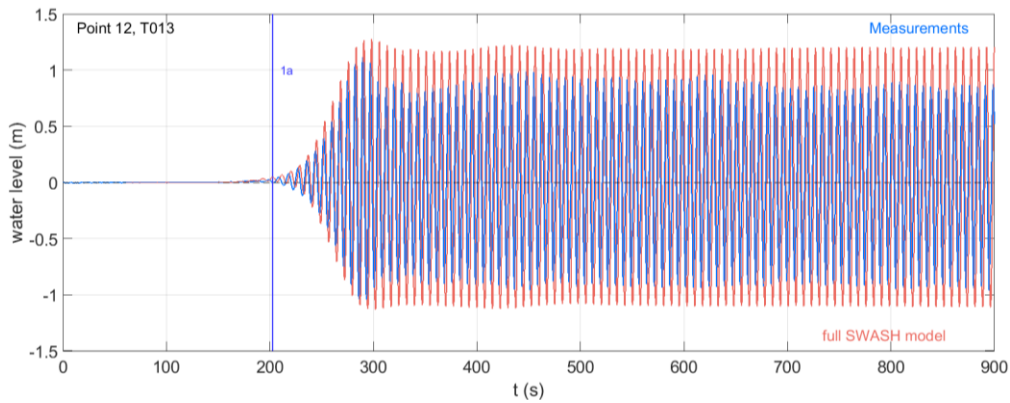
Figure K.12 - T013, Point 12: Comparison of the measured water level time series to the full 2D SWASH outputs.

K.2 Comparison of the steady state in the measurements to the outputs of the 2D SWASH model representing the full layout 1
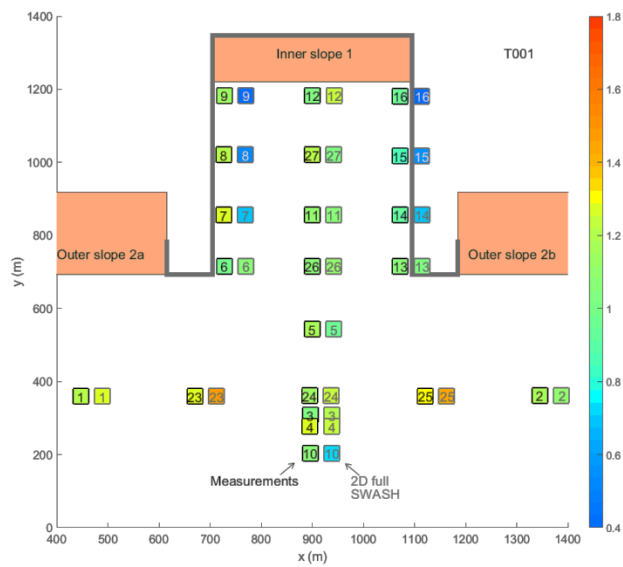
Figure K.13 –2D full model results for T001: Top view of the ratio $H_{steady\ state}/H_{incoming}$ at the output locations included in the measurements. The colours indicate the ratio values.

Table K.1 - 2D full model results for T001: The exact values of ratio $H_{steady\ state}/H_{incoming}$ at the output locations included in the measurements.

Outside the harbour basin				Inside the harbour basin			
Wave Gauge	Measured $H_{steady\ state}/H_{inc}$	2D full $H_{steady\ state}/H_{inc}$	Difference (%)	Wave Gauge	Measured $H_{steady\ state}/H_{inc}$	2D full $H_{steady\ state}/H_{inc}$	Difference (%)
1	1.20	1.27	6	6	1.00	1.07	7
2	1.18	1.11	-6	7	1.27	0.69	-45
3	1.03	1.21	18	8	1.21	0.51	-58
4	1.26	1.24	-1	9	1.15	0.42	-64
5	1.17	0.97	-17	11	1.10	1.05	-4
10	1.08	0.71	-34	12	1.03	1.24	20
23	1.28	1.46	14	13	1.07	1.03	-3
24	1.14	1.23	8	14	0.94	0.68	-28
25	1.32	1.44	9	15	0.87	0.54	-39
			|Max|= 34	16	0.98	0.40	-59
				26	1.07	1.09	1
				27	1.20	1.04	-14
							|Max|= 64

Figure K.14 –2D full model results for T002: Top view of the ratio $H_{steady\ state}/H_{incoming}$ at the output locations included in the measurements. The colours indicate the ratio values.

Table K.2 - 2D full model results for T002: The exact values of ratio $H_{steady\ state}/H_{incoming}$ at the output locations included in the measurements.

Outside the harbour basin				Inside the harbour basin			
Wave Gauge	Measured $H_{steady\ state}$ / H_{inc}	2D full $H_{steady\ state}$ / H_{inc}	Difference (%)	Wave Gauge	Measured $H_{steady\ state}$ / H_{inc}	2D full $H_{steady\ state}$ / H_{inc}	Difference (%)
1	1.63	1.36	-16	6	1.12	1.13	2
2	1.54	1.19	-23	7	0.90	0.73	-19
3	1.36	1.02	-25	8	0.95	0.76	-20
4	1.22	1.20	-2	9	1.37	0.76	-45
5	0.50	0.71	44	11	0.99	1.12	13
10	0.81	0.87	8	12	0.96	1.22	27
23	0.46	0.87	90	13	1.17	1.14	-3
24	1.41	1.45	2	14	0.79	0.74	-7
25	0.60	0.95	59	15	1.11	0.77	-30
			|Max|= 90	16	1.06	0.77	-28
				26	1.28	1.23	-4
				27	0.94	1.16	23
							|Max|= 45

Figure K.15 –2D full model results for T003: Top view of the ratio $H_{steady\ state}/H_{incoming}$ at the output locations included in the measurements. The colours indicate the ratio values.

Table K.3 - 2D full model results for T003: The exact values of ratio $H_{steady\ state}/H_{incoming}$ at the output locations included in the measurements.

| Outside the harbour basin				Inside the harbour basin			
Wave Gauge	Measured $H_{steady\ state}/H_{inc}$	2D full $H_{steady\ state}/H_{inc}$	Difference (%)	Wave Gauge	Measured $H_{steady\ state}/H_{inc}$	2D full $H_{steady\ state}/H_{inc}$	Difference (%)
1	1.19	1.13	-5	6	1.39	1.27	-9
2	1.23	1.07	-13	7	1.27	1.01	-21
3	0.85	0.59	-31	8	0.86	0.95	10
4	1.35	1.26	-6	9	1.16	1.05	-10
5	1.21	0.97	-20	11	1.14	1.00	-12
10	0.57	0.70	24	12	1.19	1.04	-13
23	1.48	1.33	-11	13	1.03	1.25	22
24	1.51	1.66	10	14	1.11	1.02	-9
25	1.46	1.29	-12	15	0.85	0.94	10
			|Max|= 31	16	0.87	1.04	19
				26	1.11	1.17	5
				27	0.91	0.99	9
							|Max|= 22

Figure K.16 – 2D full model results for T010: Top view of the ratio $H_{steady\ state}/H_{incoming}$ at the output locations included in the measurements. The colours indicate the ratio values.

Table K.4 - 2D full model results for T010: The exact values of ratio $H_{steady\ state}/H_{incoming}$ at the output locations included in the measurements.

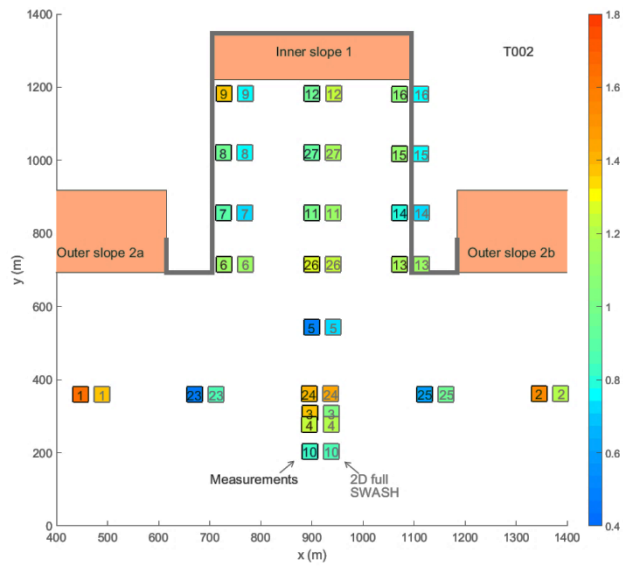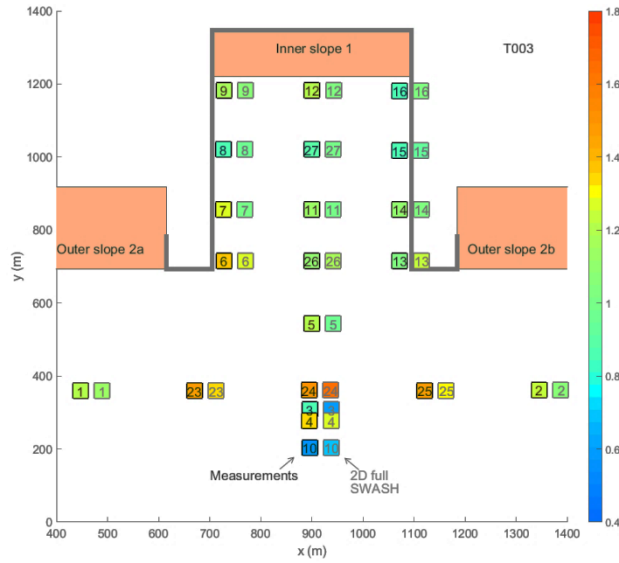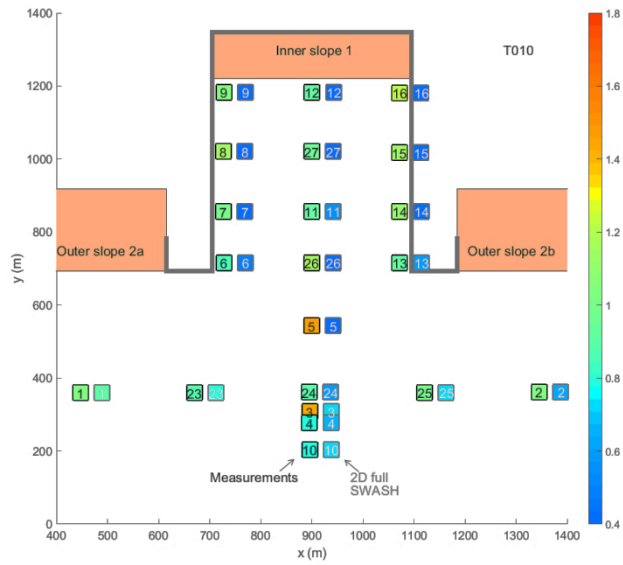| Outside the harbour basin				Inside the harbour basin			
Wave Gauge	Measured $H_{steady\ state}$ / H_{inc}	2D full $H_{steady\ state}$ / H_{inc}	Difference (%)	Wave Gauge	Measured $H_{steady\ state}$ / H_{inc}	2D full $H_{steady\ state}$ / H_{inc}	Difference (%)
1	1.03	0.90	-13	6	0.85	0.47	-45
2	1.04	0.62	-40	7	1.00	0.29	-71
3	1.43	0.72	-50	8	1.15	0.19	-83
4	0.79	0.64	-20	9	1.02	0.16	-84
5	1.47	0.38	-74	11	0.93	0.57	-38
10	0.80	0.74	-7	12	0.92	0.21	-77
23	0.89	0.78	-13	13	0.93	0.60	-35
24	0.88	0.60	-32	14	1.09	0.17	-85
25	0.99	0.73	-26	15	1.15	0.33	-71
			|Max|= 74	16	1.19	0.18	-85
				26	1.12	0.23	-80
				27	0.95	0.31	-67
							|Max|= 85

Figure K.17 –2D full model results for T011: Top view of the ratio $H_{\text{steady state}}/H_{\text{incoming}}$ at the output locations included in the measurements. The colours indicate the ratio values.

Table K.5 - 2D full model results for T011: The exact values of ratio $H_{\text{steady state}}/H_{\text{incoming}}$ at the output locations included in the measurements.

Outside the harbour basin				**Inside the harbour basin**			
Wave Gauge	Measured $H_{\text{steady state}}/H_{\text{inc}}$	2D full $H_{\text{steady state}}/H_{\text{inc}}$	Difference (%)	Wave Gauge	Measured $H_{\text{steady state}}/H_{\text{inc}}$	2D full $H_{\text{steady state}}/H_{\text{inc}}$	Difference (%)
1	1.05	0.96	-9	6	1.10	1.06	-3
2	1.10	0.87	-21	7	0.85	0.80	-6
3	1.54	1.16	-25	8	0.98	0.66	-32
4	0.43	0.80	87	9	1.09	0.70	-36
5	1.57	1.39	-11	11	1.07	1.22	14
10	1.52	0.73	-52	12	0.81	1.00	23
23	1.05	1.43	36	13	0.93	1.07	15
24	1.63	1.38	-15	14	0.93	0.81	-13
25	1.07	1.50	40	15	1.06	0.67	-37
			|Max|=87	16	1.03	0.69	-32
				26	0.99	0.83	-16
				27	0.89	1.25	40
							|Max|= 37

Figure K.18 –2D full model results for T012: Top view of the ratio $H_{steady\ state}/H_{incoming}$ at the output locations included in the measurements. The colours indicate the ratio values.

Table K.6 - 2D full model results for T012: The exact values of ratio $H_{steady\ state}/H_{incoming}$ at the output locations included in the measurements.

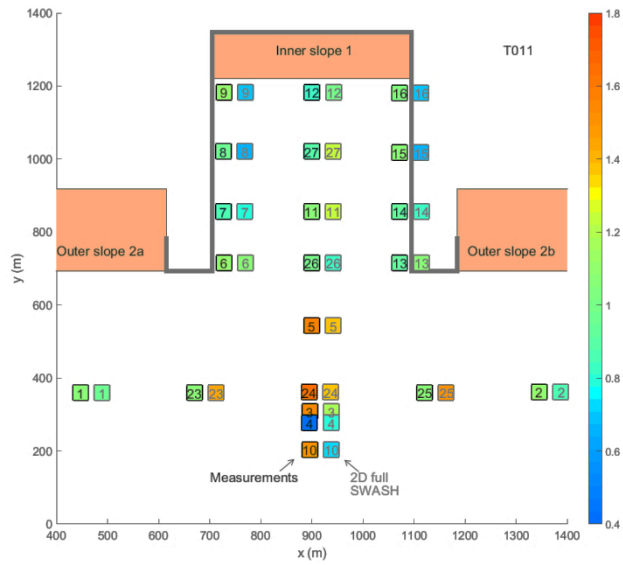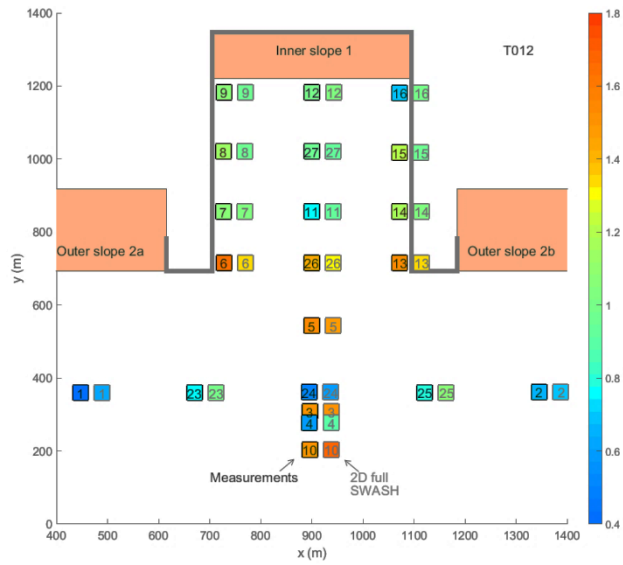| Outside the harbour basin				Inside the harbour basin			
Wave Gauge	Measured $H_{steady\ state}/H_{inc}$	2D full $H_{steady\ state}/H_{inc}$	Difference (%)	Wave Gauge	Measured $H_{steady\ state}/H_{inc}$	2D full $H_{steady\ state}/H_{inc}$	Difference (%)
1	0.33	0.61	82	6	1.63	1.33	82
2	0.67	0.69	3	7	1.06	1.03	3
3	1.52	1.51	-1	8	1.15	0.96	-1
4	0.59	0.91	55	9	1.05	0.98	55
5	1.56	1.49	-5	11	0.75	0.94	26
10	1.51	1.67	11	12	1.00	1.04	3
23	0.77	1.01	31	13	1.53	1.33	-13
24	0.47	0.58	23	14	1.16	1.02	-12
25	0.79	1.06	34	15	1.21	0.98	-20
			|Max|= 62	16	0.69	1.00	44
				26	1.43	1.29	-10
				27	0.95	0.94	-1
							|Max|= 62

Figure K.19 –2D full model results for T013: Top view of the ratio $H_{steady\ state}/H_{incoming}$ at the output locations included in the measurements. The colours indicate the ratio values.

Table K.7 - 2D full model results for T013: The exact values of ratio $H_{steady\ state}/H_{incoming}$ at the output locations included in the measurements.

Outside the harbour basin				Inside the harbour basin			
Wave Gauge	Measured $H_{steady\ state}/H_{inc}$	2D full $H_{steady\ state}/H_{inc}$	Difference (%)	Wave Gauge	Measured $H_{steady\ state}/H_{inc}$	2D full $H_{steady\ state}/H_{inc}$	Difference (%)
1	1.32	1.25	-5	6	0.99	1.07	8
2	1.22	1.10	-10	7	1.17	0.75	-36
3	0.88	1.16	31	8	1.20	0.59	-51
4	1.22	1.26	3	9	1.11	0.49	-56
5	1.04	0.91	-12	11	1.07	1.07	0
10	1.22	0.73	-40	12	0.91	1.19	30
23	1.18	1.45	23	13	1.01	1.03	2
24	1.09	1.26	15	14	1.06	0.73	-31
25	1.29	1.42	10	15	0.94	0.62	-34
			|Max|= 40	16	0.97	0.47	-51
				26	1.10	1.02	-7
				27	1.10	1.03	-6
							|Max|= 56

203

Appendix L 2D SWASH MODELS SETTINGS

L.1 The models set-up

The majority of the 1D SWASH models settings, presented in Section H.1, are also applied in the 2D SWASH models. Here only the additional or different settings are discussed.

1. Grid resolution

As a two dimensional model is more computationally demanding than the one dimensional case, a 3.5 times courser grid size (Δx=3.15m) is chosen. This choice reduces the required computational time. Each computation took approximately 12 hours on two 64-bit Linux cluster nodes with an Intel Xeon E3-1276 CPU @ 3.6GHz and 32 GB RAM. However, for a few test case, the new grid size results in a low number of grid points per wave length as show in in Table L.1. This is related to the accuracy problems observed for tests T010 and T011 (see Chapter 8). For the aforementioned tests the wave are relatively higher (H/h =0.2 instead of 0.1) and the number of grid point per cells should be higher.

Table L.1 – The ratio wave height to water depth H/h and the number of grid cells per wave length for each of the 7 selected tests.

Test	H (m)	h (m)	H/h (m)	L (m)	Δx (m)	Cells per wave length
T001	0.99	19.8	0.1	80.48	3.15	26
T002	1.44	19.8	0.1	120.74	3.15	38
T003	2.385	19.8	0.1	225.59	3.15	72
T010	2.97	19.8	0.2	39.38	3.15	13
T011	3.015	19.8	0.2	104.71	3.15	33
T012	2.745	19.8	0.1	197.05	3.15	63
T013	1.935	19.8	0.1	31.52	3.15	10

2. Boundaries

The incoming wave height generated by the wave maker in the physical scale model is prescribed at the offshore boundary of the model along the length from x= 45m to x=1755m. From x=0m to x=45m and from x=1755m to x=1799.33 the boundary is defined as a closed wall. This choice is made because in the physical scale model the first and the last five paddles are not used in full power (Section 2.2).The remaining three boundaries are defined as closed boundaries.

3. Sponge layer

The sponge layer has a length of 450m. Full justification of this choice is provided in Section 7.1.

4. Time step

The time step chosen is equal to 0.050 s to satisfy the CFL condition. The explicit time discretisation is applied in the simulations, resulting in an automatically selected time step which satisfies the CFL limits. In the command file the Courant number is restricted within the range 0.2 to 0.5.

5. Output locations

The output locations shown in Figure 7.2 are used.

L.2 The SWASH command files

L.2.1 Command file for the simplified 2D model

```
$**************HEADING******************************************
PROJ 'Teni' '1'
$************MODEL INPUT****************************************
CGRID REG 0.675 0 0 1798.65 1827 571 580
VERT 2
$
INPGRID BOTTOM REG 0.675 0 0 571 580 3.15 3.15
READINP BOTTOM 45. 'Harbouronly_L1_grid007_big_sponge.bot' 1 0 FREE
INPGRID POROSITY REG 0.675 0 0 571 580 3.15 3.15
READINP POROSITY 1. 'Walls_only_L1_grid007_big_sponge.por' 1 0 FREE
INPGRID PSIZE REG 0.675 0 0 571 580 3.15 3.15
READINP PSIZE 45. 'Walls_only_L1_grid007_big_sponge.psiz' 1 0 FREE
INPGRID HSTRUCTURE REG 0.675 0 0 571 580 3.15 3.15
READINP HSTRUCTURE 45. 'Walls_only_L1_grid007_big_sponge.hstr' 1 0 FREE
$
INITIAL ZERO
$
BOUND SEGMENT XY 0.675 0 45 0 BTYPE VEL UNIFORM FOURIER 0 0 0 0
BOUND SEGMENT XY 45 0 1755 0 BTYPE WEAK SMOO 1 SEC UNIFORM SERIES
'Paddle45_5_96_T002.tms'
BOUND SEGMENT XY 1755 0 1799.33 0 BTYPE VEL UNIFORM FOURIER 0 0 0 0
BOUND SIDE E CCW BTYPE VEL UNIFORM FOURIER 0 0 0 0
BOUND SIDE W CCW BTYPE VEL UNIFORM FOURIER 0 0 0 0
$
SPON N 450.45
$
NONHYDROSTATIC
$
DISCRET UPW MOM
DISCRET UPW WMOM
$
TIMEI 0.2 0.5
$
$************ OUTPUT REQUESTS ******************************

POINTS 'punt1'    447.07500000    359.50500000
POINTS 'punt2'    1345.64000000 361.75500000
POINTS 'punt3'    896.40000000    307.57500000
POINTS 'punt4'    895.45500000    277.06500000
POINTS 'punt5'    899.68500000    543.60000000
POINTS 'punt6'    727.65000000    715.50000000
POINTS 'punt7'    726.43500000    856.30500000
POINTS 'punt8'    726.66000000    1020.65000000
POINTS 'punt9'    728.19000000    1183.10000000
POINTS 'punt10'  896.17500000    203.71500000
POINTS 'punt11'  900.00000000    856.35000000
POINTS 'punt12'  900.36000000    1183.28000000
POINTS 'punt13'  1072.35000000  715.50000000
POINTS 'punt14'  1072.35000000  856.35000000
POINTS 'punt15'  1071.32000000  1017.05000000
POINTS 'punt16'  1072.08000000  1181.34000000
POINTS 'punt23'  670.36500000    359.73000000
POINTS 'punt24'  894.82500000    360.94500000
POINTS 'punt25'  1121.18000000  360.45000000
POINTS 'punt26'  900.00000000    715.50000000
```

```
POINTS 'punt27'  899.77500000     1020.51000000
$
POINTS 'punt28'  447.07500000     203.71500000
POINTS 'punt29'  447.07500000     543.60000000
POINTS 'punt30'  447.07500000     922.50000000
POINTS 'punt31'  558.72000000     203.71500000
POINTS 'punt32'  558.72000000     359.50500000
POINTS 'punt33'  558.72000000     543.60000000
POINTS 'punt34'  670.36500000     203.71500000
POINTS 'punt35'  670.36500000     543.60000000
$
POINTS 'punt40'  813.63400000     1182.57000000
POINTS 'punt41'  813.63400000     1100.98500000
POINTS 'punt42'  813.63400000     1019.40000000
POINTS 'punt43'  813.63400000     937.86800000
POINTS 'punt44'  813.63400000     856.33500000
POINTS 'punt45'  813.63400000     785.91800000
POINTS 'punt46'  813.63400000     715.50000000
$
POINTS 'punt47'  986.02900000     1182.57000000
POINTS 'punt48'  986.02900000     1100.98500000
POINTS 'punt49'  986.02900000     1019.40000000
POINTS 'punt50'  986.02900000     937.86800000
POINTS 'punt51'  986.02900000     856.33500000
POINTS 'punt52'  986.02900000     785.91800000
POINTS 'punt53'  986.02900000     715.50000000
$
POINTS 'punt54'  727.23400000     1100.98500000
POINTS 'punt55'  727.23400000     937.86800000
POINTS 'punt56'  727.23400000     785.91800000
$
POINTS 'punt57'  900.03400000     1100.98500000
POINTS 'punt58'  900.03400000     937.86800000
POINTS 'punt59'  900.03400000     785.91800000
$
POINTS 'punt60'  1072.02400000    1100.98500000
POINTS 'punt61'  1072.02400000    937.86800000
POINTS 'punt62'  1072.02400000    785.91800000
$
FRAME 'frame1' 0.675 0 0 1798.65 1827 571 580
FRAME 'frame2' 0.675 0 0 1798.65 1827 57 58
$
QUANTITY WATLEV 'WATLEV' 'WATLEV' -10 10 -999
QUANTITY HS 'HS' 'HS' 0 10 -999 0 25 MIN
$
TABLE  'punt1' HEAD 'T002_p1.tbl' TSEC XP YP WATL VKSI VETA OUTPUT 000000.000 0.10 SEC
TABLE  'punt2' HEAD 'T002_p3.tbl' TSEC XP YP WATL VKSI VETA OUTPUT 000000.000 0.10 SEC
TABLE  'punt3' HEAD 'T002_p3.tbl' TSEC XP YP WATL VKSI VETA OUTPUT 000000.000 0.10 SEC
TABLE  'punt4' HEAD 'T002_p4.tbl' TSEC XP YP WATL VKSI VETA OUTPUT 000000.000 0.10 SEC
*** same table created for all the output points****
TABLE  'punt60' HEAD 'T002_p60.tbl' TSEC XP YP WATL VKSI VETA OUTPUT 000000.000 0.10 SEC
TABLE  'punt61' HEAD 'T002_p61.tbl' TSEC XP YP WATL VKSI VETA OUTPUT 000000.000 0.10 SEC
TABLE  'punt62' HEAD 'T002_p62.tbl' TSEC XP YP WATL VKSI VETA OUTPUT 000000.000 0.10 SEC
$
TABLE 'frame1' HEAD 'T002_hs.fr' TSEC XP YP HS
TABLE 'frame1' HEAD 'FT002_wl.fr' TSEC XP YP WATL OUTPUT 000010.000 5 SEC
$
COMPUTE 000000.000 0.050 SEC 001500.000
STOP
```

$*************HEADING*************************************
PROJ 'Teni' '1'
$***********MODEL INPUT***********************************
$
CGRID REG 0.675 0 0 1798.65 1827 571 580
VERT 2
$
INPGRID BOTTOM REG 0.675 0 0 571 580 3.15 3.15
READINP BOTTOM 45. 'Bottom_grid007_big_sponge.bot' 1 0 FREE
INPGRID POROSITY REG 0.675 0 0 571 580 3.15 3.15
READINP POROSITY 1. 'Full_grid007_big_sponge.por' 1 0 FREE
INPGRID PSIZE REG 0.675 0 0 571 580 3.15 3.15
READINP PSIZE 45. 'Full_grid007_big_sponge.psiz' 1 0 FREE
INPGRID HSTRUCTURE REG 0.675 0 0 571 580 3.15 3.15
READINP HSTRUCTURE 45. 'Full_grid007_big_sponge.hstr' 1 0 FREE
$
INITIAL ZERO
$
BOUND SEGMENT XY 0.675 0 45 0 BTYPE VEL UNIFORM FOURIER 0 0 0 0
BOUND SEGMENT XY 45 0 1755 0 BTYPE WEAK SMOO 1 SEC UNIFORM SERIES
'Paddle45_5_96_T002.tms'
BOUND SEGMENT XY 1755 0 1799.33 0 BTYPE VEL UNIFORM FOURIER 0 0 0 0
BOUND SIDE E CCW BTYPE VEL UNIFORM FOURIER 0 0 0 0
BOUND SIDE W CCW BTYPE VEL UNIFORM FOURIER 0 0 0 0
$
SPON N 450.45
NONHYDROSTATIC
DISCRET UPW MOM
DISCRET UPW WMOM
TIMEI 0.2 0.5
$
$************ OUTPUT REQUESTS *****************************
$
POINTS 'punt1'   447.07500000   359.50500000
*** same coordinates defined for the simplified 2D SWASH model, as presented in L.2.1****
POINTS 'punt62' 1072.02400000   785.91800000
$
FRAME 'frame1' 0.675 0 0 1798.65 1827 571 580
FRAME 'frame2' 0.675 0 0 1798.65 1827 57 58
$
QUANTITY WATLEV 'WATLEV' 'WATLEV' -10 10 -999
QUANTITY HS 'HS' 'HS' 0 10 -999 0 25 MIN
$
TABLE 'punt1' HEAD 'T002_p1.tbl' TSEC XP YP WATL VKSI VETA OUTPUT 000000.000 0.10 SEC
 *** same table for all the output points****
TABLE 'punt62' HEAD 'T002_p62.tbl' TSEC XP YP WATL VKSI VETA OUTPUT 000000.000 0.10 SEC
$
TABLE 'frame1' HEAD 'T002_hs.fr' TSEC XP YP HS
TABLE 'frame1' HEAD 'FT002_wl.fr' TSEC XP YP WATL OUTPUT 000010.000 5 SEC
$TABLE 'frame2' HEAD 'FT002_lf.fr' TSEC XP YP WATL OUTPUT 000010.000 5 SEC
$
COMPUTE 000000.000 0.050 SEC 001500.000
STOP